

Engineering strategies for enhancement of
bio-hydrogen production by phototrophic bacterium
Rhodospseudomonas palustris

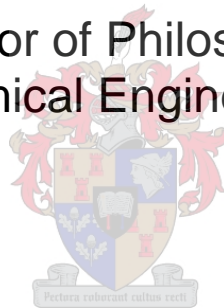
by

Jan-Pierre du Toit

Dissertation presented for the Degree

of

Doctor of Philosophy
(Chemical Engineering)



in the Faculty of Engineering
at Stellenbosch University

Supervisor

Prof. Robert W. M. Pott

The financial assistance of the National Research Foundation (NRF) towards this research is hereby acknowledged. Opinions expressed and conclusions arrived at are those of the author and are not necessarily to be attributed to the NRF.

March 2021

DECLARATION

By submitting this thesis electronically, I declare that the entirety of the work contained therein is my own, original work, that I am the sole author thereof (save to the extent explicitly otherwise stated), that reproduction and publication thereof by Stellenbosch University will not infringe any third party rights and that I have not previously in its entirety or in part submitted it for obtaining any qualification.

This dissertation includes **2** original papers published in peer-reviewed journals, and **1** paper under revision after peer review. The development and writing of the papers (published and unpublished) were the principal responsibility of myself and, for each of the cases where this is not the case, a declaration is included in the dissertation indicating the nature and extent of the contributions of co-authors.

March 2021

ACKNOWLEDGEMENTS

The work in this dissertation, and my development as a scientist have both been supported by the contributions of countless people.

I would foremost like to thank Dr Robbie Pott, my supervisor, for the patient support, advice, and critical discussions offered during the course of my PhD, which was invaluable on my path to becoming an independent researcher. I am now acutely aware that nothing in research works the first time and takes at least twice as long as anticipated.

I thank the members of our research group for their support, camaraderie and occasional commiseration. I am also grateful to the staff of the Process Engineering department for their assistance and wealth of technical expertise; in particular Jaco van Rooyen and Hanlie Botha for excellent discussions on analytical problems, and Jos Weerdenburg and Anton Cordier for their fabrication ingenuity and endless good-humour.

I would also like to acknowledge Professor Chris Howe and Dr David Lea-Smith for their mentorship and support in developing genetic modification techniques, and without whom my research visit to the University of Cambridge would not have been possible. I owe my success during this short 5-month stint to the people in the Hopkins building who made my time there both immensely enjoyable and productive: Drs Anna Git, Jeff Douglass, Jack Hervey and Laura Wey.

My postgraduate study was supported by funding from the National Research Foundation, Water Research Commission, and a Merit scholarship from Stellenbosch University; all of which I am deeply grateful for.

Finally, I would like to thank my family and friends for their unfailing support and encouragement throughout this journey.

ABSTRACT

The photosynthetic bacterium *Rhodospseudomonas palustris* demonstrates an exceptional metabolic diversity and is capable of consuming a wide variety of organic compounds including those toxic to other organisms. Anaerobic photoheterotrophic growth results in a cellular redox imbalance due to accumulation of excess reducing equivalents arising from substrate breakdown. This favourable energy state drives energy-intensive pathways including nitrogenase-mediated hydrogen production, raising the potential for generation of a clean renewable energy source from a multitude of organic waste streams. Realising the promise of biohydrogen production via photofermentation as part of a nascent circular bioeconomy requires technological development to address two key issues: i. low volumetric production rates, and ii. means of sustaining long-term continuous production. The research herein explores strategies comprising process engineering and optimisation, materials science and metabolic engineering to overcome these barriers to process feasibility.

The first objective was to definitively determine optimal temperatures for growth and hydrogen production by *R. palustris*; a fundamental process parameter with significant impact on enzyme and metabolic efficiency. By acclimatising two closely-related laboratory strains to higher temperatures, temperature optima 5 to 10°C higher than the widely-accepted 30°C were seen. Higher optima are advantageous for outdoor sunlit bioreactors which experience high temperatures, reducing considerations for temperature control. At 35°C, strain CGA009 showed 53% faster growth and 2.4-fold higher hydrogen production versus 30°C. Strain ATH 2.1.37 grew optimally at 40°C, with 86% faster growth and 4-fold higher productivity. In context of the strains' high genome similarity, long-term laboratory cultivation seems to diminish temperature resistance over time, informing selection criteria for high-temperature, catalytically-efficient strains.

Hydrogen production is not growth-associated in *R. palustris*, and non-growing biomass supports higher production rates due to reduced energetic competition from cell division. Immobilisation of cells in a suitable solid matrix is thus an attractive means of retaining

biomass in a continuous reactor independent of hydraulic retention time. To this end, a novel transparent cryogel composed of poly vinyl-alcohol was characterised and optimised to yield properties suited to entrapment of photosynthetic bacteria, aided by newly-devised *in situ* imaging techniques. High transparency, mechanical resilience and biocompatibility, and low resistance to substrate diffusion was demonstrated. Immobilised *R. palustris* showed higher specific hydrogen production rates which continued longer than planktonic controls. Continuous cultures further maintained productivity for at least 67 days, verifying suitability of the PVA cryogel for long-term photofermentation and indeed wider applications where high biocompatibility and resilience is desirable.

Metabolic engineering is a powerful tool for optimising the productivity of specific pathways including nitrogenase-mediated hydrogen production. The lack of efficient tools for genetic manipulation of *R. palustris* was thus addressed by development of a rapid, electroporation-based technique for chromosomal modification. Multiple refinements effectively halve the time required to generate markerless strains to 12 days versus previous methods. This system was used to over-express alternative nitrogenase genes with the potential to improve low enzyme efficiency; hypothesised to be rate-limiting for hydrogen production overall. By insertion of strong promoters upstream of native genes, up to 4000-fold overexpression was achieved. While hydrogen productivity was not ultimately improved, these tools facilitate further efforts and advance *R. palustris* as a biotechnological chassis for high value, energy-intensive bioproducts.

These advancements in temperature optimisation, bacterial immobilisation and metabolic engineering as an integrated strategy have the potential to enable maturation of photosynthetic biohydrogen towards larger-scale viability.

OPSOMMING

Die fotosintetiese bakterie *Rhodospseudomonas palustris* demonstreer 'n uitsonderlike metaboliese diversiteit en kan 'n wye verskeidenheid organiese samestellings verteer, insluitend die wat toksies is vir ander organismes. Anaerobiese fotoheterotrofiese groei lei tot 'n sellulêre redokswanbalans as gevolg van die akkumulering van 'n oormaat reduseerewivalente wat ontstaan vanuit substraatafbreking. Hierdie gunstige energietoestand dryf energie-intensiewe paaie insluitend nitrogenase-bemiddelde waterstofproduksie, wat die potensiaal wek vir ontwikkeling van 'n skoon, herwinbare energiebron vanuit 'n menigte organiese afvalstrome. Om die belofte van biowaterstofproduksie via fotofermentasie as deel van 'n nassente sirkulêre bio-ekonomie te realiseer, vereis tegnologiese ontwikkeling om twee sleutelkwessies aan te spreek: eerstens, lae volumetriese produksietempo's, en tweedens die vermoë om langtermyn aaneenlopende produksie te handhaaf. Die navorsing hierin ondersoek strategieë wat uit prosesingenieurswese en optimering, materiaalkunde en metaboliese ingenieurswese bestaan, om hierdie hindernisse tot die proses se uitvoerbaarheid, te oorkom.

Die eerste doelwit was om optimale temperature vir groei en waterstofproduksie deur *R. palustris* definitief te bepaal; 'n fundamentele prosesparameter met beduidende impak op ensiem- en metaboliese doeltreffendheid. Deur twee naby-verwante laboratoriumlyne na hoër temperature te akklimatiseer, is temperatuur optima 5 tot 10°C hoër as die wyd-aanvaarde 30°C, waargeneem. Hoër optima is voordelig vir buitelug, sonverligte bioreaktors wat hoër temperature ondervind, en sodoende oorwegings vir temperatuurbeheer verlaag. By 35°C, het lyn CGA009 53% vinniger groei en 2.4-keer hoër waterstofproduksie getoon, teenoor by 30°C. Lyn ATH 2.1.37 het optimaal gegroei by 40°C, met 86% vinniger groei en 4-keer hoër produktiwiteit. In konteks van die lyne se hoë genoomooreenkoms, lyk dit asof langtermyn laboratorium kultivering temperatuurweerstand oor tyd verminder, wat seleksiekriteria vir hoë-temperatuur katalitiese-doeltreffende lyne inlig.

Waterstofproduksie is nie groei-geassosieer in *R. palustris* nie, en nie-groeiende biomassa

ondersteun hoër produksietempo's as gevolg van verlaagde energieke kompetisie vanuit selverdeling. Immobilisasie van selle in 'n gepaste vaste matriks is dus 'n aantreklike manier om biomassa in 'n kontinue reaktor, onafhanklik van hidrouliese retensietyd, te behou. Hiertoë is 'n nuwe deursigtige kriojel, saamgestel uit polivinielalkohol (PVA), gekarakteriseer en optimeer om eienskappe gepas tot verstrikking van fotosintetiese bakterieë te lewer, met behulp van nuut-ontwerpte *in situ* beeldvormingstegnieke. Hoë deursigtigheid, meganiese veerkragtigheid en bioverenigbaarheid, en lae weerstand tot substraat diffusie is gedemonstreer. Geïmmobiliseerde *R. palustris* het hoër spesifieke waterstofproduksietempo's getoon wat langer aangehou het as planktoniese kontroles. Verder het kontinue kulture produktiwiteit vir ten minste 67 dae gehandhaaf, wat geskiktheid van die PVA-kriojel vir langtermyn fotofermentasie verifieer en so ook wyer toepassings waar hoë bioverenigbaarheid en veerkragtigheid na wense is.

Metaboliese ingenieurswese is 'n kragtige instrument om die produktiwiteit van spesifieke paaie te optimeer, insluitend nitrogenase-bemiddelde waterstofproduksie. Die gebrek aan doeltreffende instrumente vir genetiese manipulasie van *R. palustris* was dus geadresseer deur ontwikkeling van 'n vinnige elektroporasie-gebaseerde tegniek vir chromosoommodifikasie. Verskeie verfynings het die tyd wat dit neem om merkervrye lyne te genereer, na 12 dae gehalveer teenoor vorige metodes. Hierdie sisteem is gebruik vir die ooruitdrukking van alternatiewe nitrogenasegene met die potensiaal om lae ensiemdoeltreffendheid te verbeter; wat gehipoteseer is om tempo-beperkend te wees vir waterstofproduksie oor die algeheel. Deur sterk promotors stroomop van inheemse gene by te voeg, is tot en met 4000-maal ooruitdrukking bereik. Terwyl waterstofproduktiwiteit nie op die lange duur verbeter het nie, het hierdie instrumente verdere pogings gefasiliteer en *R. palustris* as 'n biotegniese raamwerk vir hoë waarde, energie-intensiewe bioprodukte bevorder.

Hierdie vordering in temperaturoptimering, bakteriese immobilisasie en metaboliese ingenieurswese as 'n geïntegreerde strategie het die potensiaal om rypwording van fotosintetiese biowaterstof tot groter skaal uitvoerbaarheid in staat gestel.

TABLE OF CONTENTS

ACKNOWLEDGEMENTS	I
ABSTRACT.....	II
OPSOMMING.....	IV
LIST OF FIGURES	IX
LIST OF TABLES.....	XI
CHAPTER 1 INTRODUCTION: CENTRAL AIM AND SUMMARY OF RESEARCH.....	1
1.1 Central aim	2
1.2 Introduction.....	3
1.3 Summary of research.....	4
1.4 Articles arising from this work	5
CHAPTER 2 INTRODUCTION TO BIOHYDROGEN PRODUCTION BY <i>RHODOPSEUDOMONAS PALUSTRIS</i> AND ASSOCIATED BIOPROCESS CONSIDERATIONS	6
2.1 <i>Status quo</i> of energy economy & environmental outlook	7
2.2 Hydrogen as an alternative energy carrier	8
2.3 Biological hydrogen production	9
2.3.1 Biophotolysis	9
2.3.2 Dark fermentation.....	10
2.3.3 Photofermentation	10
2.4 <i>Rhodopseudomonas palustris</i>	11
2.4.1 Taxonomy and microbiology	11
2.4.2 Metabolism and photosynthesis	13
2.4.3 Substrates and industrial applications	17
2.5 Influence of temperature on hydrogen production	19
2.6 Influence of light on hydrogen production	21
2.7 Mechanisms of control over nitrogenase expression and activity in <i>R. palustris</i>	23
2.8 Microbial immobilisation for bioprocess optimisation	27
2.8.1 PVA cryogels.....	30
2.9 Conclusion.....	32
CHAPTER 3 HEAT-ACCLIMATISED STRAINS OF <i>RHODOPSEUDOMONAS PALUSTRIS</i> REVEAL HIGHER TEMPERATURE OPTIMA WITH CONCOMITANTLY ENHANCED HYDROGEN PRODUCTION RATES.....	34
3.1 Context	35
3.2 Abstract	35
3.3 Introduction.....	36
3.4 Methods:.....	39
3.4.1 Bacteria and culture methods.....	39
3.4.2 Photobioreactor setup	39
3.4.3 Analytical	40
3.4.4 Bioinformatics.....	41
3.5 Results and discussion	43

3.5.1	Growth is enhanced at temperatures exceeding 30°C	43
3.5.2	Increased temperatures support faster hydrogen production rates	47
3.5.3	Temperature influences substrate conversion efficiency	50
3.6	Conclusion.....	52
3.7	Acknowledgements	53
3.8	Author contributions	53
CHAPTER 4 TRANSPARENT POLY VINYL-ALCOHOL CRYOGEL AS IMMOBILISATION MATRIX FOR CONTINUOUS BIOHYDROGEN PRODUCTION BY PHOTOTROPHIC BACTERIA		54
4.1	Context	55
4.2	Abstract	55
4.3	Introduction.....	57
4.4	Materials and Methods.....	61
4.4.1	Cryogel sample preparation	61
4.4.2	Mechanical testing.....	61
4.4.3	Optical characterisation.....	61
4.4.4	Diffusive properties.....	62
4.4.5	Bacteria and culture methods.....	62
4.4.6	Photobioreactor setup	62
4.4.7	<i>R. palustris</i> immobilisation.....	63
4.4.8	Microscopic imaging.....	64
4.4.9	Bacterial membrane integrity determination	64
4.4.10	Analytical	65
4.5	Results and discussion	66
4.5.1	Transparency of cryogels for use with phototrophic organisms.....	66
4.5.2	Mechanical properties of transparent cryogels for bioprocess use.....	69
4.5.3	Morphological differences between conventional and transparent cryogels.....	72
4.5.4	Diffusive properties of cryogels	74
4.5.5	Assessment of PVA immobilisation procedure on cell viability	76
4.5.6	Phototrophic bio-hydrogen production by PVA cryogel-entrapped <i>R. palustris</i>	80
4.6	Conclusion.....	84
4.7	Acknowledgments	85
4.8	Author contributions	86
CHAPTER 5 EXPRESSION OF ALTERNATIVE NITROGENASES IN <i>RHODOPSEUDOMONAS PALUSTRIS</i> IS ENHANCED USING A NOVEL GENETIC TOOLSET FOR RAPID, MARKERLESS MODIFICATIONS.....		87
5.1	Context	88
5.2	Abstract	88
5.3	Introduction.....	89
5.4	Methods.....	92
5.4.1	Media and culture conditions.....	92
5.4.2	Plasmid construction	92
5.4.3	Optimised <i>R. palustris</i> transformation and markerless strain generation	93
5.4.4	Electroporation procedure refinement	96
5.4.5	Optimised RNA isolation	96
5.4.6	Gene expression analysis by RT-qPCR	97
5.4.7	Western blot.....	100

5.4.8	Photobioreactor configuration and conditions	100
5.5	Results and discussion	101
5.5.1	Generation of plasmids and identification of promoters for over-expression of genes encoding nitrogenase subunits	101
5.5.2	Optimisation of a rapid electroporation-based genetic modification protocol.....	103
5.5.3	Development of an optimised RNA extraction method for analysis of overexpressed genes.....	108
5.5.4	Quantifying gene expression of recombinant strains	110
5.5.5	Nitrogenase protein expression.....	112
5.5.6	Hydrogen production by modified strains	114
5.6	Conclusion.....	118
5.7	Acknowledgements	118
5.8	Author contributions	119
CHAPTER 6 CONCLUSIONS AND FUTURE PERSPECTIVES		120
6.1	Conclusions.....	121
6.2	Further work	124
REFERENCES		128
APPENDICES		143
APPENDIX 1.	Supplementary information for Chapter 3.	143
APPENDIX 2.	Supplementary information for Chapter 4.	149
APPENDIX 3.	Supplementary information for Chapter 5.	151
APPENDIX 4.	Light source selection, calibration and conversion factors.....	153
APPENDIX 5.	Calibration curves for determination of biomass and glutamate concentration ..	155
APPENDIX 6.	Protocols	156
Protocol A.	Modified <i>Rhodospirillacea</i> minimal medium	156
Protocol B.	Transparent PVA cryogel bead immobilisation procedure.....	157
Protocol C.	<i>R. palustris</i> electrocompetent cell preparation	159
Protocol D.	<i>R. palustris</i> electro-transformation procedure	160
Protocol E.	Optimised RNA isolation procedure	161

LIST OF FIGURES

Figure 2.1. Budding cell division cycle of <i>R. palustris</i> .	12
Figure 2.2. Schematic of <i>R. palustris</i> metabolism under photoheterotrophic, nitrogen-fixing conditions.	14
Figure 2.3. Diagram of cyclic photophosphorylation and electron transport chain in the photosynthetic membrane, and relationship to H ₂ production in <i>R. palustris</i> .	15
Figure 2.4 Control over Nif nitrogenase expression and activity in response to fixed nitrogen availability is exerted on 3 levels, controlled by PII proteins.	26
Figure 2.5. Conceptual diagram of the formation of polymeric cryogels.	30
Figure 3.1. Phylogenetic tree of <i>Rhodopseudomonas palustris</i> strains based on whole genome comparison.	43
Figure 3.2. Growth of 35°C-acclimatised <i>R. palustris</i> under varying temperatures.	44
Figure 3.3. Hydrogen production characteristics of <i>R. palustris</i> under varying temperature.	48
Figure 4.1. Influence of cryogel composition on material transparency.	67
Figure 4.2. Compressive characteristics of cryogels comprised of PVA with varying molecular weights.	70
Figure 4.3. Confocal laser scanning microscopy (CLSM) visualisation of pore structure in different PVA cryogels.	73
Figure 4.4. Characterisation of diffusive properties of PVA cryogels for bioprocess applications.	75
Figure 4.5. Characterisation of biocompatibility of PVA cryogels for bacterial immobilisation.	77
Figure 4.6. CLSM micrograph of LIVE/DEAD stained <i>R. palustris</i> entrapped in PVA cryogel bead.	79
Figure 4.7. Phototrophic hydrogen production by non-growing PVA-immobilised <i>R. palustris</i> in batch mode.	81
Figure 4.8. Phototrophic hydrogen production by non-growing PVA-immobilised <i>R. palustris</i> in long-term continuous mode.	83
Figure 5.1 Organisation of nitrogenase genes in <i>R. palustris</i> (A) and summary of promoter insertion modifications (B).	103
Figure 5.2 Timelines for transformation and generation of unmarked strains in <i>R. palustris</i> .	104
Figure 5.3 Genotyping of promoter-modified strains by PCR.	107
Figure 5.4 Test of kit-based RNA isolation from <i>R. palustris</i> .	108
Figure 5.5 Evaluation of cell lysis pre-treatments for RNA extraction from <i>R. palustris</i> cultures.	109
Figure 5.6. Quantification of gene expression by RT-qPCR from modified nitrogenase operons under control of <i>pucBa</i> (P_{puc}) or <i>cisY</i> (P_{cit}) promoters.	111
Figure 5.7. Quantification of nitrogenase protein in promoter-modified strains.	112
Figure 5.8 Growth and hydrogen production by nitrogenase promoter-modified strains under nitrogen-fixing conditions.	115
Figure A1.1. Setup of temperature-controlled 0.5 L test photobioreactors for growth and hydrogen production studies.	148
Figure A2.1. The minimum residual error (solid line) decreases asymptotically as the mass transfer coefficient kL increases, indicating practical unidentifiability.	150
Figure A2.2. Model predictions (solid line) using $Deff = 7.32 \times 10^{-6} \text{ cm}^2 \cdot \text{s}^{-1}$, compared to experimental measurements (circles) for diffusion of glycerol from transparent cryogel.	150
Figure A3.1. Codon quality distribution and codon quality plot of <i>vnfH_{opt}</i> .	151

Figure A4.1. Spectra of commonly-used indoor light sources at 500 lux.	153
Figure A4.2. Irradiance intensity spectrum at inner surface of photobioreactors provided by 100 W incandescent lightbulbs.	153
Figure A4.3. Photon flux intensity spectrum at inner surface of photobioreactors illuminated by 100 W incandescent lightbulbs.	154
Figure A5.1. Calibration curve for determination of biomass concentration using optical density at a wavelength of 660 nm.	155
Figure A5.2. Calibration curve for determination of glutamate concentration using absorbance of ninhydrin colorimetric assay at a wavelength of 590 nm.	155

LIST OF TABLES

Table 2.1. Growth modes of <i>R. palustris</i>	13
Table 3.1. Doubling times for acclimatised <i>R. palustris</i> strains.	47
Table 3.2. Hydrogen production rates of acclimatised <i>R. palustris</i> strains under varying temperature.	48
Table 3.3. Substrate-to-hydrogen conversion efficiencies of acclimatised <i>R. palustris</i> strains.....	51
Table 4.1. Summary of key examples of materials applied to immobilisation of phototrophic bacteria.	60
Table 5.1. Plasmids used in this study	94
Table 5.2. Genotyping PCR Primers used in this study	95
Table 5.3. qPCR Primers used in this study.....	99
Table 5.4. Rate of false-positive transformants with wild-type genotype after selection on 200 µg.mL ⁻¹ kanamycin.	106
Table A3.1. PCR Primers used to generate fragments for plasmid construction by Gibson assembly.	152

CHAPTER 1

INTRODUCTION: CENTRAL AIM AND SUMMARY OF RESEARCH

1.1 Central aim

The alarming consequences of global climate change brought about by anthropogenic carbon emissions are already being felt, and their manifestations are only set to accelerate. With an expanding world population, satiating surging energy demand while balancing environmental responsibility is increasingly challenging. To this end, replacing finite fossil fuels as a default energy source is a key development ambition. Combining potential waste degradation with generation of a clean source of energy, hydrogen production in photosynthetic bacteria is a promising prospect for a sustainable bioeconomy, requiring technological development to realise.

The phototrophic purple non-sulfur bacterium *Rhodospseudomonas palustris* displays a vast metabolic repertoire in addition to a capacity to convert organic substrates into hydrogen as a means of balancing the redox environment in the cell. Successful application of this pathway requires comprehensive understanding of the complex interplay of competing metabolic processes, which has progressed significantly as a result of significant research effort in recent years. The main obstacle to practical feasibility however remains process related: low volumetric production rates due to firstly, non-optimal process conditions and secondly, metabolic obstacles.

In an effort to address these challenges with a view towards eventual industrial implementation, the research in this dissertation applies a synergistic combination of process engineering, process optimisation, materials science and metabolic engineering strategies to upgrade hydrogen production efficiency from photofermentation, with potential wider applications to other processes using the unique metabolic capabilities of *R. palustris* as a biotechnological platform.

1.2 Introduction

This dissertation explores strategies with the potential to improve the rate of hydrogen production by *R. palustris*, advancing incrementally towards the long-term goal of feasibility for commercial application. The complex metabolism of *R. palustris* underlies the organism's usefulness both for hydrogen production and diverse biotechnological applications, driven by the favourable cellular redox state enabled by phototrophic growth.

Literature on previous research relevant to biohydrogen production, the metabolism of *R. palustris* and key process engineering considerations are reviewed in Chapter 2.

Chapters 3, 4 and 5 detail the three main studies comprising the research conducted.

Chapter 3 examines the temperature dependence of hydrogen production, and the impact of acclimation on the growth and hydrogen production rate at elevated temperatures. Differences in temperature optima and tolerance are also explored in two strains of *R. palustris* with highly similar genomes in order to inform appropriate strain selection and maintenance criteria for high optimal temperatures.

Chapter 4 presents the development and optimisation of a transparent immobilisation matrix, based on poly vinyl-alcohol (PVA) cryogel, tailored to long-term hydrogen production under continuous, non-growing cultivation. Key properties of the cryogel material were characterised to identify ideal composition. The effect of immobilisation on hydrogen production was assessed, and the long-term hydrogen production potential of immobilised bacteria was investigated over several months.

Chapter 5 describes the design of a high-efficiency genetic modification technique for metabolic engineering of *R. palustris*, based on electroporation instead of time-consuming conjugation. The optimised technique was used to over-express alternative nitrogenase enzymes which have the potential for higher hydrogen productivity. Over-expression was confirmed, and the hydrogen productivity of the modified strains were determined.

Chapter 6 presents the conclusions on the studies conducted and gives recommendations for future research to advance the field.

1.3 Summary of research

Part 1 - Hypothesis: 30°C is not the innate optimal growth or hydrogen production temperature for *R. palustris*

- Strains CGA009 and ATH 2.1.37 were acclimated to 35°C over multiple passages.
- Growth and hydrogen production rates, and substrate conversion efficiency were determined over a temperature range of 30 – 42°C in test-scale photobioreactors.
- Both strains were confirmed to have higher but distinct temperature optima, with correspondingly enhanced growth rate, hydrogen productivity and substrate conversion efficiency.

Part 2 - Objective: To develop a transparent poly vinyl-alcohol (PVA) cryogel material with favourable properties for immobilisation of hydrogen-producing phototrophic bacteria

- Cryogels with various PVA molecular weight and glycerol-water solvent compositions were characterised.
- Material strength, transparency, resistance to diffusion and biocompatibility were determined, and optimal compositions identified for bioprocess use. To enable this, a method for examining the viability of entrapped cells *in situ* was developed.
- Hydrogen production by immobilised *R. palustris* was compared to identical planktonic cultures, and the long-term productivity of immobilised cultures was investigated using continuous culture over several months.

Part 3 - Objective: To design an efficient genetic engineering technique for rapid metabolic engineering of *R. palustris*

- A chromosomal modification technique based on transformation of a homologous recombination vector using electroporation was refined to decrease time required for successful generation of markerless strains.
- The refined technique was used to overexpress alternative *vnf* and *anf* nitrogenase genes in *R. palustris* by insertion of strong promoters upstream of operons.
- Over-expression was confirmed by quantification of RNA transcripts and protein concentrations, and the hydrogen productivity of the modified strains compared to unmodified wild-type.

1.4 Articles arising from this work

- Transparent poly vinyl-alcohol cryogel as immobilisation matrix for continuous biohydrogen production by phototrophic bacteria.

Jan-Pierre du Toit and Robert W. M. Pott

Biotechnology for Biofuels **13**, 105 (2020)

DOI: <https://doi.org/10.1186/s13068-020-01743-7>.

Published 9 June 2020.

- Heat-acclimatised strains of *Rhodopseudomonas palustris* reveal higher temperature optima with concomitantly enhanced hydrogen production rates.

Jan-Pierre du Toit and Robert W. M. Pott

International Journal of Hydrogen Energy

DOI: <https://doi.org/10.1016/j.ijhydene.2021.01.068>

Published 4 February 2021.

- Expression of alternative nitrogenases in *Rhodopseudomonas palustris* is enhanced using a novel genetic toolset for rapid, markerless modifications.

Jan-Pierre du Toit, David J. Lea-Smith, Anna Git, John R. D. Hervey, Christopher J. Howe, Robert W. M. Pott.

Submitted September 2020, currently undergoing revision after peer review for publication in *ACS Synthetic Biology*.

CHAPTER 2

INTRODUCTION TO BIOHYDROGEN PRODUCTION BY *RHODOPSEUDOMONAS* *PALUSTRIS* AND ASSOCIATED BIOPROCESS CONSIDERATIONS

2.1 *Status quo* of energy economy & environmental outlook

Since the advent of the fossil fuel economy during the industrial revolution, atmospheric concentrations of greenhouse gases have grown to far exceed the natural range over the last 650,000 years (Karl & Trenberth, 2003). Large-scale anthropogenic emission of these gases, including CO₂ and methane, have been strongly linked to an increase in the surface temperature of the Earth, amounting to between 0.8 and 1.2°C to date by latest estimates from the Intergovernmental Panel on Climate Change (Allen et al., 2018).

The detrimental ramifications of global climate change are wide-ranging and these changes are already detectable in global weather patterns on a single-day timescale (Sippel et al., 2020). Increased temperatures heighten the risk of rising sea levels destroying coastal communities, ocean acidification and ecological disruptions (Karl & Trenberth, 2003; Arnell et al., 2019), and changes in rainfall patterns leading to water scarcity and compromised food security (Fujimori et al., 2019).

In light of these imminent risks, a guideline global warming limit of 1.5 – 2°C relative to pre-industrial levels has been adopted by 195 countries as part of the 2015 Paris Agreement (Schleussner et al., 2016). This aim requires massive reduction in the ever-accelerating rate of greenhouse gas emissions (Roelfsema et al., 2020). Thus, development of renewable carbon-neutral energy sources is crucial to facilitate the shift away from fossil fuels.

In recent years there has been a shift towards a bio-economy approach, in which wastes are used as feedstocks for novel bioprocesses producing desirable products, including renewable fuels. In this way, maximum value is extracted from available resources while reducing the ecological impact of meeting energy demand (Ubando, Felix & Chen, 2020).

2.2 Hydrogen as an alternative energy carrier

With global energy demand expanding exponentially, the dual challenges of restraining greenhouse gas emissions and replacing unsustainable fossil fuels have prompted a surge in development of viable substitutes. Hydrogen has gained significant attention in recent decades as an alternative energy carrier with one of the highest energy contents known, which at 122 kJ/g is around 2.7-fold that of typical hydrocarbon fuels (Gupta et al., 2013). However, as a low-density gas, hydrogen is difficult to store and requires energy-intensive compression for practical use. Numerous storage and distribution technologies are thus under development in pursuit of a sustainable hydrogen economy, including chemical sorption of hydrogen gas as ammonia or metal hydrides, and physical sorption in novel nanomaterials such as porous metal organic frameworks. (Moradi & Groth, 2019; Boateng & Chen, 2020). Such approaches have the potential to attain high hydrogen storage densities without the need for gas compression.

Hydrogen is by nature non-polluting, producing only water upon combustion or high-efficiency conversion to electricity in fuel cells. This makes it attractive as a transport fuel since this diffuse source of emissions, making up 18% of global energy use, is particularly difficult to address with current carbon-neutral energy strategies (Staffell et al., 2019; Acar & Dincer, 2020). Besides its value as an energy carrier, hydrogen is also a valuable industrial feedstock with a range of uses including in chemical, electronics and steel production, hydrogenation in food manufacturing and detoxification of pollutants (Kapdan & Kargi, 2006). This sizeable, mature industry presents a solid foundation upon which to expand an energy economy based on hydrogen. The main barriers to adoption of hydrogen power on a large scale are low volumetric energy density and a lack of renewable sources of hydrogen gas, which require technological advancement to address.

Currently, around 95% of hydrogen is produced from hydrocarbon reformation, primarily natural gas, light oil and coal (El-Emam & Özcan, 2019), which merely shifts the carbon and pollutant emission footprint to an upstream step in the fossil fuel paradigm. To realise the

potential of carbon-neutral hydrogen, low-cost sustainable production from renewable sources is a subject of widespread study, via a variety of methods.

Electrolysis of water and biomass reformation processes are incredibly energy intensive. They require either large amounts of electricity or heat in addition to generating large amounts of pollution in the case of reformation and are therefore inefficient strategies (Ayers et al., 2019; Li et al., 2019). From this point of view, biological hydrogen production is of particular interest.

2.3 Biological hydrogen production

A variety of microorganisms catalyse the formation of hydrogen using enzymes at ambient temperature and pressure. Capitalising on the evolution-driven efficiency of these molecular-scale processes avoids the need for high temperatures and expensive platinum-based catalysts otherwise required by classical reformation processes (Crabtree, Dresselhaus & Buchanan, 2004). Further, the low aqueous solubility of hydrogen makes it an ideal bioproduct, as it readily evolves into the gaseous phase (Ghosh, Tourigny & Hallenbeck, 2012). It thus requires minimal purification which offers a clear advantage in comparison to liquid biofuels such as ethanol.

There are three chief biological routes for hydrogen production, namely oxygenic biophotolysis, dark- and photofermentation.

2.3.1 Biophotolysis

Biophotolysis occurs in certain photosynthetic microalgae and cyanobacteria, whereby energy captured from light in the form of reduced ferredoxin is in turn used to reduce protons to molecular hydrogen. Though this process uses only water as a substrate and consumes CO₂, it is fundamentally limited by the generation of oxygen that the hydrogenase enzyme is extremely sensitive to. As discussed by Hallenbeck and colleagues, while work has been ongoing since the 1970s, energy conversion efficiencies have not improved appreciably since then despite being a key area of focus in biohydrogen research (Hallenbeck et al., 2009).

2.3.2 Dark fermentation

Dark, or more specifically light-independent fermentation is the anaerobic degradation of organic carbon substrates by mesophilic bacteria, normally via acidogenic processes yielding mainly organic acids such as acetate and butyrate (Chong et al., 2009). This process has the advantage of requiring a relatively simple bioreactor and using a variety of carbohydrate substrates and naturally occurring microbial consortia. High hydrogen production rates have been observed, but process limitations such as controlling the composition of feedstock and biocatalyst, as well as low practical yields are significant barriers to scale-up and overall economic feasibility (Dahiya et al., 2021). The major metabolic obstacle is the need to regenerate the electron carrier NAD^+ for various cellular processes, thus shuttling reducing equivalents away from hydrogen production (Lee, Salerno & Rittmann, 2008), which consequently only accounts for around 17% of reduced electrons (Lee et al., 2009). The resulting thermodynamic disadvantage also leads to incomplete substrate oxidation and consequently optimised hydrogen yields of only around 25% of theoretical stoichiometric maximums, which themselves are limited to 33% of the energy content of the substrate (Hallenbeck & Ghosh, 2009). Incomplete breakdown of the substrate results in generation of organic acids as downstream waste products, which require further treatment for disposal. Combining photofermentation sequentially with dark fermentation has thus been widely studied as a means of improving conversion efficiency and biohydrogen yields by allowing consumption of the leftover breakdown products (Mishra et al., 2019).

2.3.3 Photofermentation

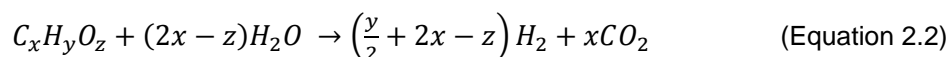
Photofermentation has been identified as a key frontier in biohydrogen, as it allows for far higher conversion efficiencies since hydrogen production is driven by energy in the form of ATP derived from light. Thermodynamically unfavourable reactions are thus overcome, allowing complete substrate oxidation and improving conversion efficiency potential (Hallenbeck & Benemann, 2002).

In this anaerobic process, the highly-conserved enzyme nitrogenase catalyses the fixation of dinitrogen into ammonia under nitrogen limiting conditions, along with hydrogen gas as an obligate by-product. In the absence of dinitrogen, hydrogen is the sole product formed according to the reaction:



Electrons derived from degradation of carbon source are supplied via reduced ferredoxin. Being an ATP-driven reaction, it is by nature essentially irreversible and thus does not suffer from inhibitory feedback via product accumulation (McKinlay & Harwood, 2010a). This allows pressurized hydrogen production, as long as the required energy is available, which raises the possibility of reducing the cost of downstream compression for practical distribution and use.

Complete oxidation of substrates can be characterized thus (Turner et al., 2008):



Similar in character to the hydrogenase enzyme, nitrogenase is sensitive to inhibition by oxygen, but since this reaction is not oxygenic this presents minimal process consideration.

The purple non-sulfur bacteria have been the most intensively studied candidate organisms for anoxygenic photo-production of hydrogen and of these *Rhodopseudomonas palustris* is attractive for several reasons.

2.4 *Rhodopseudomonas palustris*

2.4.1 Taxonomy and microbiology

R. palustris is mesophilic purple non-sulfur bacteria (PNSB) belonging to the class of alphaproteobacteria. The PNSB are a highly diverse non-taxonomic group of facultative phototrophic anaerobes found in a wide range of natural environments, mostly aquatic and rich in organic matter and include some species isolated from challenging extremes of heat, cold and salinity (Madigan & Jung, 2009). They are capable of anoxygenic photosynthesis, with a reaction centre containing bacteriochlorophyll a or b, which absorbs light primarily in

the infrared range of 800 – 900 nm, in contrast to the visible light utilised by chlorophyll a found in organisms such as plants and cyanobacteria using classical oxygenic photosynthesis. As such, PNSB obtain electrons from inorganic or organic donors instead of water, accounting for their ecological distribution.

R. palustris reproduces via a budding life cycle, which results in two distinct stages: a non-motile mother cell, and a smaller motile daughter or swarmer cell, as shown in **Figure 2.1** from Westmacott & Primrose (1976). The swarmer cell (a) extends a slender, translucent tube at the end opposite the flagellum (b) and in so doing becomes non-motile. This tube (b, c) develops into a bud (d), which swells into what will become the nascent cell (e). Separation between the tube and newly formed motile swarmer cell completes the division process (f). The mother cell develops a “sticky holdfast” on the pole opposite the tube, resulting in multiple mother cells joining to form rosette structures which become more prevalent in older cultures. Mother cells also reproduce more quickly than swarmer cells since the tube is retained, and this complexity results in a heterogeneous population of different cell stages within a culture, which may not conform to simple exponential growth in experiments.

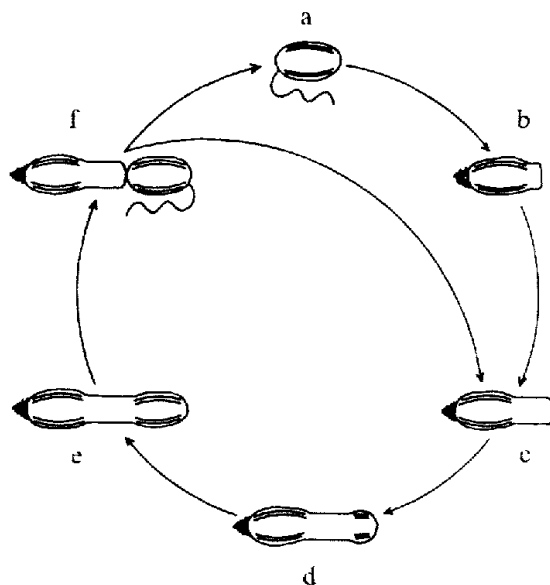


Figure 2.1. Budding cell division cycle of *R. palustris*.

Stages **a** to **f** are described in the text.

Reproduced from Westmacott and Primrose (1976) with permission from *Microbiology Society*.

2.4.2 Metabolism and photosynthesis

R. palustris possesses an unusual metabolic flexibility resulting from adaptation to sediment microenvironments, as implied by the species name *palustris*; Latin for marsh or swamp. Complete genomic sequencing performed by Larimer et al. (Larimer et al., 2004) revealed *R. palustris* as one of the most metabolically versatile organisms known. It is capable of surviving by all four main modes of metabolism: chemoautotrophic, chemoheterotrophic, photoautotrophic and photoheterotrophic, as summarised in **Table 2.1**. In addition, various strains have been isolated in which varying degrees of metabolic specialization have occurred in order to take further advantage of specific microenvironments (Oda et al., 2008).

Photoheterotrophic metabolism is the preferred mode of growth for the organism and takes place under illumination using substrates such as organic acids as both source of carbon and electrons to be energized by the photosystem, which is expressed under anaerobic conditions. Since energy is primarily generated from cyclic photophosphorylation, excess electrons derived from oxidation of the carbon substrate (not directly assimilated into biomass) are used to fix CO₂ via the Calvin cycle in order to maintain redox balance in the cell.

Table 2.1. Growth modes of *R. palustris*

Growth mode	Light required	Oxygen required	Electron / Energy source	Carbon source	H ₂ production
Chemoautotrophic	No	Aerobic ^a	H ₂ , thiosulfate, inorganic electron donors	CO ₂	H ₂ consumption
Chemoheterotrophic	No	Aerobic	Organic carbon	Organic carbon	None
Photoautotrophic	Yes	Anaerobic	H ₂ , thiosulfate, Fe ²⁺ , S ²⁻ , inorganic electron donors / light	CO ₂	H ₂ consumption
Photoheterotrophic	Yes	Anaerobic	Organic carbon / light	Organic carbon	H ₂ production (if ammonia absent)

^a Growth without oxygen possible if alternative terminal electron acceptor is present e.g. nitrate

Under nitrogen limitation, hydrogen production as an obligate by-product of the nitrogen fixation pathway is enabled, referred to as nitrogen-fixing conditions, as depicted in **Figure 2.2**. Hydrogen production serves as an additional electron sink, which can be used to maintain the redox status of the cell by unburdening energy and electron carriers (ATP and NADH).

The bacterial photosystem, though vaguely resembling photosystem II of eukaryotic plants, is capable of absorbing incident light over a wider spectrum range from 400 to 1000 nm, thus making efficient use of available photons. Significantly, the simpler photosynthetic apparatus does not possess a counterpart to the water-splitting complex of eukaryotic PSII, and PNS bacteria thus do not evolve oxygen (Robert, Cogdell & van Grondelle, 2003).

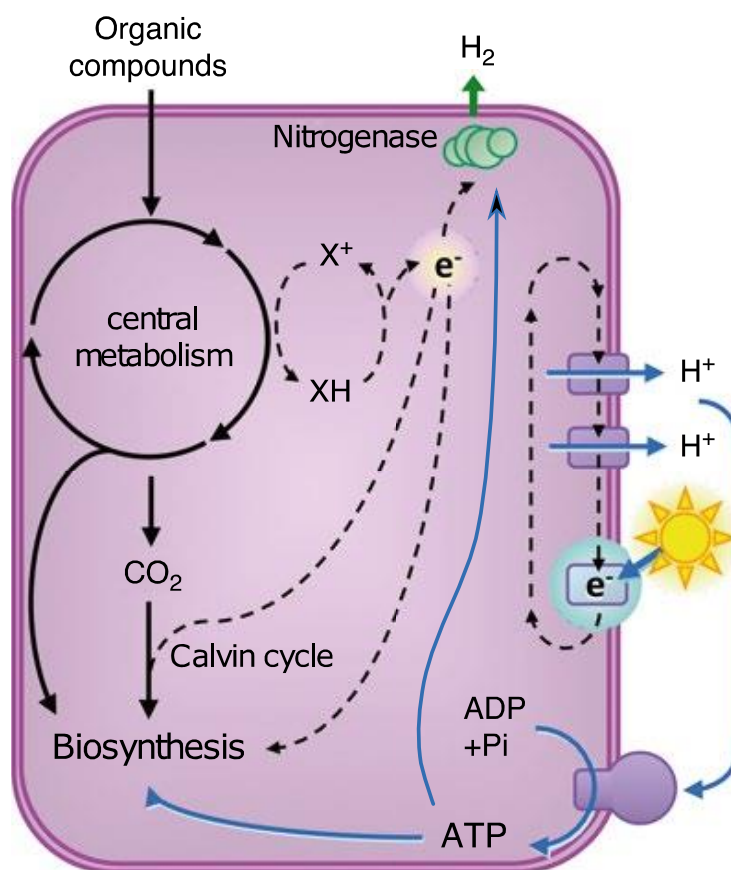


Figure 2.2. Schematic of *R. palustris* metabolism under photoheterotrophic, nitrogen-fixing conditions.

X+: oxidised electron carriers; XH: reduced electron carriers.

Figure adapted from McKinlay (2014) with permission from *Springer Nature*.

In addition, the photosystem is highly sensitive to oxygen and as such expression is tightly repressed by aerobic conditions (Young & Beatty, 2003). This has interesting implications for integrating photosynthetic growth with anaerobic conditions; distinct from conventional photosynthesis performed by organisms such as cyanobacteria.

In PNSB, the photosynthetic apparatus is housed in extensive, specialised intracellular membrane lamellae, which facilitate the generation of proton gradients, as illustrated in **Figure 2.3**. Peripheral light harvesting antennae (LH2–4) absorb photons using the bacteriochlorophyll a and carotenoid pigments contained within. These antennae are variably expressed depending on light intensity and redox status of the cell, with increasing expression under high metabolic load (Fixen, Oda & Harwood, 2019). The absorbed energy is then transferred to the photochemical reaction centre (RC) along with that from core LH1 antenna. Charge separation in the RC results in the lipid-phase electron carrier ubiquinone (Q) being doubly reduced. Reduced ubiquinone (QH₂) freely diffuses in the lipid bilayer and passes electrons on to cytochrome *bc*1. Cytochrome *bc*1 uses the energy to pump protons across the membrane in order to generate a proton gradient, while aqueous cytochrome *c* mediates the

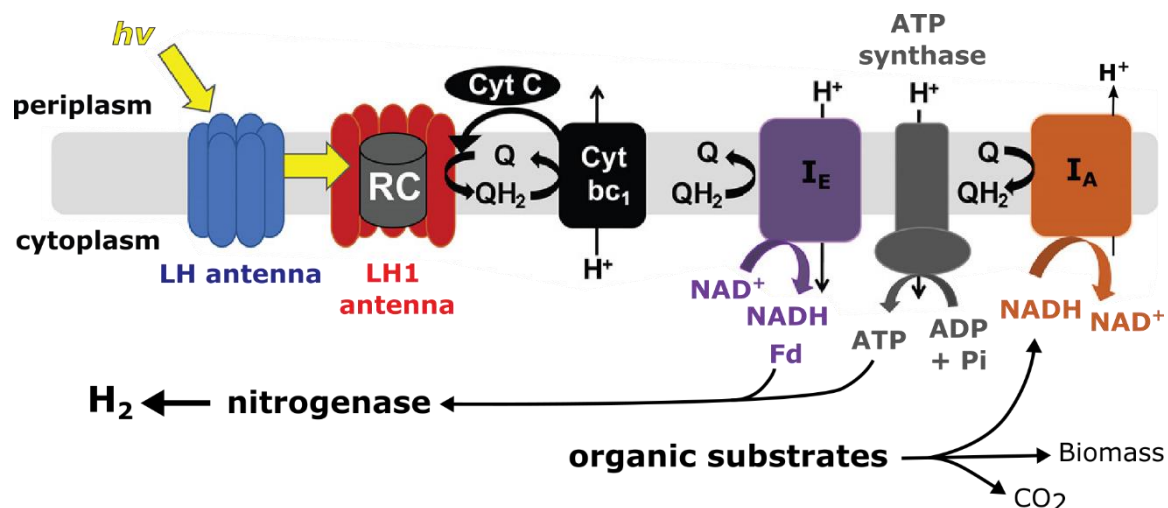


Figure 2.3. Diagram of cyclic photophosphorylation and electron transport chain in the photosynthetic membrane, and relationship to H₂ production in *R. palustris*.

RC: reaction centre, LH: light harvesting, Cyt: cytochrome, Q: quinone, QH₂: reduced quinone, I_E and I_A: oxidoreductases, Fd: ferredoxin, H⁺: protons

Figure adapted from Fixen et al. (2019) with permission from *American Society for Microbiology*.

Additional information from Yang et al. (2017) and McKinlay and Harwood (2010a).

re-reduction of the RC thus completing the electron transport chain. The proton gradient is subsequently used by ATP synthase to drive ATP formation from ADP and phosphate. This process, despite being termed cyclic photophosphorylation, is not a closed loop system and serves as a balancing mechanism for electron flux in the cell (Yang et al., 2017). Electrons derived from oxidation of organic substrates are shuttled via NADH and oxidoreductase I_A to the pool of reduced ubiquinone. The pool of reduced ubiquinone in turn also interacts with oxidoreductases such as I_E, which transfer electrons to NADH and reduced ferredoxin. NADH is used for carbon fixation via the Calvin cycle while ferredoxin along with ATP is used by the nitrogenase-catalysed nitrogen fixation pathway to produce hydrogen.

In non-growing cells particularly, carbon sources are completely degraded instead of being incorporated into biomass. Under these conditions hydrogen production becomes an essential means of balancing cellular redox state, and allows excess energy to be unloaded for the regeneration of electron- (ferredoxin) and energy carriers (ADP) (Muzziotti et al., 2016). Hydrogen is thus not a growth-associated product (Melnicki et al., 2008), which allows continuous production in the absence of additional biomass accumulation. Further, this recycling mechanism presents a convenient means of selecting for more efficient hydrogen-producing strains, since offloading of electrons would be essential for regeneration of electron carriers and facilitate growth on highly-reduced substrates (Rey, Heiniger & Harwood, 2007). Such a selection mechanism is important to maintain enzyme activity, since loss of function from accumulation of deleterious mutations occurs when metabolic pathways are not essential for the organism's survival.

An additional redox balancing process occurs via directing reducing equivalents to the Calvin-Benson-Bassham (CBB) pathway (or Calvin cycle), which fixes CO₂ into carbon storage molecules such as poly(hydroxybutyrate) (PHB) (McKinlay & Harwood, 2010b). Carbon fixation partially explains low percentages (<3%) of CO₂ seen in the gaseous product of various photofermentation studies employing *R. palustris* grown on glycerol, alongside absorption into the water displaced as part of the hydrogen collection method (Pott, Howe &

Dennis, 2013). The refixation of CO₂ is interesting due to the potential for rendering photofermentation a carbon-*negative* process instead of merely carbon-neutral, while concurrently producing a highly pure hydrogen product albeit at the expense of reduced hydrogen yield due to the metabolic demand. Conversely, inactivation of the Calvin cycle by deletion of phosphoribulokinase increased both yield and specific hydrogen productivity from acetate by reducing competition for the cellular energy pool in the NifA* strain of *R. palustris*, which expresses nitrogenase constitutively (McCully & McKinlay, 2016). However, when using highly reduced substrates such as butyrate, hydrogen production has been shown to be essential for cell growth, since Calvin cycle flux is an insufficient sink for excess reducing equivalents in the absence of additional CO₂ being supplied to the system (McKinlay & Harwood, 2011). The efficiency of hydrogen production is thus less adversely affected by carbon fixation activity when growing on highly reduced substrates, with implications for feedstock selection.

2.4.3 Substrates and industrial applications

As a result of its diverse geographic distribution, *R. palustris* has well-characterised and wide substrate versatility. Within this gamut, certain strains have been shown to adapt to the specific set of prevailing conditions (Oda et al., 2008). Possible carbon sources include organic and fatty acids, sugars, and even halogenated and aromatic compounds; challenging compounds to degrade using most other organisms. Genetic studies reveal genes encoding five benzene ring cleavage pathways (Larimer et al., 2004), and certain strains demonstrate the most comprehensive aromatic degradation abilities of any known organism (Harwood & Gibson, 1988). This capability underlies the organism's usefulness in waste water treatment, the most common application of the Rhodospirillacea to date (Siefert, Irgens & Pfennig, 1978; Kim et al., 2004); simultaneously an indication of a level of robustness suitable for use in an industrial bioprocess, perhaps no better typified than by its use in uranium waste bioremediation (Llorens et al., 2012).

Indeed, the ability to simultaneously degrade even recalcitrant compounds found in a wide variety of waste streams and convert them to valuable products is an exceedingly attractive prospect. By adopting this type of bio-economy paradigm, latent value of biomass contained in essentially worthless waste streams is released in the form of a clean energy source while simultaneously reducing chemical oxygen demand (COD) for downstream disposal. Inversion of the economics of classical waste management towards net benefit would be of great help in mitigating the strain on the natural environment posed by ever-accelerating population growth.

Study of substrates specifically for hydrogen production have mostly been concentrated on organic acids, such as acetic (Barbosa et al., 2001) and butyric acids (Chen et al., 2007). These are frequently found in the organism's habitat as well as being the predominant products of dark anaerobic fermentation processes. Thus, there exist numerous reports on the possibility of linking dark- and photofermentation in sequential processes to extract maximum yield and substrate conversion efficiency (Oh et al., 2004; Azbar & Cetinkaya Dokgoz, 2010; Lazaro, Varesche & Silva, 2015).

Other low-cost waste streams reported to be potentially suitable for photofermentation are represented in most biomass-related industries: effluent from food manufacturing such as dairies (Seifert, Waligorska & Laniecki, 2010a) and breweries (Seifert, Waligorska & Laniecki, 2010b), sugar cane processing (Keskin & Hallenbeck, 2012), agricultural waste containing aromatic compounds (Austin et al., 2015) and glycerol from biodiesel production (Sabourin-Provost & Hallenbeck, 2009; Pott, Howe & Dennis, 2014).

Notably, glycerol exhibited remarkable conversion efficiencies at around 96% of stoichiometric limit (Ghosh, Sobro & Hallenbeck, 2012), which was confirmed to be among the highest for a range of substrates examined including organic acids (Pott, Howe & Dennis, 2013). Glycerol is a significant by-product of biodiesel manufacturing via transesterification, amounting to around 12% of the mass of biodiesel produced; quantities far outstripping industrial demand (Ciriminna et al., 2014). Many countries including the UK and South Africa

(National Energy Act 34/2008) have enacted biofuels legislation mandating that at least 5% of diesel consumption be met from renewable sources, further exacerbating oversupply and creating burgeoning disposal issues. Efforts have been made to upgrade this waste stream for use as a bioprocess feedstock, and cost-effective methods for successful removal of key inhibitory compounds such as saponified fatty acids have been devised (Pott, Howe & Dennis, 2014). Implementation of such processes along with consolidation of highly-distributed point sources may allow further beneficiation of waste glycerol. In addition, as a highly reduced substrate, glycerol is an excellent source of electrons and would thus be a fortuitous candidate substrate for high efficiency photoproduction of hydrogen.

2.5 Influence of temperature on hydrogen production

Temperature is a central engineering parameter for the operation of any process, since reaction rates are often exponentially related to temperature, as described by the classical Arrhenius Equation:

$$k = Ae^{-E_a/RT} \quad (\text{Equation 2.3})$$

Where k = rate constant; A = pre-exponential factor; E_a = activation energy; R = universal gas constant; T = absolute temperature (K).

Temperature is especially important when using biological catalysts in the form of bacteria, since catalytic rate improves up to a limit where irreversible inhibition occurs. Organisms have evolved enzymatic pathways with very specific temperature tolerances adapted to their natural environments, and being proteinaceous in nature, enzymes are prone to loss of conformation and activity at excessive temperatures (Arnold et al., 2001). For maximum bioprocess efficiency, it is thus essential to comprehensively characterize physiological temperature limits for the candidate organism.

Since first being described as part of a detailed study of PNSB by Van Niel over 75 years ago (van Niel, 1944), little work has been done to rigorously characterize the temperature tolerance of *R. palustris*. Most of the studies relating to biohydrogen production to date assume 30°C as

the ideal temperature for purple nonsulfur bacteria; however, Van Niel in fact identified a higher possible maximum. Good growth was seen at 37°C, although complicated by strain-dependent differences. Significant strain-related differences were also seen in further studies of closely-related *R. capsulata*, which displayed optima between 35 – 40°C; in turn higher than the 30°C maximum reported by Van Niel (Weaver, Wall & Gest, 1975). Putative strains of *R. palustris* have been identified with optimal temperatures of 45°C, furthering the potential for higher production temperatures (Singh, Srivastava & Pandey, 1994). Following on from the Arrhenius model, enzymes typically double their rate of activity for every 10°C increase in temperature (Bergmeyer, 2012), such that developing thermostable enzymes has been the focus of much research to bring down costs in industrial conversion processes by reducing enzyme concentration needed for high productivity (Zamost, Nielsen & Starnes, 1991).

Raising the temperature of hydrogen production from the low baseline of 30°C would thus substantially enhance the rate of hydrogen evolution mediated by nitrogenase enzyme activity. Although not accounting for other potential metabolic bottlenecks such as availability of ATP or reducing equivalents, this poses potentially major positive implications for the feasibility of biohydrogen production, in context of sufficiently high production rate being the main obstacle to economic feasibility (Hallenbeck et al., 2009). Further benefits of higher temperatures may be mediated by the increase of membrane fluidity, since membrane-bound photosystems rely on diffusion of reduced ubiquinone to shuttle electrons between components of the electron transport chain. More efficient diffusion may offer additional benefits for optimal supply of electrons and ATP to the nitrogen fixation pathway (Mullineaux & Liu, 2020).

As further benefit of higher temperatures, large-scale photobiological hydrogen production would require using sunlight for illumination, with the concomitant problem of raising the temperature of a photobioreactor system under intense, direct illumination. Higher operating temperatures would be a great advantage to process feasibility since engineering complexity of temperature control and cooling measures would be partially mitigated.

2.6 Influence of light on hydrogen production

The second central consideration for photosynthetic hydrogen production is the availability of light for ATP synthesis via photophosphorylation and sufficient reducing equivalents. Nitrogenase-mediated proton reduction to H₂ is driven by ATP, with a minimum of 4 moles required per mole hydrogen formed (**Equation 2.1** in **section 2.3.3**). In the absence of light, nitrogenase activity is repressed in order to limit this energetic expense (Yoch & Gotto, 1982). Optimisation of light intensity is therefore important for providing sufficient energy for high-rate hydrogen production.

The single bacterial photosystem found in PNSB is simpler than the classical eukaryotic arrangement, and differs in that its bacteriochlorophylls primarily absorb incident light in the near infrared range (NIR) with peaks between 800 – 1000 nm (Vredenberg & Ames, 1966). This is consistent with the species' adaptation to relatively low-light aquatic sediment microenvironments where longer wavelengths of light prevail (Oda et al., 2008), since the major photosynthetic wavelengths are rapidly depleted by algae in the upper phototrophic zone. Different ecotypes are able to adapt the levels of photosystem expression to suit different light intensities, varying the numbers and sizes of the photosystems in addition to the total area of the intracellular photosynthetic membrane system (Firsow & Drews, 1977). Expression of different types of photosystem with varying absorbance characteristics have also been reported (Giraud et al., 2005; Scheuring et al., 2006), and different strains of *R. palustris* show distinct differences in both genetic complement and expression at varying light intensities (Fixen, Oda & Harwood, 2016). Adaptation to low-light conditions, however, reduces photosynthetic efficiency at high light intensities due to mutual shading of bacteria expressing high levels of pigments (Vasilyeva et al., 1999). Reducing pigment density has been the subject of some study. A doubling of hydrogen production rate was seen for mutant *Rhodobacter sphaeroides* strains expressing bacteriochlorophyll and carotenoids at ~50% of the wild-type (Kondo et al., 2002), raising the possibility of tuning the light absorption characteristics of *R. palustris* for bioreactor use.

High light intensities however also tend to reduce photosynthetic efficiency in individual cells, since the metabolic stress of excessive energy influx needs to be mitigated to avoid damage (Hellingwerf et al., 1994; Golomysova, Gomelsky & Ivanov, 2010). Lower hydrogen production efficiencies at high light intensities have been attributed to the saturation of the hydrogen production pathway, leading to the surfeit energy being channelled to biosynthetic pathways as supplemental energy sinks. Cells grown under high light intensity showed 4-fold higher cellular dry weight compared to low-light growth (Muzziotti et al., 2016). This is supported by similar observations of PHB accumulation up to 30% of cell weight in non-growing, nitrogen-limited cultures, despite 3.5-fold increased hydrogen production (McKinlay et al., 2014). Biosynthesis of storage compounds such as PHB is a less efficient, slower process and thus an inferior energy sink (Muzziotti et al., 2016), suggesting nitrogenase activity was insufficient to consume available reducing power load in the absence of growth. The availability of energy is thus not likely to be the primary inherent limitation in the hydrogen production pathway, and thus is not of critical importance for process efficiency until other pathways limitations can be alleviated.

The bacterial photosystem is less powerful than the canonical system in green plants, with around half the oxidative potential due to absence of a homolog of the oxygen evolving complex of photosystem II thus lacking the ability to split water (Barber & Andersson, 1992). Lower energies involved result in reduced danger from highly-oxidising intermediates, which is mitigated by the quenching action of carotenoids under high light conditions such that photoinhibition is not as typically encountered as for eukaryotic systems (Cogdell & Frank, 1987; Hashimoto, Uragami & Cogdell, 2016). Cultures of *R. palustris* have also been shown to rapidly acclimate to high light intensities of $1500 \mu\text{mol photons m}^{-2}\cdot\text{s}^{-1}$ (Muzziotti et al., 2017). Further, microarray analysis of *Rhodobacter capsulatus* revealed that expression of photosynthetic reaction centre genes were downregulated to protect the photosynthetic membrane from overload under high light intensity at $570 \text{ W}\cdot\text{m}^{-2}$, while electron transport and nitrogen fixation genes were upregulated to enhance the cell's ability to offload energy

(Gürkan et al., 2020). Nevertheless, oxidative stress still poses a risk to intracellular components and proteins at high light intensity despite energy offloading to the nitrogenase and biosynthetic pathways.

The current body of literature on optimal light intensity suffers from a lack of reproducibility, since values are commonly reported in lux. This perhaps relates to the ready availability of equipment measuring light intensity for photographic use. As a unit of illuminance weighted to human visual perception between 400 – 700 nm via the luminosity function, lux is a wholly inappropriate measure for organisms relying on near-infrared light wavelengths beyond the range of the human eye. In addition, lux values for different light sources are not comparable since significant differences in emission spectra beyond this range are not accounted for. Other studies report values relating to the photosynthetically active range (PAR) for eukaryotic plants (300 – 700 nm) and are thus also inappropriate for comparing irradiance intensity relevant to bacterial photosystems. The standard SI unit of $\text{W}\cdot\text{m}^{-2}$ is used in the present work, in the range 500 – 1100 nm appropriate for bacterial photosynthesis. Additional clarification on ideal light intensities specifically in the bacterial PAR range is thus required, specifically up to sunlight-level intensities.

2.7 Mechanisms of control over nitrogenase expression and activity in *R. palustris*

A classical challenge in the development of bioprocesses is the need to co-opt bacterial metabolism to produce a specific product in high volumes. Due to the strict selective pressures applied during the evolution of these biochemical pathways, tight genetic and metabolic control is exerted over the activity of enzymes in order to efficiently use available energy and thus ensure long-term survival of organisms in changing and often-adverse conditions (Oda et al., 2008).

Obtaining bioavailable nitrogen is one such pathway essential to the ability of bacteria to grow and replicate, as evidenced by the multifactorial control systems governing it. Central to this system is the nitrogenase fixation pathway, which catalyses the energy-intensive process of

reducing relatively inert dinitrogen absorbed from the atmosphere to usable ammonia, driven by ATP hydrolysis via the enzyme nitrogenase (Burris, 1991):



Hydrogen is an obligate by-product of this process and in the absence of N_2 , reducing equivalents are directed entirely to hydrogen production, which is thus increased by four fold (Burris, 1991):



R. palustris possesses 3 nitrogenase isozymes, characterized by their respective metal cofactors. The molybdenum-containing (Mo) nitrogenase (Nif) is the most efficient isozyme (reflected in **Equation 2.4**) and therefore expressed by default under nitrogen-limiting conditions. Two additional isozymes, with vanadium (Vnf) and iron cofactors (Anf), are termed the alternative nitrogenases since they are expressed only under severe fixed nitrogen (Oda et al., 2005a) or transition metal limitation (Schüddekopf et al., 1993; McRose et al., 2017). This sequential expression cascade, with the vanadium nitrogenase in turn expressed in preference to the iron nitrogenase, reflects the relative energy efficiency of the isozymes in fixing nitrogen. These inefficiencies from the microbial point-of-view translate to much-improved hydrogen yields under N_2 -replete conditions (McKinlay & Harwood, 2010a), which are 3- to 9-fold higher in comparison to Mo-nitrogenase (**Equation 2.4**) as shown below:

V-nitrogenase (Eady, 1996):



Fe-nitrogenase (McKinlay & Harwood, 2010a):



In practice, the inherently higher affinity of these alternative nitrogenases for protons is reflected in a two- to four-fold higher hydrogen production normalized to biomass concentration in mutant strains expressing only V- and Fe-nitrogenases respectively (Oda et al., 2005a). These results were obtained during nitrogenase activity assays; thus, production

rates are likely to be superior in the absence of concomitant nitrogen-reducing activity under N₂-free conditions. De-repression of alternative nitrogenase expression in *Rhodobacter capsulatus* allowed 25% higher maximum hydrogen production rate and up to 40% increased yield (Yang et al., 2015). The Fe-nitrogenase has a higher affinity for protons underlying its improved hydrogen output (Schneider et al., 1997), which may yield insights for rational directed modification towards ideal enzymes for bioprocess use.

As discussed in **section 2.5** above, hydrogen production is a means of offloading excessive energy captured under high light intensity, yet saturation is readily achieved resulting in reduced efficiency due to redirection of reducing power to alternative energy sinks. In context of the slow turnover rate of the Mo-nitrogenase of around 5 molecules per second (McKinlay & Harwood, 2010a), saturation is likely to occur quickly despite high nitrogenase concentrations under high light, up to 40% of cellular protein (Jouanneau, Wong & Vignais, 1985). Upregulation of the Fe-nitrogenase levels would represent an inherently superior energy sink at equivalent enzyme levels, concomitant to higher stoichiometric production of hydrogen per enzyme cycle. Circumventing genetic controls over expression of alternative nitrogenases would thus be attractive targets for process improvement.

Due to the energy-intensive nature of nitrogen fixation, and the complicated synthesis and assembly of nitrogenases (Rubio & Ludden, 2005), expression and activity of the pathway is strongly repressed by availability of ammonia – the preferred source of fixed nitrogen. This control is exercised on three levels policed by the PII family of regulator proteins, as summarized in **Figure 2.4** from Heiniger et al. (2012a).

At the top level, the NtrBC system responds to levels of fixed nitrogen via intracellular glutamine as proxy for nitrogen availability (Zumft & Castillo, 1978). Under limiting conditions (N₂; right panel), NtrB activates NtrC by phosphorylation, which in turn upregulates expression of genes linked to nitrogen starvation, including *NifA*.

The second level is mediated by *NifA* – the master transcriptional activator for *Nif* (Mo-nitrogenase) along with auxiliary genes in the regulon for co-factor and assembly proteins.

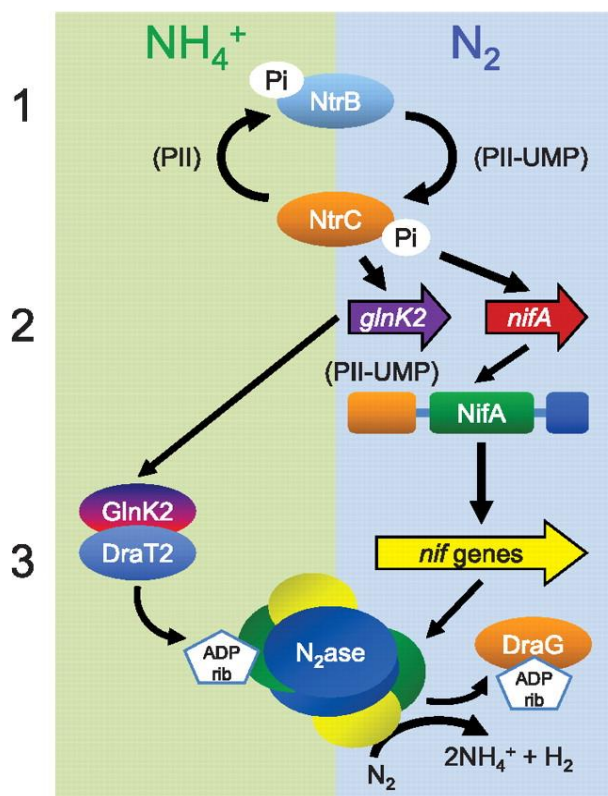


Figure 2.4 Control over Nif nitrogenase expression and activity in response to fixed nitrogen availability is exerted on 3 levels, controlled by PII proteins.

Figure reproduced from Heiniger et al. (2012) with permission from *American Society for Microbiology*.

Under nitrogen limitation, NifA subsequently undergoes a conformation change via interaction with PII-UMP, which initiates its transcription-activating ability. The alternative nitrogenase transcriptional activators VnfA and AnfA are hypothesized to be similarly upregulated primarily in response to increasing nitrogen limitation (Oda et al., 2005a), and repressed by availability of molybdenum (Kutsche et al., 1996).

Post-translational modification of the nitrogenase enzyme constitutes the third level of control, allowing rapid adaptation to changing conditions by modifying the activity of the nitrogenase complement already present. In response to increasing ammonium concentration the PII protein GlnK2, also under transcriptional control by NtrC as a means of feed-forward control, binds to DraT2. A constitutively expressed protein, DraT2 then effects ADP-ribosylation of nitrogenase to reversibly inhibit activity. Removal of ADP-ribosyl by DraG restores activity upon ammonium depletion. These mechanisms are key to controlling the

activity of nitrogenase, and present targets for metabolic engineering efforts to enhance the hydrogen production potential of *R. palustris*.

The *nifA** mutant strain of *R. palustris* expresses NifA in a form not requiring activation by conformational change, such that basal expression levels resulted in high nitrogenase activity irrespective of NtrBC control mechanisms. Since GlnK2 expression is not activated by NtrC under nitrogen limitation, all three level of control over nitrogenase are circumvented. This strain therefore produces hydrogen constitutively, and in the presence of ammonium although DraT2 inactivation showed further improvement (Heiniger et al., 2012a).

Inactivation of GlnK2 and DraT2 are thus proven targets for boosting hydrogen production efficiency up to 5-fold, without negatively affecting growth of the bacterium (Rey, Heiniger & Harwood, 2007; Wu et al., 2016). In addition, the removal of ammonium repression widens the possible array of substrates for large-scale biohydrogen production from organic wastewaters, which are likely to contain significant levels of ammonium (McKinlay & Harwood, 2010a). Combining overexpression of the alternative Vnf and Anf nitrogenases with elimination of repressive mechanisms are interesting prospects for further development towards economically feasible high-rate biohydrogen production.

2.8 Microbial immobilisation for bioprocess optimisation

In development of bioprocesses at all scales, immobilisation of the microorganisms is a widely used strategy to better control key process parameters by allowing easy separation of biomass from the liquid medium. The classic microbiological approach involving suspended culture systems offers excellent mass transfer between growth medium and organism but provides minimal buffering of adverse conditions, and when operating continuously is susceptible to biomass wash-out under high dilution rates or low growth rates. By immobilising the cells into a solid support, a more favourable microenvironment is created, thus increasing operational stability by shielding against pH extremes, thermal shock and mechanical shear forces (Willaert & Baron, 1996). Immobilised systems allow cultures to be used over a longer time, and are also less sensitive to contamination of the desired microbial composition (Plieva

et al., 2008), which is of note in systems potentially using non-sterile wastewaters as feedstock. Finally, it may protect against toxic or inhibitory substances. *Pseudomonas* entrapped in alginate hydrogel was able to degrade 2-fold higher phenol concentration with correspondingly shorter degradation times, hypothesized to be due to formation of microcolonies inside the matrix (Bettmann & Rehm, 1984). These effects further extended to a doubling of hydrogen production rate from aromatic acids when *R. palustris* was immobilised (Fißler, Kohring & Giffhorn, 1995), showing direct benefit for biohydrogen production from challenging waste streams.

In the case of photofermentative hydrogen production, a central obstacle is the low volumetric production rate (Hallenbeck et al., 2009; Tian et al., 2009). Concentrated biomass loading (to maximise available biosynthetic capacity) and optimising hydraulic retention time (HRT) of the feedstock (to increase substrate turnover) independent of biomass retention time are key strategies for increasing production rates. Firstly, at high flow rates in suspension systems, the doubling time for the organism exceeds the residence time of the growth medium, thus wash-out of the organism occurs, since growth is not sufficient to replace biomass lost to effluent. This makes balancing sufficient influx of substrate with maintenance of optimal biomass concentration difficult. Here immobilisation is advantageous, since microbial biomass retention is separated from HRT and optimal loading is continually maintained irrespective of flow rate. To date, few studies on separation of biomass and hydraulic retention times in photosynthetic systems have been reported.

Secondly, non-growing *R. palustris* exhibits greatly improved hydrogen production capability since energy and carbon is not diverted to microbial biomass synthesis (McKinlay & Harwood, 2010a). Studies of non-growing cultures consuming acetate also revealed metabolic shifts from the glyoxylate shunt to the more efficient tricarboxylic acid cycle in which substrates are more fully oxidized, and the resultant reducing power drove 3.5 times higher hydrogen production than growing cells (McKinlay et al., 2014). In this respect, *R. palustris* is ideally suited for long-term use, since the ability to maintain an ample supply of ATP using

light allows cell maintenance in the absence of growth, resulting in minimal decreases in viability over many months of growth arrest (Pechter et al., 2017). Large-scale transposon mutagenesis studies of growth-arrested *R. palustris* showed that genes involved in translation are required for survival, and while ribosome abundance decreases, protein synthesis is essential for the cell to be able to effectively turn over the enzyme complement in the cell and maintain key metabolic processes (Yin et al., 2019). Hydrogen production would also likely be maintained by continual renewal of the nitrogenase complement in the cell.

Biomass could thus be grown under optimum pre-culture conditions and the inoculum subsequently immobilised in a suitable matrix for the required bioreactor loading. *R. palustris* possesses genes involved in quorum sensing, whereby microbial population density is detected (Larimer et al., 2004), thus potentially resulting in a large stable population of non-growing of cells within the immobilisation matrix efficiently evolving hydrogen.

An appropriate matrix should possess certain required characteristics:

1. It should be mechanically, chemically and thermally robust under process conditions,
2. It should be transparent, since hydrogen production is light-driven,
3. It should be biocompatible with the immobilised organism at all stages, yet resist degradation by it, and
4. It should have low resistance to diffusion so as not to limit movement of substrates and product through it.

To this end, numerous potential immobilisation methods have been explored; of which cell entrapment in porous polymer hydrogels show the most promise due to versatility and ease of handling. However, the majority of candidate hydrogels have proven dissatisfactory: alginate and other chelatotropic polymers are weak and chemically unstable, while synthetic polymers such as polyacrylamide require toxic crosslinking agents (Lozinsky, 2009). In this respect, novel hydrogels based on cryo-crosslinking of synthetic poly vinyl-alcohol are particularly attractive since they have the potential to meet all the requisite requirements for

an immobilisation matrix. Immobilisation materials applied to photosynthetic bacteria are further discussed in **section 4.3**, along with a summary given in **Table 4.1**.

2.8.1 PVA cryogels

Poly vinyl-alcohol, or PVA, is a synthetic polymer widely used in industry and manufacturing, including biotechnological applications such as chromatography, and is thus a readily available, low-cost material. PVA hydrogels are non-toxic and show inherently suitable biocompatibility (Baker et al., 2012), however, achieving the necessary crosslinking with chemical agents such as glutaraldehyde (Gough, Scotchford & Downes, 2002) or boric acid (Wu & Wisecarver, 1992) is often toxic to microbes under the requisite conditions.

Cryogels based on PVA, in which crosslinking is achieved by purely physical cryotropic effects, have thus been studied since the late 1980s (Ariga et al., 1987). In this process, exposure to low temperature causes water to freeze, with the phase separation forcing PVA out of solution into regions of high concentration. The resulting proximity of PVA polymers allows hydrogen bonding to take place between the chains to form a robust hydrogel network, enhanced by freeze-thaw cycling (Holloway, Lowman & Palmese, 2013a). As depicted in **Figure 2.5**, ice crystals serve as porogens in the hydrogel forming a highly macroporous structure with excellent diffusion characteristics; rendering them superior to other hydrogels (Lozinsky et al., 2003). These cryogels are also very durable, abrasion resistant and non-brittle,

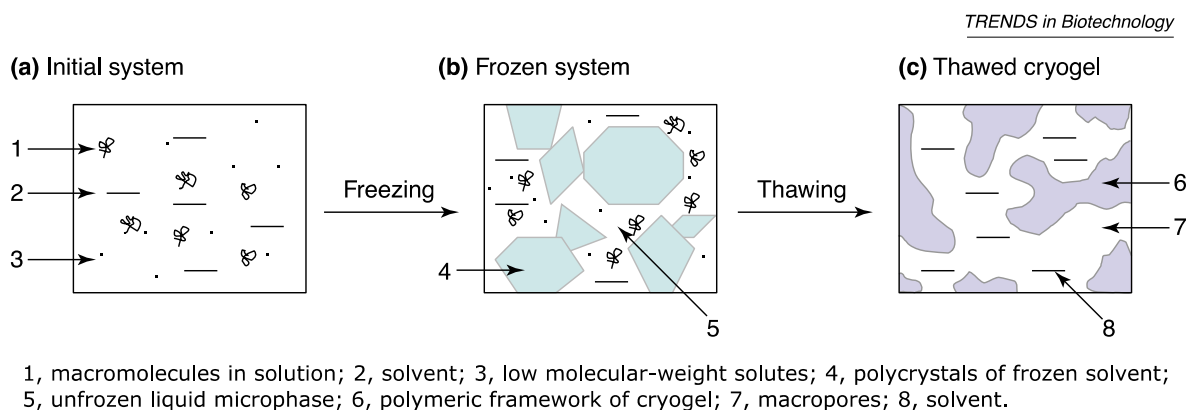


Figure 2.5. Conceptual diagram of the formation of polymeric cryogels.

Figure reproduced from Lozinsky et al. (2003) with permission from *Trends in Biotechnology*.

with a combination of elasticity and plasticity allowing non-destructive deformation (Lozinsky et al., 1986; Lozinsky & Plieva, 1998).

Tests of immobilised bacteria in a variety of microbial culture media showed no deterioration of the matrix, even over many months (Okazaki et al., 1995). A cross-section of studies using various organisms from bacteria to yeast immobilised in PVA cryogels reported improved yields and successful scale-up, as reviewed by Lozinsky (Lozinsky, 2009).

Despite all these advantages, PVA cryogels have not been investigated for use with photosynthetic organisms due to their opacity. However, changing the solvent properties by addition of a low molecular weight co-solvent results in a transparent matrix. Hyon et al (1989) developed a cryogel with 99% light transmittance using 80% DMSO (Hyon, Cha & Ikada, 1989); a concentration toxic to microbes and thus not appropriate for immobilisation. Polyols such as glycerol have also been reported as possible co-solvents (Cha, Hyon & Ikada, 1992; Lozinsky et al., 1995), which is an appealing option since glycerol is a widely-used cryoprotectant when freezing stock cultures for long-term preservation. The cryoprotectant effect is mediated by impeding formation of ice crystals that damage cell walls, and the presence of glycerol would likely limit adverse effects on microbial viability during the immobilisation procedure. Interestingly, PVA shares this property under certain conditions (Wowk et al., 2000), presenting the potential for a synergistic cryoprotectant effect. Freezing-related damage to cells could thus be averted, maximising biocompatibility of the cryogel immobilisation matrix. Due to the nature of cryogelation, incorporating glycerol into a PVA cryogel may affect the desired physical properties of the matrix and requires further investigation:

The transparency of DMSO cryogels was hypothesized to be a consequence of a homogeneous distribution of fine (<1 μm) pores limiting the scattering of light (Hyon, Cha & Ikada, 1989). Indeed, neutron scattering studies by Kanaya et al (2012) showed that liquid-liquid phase separation, or spinodal decomposition, was the origin of opacity in conventional cryogels (Kanaya et al., 2012). The addition of a co-solvent results in a homogenous material by

depressing the freezing point of the system. The sacrifice of macroporosity in order to gain transparency may be an obstacle to attaining optimal diffusion in a PVA-glycerol matrix. However, since the tortuosity of the pores ultimately determines the diffusive characteristics (Barrande, Bouchet & Denoyel, 2007), the lack of macropores may not be a significant constraint in an otherwise very highly hydrated gel matrix. A material composed mostly of water would not be likely to present significant resistance to diffusion.

Additional background on PVA cryogels is discussed in more detail in **section 4.3**.

2.9 Conclusion

Photofermentative hydrogen production using *R. palustris* fed on wastewater substrates has promise as a bio-economy solution to the dual problems of waste remediation and energy production, but technological improvements are key to realising this potential.

On a fundamental level, careful characterisation of the temperature optima and limits of *R. palustris* is essential to exact maximal overall metabolic performance of the organism, and to inform engineering decisions for further process and bioreactor development.

The hydrogen production process, catalysed by nitrogenases as an obligate by-product, is driven by the need to maintain redox balance resulting a surfeit of electrons and energy generated during photoheterotrophic growth. Additional sinks compete with hydrogen production for this pool of electrons, including carbon fixation and biomass synthesis. The energy flux through nitrogenase could thus be enhanced by maintenance of a non-growing culture, in which biomass synthesis is significantly reduced. This aim would be supported by microbial immobilisation in a material specifically optimised with photosynthetic bacteria in mind as a means of keeping a stable, non-growing culture decoupled from substrate hydraulic retention time. Here transparent PVA cryogels show promise as suitable matrices, requiring further characterisation to determine the ideal composition.

Further, the competitive efficiency of the nitrogen fixation pathway for reducing power may be enhanced by metabolic engineering, since there is evidence that the low catalytic activity

of the classical Nif nitrogenase complex is rate limiting for hydrogen production. The presence of alternative nitrogenase isozymes with more favourable catalytic stoichiometries provides a target for production rate improvement by over-expression of these tightly repressed genes. Each of these advancements have the potential to contribute technologically to a validated, integrated bioprocess optimisation strategy for high-rate hydrogen production.

CHAPTER 3

HEAT-ACCLIMATISED STRAINS OF *RHODOPSEUDOMONAS PALUSTRIS* REVEAL HIGHER TEMPERATURE OPTIMA WITH CONCOMITANTLY ENHANCED HYDROGEN PRODUCTION RATES

Adapted from:

Jan-Pierre du Toit and Robert W. M. Pott.

International Journal of Hydrogen Energy

DOI: <https://doi.org/10.1016/j.ijhydene.2021.01.068>

Published online 4 February 2021.

3.1 Context

Temperature is a fundamental bioprocess parameter, inherently affecting the catalytic activity of enzymes and other cell components responsible for biohydrogen production. The work in this chapter thus investigates the hypothesis that 30°C is not the optimal growth or hydrogen production temperature for *R. palustris*, in order to determine ideal standard cultivation temperatures for subsequent investigations in this dissertation. Pre-acclimation of two closely-related laboratory strains to 35°C reveals significantly higher optimum temperatures, suggesting that long-term cultivation under mild conditions leads to loss of innate temperature resistance. Higher temperatures translated to a peak of 4-fold enhanced hydrogen productivity; a dual advantage to process feasibility by reducing cooling requirements for outdoor sunlight-driven bioreactors. These results further inform strain selection criteria for enhanced hydrogen productivity, since higher temperature resistance and thus metabolic efficiency may be supported by novel isolates of *R. palustris* instead of potentially-compromised laboratory strains.

3.2 Abstract

Successful optimisation of bioprocesses requires detailed knowledge of process parameters; chiefly ideal temperatures for maximal production. Biohydrogen production via photofermentation by purple nonsulfur bacteria, such as *Rhodospseudomonas palustris*, has been the subject of extensive research but realisation of this clean energy source is limited by comparatively low productivity. Assessment of the growth and hydrogen productivity of two closely-related strains of *R. palustris* at progressively increasing temperature showed markedly higher strain-dependent optima than the 30°C previously reported and widely accepted, likely due to historical adaptation to conservative laboratory cultivation conditions and a degree of atrophy in temperature resistance in CGA009. Strain CGA009 showed 53% faster growth at 35°C, with 2.4-fold higher hydrogen production rate. Strain ATH 2.1.37 had a wider temperature range with an optimum of 40°C, resulting in 86% faster growth and 4-fold higher hydrogen production rate, along with the advantage of higher specific production

and substrate conversion efficiency. These results reaffirm the necessity of verifying temperature optima for specific process aims in order to realise maximum innate potential of candidate organisms with variable, strain-dependent characteristics in spite of highly similar genomes. In addition, caution is advised when using laboratory strains to investigate properties which may be diminished as an artefact of long-term cultivation under mild conditions.

3.3 Introduction

Since isolation over 100 years ago, *Rhodospseudomonas palustris* has emerged as an organism of great biotechnological interest due to its impressive metabolic versatility and ability to use a wide variety of organic substrates (Larimer et al., 2004). As a photosynthetic purple non-sulfur bacterium (PNSB), it is able to use energy from light in the form of ATP combined with electrons from breakdown of organic compounds to produce hydrogen gas using the enzyme nitrogenase (McKinlay & Harwood, 2010a). Production of biohydrogen as a clean alternative fuel with concomitant degradation of organic waste streams is thus an attractive bioeconomy development goal, and the subject of intense research for the past few decades (Pott, Howe & Dennis, 2013; Hallenbeck & Liu, 2016; Adessi, Corneli & De Philippis, 2017).

In spite of this focus, hydrogen production rates remain enduringly low in comparison to other hydrogen production methodologies, presenting a barrier for further development. Numerous approaches from bioreactor design to metabolic engineering have been presented as potential solutions (Tiang et al., 2020). However, one of the key fundamental parameters of bioprocess optimisation, temperature, has received comparatively little attention. Since hydrogen production is an enzyme-mediated process, the kinetics are intrinsically affected by temperature. *In vitro*, the activity of model nitrogenases have shown linear Arrhenius kinetics over a wide temperature range from 12 to 40°C (Thorneley, Eady & Yates, 1975). Enzyme activity is therefore exponentially related to temperature, highlighting the importance of careful temperature optimisation to realise maximum productivity where a difference of a few degrees can have a major impact. Moreover, temperature parameters significantly affect

engineering considerations for ultimate development of the photofermentation process towards larger-scale feasibility, which will require sunlight for cost-effective operation with the associated challenges of preventing overheating (Uyar & Kapucu, 2015). Here a higher standard operating temperature would reduce both energy and equipment requirements for temperature control. The vast majority of studies examining *R. palustris* biohydrogen production have been performed at 30°C (Adessi, Corneli & De Philippis, 2017), despite limited evidence that this is indeed the innate optimal temperature. Strains of *R. palustris* have been found in alkaline hot springs in Russia at a constant temperature of 54°C (Namsaraev et al., 2003). Similarly, thermotolerant *Rhodospseudomonas* species with temperature optima of 40°C were isolated from hot springs in Japan (Hisada, Okamura & Hiraishi, 2007), extending the expected feasible range of cultivation temperatures. As far back as 1944, one of the earliest characterisations of *R. palustris* by C.B. van Niel indicated that good growth was possible at 37°C, although strain-dependent differences and lower temperature optima were seen in isolates cultivated under laboratory conditions over extended periods (van Niel, 1944). Attempts to optimise temperatures specifically for biohydrogen production have not to date accounted for this acclimatisation process (Carlozzi & Lambardi, 2009; Wang et al., 2010, 2011; Guo et al., 2011), and the low 30°C optima identified may thus be an artefact of cultivation history. Further, characterisations have been based on assumptions that optimal temperatures for growth and hydrogen production are the same (Carlozzi & Lambardi, 2009), despite hydrogen production not being a growth-associated (Oh et al., 2004) and thus potentially needing to be specifically optimised.

The versatile metabolism of *R. palustris* belies a high level of biochemical specialisation in individual cells exposed to specific environmental factors, and transcriptional reprogramming is required for adaptation to changing conditions (Karpinets et al., 2009). *R. palustris* showed both increased hydrogen productivity and yield when acclimatised to growing on succinate for longer periods, allowing for comprehensive adaptation to the substrate (Hanipa et al., 2020). Preculture conditions, inoculum growth state and density have

been demonstrated to have a significant impact on biohydrogen production in batch cultures with the PNSB *Rhodobacter sphaeroides*, with the highest productivity gained when using log-phase inoculum in which cellular metabolism is primed for peak activity (Sasikala, Ramana & Raghuveer Rao, 1991; Laurinavichene & Tsygankov, 2018). Further, initial characterisation of a photosynthetic PNSB consortium, which included *R. palustris* and was routinely grown at 30°C, unsurprisingly showed an optimal hydrogen production temperature of 30.5°C (Lu et al., 2016). However, subsequent investigation of the thermophilic potential of this consortium resulted in an optimum of 39.6°C, higher than any of the component species, and resulting in a 60% increase in maximum hydrogen production rate (Hu et al., 2017). Adequate pre-acclimatisation to culture conditions is therefore essential for accurate determination of the inherent potential of different strains for desired process outcomes, without the confounding influence of this adaptation process.

In order to better understand the innate temperature-related characteristics of *R. palustris*, we examined growth and hydrogen production potential of two widely used strains in batch culture under progressively increasing temperatures for extended periods in order to allow complete adaptation. Our results indicate that optimal growth in both strains indeed occurs at higher temperatures, along with substantially improved hydrogen production rates, confirming the importance of careful verification of this fundamental process parameter even in closely-related strains.

3.4 Methods:

3.4.1 Bacteria and culture methods

Rhodopseudomonas palustris strain ATH 2.1.37 (NCIB 11774) was obtained from ATCC (ATCC® 17007™). Strain CGA009 was obtained from C.J. Howe, University of Cambridge. Strains were initially cultured at 30°C before acclimatisation at 35°C for at least 3 passages of 1 week each. Rapid routine growth on plates was achieved using Van Niel's yeast agar with 50 mM glycerol (referred to as VNG agar; 1 g K₂HPO₄, 0.5 g MgSO₄, 10 g yeast extract, 15 g agar; L⁻¹), incubated at 35°C, which also served to quickly detect any potential culture contamination both prior to and after experiments. Glycerol was used as standard carbon source for all cultivation to maintain a high degree of substrate adaptation.

For growth and hydrogen production studies, strains were grown in modified *Rhodospirillacea* minimal medium consisting of (L⁻¹): 0.57 g KH₂PO₄, 1.86 g K₂HPO₄, 0.4 g NaCl, 0.2 g yeast extract, 0.25 g Na₂S₂O₃·5H₂O, 0.2 g MgSO₄·7H₂O, 0.05 g CaCl₂·2H₂O, 0.005 g Ferric citrate, 0.002 g para-aminobenzoic acid. Medium buffer system was formulated to yield pH ~7.2 after autoclaving, with 50 mM glycerol, 10 mM glutamate (monosodium) and 1 mL·L⁻¹ trace element solution (Pott, Howe & Dennis, 2013) added from sterile stocks. Trace element solution consisted of (L⁻¹): 70 mg ZnCl₂, 100 mg MnCl₂·4H₂O, 60 mg H₃BO₃, 200 mg CoCl₂·6H₂O, 20 mg CuCl₂·2H₂O, 20 mg NiCl₂·6H₂O and 40 mg NaMoO₄·2H₂O; filtered sterile. (Pott, Howe & Dennis, 2013). A protocol for medium preparation is provided in **Appendix 6 (Protocol A)**.

3.4.2 Photobioreactor setup

Test-scale photobioreactors were composed of 500 mL working-volume glass reagent bottles (Simax) and GL45 polypropylene lids adapted by the addition of gastight stainless-steel liquid and gas sampling tubes. Reactors were sterilised by autoclave. Cultures were inoculated to a starting OD₆₆₀ of 0.05 from 3-day precultures grown at 35°C under identical conditions (~1% inoculum). Sparging with technical grade argon gas (>99.9%) sterile-filtered through a 0.2 µm PTFE filter for 10 – 15 min served to induce anaerobic, N₂-free conditions required for

hydrogen production. Cultures were agitated by magnetic stirring at ± 200 RPM with 50 mm PTFE-coated stirrer bars. Illumination provided by 100 W tungsten-filament incandescent lightbulbs (Eurolux) was adjusted to an irradiance intensity of $200 \text{ W}\cdot\text{m}^{-2}$ (± 20) in the wavelength range 500 – 1100 nm at the inner surface of the bioreactors, using a compact spectrometer with cosine correcting probe (RGB photonics Qmini VIS-NIR). Reference irradiance spectra are shown in **Appendix 4**. Temperature was maintained by immersing bioreactors in a water-filled glass tank with a heating circulator and cooling loop and controlled to $\pm 0.2^\circ\text{C}$ of applicable setpoint, as shown in **Appendix 1**. Gas production was quantified by displacement in inverted, water-filled 1 L measuring cylinders connected to each bioreactor sampling port with low hydrogen-permeability tubing (Tygon E-3603, Saint-Gobain) and one-way valves to prevent reflux.

At each indicated timepoint, a 3 mL sample was taken aseptically via the liquid sampling port for determination of optical density; the remainder was centrifuged to pellet cells and the supernatant frozen at -20°C for glycerol quantification at a later point.

3.4.3 Analytical

Biomass concentration was determined by optical density at 660 nm and converted to dry cell weight with a standard curve generated by filtering triplicate 15 – 30 mL culture aliquots through pre-dried $0.2 \mu\text{m}$ nylon filters and drying at 60°C until constant weight (OD_{660} : 0.05 – 1.3). Standard curve is shown in **Appendix 5**. Samples with $\text{OD}_{660} > 1.3$ were diluted for accurate measurement, and the dilution factor applied to calculate the actual concentration.

The growth rate constant, k , was determined using the linear regression slope from a semi-log plot of biomass versus time, and the doubling time, g , calculated using the equation $g = \ln(2)/k$.

Glycerol was quantified by high performance liquid chromatography (HPLC), using a Dionex UltiMate 3000 system fitted with a Biorad HPX-87H 250 x 7.8 mm column with guard cartridge and ERC Refracto Max520 refractive index detector. 20 μL of each sample (pre-filtered using $0.2 \mu\text{m}$ nylon syringe filters) was injected and eluted with 0.005 M H_2SO_4 mobile phase at 0.6 mL/min and column temperature of 65°C .

A Global Analyser Solutions CompactGC gas chromatograph with argon carrier stream and thermal conductivity detector was employed to confirm the relative composition of the gas produced. H₂ and CO₂ were quantified and reported as relative percentages; any contaminating nitrogen or oxygen was discounted as artefact of the sampling procedure. Typical gas composition (n = 4) fell within the range of 94.1 ± 0.4% H₂, 5.9 ± 0.4% CO₂.

Substrate conversion efficiency was assessed as the molar ratio of hydrogen yield to glycerol consumed as a percentage theoretical maximum (7 mol H₂: mol glycerol), calculated using the molar volume of H₂ at NTP and the composition of typical gas samples: 94.1 ± 0.4% H₂, 5.9 ± 0.4% CO₂. Monte Carlo simulations were performed for uncertainty propagation of calculated values, using the NIST Uncertainty Machine (Albert, 2020) with a sample size of 10⁶.

Data was analysed and visualised using GraphPad Prism 7. Two-way ANOVA with Tukey's multiple comparison tests were used to determine statistical significance at a threshold of $\alpha = 0.05$.

3.4.4 Bioinformatics

Accession numbers of genome sequences used are: *R. palustris* CGA009 (BX571963.1), *R. palustris* ATH 2.1.37 (QYYC01), *R. palustris* ELI 1980 (CM001782.1), *R. palustris* DSM 126 (NRS101), *R. palustris* TIE-1 (ASM2044v1), *R. palustris* (*rutila*) R1 (QWVU01), *R. palustris* PS3 (CP019966.1), *R. palustris* YSC3 (CP019967.1), *R. palustris* XCP (QKQS01), *R. palustris* 42OL (LCZMO1), *R. palustris* DX-1 (CP002418.1, NC014834.1), *R. (pseudo)palustris* DSM 123 (PRJEB16943), *R. palustris* BisB5 (CP000283.1), *R. palustris* HaA2 (CP000250.1), *R. palustris* strain 2.1.18 (QYYD01), *R. palustris* strain BAL398 (ASM93520v1), *R. palustris* JSC-3b (AYSU00000000.1), *R. palustris* BisA53 (CP000463.1), *R. palustris* BisB18 (CP000301.1).

The phylogenetic tree was generated using the codon trees method in PATRIC, the Pathosystems Resource Integration Centre (Wattam et al., 2017). From 1153 single-copy genes occurring in all 19 genomes, 1000 were automatically selected from PATRIC's global Protein Families (PGFams). Alignments of both nucleotides and amino acids were used to determine the phylogenetic relationships using RaxML, with support values determined by 100 rounds

of rapid bootstrapping (Stamatakis, 2014). The resultant tree was visualised with iTOL (Letunic & Bork, 2019). Multiple sequence alignments of RefSeq-annotated genes were performed using nucleotide and amino acid alignment functions in PATRIC.

3.5 Results and discussion

3.5.1 Growth is enhanced at temperatures exceeding 30°C

Pre-adaptation of cells to growing conditions is important for accurate determination of the innate growth and hydrogen-producing characteristics for appropriate process optimisation. We investigated this effect using CGA009 and ATH 2.1.37, two closely related strains of *R. palustris* based on global Protein Families (PGFams; **Figure 3.1**) which share an average nucleotide identity (ANI) of 99.9% (Imhoff, Meyer & Kyndt, 2020). These strains were thus expected to be highly similar functionally. The strains were routinely cultivated in the laboratory using glycerol, an ideal substrate for high-rate hydrogen production (Pott, Howe & Dennis, 2013) with the benefit of not being prone to detrimental pH swings over time as is the case for more commonly-investigated organic acids (Laurinavichene & Tsygankov, 2018). Previously maintained at 30°C, both strains were acclimatised to a higher temperature of 35°C over 3 weeks prior to investigation of the growth and hydrogen production over a range of temperatures in batch culture experiments using test-scale bioreactors. The growth rate of

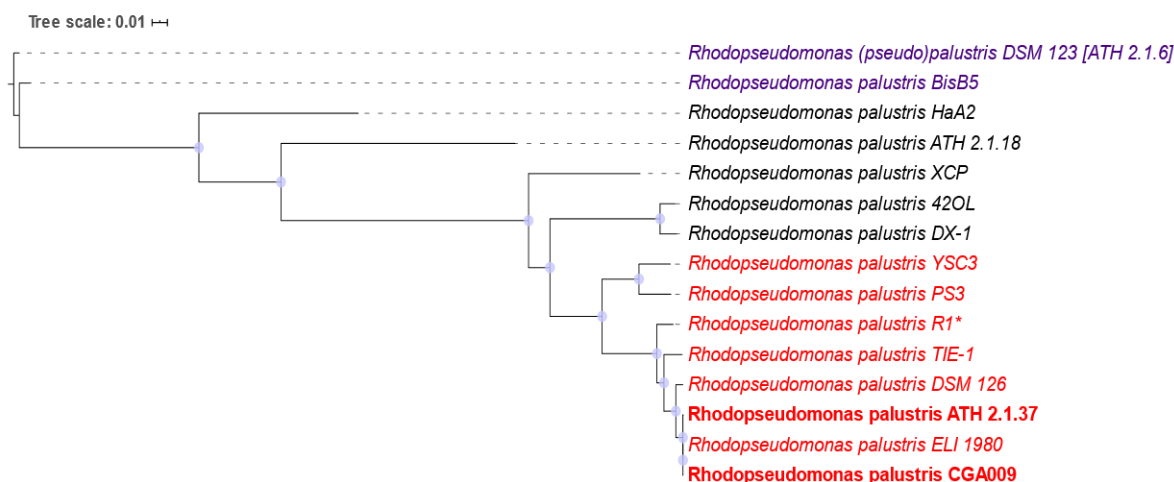


Figure 3.1. Phylogenetic tree of *Rhodopseudomonas palustris* strains based on whole genome comparison.

The phylogenetic relationships were determined by the codon tree method in PATRIC, using protein and coding sequence alignments of 1000 single-copy genes selected from PGFam homology groups, generated with RAXML. Tree visualised with iTOL. Blue circles represent 100% bootstrap values for branch points. Strains are colour coded by groups proposed to be distinct species by Imhoff et al (2020).

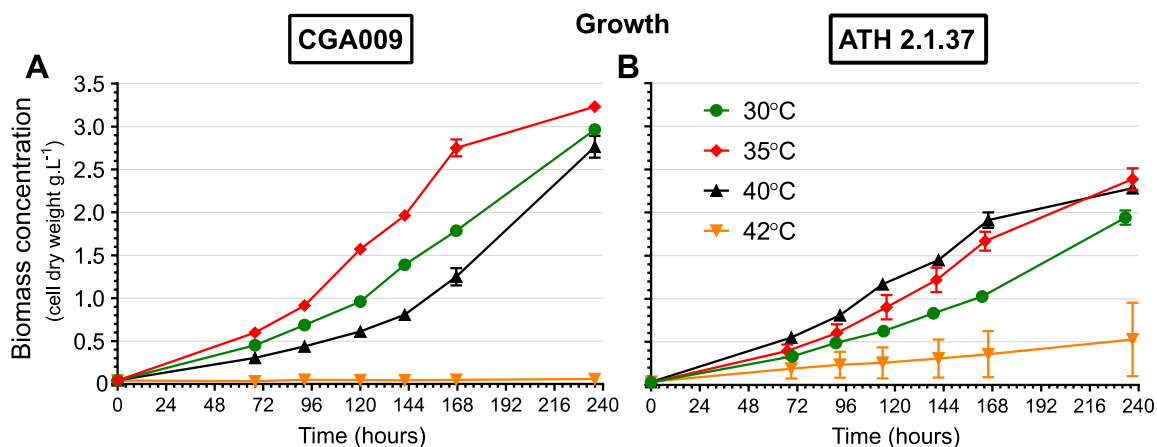


Figure 3.2. Growth of 35°C-acclimatised *R. palustris* under varying temperatures.

Strains CGA009 (A) and ATH 2.1.37 (B) were grown at 30 – 42°C in batch culture under photoheterotrophic conditions. Biomass concentration determined by measurement of OD₆₆₀. Datapoints represent mean ± SEM for 4 – 6 biological replicates.

both strains was enhanced at temperatures higher than the 30°C baseline (Figure 3.2), confirming our hypothesis that this is not the optimal growth temperature. Strain CGA009 grew best at 35°C, resulting in considerably higher biomass concentration after 7 days compared to 30°C (Figure 3.2A; 168 hours; 54 ± 4 %, $p < 0.001$), while growth at higher temperatures was impaired. Strain ATH 2.1.37 showed a wider favourable temperature range with comparative day-7 biomass concentrations 63 to 86% higher at 35 and 40°C respectively (Figure 3.2B; both ± 9 %, $p < 0.001$). A higher maximum temperature was also evident, since growth occurred at 42°C whereas CGA009 was completely arrested at this temperature. The high variation between replicate reactors, possibly reflecting stochastic effects in the initial inoculum, may also indicate the possibility of a degree of further adaptation to growth at higher temperatures approaching the upper limit. Although higher overall biomass densities were achieved quickly by CGA009, this comes at the cost of a reduced permissible temperature range. CGA009 is the most commonly-used laboratory strain of *R. palustris*; itself a derivative of earlier laboratory strains (Kim & Harwood, 1991), and thus has a long history of cultivation at mild, controlled temperatures. This may plausibly be accompanied by a degree of selection for fast growth under these conditions to satisfy experimental demands,

over the course of many passages in the decades since initial isolation. As noted by van Niel, strains subjected to long-term laboratory cultivation exhibited significantly reduced temperature ranges (van Niel, 1944), consistent with the present study of CGA009. In the case of ATH 2.1.37, an original isolate from van Niel's culture collection, this adaptation process has likely been far less extensive or at least reversible, perhaps more closely reflecting the inherent capabilities of the organism. Here it may be advisable to use recent environmental isolates from locations experiencing high average temperatures to maximise the permissible process temperature, and to maintain these strains at higher temperatures so as to prevent potential debilitation.

Based on comparative genomics and re-evaluation of original type strains, Imhoff et al have recently presented evidence that strains designated *R. palustris* are actually multiple distinct species, as indicated in **Figure 3.1** (Imhoff, Meyer & Kyndt, 2020). The group including CGA009 and ATH 2.1.37 is most closely represented taxonomically by the type strain *R. rutila* R1; physiologically distinct from *R. palustris* as represented by type strain DSM123. This further highlights the importance of strain-specific characterisation in species which may be highly heterogeneous, and even strains with highly similar genomes may nevertheless display distinct traits.

General stress responses in *R. palustris* are mediated by hopanoids, steroid-like pentacyclic bacterial lipids which have been associated with successful growth at higher temperatures. By tuning the fluidity and rigidity of the extensive membrane systems, which contain a high proportion of unsaturated lipids, hopanoids provide stabilisation against thermal disorder (Neubauer et al., 2015). Increasing from 30 to 38°C, hopanoid content increased 25% in *R. palustris* TIE-1 and disruption of either hopanoid biosynthesis or correct localisation in the outer membrane significantly impaired growth at 38°C (Doughty et al., 2011). Investigation of hopanoid-related biosynthesis and transport genes using sequence alignments however revealed no mutations in coding sequences (**Appendix 1**). This does not exclude the possibility of changes in gene regulatory elements which have not been comprehensively characterised.

Since hopanoids are not essential for growth at mild temperatures, maintenance of these pathways in laboratory strains would not be under selective pressure. Similarly, changes in regulatory mechanisms for other pathways involved in successful response to heat stress, such as heat shock proteins, may underlie the diminished temperature range of CGA009 and would likely be subtle in context of the highly similar genomes, although this requires further study. The provenance and cultivation history of strains thus seem to be important considerations in the development of processes utilising *R. palustris*, where long-term maintenance under unfavourable non-selective conditions may lead to atrophy of potentially desirable characteristics. The wider temperature tolerance and higher optimal growth temperature of ATH 2.1.37 is an advantage for the feasibility of sunlight-driven photofermentation where temperatures are likely to be high, along with catalytic implications for the hydrogen production pathway. PNSB grown in outdoor, sunlit bioreactors have been reported to commonly experience lethal temperatures in excess of 45°C, requiring cooling mechanisms to control (Uyar, 2016). These measures add technical complexity and cost to the process; thus, a higher standard operating temperature may partially mitigate these challenges to reaching overall photofermentation process feasibility.

The differences seen in biomass concentration diminished at the start of stationary phase after 10 days (**Figure 3.2**; 240 hours), likely due to biomass density approaching the maximum supportable at the constant light intensity used here. At this critical density, light limitation due to mutual shading results in only enough energy being produced for cell maintenance, thus precluding further growth (Clark et al., 2018). At the 500 mL reactor scale used, light limitation is likely since substantial biomass concentrations (exceeding 0.5 g.L⁻¹) are required for industrially-relevant hydrogen production rates, as evidenced by the calculated doubling times (**Table 3.1**) which are significantly longer than reported exponential phase doubling times of 8 – 11 hours for strain CGA009 (Rey & Harwood, 2010). Despite this light limitation, higher

temperatures still resulted in faster growth up to the respective optima, reflecting increased efficiency in energy supply and/or utilisation as well as biomass synthesis for cell division. In the PNSB *Rhodospirillum rubrum*, both photosynthetic electron transport and respiration are enhanced, conforming to Arrhenius kinetics, up to 41°C (Kaftan, Bína & Koblížek, 2019). The photosynthetic reaction centres are highly conserved amongst PNSB, and this degree of thermostability could facilitate more effective use of available light for energy production and thus faster growth at higher temperatures, as demonstrated here.

Table 3.1. Doubling times for acclimatised *R. palustris* strains.

Temperature (°C)	Doubling time (h) ^a	
	CGA009	ATH 2.1.37
30	115.0 ± 3.4	134.8 ± 5.4
35	103.7 ± 3.8	107.3 ± 6.3
40	115.6 ± 6.2	126.8 ± 4.7
42	NG ^b	307.0 ± 145.1

^a Mean ± SEM for 3 – 6 biological replicates

^b No growth

3.5.2 Increased temperatures support faster hydrogen production rates

The ability to endure higher temperatures has significant consequences for the catalytic efficiency of all cellular pathways, as demonstrated by increased biomass synthesis. As anticipated, hydrogen production was similarly enhanced at higher temperatures (**Figure 3.3A**). Remarkably, CGA009 produced more than double the total hydrogen at 35°C versus 30°C, and while this difference was less pronounced with ATH 2.1.37, the hydrogen production rates were similarly increased in both strains by 2.4 to 2.7 fold (**Table 3.2**; $p < 0.05$), with no significant difference between strains ($p = 0.99$).

The temperature range for hydrogen production by ATH 2.1.37 was again superior, showing peak productivity and yield at 40°C (**Figure 3.3A**). This was also reflected in the highest overall hydrogen production rate observed; 4-fold higher than the 30°C baseline for the strain

(Table 3.2; ± 0.5 , $p < 0.001$). ATH 2.1.37 thus offers dual advantages of a wider temperature range coupled with significantly enhanced hydrogen production.

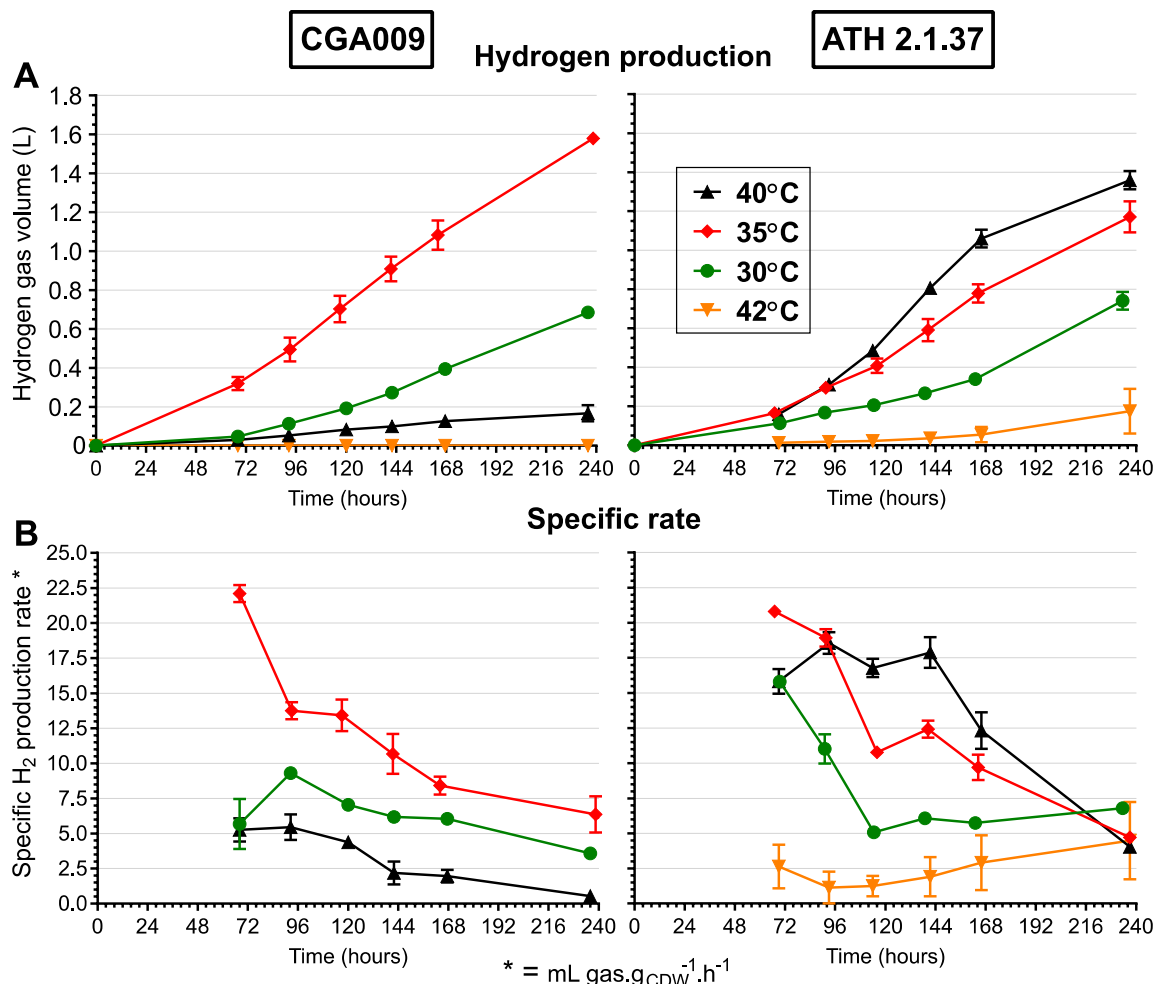


Figure 3.3. Hydrogen production characteristics of *R. palustris* under varying temperature. Strains CGA009 and ATH 2.1.37 were grown at 30 – 42°C in batch culture under photoheterotrophic conditions. Hydrogen production (A) was normalised to average biomass (cell dry weight) in bioreactor between timepoints to yield specific hydrogen production rate (B). Datapoints represent mean \pm SEM for 4 – 6 biological replicates.

Table 3.2. Hydrogen production rates of acclimatised *R. palustris* strains under varying temperature.

Temperature (°C)	Hydrogen production rate (mL.h ⁻¹) ^a	
	CGA009	ATH 2.1.37
30	3.4 \pm 0.2	2.8 \pm 0.5
35	8.1 \pm 0.8	7.7 \pm 1.3
40	1.0 \pm 0.1	11.0 \pm 0.9

^a Mean \pm SEM for 3 – 6 biological replicates

During photoheterotrophic growth, ATP is produced via cyclic electron transport driven by photosynthesis, without requiring a terminal electron acceptor. The reduced electron carriers (NADH, NADPH and ferredoxins) generated from breakdown of organic substrates thus need to be re-oxidised in order to maintain redox balance and keep cellular metabolism functioning (McKinlay & Harwood, 2010a). In addition, the oxidation state of the substrate contributes to the electron surplus, depending on the oxidative pathway used. The oxidation state of glycerol is -1 in comparison to -0.5 for *R. palustris* biomass, similar to that of butyrate which was shown to considerably boost electron supply and thus hydrogen yield in metabolic flux studies (McKinlay & Harwood, 2011). Alongside hydrogen production, carbon fixation and biomass synthesis are two key sinks for offloading surplus electrons to maintain cellular redox balance, and these pathways are thus in direct competition for reducing equivalents in these experiments. The fact that higher growth rates coincide with higher hydrogen production rates indicates a greater degree of energetic uncoupling from biomass synthesis, likely due to a more favourable redox state resulting from improved activity of rate limiting steps at higher temperatures, as observed in *Rb. sphaeroides* (Kaiser & Oelze, 1980). The transfer of electrons to nitrogenase incurs an energetic cost in the form of ATP, which decreases significantly under highly reduced states due to the reduced energy barrier, consequently improving the efficiency of nitrogenase activity and thus hydrogen production (Hallenbeck, 1983). Enhanced catalytic activity and electron transport in combination with a more favourable redox state facilitated at higher temperatures thus have the potential to act in synergy to improve hydrogen production.

In order to realise the highest possible biohydrogen production rate, the specific productivity per cell will need to be optimised to reduce unnecessary biomass accumulation which diverts energy away from product formation, potentially creating an additional undesired by-product and complicating process development. Higher operating temperatures support much-improved specific hydrogen production rates, particularly at lower culture densities where deep light penetration allows optimal ATP regeneration (**Figure 3.3B**; 70 hours), increased by 4.2-fold in CGA009 at 35°C (± 0.2 -fold; $p < 0.001$). Increases for ATH 2.1.37 were

more modest, however specific production rates remained higher for much longer periods at 35 – 40°C since biomass concentration was lower overall than CGA009. Slower growth is thus a comparative advantage here, allowing more energy to be directed to high-rate hydrogen production instead of biomass. Between 114 and 141 hours, ATH 2.1.37 supported on average 1.9-fold higher specific hydrogen production rates at 35°C (1.7 – 2.1-fold; $p < 0.001$), increasing to 2.6-fold at 40°C (2.1 – 2.9-fold; $p < 0.005$). Since biomass densities were elevated proportionally with temperature (**Figure 3.2**), these cultures experienced a greater degree of mutual shading thus reducing the average irradiance intensity available to drive photosynthesis. According to Beer-Lambert law, at an optical density of 1.5 (approximately 1.1 g.L⁻¹ biomass) light transmission is attenuated by 97% at a depth of 1 cm. Despite this degree of light limitation in reactors with an 8 cm diameter and non-optimised surface-volume ratio, higher specific hydrogen production rates were still achieved by increasing temperature, indicating substantial improvement in photosynthetic efficiency to generate sufficient ATP in support of energy-intensive hydrogen production. Alternatively, expression of light-harvesting antenna complexes may play a role, since they have been shown to be regulated by a redox sensing mechanism (Fixen, Oda & Harwood, 2019), thus responding to cellular energy demands instead of merely the prevailing light intensity. Assuming that higher temperatures increase the activity of the nitrogen fixation and electron transport pathways and result in a higher energetic flux, raising expression of antenna complexes may allow better utilisation of transient exposure to high irradiance, mitigating the lower average irradiance at these high biomass densities (at the expense of exacerbating mutual shading overall). It is likely that improved activity of the numerous pathways necessary for hydrogen production, including photosynthesis, ATP regeneration, electron transport and nitrogenase components, contribute in tandem to the enhanced productivity at higher temperatures.

3.5.3 Temperature influences substrate conversion efficiency

Alongside specific productivity, substrate conversion efficiency is a further key consideration for the feasibility of biohydrogen production. Up to their respective temperature optima, both

strains bore higher glycerol conversion efficiencies, as a percentage of the maximum theoretical hydrogen yield of 7 mol H₂/mol glycerol. Perhaps due to the slower growth rate of ATH 2.1.37 at lower temperature resulting in reduced competition for ATP and electrons, 70% higher glycerol conversion efficiency was seen versus CGA009 at 30°C (**Table 3.3**; $\pm 15\%$; $p = 0.0021$). With this baseline, CGA009 had a 2-fold higher conversion efficiency at 35°C (**Table 3.3**; $\pm 15\%$; $p < 0.0001$), whereas ATH 2.1.37 improved by 29% at 40°C ($\pm 9\%$; $p = 0.035$); which was also the highest conversion efficiency seen although not statistically different compared to the result at 35°C. Higher temperatures thus seem to advantage substrate conversion efficiency, shifting the cellular energy budget in favour of hydrogen production while competing pathways perhaps fail to derive equal advantage from temperature-related catalytic or activity enhancements.

Table 3.3. Substrate-to-hydrogen conversion efficiencies of acclimatised *R. palustris* strains

Temperature (°C)	Glycerol conversion efficiency (%) ^a	
	CGA009	ATH 2.1.37
30	29.9 \pm 2.1	50.7 \pm 7.1
35	60.3 \pm 3.4	58.6 \pm 10.9
40	8.3 \pm 3.6	65.6 \pm 6.0

^a Percentage of maximum theoretical yield; mean \pm SD for 3 – 6 biological replicates

The nitrogen fixation pathway responsible for hydrogen production is complex and relies on many accessory proteins to manage electron flow to nitrogenase, with rate-limiting steps restricting catalytic activity to a meagre ~6 reactions per second (Yang et al., 2016). Improvements in catalytic efficiency of this energy intensive process, combined with the potential for reduced energetic cost of electron transfer at higher temperatures may thus result in a superior sink which better competes for available reduced electron carriers. Even greater hydrogen productivity and substrate efficiency is therefore likely using non-growing cells at

their higher temperature optima, where absence of competition from biomass synthesis has been demonstrated to increase hydrogen yield 3.5-fold (McKinlay et al., 2014).

The performance enhancements in terms of growth rate, hydrogen productivity and substrate conversion efficiency at increasing temperatures identified here are unlikely to be the maximum possible, due to the limits imposed by light penetration due to culture density and reactor geometry in these experiments. Application of strains acclimatised at higher growth temperatures to biohydrogen production using optimised reactors with surface-volume ratios conducive to homogeneous illumination will thus allow realisation of the maximum innate potential of suitably robust strains such as ATH 2.1.37, contributing to advancement in the development of high-rate biohydrogen production towards feasibility.

3.6 Conclusion

The hypothesis that *R. palustris* is capable of efficient growth and hydrogen production at temperatures above 30°C was tested by acclimating two closely-related strains at 35°C over multiple passages, and investigating temperature-related performance up to 42°C. The results demonstrated that temperature optima are indeed 5 to 10°C higher than previously accepted, with significant implications for hydrogen productivity which improved by up to 4-fold compared to the 30°C baseline. In addition, enhancement of specific hydrogen production rate and substrate conversion efficiency were demonstrated. Strain CGA009 showed an optimum temperature of 35°C, while that of ATH 2.1.37 was 40°C with a higher overall temperature resistance. It is theorised that long-term cultivation of laboratory strains under lenient conditions results in loss of innate temperature resistance over time. These differences in strains with 99.9% genome similarity are remarkable and may reflect subtle changes in expression of heat resistance mechanisms, which require additional characterisation. As such, higher process temperatures and maximal metabolic efficiency may be elucidated by using fresh environmental isolates as candidate strains for further study.

3.7 Acknowledgements

We would like to thank Jaco van Rooyen and Levine Simmers for assistance with HPLC analysis, and Jos Weerdenberg for fabrication of reactor components as well as engineering and problem-solving advice. This work was supported by funding from the Water Research Commission (WRC) of South Africa.

3.8 Author contributions

Declaration by the candidate:

With regard to Chapter 3, the nature and scope of my contribution were as follows:

Nature of contribution	Extent of contribution (%)
Conceptualisation	90%
Methodology	
Investigation	
Data analysis & Visualisation	
Writing & Editing	

The following co-author has contributed to Chapter 3:

Name	e-mail address	Nature of contribution	Extent of contribution
Robert W. M. Pott	rpott@sun.ac.za	Conceptualisation & discussion Review & Editing	10%

Signature of candidate: Jan-Pierre du Toit Date: 29 January 2021

Declaration by co-author: The undersigned hereby confirm that

1. the declaration above accurately reflects the nature and extent of the contributions of the candidate and the co-authors to Chapter 3,
2. no other authors contributed to Chapters 3 besides those specified above, and
3. potential conflicts of interest have been revealed to all interested parties and that the necessary arrangements have been made to use the material in Chapters 3 of this dissertation.

Signature	Institutional affiliation	Date
Robert W. M. Pott	Stellenbosch University	29 January 2021

Declaration with signatures in possession of candidate and supervisor

CHAPTER 4

TRANSPARENT POLY VINYL-ALCOHOL CRYOGEL AS IMMOBILISATION MATRIX FOR CONTINUOUS BIOHYDROGEN PRODUCTION BY PHOTOTROPHIC BACTERIA

Adapted from:

Jan-Pierre du Toit and Robert W. M. Pott

Biotechnology for Biofuels **13**, 105 (2020)

DOI: <https://doi.org/10.1186/s13068-020-01743-7>.

Published 9 June 2020.

4.1 Context

Bioprocess optimisation requires technological means to control important process parameters. To enable continuous biohydrogen production, a method of isolating biomass from the liquid medium is necessary to prevent biomass washout under high dilution rates or due to slow bacterial growth. In addition, biohydrogen production by PNSB is not growth-associated and non-growing cells produce hydrogen more efficiently, making effective retention of biomass essential under these conditions. This chapter thus details the development of a transparent immobilisation matrix based on poly-vinyl alcohol (PVA), to allow biomass to be retained in a bioreactor. Key characteristics of the cryogel were determined and the material composition optimised to maximise compatibility with photosynthetic bioprocess requirements, including studies of hydrogen production by immobilised bacteria at the higher temperature optima identified in the previous chapter. In addition, imaging techniques employing confocal microscopy and fluorescent staining were developed to enable *in situ* investigation of PVA porosity and biocompatibility under native, non-denaturing conditions.

4.2 Abstract

Phototrophic purple nonsulfur bacteria (PNSB) have gained attention for their ability to produce a valuable clean energy source in the form bio-hydrogen via photofermentation of a wide variety of organic wastes. For maturation of these phototrophic bioprocesses towards commercial feasibility, development of suitable immobilisation materials is required to allow continuous production from a stable pool of catalytic biomass in which energy is not diverted towards biomass accumulation, and optimal hydrogen production rates are realised. Here the application of transparent poly vinyl-alcohol (PVA) cryogel beads to immobilisation of *Rhodospseudomonas palustris* for long term hydrogen production is described.

The addition of glycerol co-solvent induces favourable light transmission properties in normally opaque PVA cryogels, especially well-suited to the near-infrared light requirements of PNSB. Material characterisation showed high mechanical resilience, low resistance to

diffusion of substrates and high biocompatibility of the material and immobilisation process. The glycerol co-solvent in transparent cryogels offered additional benefit by reinforcing physical interactions to the extent that only a single freeze-thaw cycle was required to form durable cryogels, extending utility beyond only phototrophic bioprocesses. In contrast, conventional PVA cryogels require multiple freeze-thaw cycles which compromise viability of entrapped organisms. Hydrogen production studies of immobilised *R. palustris* in batch photobioreactors showed higher specific hydrogen production rates that continued longer than planktonic cultures. Continuous cultivation yielded hydrogen production for at least 67 days from immobilised bacteria, demonstrating the suitability of PVA cryogel immobilisation for long-term phototrophic bioprocesses. Imaged organisms immobilised in cryogels showed a monolithic structure to PVA cryogels, and demonstrated a living, stable, photofermentative population after long-term immobilisation.

Transparent PVA cryogels thus offer ideal properties as an immobilisation matrix for phototrophic bacteria and present a viable photobioreactor technology for the further advancement of biohydrogen from waste as a sustainable energy source, as well as development of alternative photo-bioprocesses exploiting the unique capabilities of purple non-sulfur bacteria.

4.3 Introduction

Phototrophic purple nonsulfur bacteria (PNSB) have garnered much attention for their ability to produce high-purity hydrogen from organic wastes via photofermentation. In recent decades significant effort has been devoted to developing this potential clean, sustainable energy source to commercial feasibility and in particular overcoming the barrier of enduringly low production rates. In addition to metabolic enhancement, bacterial immobilisation has been identified as key strategy for improving productivity (Adessi, Corneli & De Philippis, 2017). Hydrogen production occurs independent of growth; thus, the cells can be used as biocatalysts while in stationary phase, with immobilisation facilitating optimal continuous operation of the process. Conventional suspended cell systems require balancing of dilution rates with cell growth to prevent biomass washout (Obradovic et al., 2004), thus constraining reactor dynamics to potentially unfavourable parameters. Here cell immobilisation is advantageous, resulting in phase separation of the cells and liquid medium. A stable pool of catalytic biomass is thus maintained within the reactor, irrespective of feed rates, allowing the hydraulic and solids retention times to be precisely tuned independently of each other for maximal production rate.

Immobilisation offers myriad additional benefits to the bioprocess engineer:

- i) Volumetric biomass loading can be increased over planktonic cells
- ii) Less metabolic energy needs to be diverted to cell multiplication, resulting in higher product yields
- iii) Lower risk of genetic drift or reversion
- iv) Cells are protected from shear stresses and pH, temperature or chemical concentration fluctuations within the reactor

(Dervakos & Webb, 1991; Nedovic & Willaert, 2013; Žur, Wojcieszynska & Guzik, 2016).

While a host of immobilization matrices have historically been applied to heterotrophic organisms [for an extensive review see Willaert & Baron (1996)], fewer options have been

critically investigated for phototrophic bacteria: the key difference being that phototrophic organisms require a high level of transparency for substantial light penetration. Many materials previously studied do not or only partially meet additional key requirements, namely: biocompatibility, chemical and mechanical durability for long-term use, and possessing low barriers to diffusion of substrates (Tsygankov & Kosourov, 2014), as illustrated in **Table 4.1**.

The early staples of cell immobilisation, agar and alginate, offer good transparency, diffusion properties and biocompatibility, but are exceedingly fragile, and thus unsuitable for long term industrial use (Bucke C. et al., 1983; Buitelaar et al., 1996). Alginate is also vulnerable to dissolution in the presence of monovalent cations or chelators (Smidsrød & Skjåk-Braek, 1990), placing unrealistic limitations on potential feedstocks. Conversely, robust materials such as polyacrylamide are limited by potentially toxic monomers and adverse polymerisation conditions which compromise cell viability (Bucke C. et al., 1983).

One underexplored potential immobilisation material is a glycerol co-solvent poly vinyl-alcohol (PVA) cryogel. Cryo-gelation uses low temperature cycling to solidify an initially homogeneous liquid polymer solution. Hydrogels formed in this way avoid the use of toxic crosslinking agents, resulting in improved biocompatibility. The extensive physical interactions between hydrophilic polymer chains underlying the gel formation gives PVA cryogels a high mechanical strength (Holloway, Lowman & Palmese, 2013b), along with resistance to chemical and enzymatic degradation under typical culture conditions (Lozinsky, Zubov & Titova, 1996). PVA cryogels exhibit a porous structure (Lozinsky, 2009) which combined with high hydration levels presents minimal barrier to diffusion through the material. As a bulk industrial commodity, PVA is also a very low-cost material for immobilisation at less than 2 USD per kilogram (Alibaba.com, 2019).

PVA-based cryogels have been successfully applied to a variety of fermentation processes over the past few decades, most recently including phenolic degradation (See et al., 2015), and production of ethanol (Stepanov & Efremenko, 2017). However, the non-ideal optical

properties of conventional cryogels is a barrier to their use for photosynthetic applications. Typical PVA cryogels are functionally opaque, due to the occurrence of pores formed by frozen inclusions, which scatter light. Transparency can be induced by the addition of a polyol co-solvent, such as glycerol (Lozinsky et al., 1995), which potentially enhances the cryoprotectant effect of PVA itself (Wowk et al., 2000). While mechanisms for inducing transparency have been described since the late 1980s (Hyon, Cha & Ikada, 1989), exploration of transparent cryogels for the immobilisation of phototrophic bacteria has not yet been undertaken. Further, very little physical characterisation of PVA-glycerol cryogel matrices have been conducted to date as specifically pertains to bioprocess use, such as directly examining the mechanical resilience, long-term biocompatibility or productivity of organisms immobilised within the material with the ultimate objective of application to large-scale bioprocesses.

This article demonstrates the successful application of transparent PVA cryogels to photofermentation using the PNSB *Rhodospseudomonas palustris*, a stalwart of biohydrogen research owing to its robustness and extraordinary metabolic versatility (Harwood, 2008). Comprehensive investigation of the material properties showed ideal transparency, high biocompatibility, minimal resistance to diffusion of substrates, as well as excellent mechanical resilience which exceeded that of conventional cryogels after a single freeze-thaw cycle. These characteristics were further validated by batch cultures of cryogel-immobilised *R. palustris* which had higher hydrogen production rates which continued for longer than planktonic cultures, and long-term continuous production in excess of 67 days. Biohydrogen produced from organic waste has great potential as a future green energy source, and optimised immobilisation materials such as transparent PVA cryogels are necessary to coax maximum efficiency from photofermentation processes. Integration of such materials with new photobioreactor designs, along with metabolic engineering of the candidate organisms, has the potential to significantly advance the feasibility of photosynthetic bioprocesses towards commercial scales.

Table 4.1. Summary of key examples of materials applied to immobilisation of phototrophic bacteria.

Matrix material	Organism immobilized	Bio-compatibility	Transparency	Diffusion resistance	Mechanical stability	Chemical stability	References
Alginate	<i>Rhodopseudomonas palustris</i> Photosynthetic consortium <i>Chlorobium thiosulfatophilum</i> ¹	Good	Good	Good	<i>Poor</i>	<i>Poor</i>	Kim, Kim & Chang, (1990); Smidsrød & Skjåk-Braek, (1990); Fißler, Kohring & Giffhorn, (1995); Zhang et al., (2017)
Agar	<i>Rhodopseudomonas palustris</i>	Fair – Good	Good	Fair	<i>Poor</i>	<i>Poor</i>	Vincenzini et al., (1982); Bucke C. et al., (1983); Fißler, Kohring & Giffhorn, (1995)
Poly-acrylamide	<i>Rhodospirillum rubrum</i>	<i>Poor</i>	Good	Fair – Good	Good	Good	Hirayama et al., (1986); Tsygankov & Kosourov, (2014)
Carrageenan	<i>Rhodopseudomonas capsulata</i> <i>Rhodospirillum rubrum</i> <i>Rhodopseudomonas palustris</i>	Fair – Good	Good	Good	<i>Poor</i>	<i>Poor</i>	Francou & Vignais, (1984); Hirayama et al., (1986); Fißler, Kohring & Giffhorn, (1995)
Chitosan	<i>Rhodobacter sphaeroides</i>	Fair	Fair	Fair	Fair	Fair	Zhu et al., (1999)
Boric acid crosslinked PVA	<i>Rhodopseudomonas palustris</i> <i>Rhodobacter sphaeroides</i>	Poor – Fair	Good	Good	Good	Good	Nagadomi et al., (1999); Takei et al., (2012)
PVA cryogel	Various; non-photosynthetic	Fair – Good ²	<i>Poor</i>	Good	Good – Excellent ²	Excellent	Lozinsky & Plieva, (1998); Szczęśna-Antczak & Galas, (2001); Plieva et al., (2008); Mattiasson, (2014)
PVA-glycerol cryogel	<i>Rhodopseudomonas palustris</i>	Good	Good	Good	Excellent	Excellent ³	This study ³ Lozinsky, Zubov & Makhlis, (1996)

¹ Non PNSB (phototrophic green sulfur bacterium)² Depending on number of freeze-thaw cycles used to form hydrogel; increasing cycles sacrifice cell viability for material strength

4.4 Materials and Methods

All reagents used were of minimum reagent grade and purchased from Sigma-Aldrich unless otherwise stated. Atactic poly vinyl-alcohol (PVA) with approximate molecular weights ranging between 61 and 195 kDa and at least 98% hydrolysis (except 96% for the 95 kDa PVA) were used: Aldrich, Mowiol®: 61 kDa (10-98), 125 kDa (20-98) and 195 kDa (56-98); Scientific Polymer Products (NY, USA): 88 kDa (Cat# 362) and 95 kDa (#351); Polysciences Inc. (PA, USA): 78 kDa (Cat# 15130). 10% w/v aqueous solutions were prepared in either deionised water or 50% v/v glycerol by heating to ~95°C under magnetic stirring for 8 hours in capped reagent bottles to minimise evaporation.

4.4.1 Cryogel sample preparation

Hot (~60°C) PVA solutions were poured into either cubic silicone moulds (20 x 20 x 19 mm) or 3 mL polystyrene cuvettes and subjected to the indicated number of freeze-thaw cycles to form cryogels: cooling to -20°C for 12 hours, followed by thawing at ambient temperature for 4 hours. Cubes were washed 5 times in excess volume deionised water over at least 10 days to hydrate the cryogel and remove glycerol co-solvent.

4.4.2 Mechanical testing

A benchtop universal testing machine (Lloyd instruments) was used to determine the Young's Modulus (in the linear viscoelastic region) and yield stress of cryogel cubes at controlled room temperature (~20°C) under a constant unconstrained uniaxial compression rate of 20 mm.min⁻¹ (n ≥ 4). The modulus of resilience was calculated using the formula:

$$E_r = \frac{\text{Yield stress}^2}{2(\text{Young's Modulus})}$$

In samples which did not rupture below 95% strain, maximum stress was used as surrogate for yield stress.

4.4.3 Optical characterisation

The optical density of swelled PVA samples in polystyrene cuvettes (n = 4) with path length

of 1 cm was measured in scanning mode over a wavelength range of 450 to 900 nm in a UV-Vis spectrophotometer (Varian Cary 1E).

4.4.4 Diffusive properties

PVA cryogel cubes (~6 cm³) were equilibrated to desired substrate concentration with 5 changes of solution over at least 5 days (Glycerol: 120 mM, monosodium glutamate: 60 mM; high purity in deionised water). Cubes were pre-warmed to 35°C in the equilibration solution, blotted dry, measured to 0.1 mm accuracy and added to 40 mL distilled water in a sealed 100 mL temperature-controlled reactor at 35°C with magnetic stirring at 250 RPM. 200 µL samples were taken at intervals to measure effusion of substrate from the cubes. The diffusion coefficient was calculated by solving for the diffusion inside and flux out of the cube, where the cube was treated as a sphere with a diameter equal to the Sauter mean diameter of the cube. The diffusion coefficient was then regressed to the time series measurements of bulk concentration. Supplementary method details with sample calculations can be found in **Appendix 2**.

4.4.5 Bacteria and culture methods

Rhodospseudomonas palustris strain ATH 2.1.37 (NCIB 11774) was used for this study and grown in modified *Rhodospirillacea* minimal medium with 50 mM glycerol and 10 mM glutamate, as described in **Section 3.4.1**. Nitrogen-free media used for non-growing hydrogen production studies omitted yeast extract and glutamate. For rapid preparation of immobilisation biomass, Van Niel's Yeast Medium with 50 mM glycerol was used (VNG medium; 1 g K₂HPO₄, 0.5 g MgSO₄, 10 g yeast extract.L⁻¹). Cultures were streaked onto VNG agar plates to confirm absence of contaminating organisms before further use.

4.4.6 Photobioreactor setup

Cultures were grown in 500 mL test scale photobioreactors at 35°C, as described in **Section 3.4.2**. For long term continuous production studies, bioreactors were fed via precision-calibrated peristaltic pump and tubing with sterile, anaerobic nitrogen-free minimal medium containing 50 mM glycerol at a feed rate of 5 mL.h⁻¹, for a dilution rate of 0.01 h⁻¹. The

feedstock container (10 L borosilicate reagent bottle) was connected via sterile 0.2 µm PTFE filter to a 10 L PVF gas bag filled with argon gas to avoid entrainment of oxygen or nitrogen into the anaerobic, nitrogen-free bioreactors. Concurrently, waste media was removed at equal flow rate via a liquid sampling tube and peristaltic pump calibrated to precisely match the feed rate to maintain constant volume in the reactor.

4.4.7 *R. palustris* immobilisation

4-day cultures in VNG medium were centrifuged at 5000 x g for 15 min in 250 mL centrifuge bottles (Nalgene), washed twice with 100 mL aliquots of sterile PBS, each followed by 5 min. centrifugation. Cell pellets were weighed and resuspended in sterile 50% glycerol; bacterial biomass loading was calculated on a 1.5% wet cell weight: PVA volume basis (equating to 0.213% w/w dry cells: PVA) and the volume of 50% glycerol adjusted accordingly. 10 mL of bacterial suspension was dispersed evenly in 90 mL autoclaved 11% PVA-glycerol solution (previously melted and allowed to cool to 45°C) for a final PVA concentration of ~10%. The temperature of the mixture was held at 40°C with stirring to maintain sufficiently low viscosity while being dripped via peristaltic pump and sterile silicone tubing into liquid nitrogen to form beads 2 – 3 mm in diameter. Frozen beads were immediately transferred to sterile containers and stored at -80°C prior to use. A comprehensive immobilisation protocol is provided in **Appendix 6 (Protocol A)**.

For cultivation, beads were weighed, allowed to thaw completely at room temperature and washed twice in 500 mL aliquots of sterile phosphate buffered saline (PBS, pH 7) with 1 hour stirring to partially remove glycerol co-solvent and unbound cells on the surface of the beads. Anaerobic incubation in excess volume nitrogen-free media (without yeast extract) overnight at 35°C under illumination served to further remove the glycerol co-solvent without adversely affecting bacterial metabolic state and nitrogenase activity. 100 – 160 g of beads were loaded into each bioreactor with 400 mL of nitrogen-free media containing 50 mM glycerol as carbon source. Control bioreactors were inoculated with equal bacterial pellet weight as contained in the PVA beads (and from the same starting culture), resuspended in nitrogen-free medium to

prevent growth and additional biomass accumulation. At each timepoint 3 mL of medium was drawn, of which 1 mL was used for biomass quantification by optical density. The remaining 2 mL was centrifuged, the cell-free supernatant decanted and frozen at -20°C for later substrate quantification.

4.4.8 Microscopic imaging

To characterise the porous properties of PVA cryogels, fluorescent staining of the material was performed by forming the cryogel as a thin layer on microscope slides. 10 μL of warm PVA solution containing ~1% w/w wet pellet weight *R. palustris* was spread in a thin (<0.5 mm) even layer on a glass microscope slide and subjected to the minimum freeze-thaw cycles required to form a stable cryogel (PVA-glycerol: 1 cycle, PVA-water: 5 cycles) and washing in PBS (pH 7) at 4°C overnight. Slides were negatively stained with $0.5 \text{ ng}\cdot\text{mL}^{-1}$ fluorescein (Sigma-Aldrich) in PBS (pH 9.5) for 30 min in the dark, followed by brief rinsing with deionised water to remove unpermeated stain. Imaging was performed on a Zeiss LSM 780 confocal laser scanning microscope (CLSM) using a 63x/1.4 plan apochromat objective, with z-stack optical sectioning at 10 – 20 μm . Fluorescein negative staining showed areas of lower relative cryogel density with a green fluorescence signal, whereas *R. palustris* autofluorescence in red (600 – 750 nm) was visualised with excitation from a 405 nm laser.

4.4.9 Bacterial membrane integrity determination

Determination of cell membrane integrity in cultures of *R. palustris* before and after immobilisation was performed using differential fluorescent staining using propidium iodide (PI) and Syto9 (LIVE/DEAD BacLight™ bacterial viability assay, Thermofisher Scientific), with microscopic imaging by CLSM. For pre-immobilisation samples, 1 mL of a 3-day culture grown in VNG medium was centrifuged ($6500 \times g$, 5 min) and resuspended in PBS. 100 μL aliquots of cell suspension were stained with addition of PI and Syto9 to final concentrations of 30 and $0.334 \mu\text{M}$ respectively, followed by 10-minute incubation in the dark prior to imaging. Beads of PVA cryogel-entrapped cultures were collected after cultivation, rinsed in PBS and cut in half, followed by incubation in 2X staining solution ($60 \mu\text{M}$ PI, $0.668 \mu\text{M}$ Syto9

in PBS) for 10 min in the dark. Beads were placed cut-side down in an 8-well chambered cover glass for imaging (Nunc Lab-Tek™, ThermoFisher Scientific). A minimum of 3 beads/samples were imaged for each timepoint, with 4 randomly chosen fields of view each (which did not contain non-bacterial debris). 6-layer z-stacks were acquired for each field of view, at a depth of 1.3 µm per layer. For image analysis, sequential pairs of z-stack layers were exported as single maximum intensity orthogonal projections, with identical channel intensity settings for all images.

Cell counting was performed using the BioFilmAnalyzer tool (Bogachev et al., 2018). Settings for cell size range and threshold were determined by closely matching output to the values from manual counts performed on 4 sample images. Viability was assessed as the proportion of membrane-intact cells to total cells (intact and compromised), expressed as percentage.

4.4.10 Analytical

Culture growth was quantified by optical density at 660 nm and correlated to dry cell weight using a standard curve, as described in **Section 3.4.3**.

Glutamate concentration was determined by colorimetric ninhydrin assay (Mitsukawa, Shimizu & Nishi, 1971), modified by increasing ethanol concentration to minimise the effect of sample pH and to both enhance and stabilise chromophore formation. Briefly, 400 µL of 4 mM ninhydrin in absolute ethanol was added to 100 µL of 0.2 µm-filtered sample in 1.5 mL microfuge tubes and incubated in a water bath at 80°C for 15 min. 200 µL of each reaction, including standards, was pipetted in duplicate into a wells of a flat-bottom 96-well plate (Greiner) and absorbance read at 590 nm in a microplate reader (ELx800, BioTek instruments) within 30 minutes. A sample standard curve is shown in **Appendix 5**.

Glycerol was quantified by HPLC and gas composition by GC, both as described in **Section 3.4.3**. One- or Two-way ANOVA followed by Tukey's or Sidak's multiple comparisons tests respectively was used to determine statistical significance at $p < 0.05$. Significance level is indicated by ****: $p < 0.0001$; ***: $p < 0.001$; **: $p < 0.01$; *: $p < 0.05$; ns: not significant. Error bars indicate SD or SEM and sample size (n) is given for each figure.

4.5 Results and discussion

4.5.1 Transparency of cryogels for use with phototrophic organisms

In order to develop a matrix with high light transmittance for photosynthetic organisms, the relationship between the concentration of glycerol in the solvent and the transparency of resultant PVA cryogels was determined (**Figure 4.1A-C**). Light transmittance increases suddenly above 40 vol % glycerol in all wavelength ranges between 450 and 900 nm (**Figure 4.1B**), which correspond closely to photosynthetically active ranges for most microorganisms. Near infrared (NIR) radiation is particularly important for PNSB relying on bacteriochlorophylls, owing to their evolutionary adaptation to aquatic sediment microenvironments (Oda et al., 2008). Transparency in this band between 700 and 900 nm is especially high for solvent systems exceeding 40% glycerol (**Figure 4.1A**), likely due to the reduced attenuation potential of longer wavelengths of light. While light attenuation resulting from concentrations between 40 to 60% were uniformly low, there was a statistically significant optimum concentration of 50%.

As hypothesised by Hyon et al. (Hyon, Cha & Ikada, 1989), transparency is induced when phase separation is prevented by depression of the freezing point of the system. This effect was clearly seen in cryogels in the frozen state, with only samples of less than 40% glycerol showing frozen inclusions (**Figure 4.1C**), which in turn is supported by the reported freezing points for glycerol solutions. In pure water-glycerol systems in the range of 40 and 60% v/v glycerol concentration, freezing occurs at -16°C to -34°C (Lane, 1925); low enough to prevent significant phase separation under the cryogelation temperature employed (not accounting for the presence of PVA). At temperatures above -20°C , rate of phase separation via spinodal decomposition (a form of liquid-liquid phase separation) exceeds the rate of PVA crystallisation, leading to a non-homogeneous material (Takeshita et al., 2002). Tuning the solvent properties of water with increasing amounts of glycerol likely allows widespread crystallisation between PVA chains to occur (Lozinsky et al., 1995), but concurrently limits crystallite size. Smaller, more numerous PVA crystallites thus minimises scattering of light,

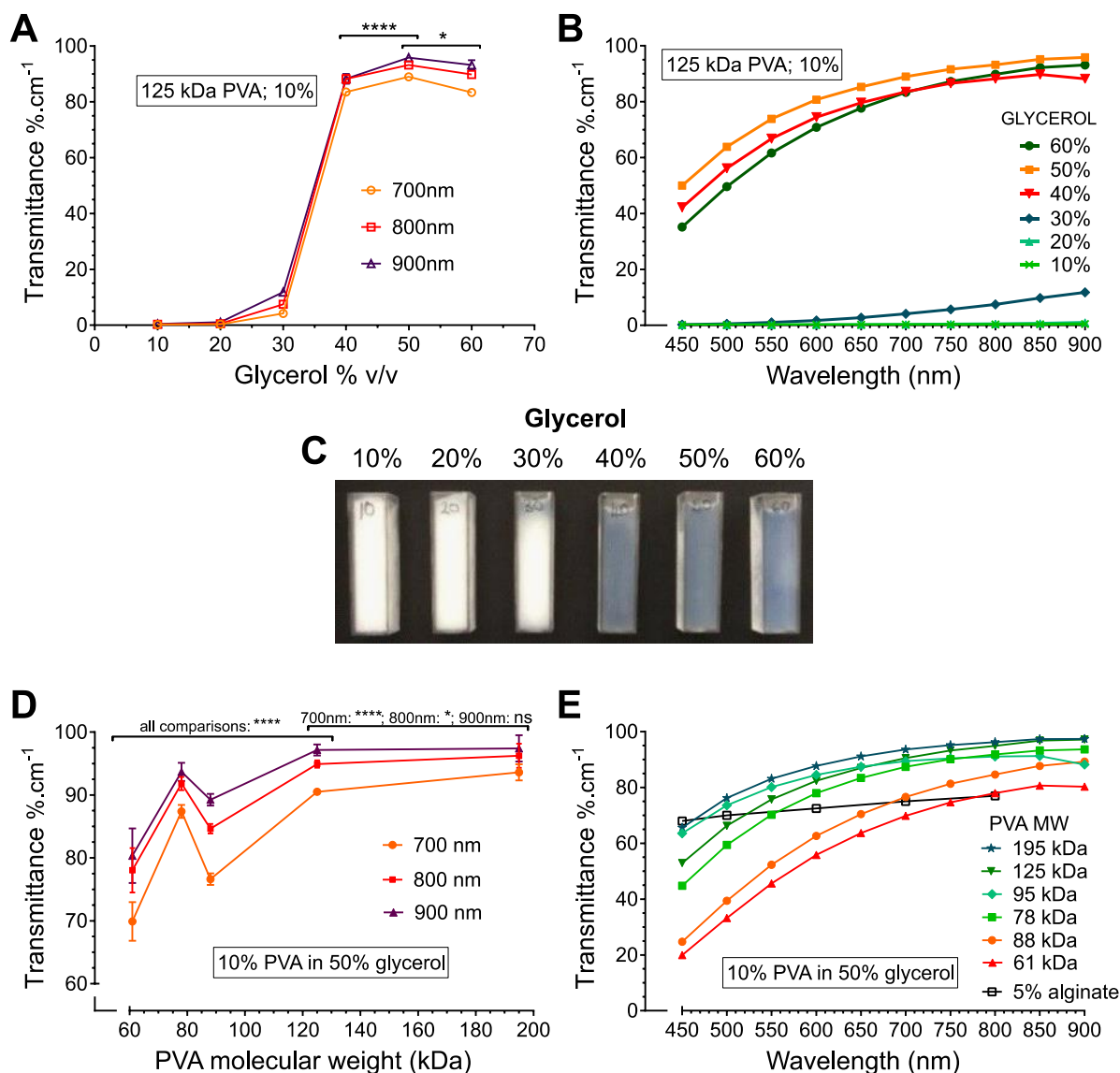


Figure 4.1. Influence of cryogel composition on material transparency.

Effect of glycerol co-solvent concentration (**A–C**) and PVA molecular weight (**D, E**) on cryogel transparency was characterised. Light transmission quantified in the near-infrared (**A, D**), and overall photosynthetic wavelength ranges (**B, E**) in 10% w/v PVA cryogel after 1 freeze-thaw cycle. PVA samples in cuvettes frozen at -20°C show changes in opacity relating to glycerol concentration (**C**). Light transmission in 5% Ca-alginate gel films included in panel **E** for comparison from Pereira et al. (2013). Data shown is the average of 4 samples, with error bars representing SD. Statistical significance for One-way ANOVA with Tukey's multiple comparison indicated by ****: $p < 0.0001$; *: $p < 0.05$.

resulting in a stable and optimally transparent gel.

Interaction between PVA chains underlies the physical gelation mechanism for cryogels, with longer chains having a higher cross-linking potential. The effect of PVA molecular weight on

transparency was thus investigated (**Figure 4.1D, E**). All molecular weights of PVA tested showed good light transmission, particularly in the critical near-infrared wavelength range between 700 and 900 nm (**Figure 4.1D, E**). Light transmission in this range was typically superior to 5% calcium alginate hydrogels (Pereira et al., 2013), the most widely-studied immobilisation material for photosynthetic applications due to its transparency (Smidsrød & Skjåk-Braek, 1990).

A trend of transparency increasing with PVA molecular weight was seen (**Figure 4.1E**), but was slightly obfuscated by the relatively low specification in terms of hydrolysis of the PVA used ($\geq 98\%$) and the complex interplay between the factors affecting the physical gelation process and the resultant optical properties. With increasing degree of hydrolysis, the overall hydrogen bonding capacity of the polymer increases significantly. Between 95 and 100% hydrolysis, hydrogen bonding capacity increases by approximately 30%, leading to preferential interactions between PVA chains over those with water (Ping et al., 2001). Subtly lower degrees of hydrolysis would appreciably reduce the rate of crystallite formation, thus shifting the equilibrium towards phase separation in advance of extensive gelation and subsequently impacting material homogeneity.

While ideal transparency is important for photosynthetic bioprocesses, using widely available inexpensive industrial grades of PVA would not greatly impact the optical properties of the gel or its suitability as an immobilisation matrix. PVA with both a higher degree of hydrolysis and molecular weight is preferable for optimal transparency, as long as solution viscosity remains practical for the immobilisation procedure. High PVA molecular weights result in solutions with commensurately high viscosity, which complicates the dripping procedure used in this study to form cryogel beads. A balance between such practical considerations and ideal optical properties should be found for the particular protocol employed, and recommendations will be discussed.

In the NIR wavelength range, all except the lowest of the PVA molecular weights tested exhibited acceptable transparency for use with photosynthetic bacteria (**Figure 4.1E**). Since the ultimate thickness of the matrix would be on the order of a few millimetres to avoid limiting

diffusion of solutes within the material (Tsygankov & Kosourov, 2014), the matrix would offer insignificant impedance to incident light in contrast to other materials which are functionally opaque.

4.5.2 Mechanical properties of transparent cryogels for bioprocess use

Industrial application of immobilisation matrices will require high material resilience to withstand shear stresses and abrasion present in bioreactor environments, both for long term production and reuse of the biocatalyst. As cryogel structure and integrity is dependent on the number freeze-thaw cycles it is subjected to, the compressive strength characteristics of conventional (water solvent) and transparent (50% glycerol co-solvent) cryogels were determined after single and multiple freeze-thaw cycles (**Figure 4.2**), as an indication of how well these materials will fare in mechanically challenging bioreactor environments.

Values of Young's Modulus, a measure of the elastic compressibility or stiffness of the material, demonstrated a very elastic and compliant material with the transparent cryogels exhibiting marginally lower levels of stiffness (**Figure 4.2A**) and thus resilience (**Figure 4.2B**) than conventional cryogels, but nonetheless remained high. While all PVA molecular weights in both solvent systems formed stable cryogels after 6 freeze-thaw cycles, forming stable conventional PVA cryogels after a single freeze-thaw cycle was not feasible, and only the 88 kDa samples formed very diffuse gels with low fracture stresses of less than 70 kPa (**Figure 4.2C**).

Higher molecular weights of PVA would be expected to increase cryogel strength due to the higher propensity for interactions between polymer chains as their average length increases. However, there was no clear trend of resilience increasing with molecular weight (**Figure 4.2B**). PVA gelation is a complex, multifactorial process depending on the intrinsic properties of the sample used. Factors include not only molecular weight and degree of hydrolysis as discussed previously, but also the specific polymer stereoregularity, polydispersity of chain

CHAPTER 4: Transparent poly vinyl-alcohol cryogel as immobilisation matrix for phototrophic bacteria

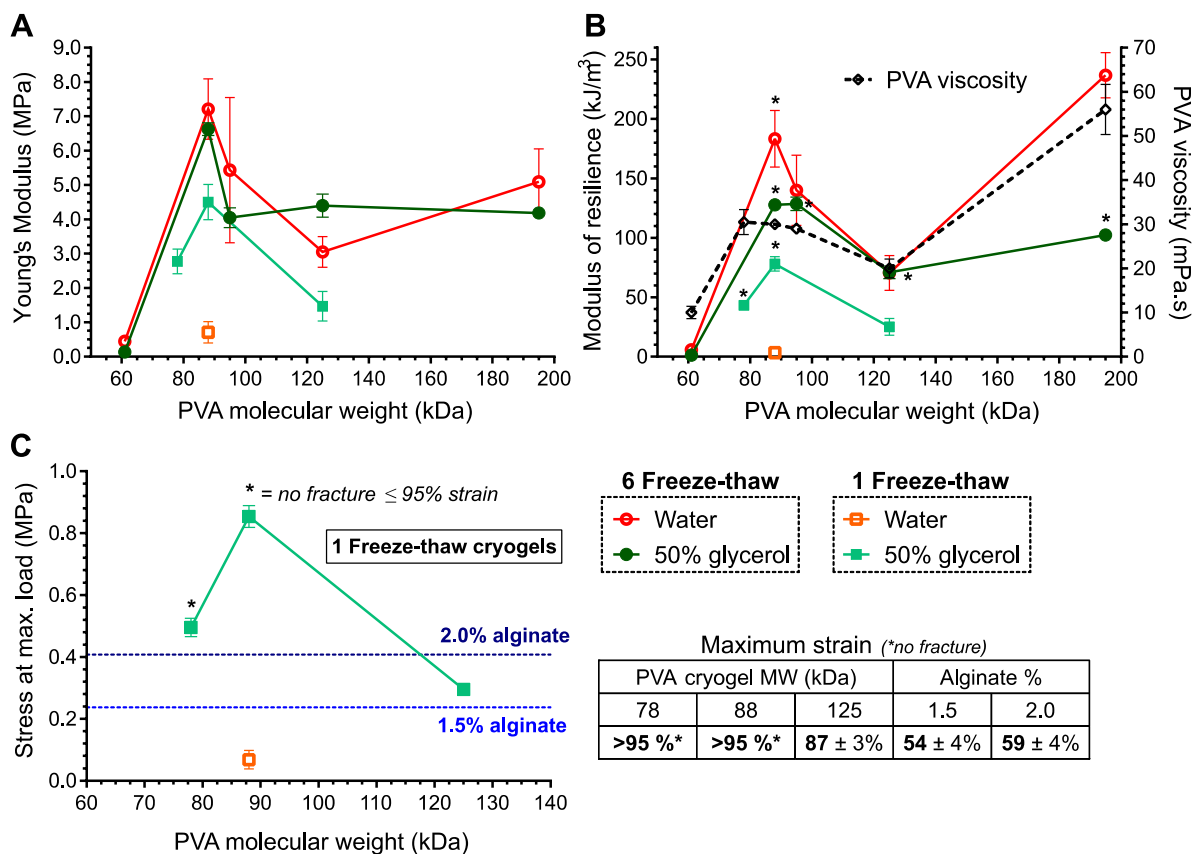


Figure 4.2. Compressive characteristics of cryogels comprised of PVA with varying molecular weights.

Cryogels formed from 10% w/v PVA solution in either 50% v/v glycerol (transparent) or pure water (conventional). 4 – 8 samples were used to determine average Young's Modulus (compressive modulus, **A**), modulus of resilience (**B**) and load under maximum stress (**C**) after the indicated number of freeze-thaw cycles (FT). Standard dynamic viscosities (4% solution, 20°C) from manufacturer's specifications for PVA samples tested show correlation to cryogel resilience (**B**). Reference fracture stresses and strains indicated for 1.5 (Mancini, Moresi & Rancini, 1999) and 2% alginate hydrogels (Fu et al., 2011) (**C**). Error bars represent SD. Data not shown for samples which did not form stable cryogels under specified conditions (1FT, transparent 95 and 195 kDa; 6FT: 78 kDa were not investigated).

length and both the thermal history and degree of dissolution of the PVA in solution (Alves et al., 2011). As reported by Lozinsky et al, increasing polymer chain length also seems to be hindrance to efficient interchain interactions, since the concomitantly increasing viscosity in solutions of higher molecular weight PVA constrains mobility during the gelation process (Lozinsky et al., 2007). Similarly, higher cryogel strength was reported for 86 kDa PVA samples compared to 115 and 66 kDa, closely replicating the local optimum seen here at 88

kDa. Modifying PVA concentration was thus seen as a better tool for controlling cryogel properties in place of increasing molecular weight beyond this balancing point for intermolecular interaction propensity. In turn, comparison of manufacturer specifications for the PVA samples used showed a degree of correlation between standardised dynamic viscosity values and the resilience of the cryogel formed (**Figure 4.2B**). While these single-point values do not reflect the intrinsic viscosity properties of the PVA sample, which would provide better prediction of material properties via more comprehensive rheological characterisation (Bercea, Morariu & Rusu, 2012), they provide a rough guide for selection of suitable PVA samples. Standard viscosity values in the range of 30 mPa.s were shown to offer acceptable cryogel strength while maintaining sufficient solution fluidity to facilitate the formation of cryogel beads via the dripping method used in this study.

As in the case of inducing transparency, the presence of the glycerol co-solvent is again advantageous for cryogel integrity. During the gelation process, lowering temperature constrains molecular mobility and facilitates crystallite formation as long as the system remains in solution (Hassan & Peppas, 2000). At the point of freezing, further crystallite formation is inhibited and thus the extent of gelation is dependent on cooling rate up to the freezing point. Depression of the freezing point of solutions containing glycerol allows optimal crystallite formation independent of cooling rate, since the freezing point is reached more slowly (or not at all). In the absence of sophisticated control of freezing rate, conventional PVA-water solutions thus require multiple freeze-thaw cycles to allow widespread crystallite formation to form stable gels.

Synergistically, the kosmotropic effect of glycerol further reinforces the gel structure by favouring physical bonding between polymer chains over polymer-solvent interactions, significantly increasing both gel strength and thermostability (Lozinsky et al., 1995; Kolosova et al., 2018). Here the transparent cryogels offer an advantage in terms of simplicity of immobilisation protocol and minimising deleterious impact on entrapped cells. While conventional cryogels exhibited slightly higher resilience and thus robustness to deformation

than transparent gels after multiple freeze-thaw cycles (**Figure 4.2B**), yielding a strong material after a single freeze thaw cycle is a significant advantage for microbial immobilisation. Successive cycles of varying temperature are detrimental to living cells, so minimising such adverse process conditions to a single freeze-thaw cycle would best preserve the viability of entrapped organisms as explored further in **section 4.5.5**. We thus focused exclusively on the single freeze-thaw cycle transparent cryogels for further characterisation. These cryogels compared favourably to alginate gels (**Figure 4.2C**) since both fracture stress and strains reported for 1.5 (Mancini, Moresi & Rancini, 1999) and 2% alginate (Fu et al., 2011) were much lower than those resisted by single freeze-thaw transparent cryogels. At 95% strain, 88 kDa cryogels withstood at least double the fracture stress of 2% alginate which failed at only ~60% deformation.

Indeed, the resilience shown reflects only the bare minimum values, as the majority of samples did not actually fracture below the very high maximum strain of 95% investigated here (**Figure 4.2C**). Single-freeze-thaw cycle 88 kDa transparent cryogels withstood in excess of 10 such compressions with no significant change in Young's Modulus or maximum stress (data not shown). These conditions exceed forces likely present under even very vigorously mixed bioprocess conditions, and no discernible degradation of the PVA beads was seen after multiple-month use under constant robust agitation.

Transparent cryogels are thus demonstrably extremely robust materials, outperforming conventional cryogels by realising these properties after single freeze-thaw cycles, and thus showing promise for even non-phototrophic bioprocesses where maximum viability of entrapped entities is required or desirable with the additional benefit of a faster, simpler procedure.

4.5.3 Morphological differences between conventional and transparent cryogels

A hallmark of conventional PVA cryogels is a macroporous structure (Lozinsky, 2009), which in turn underlies the opacity of the material. Transparent cryogels are conversely less porous in nature, allowing high transmittance of photosynthetically active wavelengths of light. A

technique was thus devised employing confocal microscopy to image conventional and transparent cryogels negatively stained with fluorescein in order to reveal subtle differences in cryogel density indicative of porosity. These results further support the hypothesis that transparency is due to the formation of a homogeneous, monolithic, material. Imaging of gels in such a way in the native hydrated state avoids sample preparation artefacts introduced by alternative techniques such as scanning electron microscopy (SEM), which tends to collapse gel structure during the requisite freeze-drying process (Fergg, Keil & Quader, 2001) and obfuscated the subtle morphological differences between the cryogel types studied here.

In **Figure 4.3A**, porosity can be inferred from the relative concentration of the staining agent, while **Figure 4.3B** shows a much more uniform (and therefore non-porous, and monolithic) staining. The conventional gel shows porosity clearly resulting from phase separation, with high density PVA crystallites surrounded by low density features running through the gel represented by higher fluorescein fluorescence (**Figure 4.3A**). This morphology corresponds

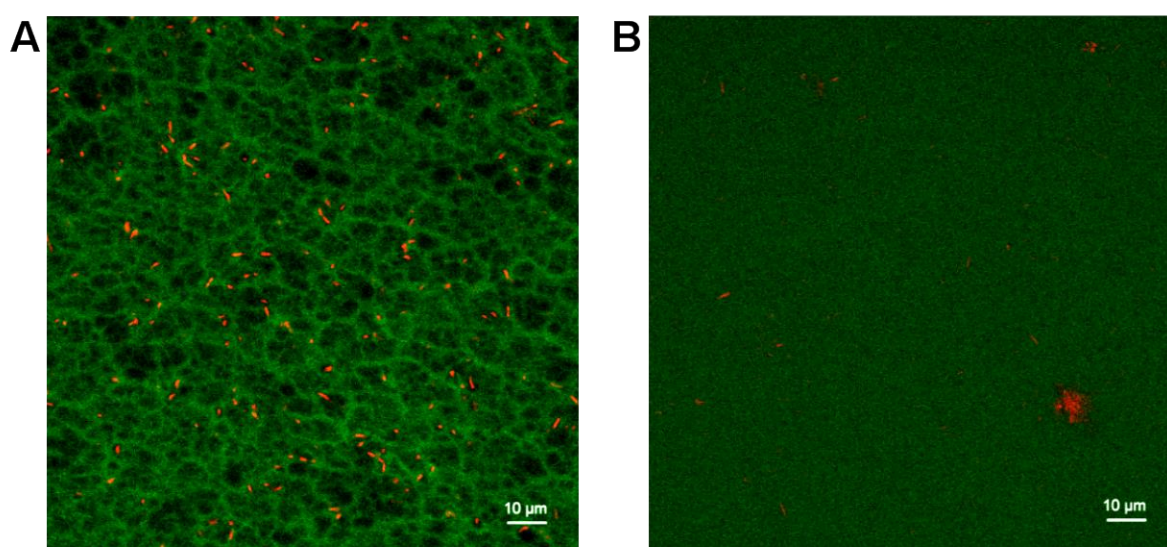


Figure 4.3. Confocal laser scanning microscopy (CLSM) visualisation of pore structure in different PVA cryogels.

Cryogels formed from 10% w/v PVA (88 kDa) in water (**A** - conventional) and 50% glycerol (**B** - transparent), with immobilised *R. palustris*. *R. palustris* autofluorescence is represented in red; negative staining with fluorescein shows lower densities of cryogel in increased green fluorescence intensity. Optical sections taken 30 – 40 µm from gel surface. Images acquired and processed identically, with contrast increased for visibility.

well to previous studies of conventional PVA cryogels (Holloway, Lowman & Palmese, 2013b). In contrast, the transparent cryogel shows uniform staining (**Figure 4.3B**) indicative of homogeneous gel density, or at least microporosity not visible using optical methods.

The resolution limit of the confocal microscopy technique used is around 0.5 μm ; any potential pores present smaller than this would still facilitate mass transport (Hamngren Blomqvist et al., 2015). Conversely, in the highly hydrated hydrogel matrix comprising around 90% water, porosity may not confer a major advantage in terms of ease of diffusion.

4.5.4 Diffusive properties of cryogels

The reduction in porosity in transparent cryogels may affect the diffusion characteristics of the material, since at first impression macroporous gels may seem to be at advantage in terms of permeability. However, porosity is not always directly correlated to diffusivity since the degree of tortuosity of the structure significantly affects mass transport (Mota, Teixeira & Yelshin, 2001); and indeed, in hydrogels diffusion through the gel is not nearly as limited as diffusion through other solids in which porosity is an important factor (such as activated carbons). In order to determine the contribution of macroporosity to the apparent diffusivity in cryogels, diffusion studies were performed by measuring effusion of glycerol and glutamate from cryogel cubes (**Figure 4.4**). These substrates are representative carbon and nitrogen sources commonly used for *R. palustris* cultivation and present a range of solute molecular weights at around 92 and 146 kDa respectively. Glycerol is an attractive substrate for biohydrogen production, and is abundant due to the worldwide glut as a waste product of biodiesel manufacture (Pott, Howe & Dennis, 2013).

Effective diffusion coefficients of both glycerol and glutamate in **Figure 4.4** showed no significant difference between conventional and transparent cryogels, indicating an apparent lack of influence of gel macroporosity. The measured diffusivity of glycerol is also in good agreement with published values for aqueous diffusion coefficients in infinite sink systems, at $10.6 \times 10^{-6} \text{ cm}^2 \cdot \text{s}^{-1}$ (Haynes, Lide & Bruno, 2016), which represents a high relative diffusivity

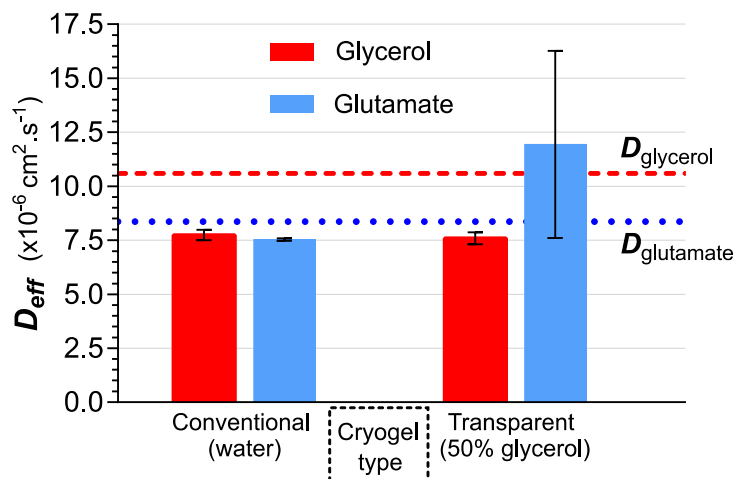


Figure 4.4. Characterisation of diffusive properties of PVA cryogels for bioprocess applications.

Diffusion of glycerol and glutamate (candidate substrate molecules) in conventional and transparent PVA cryogels quantified at 35°C, in terms of the effective diffusion coefficient, D_{eff} (A). Reference aqueous diffusion coefficients, D , are indicated by labelled dotted lines. Error bars represent SD of 2 independent replicates.

of 72% (expressed as the ratio of effective to standard aqueous diffusion coefficients). Glutamate diffusion (Figure 4.4) followed a similar trend of close correspondence to aqueous diffusion rates of $8.36 \times 10^{-6} \text{ cm}^2 \cdot \text{s}^{-1}$, albeit measured at 10°C lower and under infinite sink conditions (Ribeiro et al., 2014). Alginate, the mainstay of immobilisation matrices for its excellent permeability, has a relative diffusivity of 86% at 5% polymer concentration (Garbayo, León & Vílchez, 2002). A similar relationship was seen for a range of common carbon sources in 2% alginate hydrogels, with an average relative diffusivity of around 85% (Øyaas et al., 1995). Alginate thus offers only modestly higher permeability than the 10% PVA cryogels characterised here. Indeed, it would seem that the highly hydrated nature of the material presents minimal obstacle to passive mass transport through the material, as supported by studies of glucose diffusion in conventional cryogels, which showed very similar relative diffusion rates (Ariga, Kubo & Sano, 1994). This permeability is likely further enhanced by the swelling of the material upon removal of the glycerol co-solvent and the expansion of the gel matrix following cryogelation (Lozinsky, Zubov & Titova, 1996). Despite possessing differing molecular weights, effective diffusion coefficients for glycerol and

glutamate were not significantly different (**Figure 4.4**). Hydrodynamic radius of the diffusing molecule is more relevant to its mobility than simple molecular weight, and the structures of glycerol and glutamate suggest little difference in this respect although this could not be confirmed due to lack of reported experimental values. PVA cryogels are highly hydrophilic due to the abundance of hydroxyl groups projecting from the polymer backbone, thus the degree of hydrophilicity of the substrate molecule would likely contribute additional influence on diffusion rates through the matrix, perhaps warranting further investigation beyond the scope of the tests performed here.

From a process perspective, the high relative diffusion rates in transparent cryogels would likely result in minimal impact on substrate availability. For reference the aquaglyceroporin GlpF, responsible for glycerol transport in *Escherichia coli*, with homologs in *R. palustris* (Simmons et al., 2011), has a maximum predicted diffusion rate of $3.0 \times 10^{-6} \text{ cm}^2 \cdot \text{s}^{-1}$ (Hénin et al., 2008); or roughly half the diffusion rate through the hydrogel matrix, making transport *into* the cell slower than transport to the immobilised cell. PVA cryogels thus offer attractive mass transport properties for bioprocess use, at a similar scale as ideally permeable immobilisation materials, with the added advantages of excellent robustness and good transparency.

4.5.5 Assessment of PVA immobilisation procedure on cell viability

Exposure to low temperature has the potential to adversely affect cell viability, since formation of ice crystals can rupture cell membranes resulting in cell death. Diminished catalytic activity associated with loss of viability of entrapped bacteria is therefore a possible drawback for an immobilisation matrix formed by cryogelation. The proportions of cells with intact and compromised cell membranes was thus determined before and after immobilisation, shown in **Figure 4.5**. A ~6% drop in membrane integrity to 89% was seen in immobilised bacteria following 24-hour cultivation, from a maximum of 95% pre-immobilisation, suggesting a negligible impact on cell viability. A full cross-section through a PVA bead in **Figure 4.6** further demonstrates even distribution of intact viable cells

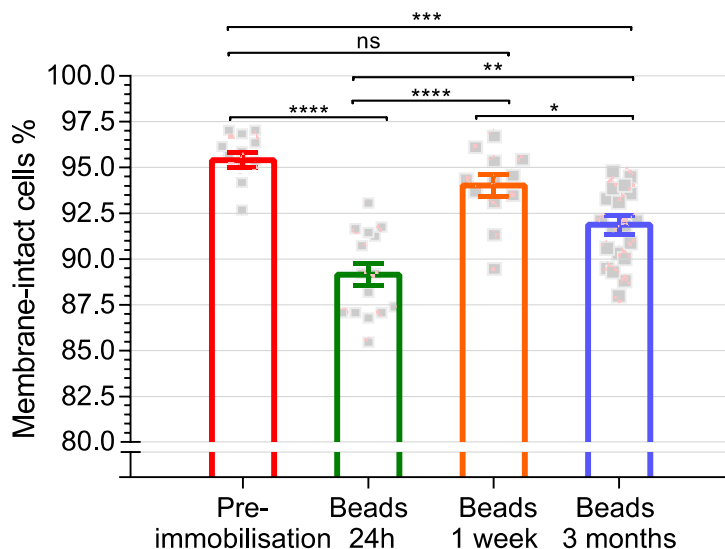


Figure 4.5. Characterisation of biocompatibility of PVA cryogels for bacterial immobilisation.

Cell viability was compared before and after immobilisation in PVA cryogel beads under continuous cultivation (**B**). Cell-membrane integrity is used as proxy for cell viability, expressed as percentage intact cells:total cells as measured by LIVE/DEAD staining and CLSM. Error bars represent SEM for minimum of 3 samples with 3 – 4 images each; datapoints shown as grey symbols. Statistical significance for One-way ANOVA with Tukey's multiple comparison indicated by ****: $p < 0.0001$; ***: $p < 0.001$; **: $p < 0.01$; *: $p < 0.05$; ns: not significant.

throughout the material, with slight non-homogeneity resulting from manual mixing of the cell suspension into the PVA solution prior to immobilisation.

Since cryoinjury occurs from ice formation both within and outside the cell, cryoprotectants are typically used to prevent damaging ice formation when cells are frozen for storage (Fowler & Toner, 2006), mediated by their colligative properties depressing the freezing point and thus reducing the propensity for ice crystal formation throughout the system. This echoes the role of the glycerol co-solvent in inducing cryogel transparency; hence, glycerol serves double duty by additionally reducing cell damage during the immobilisation process. Indeed, this protective effect extended further to the integrity of the cryogel beads formed by the immobilisation procedure employed here. Conventional PVA-water solutions fractured violently upon freezing in liquid nitrogen, likely due to large shear stresses in the material occurring during rapid crystallisation, further compromising bacterial integrity and requiring slower alternative freezing techniques (Lozinsky & Plieva, 1998).

The rapid freezing induced by dripping into liquid nitrogen, aided by the presence of glycerol, results in vitrification of the PVA beads and the cells contained within them. This glassy, amorphous state results from the rapid increase in viscosity precluding crystallisation, further limiting cryoinjury to cells (Taylor, Song & Brockbank, 2004). Upon warming, this vitreous state of the cells is vulnerable to crystal formation as temperatures increase and molecular mobility returns. PVA has shown promise as an alternative cryoprotectant due to its ability to inhibit ice recrystallisation at low concentrations (Inada & Lu, 2003), and this property potentially acts in synergy with the glycerol co-solvent to enhance the biocompatibility of the PVA cryogelation process.

Following cultivation, the proportion of membrane-intact entrapped cells rebounded to 94% after 1 week (**Figure 4.5**), suggesting that the majority of membrane damage resulting from the freezing process was not fatal, and that cells were able to recover completely to pre-immobilisation levels. Indeed, the disruption in membrane integrity represented by positive staining with propidium iodide (PI) does not necessarily equate to cell death, leading to underestimations of true overall cell viability (Rosenberg, Azevedo & Ivask, 2019). Here, the recuperation after membrane damage seems to support this observation. Notably, the recovery occurred while cultivated in minimal medium and without a nitrogen source, and entrapped cells showed only a 2% decrease in observable viability after 3 months of continuous culture under 24h illumination (**Figure 4.5**). These observations further confirm both the resilience of *R. palustris* (Harwood, 2008), and the biocompatibility of both the immobilisation process and the PVA cryogel material itself, making this technique well-suited for long-term photofermentation.

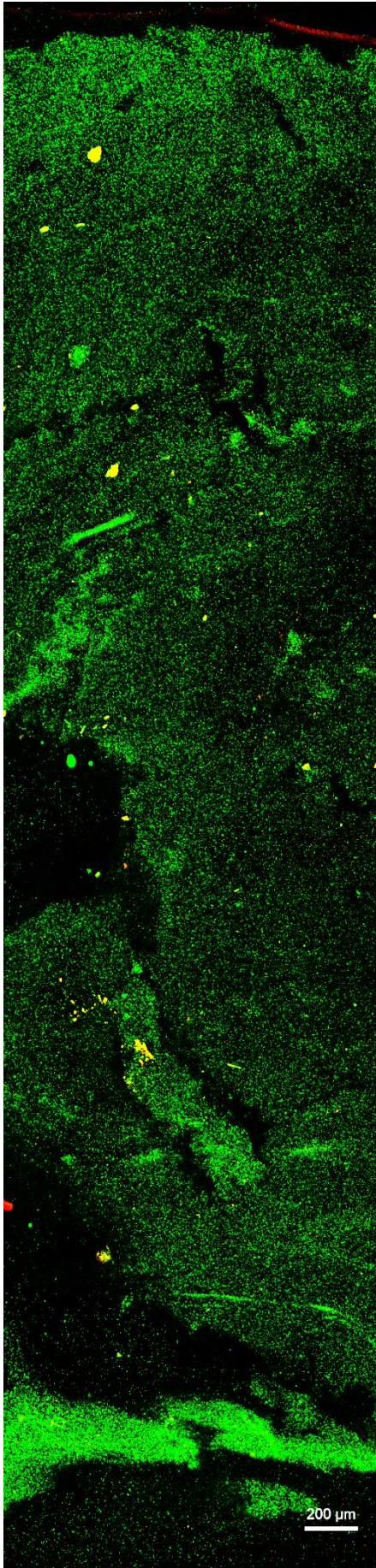


Figure 4.6. CLSM micrograph of LIVE/DEAD stained *R. palustris* entrapped in PVA cryogel bead.

Image presents entire cross-section through centre of a single PVA cryogel bead following 24 hour cultivation in minimal media under illumination. Membrane-intact cells are represented by green fluorescence (Syto9) and membrane-compromised cells in red (propidium iodide). Yellow inclusions are non-bacterial debris as artefact of immobilisation process. Image contrast enhanced for visibility equally across all channels.

4.5.6 Phototrophic bio-hydrogen production by PVA cryogel-entrapped *R. palustris*

To verify the utility of the transparent PVA cryogel as an immobilisation matrix for photosynthetic bacteria, biohydrogen production using immobilised and planktonic cultures of *R. palustris* were compared in test-scale bioreactors in batch mode with identical biomass loading (**Figure 4.7A**). Nitrogen-free media was used to maintain cells in non-growing state to allow comparison of bacterial activity from a stable, directly-comparable biomass complement free from the additional energy sink of cell replication. The non-growing state of planktonic cultures was confirmed by monitoring biomass concentration, along with levels of biomass leakage from the PVA beads (**Figure 4.7B**). Constant, negligible concentrations of planktonic biomass in the immobilised reactors confirmed robust and stable entrapment of cells within the matrix, an advantage over alternative immobilisation materials with large pores with consequently lower stability which are prone to biomass loss (Tanaka, Irie & Ochi, 1989). Immobilised *R. palustris* showed a modestly higher total hydrogen productivity compared to control cultures, suggesting a lack of any detrimental effect of the cryogelation procedure on cell viability and activity (**Figure 4.7A**). This is consistent with the analysis of post-immobilisation membrane integrity in the previous section, confirming that no discernible metabolic damage was inflicted by cryogelation. In addition, immobilised cultures displayed a higher maximum specific hydrogen production rate at $8.0 \text{ mL}\cdot\text{g}^{-1}\cdot\text{h}^{-1}$, compared to $5.1 \text{ mL}\cdot\text{g}^{-1}\cdot\text{h}^{-1}$ (**Figure 4.7A**; $p < 0.0001$). Analysis of glycerol showed a higher initial concentration for immobilised cultures, likely from residual efflux of glycerol co-solvent from the PVA cryogel (**Figure 4.7C**). A short 24-hour washing step was used to equilibrate the cryogel beads before the start of the batch culture to allow accurate comparison to planktonic cultures (see methods section 4.4.7), leading to a higher initial glycerol concentration due to residual glycerol remaining from the immobilisation procedure. The rate of glycerol consumption following the initial 24 hours of batch culture, however, was indistinguishable statistically between the groups, suggesting equilibration of glycerol concentration within and outside the beads and thus equivalent accessibility of glycerol substrate to both culture types. This lack of apparent mass transport limitation to immobilised cells (**Figure 4.7C**) was

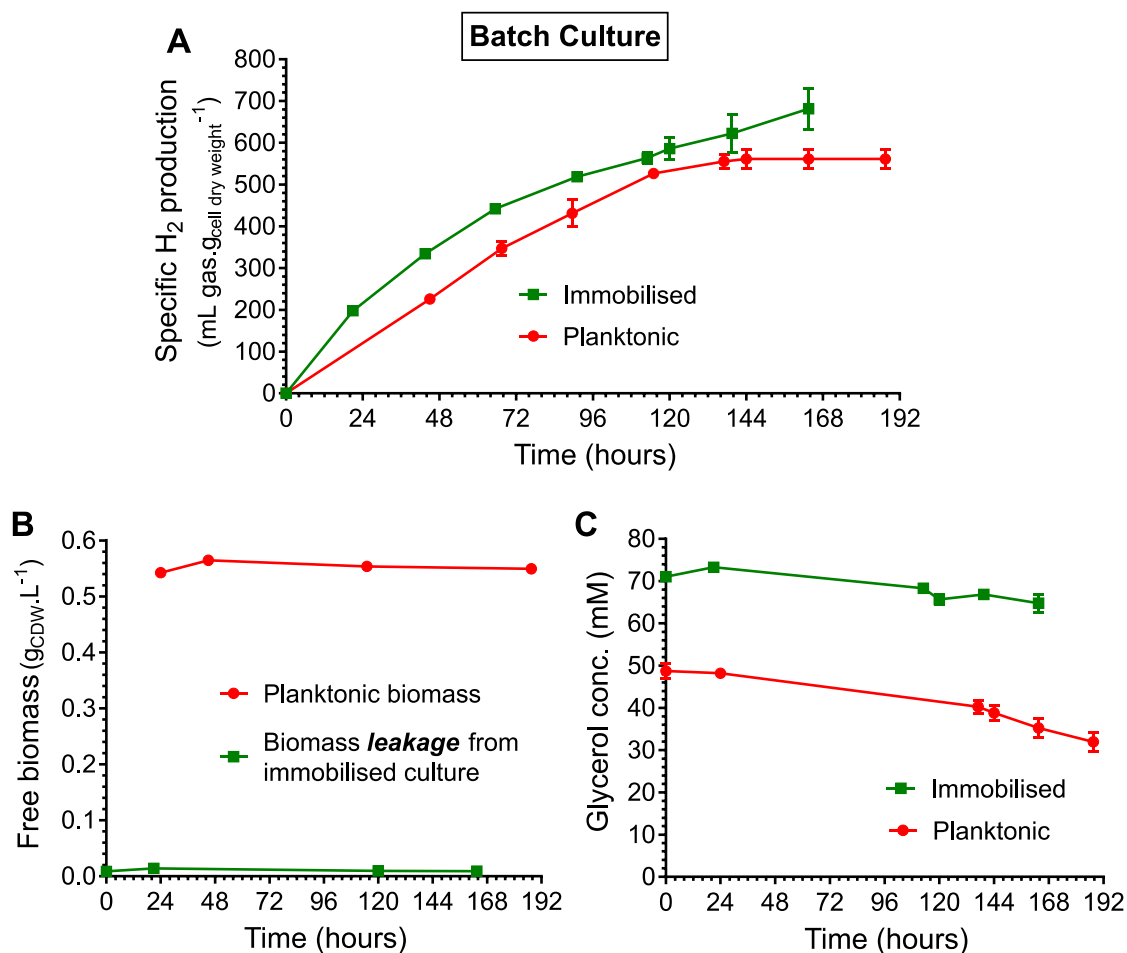


Figure 4.7. Phototrophic hydrogen production by non-growing PVA-immobilised *R. palustris* in batch mode.

Nitrogen-free minimal media with 50 mM glycerol was used for cultivation under illumination in test bioreactors. Hydrogen volume was normalised to biomass in reactor, reported as specific hydrogen production (A). Equal biomass was loaded into planktonic and immobilised reactors at the start of the experiment and concentration was tracked to confirm lack of growth and to monitor cell leakage from PVA beads (B). Glycerol concentration was measured to track carbon consumption (C). Error bars represent SD for minimum 3 replicate reactors.

supported by the glycerol diffusion experiments (Figure 4.4). For industrial applications, the presence of the glycerol co-solvent as a fermentable substrate within the immobilisation matrix would indeed likely be advantageous to foster maximal post-freezing recovery of cells. Extensive washing of the beads would therefore not be required before use as in the case of alternative transparent cryogels employing toxic DMSO as the co-solvent (Takeshita et al., 2002).

Hydrogen production from immobilised cells continued for a longer period than planktonic cultures (**Figure 4.7A**), which all but ceased after 6 days perhaps due to accumulation of deleterious waste materials, although the exact cause was not determined. Increased productivity of immobilised PNSB in terms of both rate and duration has been widely reported, and forms part of the rationale for this work. Vincenzini et al described sustained hydrogen productivity from organic acids continuing for at least 60 hours in agar-immobilised cultures, compared to 25 hours in suspension (Vincenzini et al., 1982). Fißler et al similarly reported that immobilised *R. palustris* produced hydrogen from toxic aromatic acids for longer periods than planktonic cultures (Fißler, Kohring & Giffhorn, 1995), suggesting a potential protective effect against adverse conditions offered by immobilisation. Further supporting the suitability of the cryogel matrix, entrapment within the PVA beads shows no evidence of practical limitation in terms of availability of light to drive the bioconversion process. This reinforces the observations made from the diffusion studies, and the favourable light transmission properties of the material. Although substrate diffusion and light penetration are not likely to be the rate limiting steps in the hydrogen production pathway (Hallenbeck & Benemann, 2002), the suitability of transparent PVA cryogels for photofermentation is further established.

Since long-term productivity is a key goal for immobilised bacteria, PVA-entrapped *R. palustris* was subjected to continuous non-growing cultivation in three test bioreactors fed with 50 mM glycerol in nitrogen-free media at a constant dilution rate of 0.01 h^{-1} , with varying quantities of PVA beads loaded and under axenic and non-axenic conditions, as seen in **Figure 4.8**. Hydrogen production was sustained for at least 45 days in all three reactors. The longest sustained production was seen for the lowest bead loading of 100 g (**Figure 4.8, i**), which produced hydrogen at an initial rate of 127 decreasing to 53 $\text{mL.g}_{\text{CDW}}^{-1}.\text{day}^{-1}$. Hydrogen evolution continued for at least 67 days, at which point the supply of sterile media was exhausted, representing minimum sustained productivity of over 2 months from a stable pool of catalytic biomass. Higher bead loading of 160 g resulted in a higher specific production rate of 154 $\text{mL.g}_{\text{CDW}}^{-1}.\text{day}^{-1}$ being maintained over 34 days (**Figure 4.8, ii**), followed by tapering off

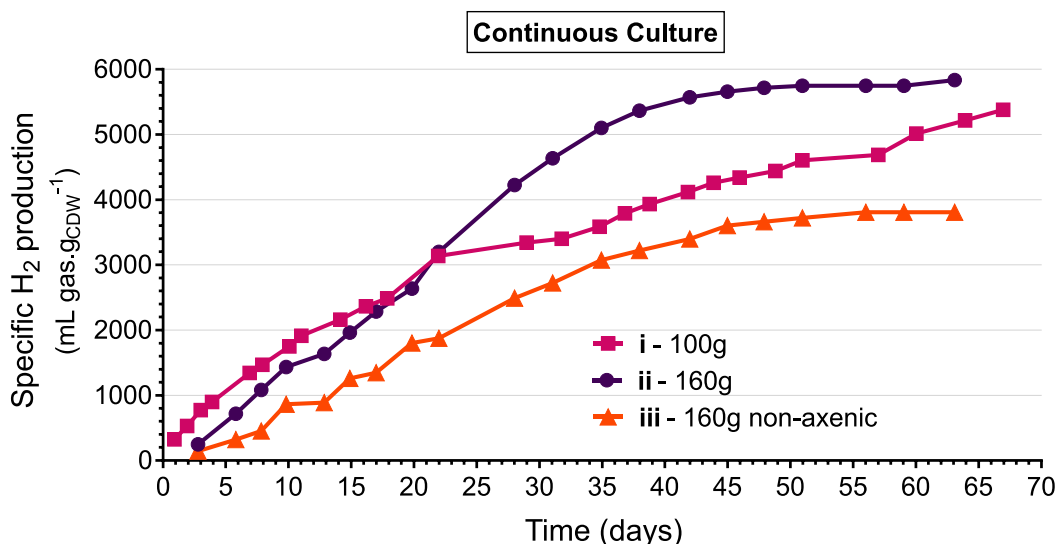


Figure 4.8. Phototrophic hydrogen production by non-growing PVA-immobilised *R. palustris* in long-term continuous mode.

Nitrogen-free minimal media with 50 mM glycerol used for cultivation under illumination in test bioreactors, fed continuously at a dilution rate of 0.01 h⁻¹. Varying quantities of PVA beads were loaded into single reactors under both axenic (i: 100 g, ii: 160 g) and non-axenic conditions (iii: 160 g). Hydrogen volume was normalised to immobilised biomass in reactor, reported as specific hydrogen production.

in hydrogen evolution. Under non-axenic conditions, average production rate decreased to 94 mL.g_{CDW}⁻¹.day⁻¹ (**Figure 4.8, iii**), likely due to competition from contaminating organisms for the available carbon. The presence of these non-PNSB organisms was detected as a white cloudiness in the culture medium and were speculated to be *Bacillus* species, which are common culture contaminants capable of glycerol utilisation. However, production in this reactor continued for a similar time period, indicating a similar performance duration for commercial-scale processes which will likely use non-sterile feedstocks to reduce input costs with the goal of reaching economic feasibility.

Interestingly, the viability of entrapped bacteria after 3 months of continuous culture remained high at 92% intact cells (**Figure 4.5**); a drop of 3% from pre-immobilisation. Cessation of hydrogen production was therefore seemingly not due to cell death but rather another metabolic cause, perhaps relating to the absence of a nitrogen source for continued enzyme production, or the low dilution rate used which may have caused nutrient limitation

due to the long hydraulic retention time (HRT). While these production rates are average in context of benchmark values of up to $45 \text{ mL.g}^{-1}.\text{h}^{-1}$ for batch culture achieved in literature (Tsygankov & Khusnutdinova, 2015), they do compare favourably to alginate immobilisation studies where maximum production rates of $3.7 \text{ mL.g}^{-1}.\text{h}^{-1}$ were reported (Fißler, Kohring & Giffhorn, 1995). The simple test bioreactor system used here is non-optimised in terms of light penetration, so does not likely reflect limitations on the part of the cryogel immobilisation matrix itself but rather the bioreactor configuration, which is the subject of ongoing improvement. HRT also has a significant influence on hydrogen production rate (Zagrodnik et al., 2015), and since the long 100-hour HRT investigated here was chosen to maximise glycerol conversion and the feasible duration of the experiment, there is much potential for improvement at the expense of lower substrate conversion. The long-term productivity facilitated by immobilisation in PVA cryogels, combined with the excellent resilience of the material, advance the candidacy of these materials for large-scale photo-bioprocess use.

4.6 Conclusion

In summary, this work posits transparent PVA cryogels as an ideally suited immobilisation material for phototrophic bacteria. The addition of 50% glycerol as a co-solvent induces optimal transparency in normally opaque cryogels by reducing ice crystal formation and fostering gel homogeneity, with an added cryoprotective effect, which preserves the viability of entrapped bacteria, visualised here *in situ*. The material displays high mechanical strength and durability, which is attractive for industrial-scale bioprocesses. Due to the reinforcing effect of the glycerol co-solvent these properties are achieved after a single freeze-thaw cycle, presenting a distinct advantage over conventional cryogels, which require multiple cycles and extending applicability beyond phototrophic processes. Diffusion studies show minimal barrier to movement of common substrates such as glycerol and glutamate through the matrix, despite the abolition of macropores in the transparent cryogel. Biohydrogen production by photofermentation with entrapped *R. palustris* continued for longer periods than equivalent planktonic cultures, and continuous cultivation yielded productivity for at

least 67 days, demonstrating the long-term applications of PVA cryogel immobilisation. The combination of these positive characteristics and the low cost of materials makes transparent PVA cryogels attractive for the advancement of industrial-scale biohydrogen production, as well as new photo-bioprocesses exploiting the unique capabilities of phototrophic bacteria.

4.7 Acknowledgments

We would like to thank Lize Engelbrecht of the Stellenbosch University Central Analytical Facility (CAF) for assistance with CLSM, Jaco van Rooyen and Levine Simmers for HPLC and analytical advice, and Dr Tobias Louw for assistance in regressing the diffusion parameters. This work was supported by funding from the Water Research Commission (WRC) of South Africa.

4.8 Author contributions

Declaration by the candidate:

With regard to Chapter 4, the nature and scope of my contribution were as follows:

Nature of contribution	Extent of contribution (%)
Conceptualisation Methodology Investigation Data analysis & Visualisation Writing & Editing	90%

The following co-author has contributed to Chapter 4:

Name	e-mail address	Nature of contribution	Extent of contribution
Robert W. M. Pott	rpott@sun.ac.za	Conceptualisation & discussion Review & Editing	10%

Signature of candidate: Jan-Pierre du Toit Date: 29 January 2021

Declaration by co-author:

The undersigned hereby confirm that

1. the declaration above accurately reflects the nature and extent of the contributions of the candidate and the co-authors to Chapter 4,
2. no other authors contributed to Chapters 4 besides those specified above, and
3. potential conflicts of interest have been revealed to all interested parties and that the necessary arrangements have been made to use the material in Chapters 4 of this dissertation.

Signature	Institutional affiliation	Date
Robert W. M. Pott	Stellenbosch University	29 January 2021

Declaration with signatures in possession of candidate and supervisor

CHAPTER 5

EXPRESSION OF ALTERNATIVE NITROGENASES IN *RHODOPSEUDOMONAS PALUSTRIS* IS ENHANCED USING A NOVEL GENETIC TOOLSET FOR RAPID, MARKERLESS MODIFICATIONS

Adapted from:

Jan-Pierre du Toit, David J. Lea-Smith, Anna Git, John R. D. Hervey, Christopher J. Howe,
Robert W. M. Pott.

Submitted September 2020 & currently undergoing revision after peer review
for publication in *ACS Synthetic Biology*.

The majority of the work in this chapter was performed during a 5-month research visit to the University of Cambridge, UK (March to August 2018), under the guidance of our collaborator Professor Christopher Howe in the Department of Biochemistry.

As such, the author list of this paper reflects the significant contributions made to the project in terms of methodology, advice and mentorship I received during this time. All work described is my own, and the individual contributions made to the article by each author are detailed at the end of the chapter.

5.1 Context

Metabolic engineering is a powerful technique for redirecting innate cellular pathways to favour desired performance in a bioprocess, or to introduce heterologous pathways for synthesis of novel products. These modifications are necessary to improve productivity of the organism beyond inherent metabolic limitations confronted once process conditions have been comprehensively optimised, as explored in the previous two chapters. The work in this chapter thus addresses the current shortage of efficient genetic tools for chromosomal modifications in *R. palustris*. This is an obstacle to widespread study required for comprehensive understanding of regulatory mechanisms governing cell metabolism pertaining to efficient hydrogen production, as well as further development of the organism as a biotechnological platform for bioproducts suited to its unique metabolic capabilities. Applied to the native hydrogen-producing metabolism, these techniques will facilitate targeted modifications to extract maximal productivity in support of overall bioprocess feasibility. In this work, these tools were used to overexpress alternative nitrogenase enzymes with the potential to allow creation of hydrogen super-producing strains

5.2 Abstract

The phototrophic bacterium *Rhodospseudomonas palustris* is emerging as a promising biotechnological chassis organism, due to its resilience to a range of harsh conditions, a wide metabolic repertoire, and the ability to quickly regenerate ATP using light. However, realisation of this promise is impeded by a lack of efficient, rapid methods for genetic modification. Here, we present optimised tools for generating chromosomal insertions and deletions employing electroporation as a means of transformation. Generation of markerless strains can be completed in 12 days, approximately half the time for previous conjugation-based methods. This system was used for over-expression of alternative nitrogenase isozymes with the aim of improving biohydrogen productivity. Insertion of the *pucBa* promoter upstream of *vnf* and *anf* nitrogenase operons drove robust over-expression up to 4000-fold higher than wild-type based on transcriptomics, with similar expression of genes in the

putative operons. Transcript quantification was facilitated by an optimised high-quality RNA extraction protocol employing lysis using detergent and heat. Over-expression also resulted in increased nitrogenase protein levels, although no increase in hydrogen productivity was demonstrated in test-scale bioreactor studies, perhaps due to saturation of enzyme assembly machinery or inadequate supply of reducing equivalents. Nevertheless, robust heterologous expression driven by the *pucBa* promoter is attractive for energy-intensive biosyntheses suited to the capabilities of *R. palustris*. Development of this genetic modification toolset will accelerate the development of *R. palustris* as a biotechnological chassis organism, while insights into the effects of nitrogenase overexpression will guide future efforts in engineering strains for improved hydrogen production.

5.3 Introduction

The phototrophic purple non-sulfur bacterium (PNSB), *Rhodopseudomonas palustris*, is a model organism used to study anoxygenic photosynthesis (Roszak et al., 2003) and extracellular electron transport (Guzman et al., 2019). Due to its extraordinary metabolic versatility, capacity for carbon fixation and resilience against toxic heavy metals and aromatic or chlorinated compounds (Larimer et al., 2004), *R. palustris* is also emerging as a potential biotechnology platform for bioremediation (Idi et al., 2015), production of bioplastics (Ranaivoarisoa et al., 2019), and possibly bioenergy generation using microbial fuel cells (Call et al., 2017). The metabolic potential of *R. palustris* has thus far mostly been applied to biohydrogen production (McKinlay & Harwood, 2010a; Hallenbeck & Liu, 2016), since this native pathway shows potential for the generation of a clean energy source from a multitude of waste materials [extensively reviewed by Adessi, Corneli & De Philippis (2017)]. During anaerobic photoheterotrophic growth, light-derived ATP synthesis drives energy-intensive H₂ production, with reducing power derived from heterotrophic metabolism (Harwood, 2008). The ready supply of ATP and electrons creates a conducive cellular energy state which has also been co-opted for the production of a wide variety of products, including methane (Fixen et al., 2016) and butanol (Doud et al., 2017). The ability of *R. palustris* to produce

abundant ATP under anaerobic phototrophic conditions also renders it a useful platform for production of redox- or oxygen-sensitive compounds and intermediates. Concomitantly, the challenges of adequate oxygenation of the aerobic organisms typically employed for demanding biosyntheses are avoided.

Hydrogen production in *R. palustris* is the obligate consequence of fixation of atmospheric nitrogen to ammonia, mediated by nitrogenase complexes. Due to the high energetic cost in terms of ATP and electrons for this reaction, expression and activity of this pathway is under strict control. Tight transcriptional repression and inactivation of nitrogenases by post-translational modification occurs, while fixed nitrogen remains available to the cell (Heiniger et al., 2012b). Despite possessing three nitrogenase isozymes, only the molybdenum-containing nitrogenase Nif is expressed under most nitrogen-fixing conditions. The alternative nitrogenases, Vnf and Anf (enzymes with vanadium and iron-only co-factors respectively), are expressed only under extreme nitrogen starvation (Heiniger & Harwood, 2015). Altering expression of these complexes shows promise for enhancing hydrogen productivity since the reaction stoichiometries of Vnf and Anf favour a 2- and 4-fold respectively higher rate of hydrogen production per unit of ammonia than Nif (Oda et al., 2005b). In the absence of N₂, energy efficiency is enhanced since ATP and electrons are directed solely to proton reduction, and thus stoichiometric yield of H₂ is increased 4-fold (McKinlay & Harwood, 2010a). Under these conditions, a further doubling in hydrogen production rates was observed in strains of the PNSB *Rhodobacter capsulatus* expressing Anf instead of Nif (Eady, 1996; Schneider et al., 1997). Additionally, since nitrogenases exhibit notoriously low catalytic rates of approximately 6 reactions per second (Yang et al., 2016), maximising gene expression and thus the total pool of nitrogenase could potentially boost hydrogen production (Oh et al., 2013; Mohanraj et al., 2019).

The potential of *R. palustris* as a biotechnology platform has been hampered by a lack of standardised, efficient engineering methods to rapidly generate both unmarked gene deletions and insertions, which are necessary for repeated genetic manipulation. Knockouts

have been widely constructed using a variety of systems, but inserted genes have been mostly limited to transient heterologous expression on non-native plasmids with non-optimised wide host range promoters and requiring antibiotics for maintenance (Xu et al., 2016; Zhai et al., 2019). Native, stably maintained plasmids have been isolated from *R. palustris* and developed as expression vectors (Inui et al., 2000). However, these have shown poor expression performance in reporter assays when compared to non-native plasmids (Doud et al., 2017). Long-term, stable expression would be better achieved by chromosomal integration with cassettes under the control of strong promoters, along with the ability to repeatedly manipulate diverse genes within the organism without the persistence of selection markers. Genomic insertions have only sporadically been reported (Rey, Heiniger & Harwood, 2007; Hirakawa et al., 2012; Jackson et al., 2018); thus we aimed to develop a rapid, reliable and versatile recombination-based genetic modification technique tailored to *R. palustris*, with the aim of metabolic engineering of the hydrogen synthesis pathway to enhance productivity. In order to circumvent innate control over alternative nitrogenase expression, we replaced native promoters upstream of the *vnf* and *anf* gene operons to generate over-expressing strains. The techniques developed allow for robust and rapid genetic modification of *R. palustris*, both in terms of insertions and deletions. Under ideal conditions, unmarked modified strains can be generated in 12 days, allowing for multiple loci to be modified in quick succession. Together, these tools advance the utility of *R. palustris* as a biotechnological chassis organism, allowing users to exploit the unique capabilities of this organism for innovative applications.

5.4 Methods

5.4.1 Media and culture conditions

Rhodopseudomonas palustris strain CGA009 was routinely cultured using Van Niel's Yeast medium (VNG) for fast growth and recovery during genetic manipulations, as described in **Section 4.4.5**. Growth and expression studies were conducted in modified Rhodospirillacea minimal medium (as in **Section 3.4.1**), with 50 mM glycerol and either 10 mM glutamate or 0.3% w/v additional yeast extract as the nitrogen source. These conditions allow for expression and function of the native Nif nitrogenase (nitrogen-fixing conditions). For non-nitrogen fixing conditions, 5 mM urea was used as nitrogen source, which avoids culture pH disturbances caused by more commonly-used ammonium salts. Vanadium for Vnf nitrogenases was supplied as NaVO₃ at a final concentration of 165 nM, equimolar to molybdenum provided in the trace element solution. Cultures were incubated at 35°C, under illumination from 100 W incandescent light bulbs for anaerobic liquid cultures and in the dark for aerobic agar plates. Irradiance intensity was calibrated in the wavelength range 500 – 1100, as described in **Section 3.4.2**. Cultures were verified as axenic using VNG agar plates to confirm absence of contaminating organisms before each experiment.

Screening of growth media for transformants was performed using YP agar (0.3% yeast extract, 0.3% peptone, 1.5% agar), tryptone soy agar (TS; BD Bacto), and nutrient agar (NA; Merck). Defined mineral medium (PM) was used as described by (Rey & Harwood, 2010).

E. coli NEB5 α (New England Biolabs) was grown in Luria Bertani (LB) medium at 37°C, with 50 $\mu\text{g}\cdot\text{mL}^{-1}$ kanamycin as required.

5.4.2 Plasmid construction

The genome sequence of *R. palustris* CGA009 (Larimer et al., 2004) was consulted via the Ensembl database (bacteria.ensembl.org). Candidate promoters were identified as the upstream intergenic sequences of *pucBa* (LH2 beta chain A; RPA2654; 350 bp) and *cisY* (Citrate synthase; RPA2907; 150 bp), referred to as the *puc* and *cit* promoters. Promoters and ~1 kb regions flanking the desired insertion site directly upstream of the target gene start codon (or

ribosome binding site –21 bp from the start codon for *vnf* modifications) were amplified by PCR using Phusion high-fidelity polymerase (Thermo Scientific) with supplied GC buffer and 3% DMSO to optimise performance on GC-rich *R. palustris* gDNA template. Primers were designed using the NEBuilder tool (nebuilder.neb.com; New England Biolabs) to generate PCR fragments suitable for Gibson assembly (Gibson et al., 2009) with minimum 30 bp overlaps, and are detailed in

Table A3.1. Promoter sequences were assembled between the 5' and 3' flanking regions in order to precisely target the insertion. In the case of *vnf* promoter-substitution strains, a maximum diversity codon-optimised sequence of the *vnfH* gene was generated using the Kazusa codon-usage database (kazusa.or.jp/codon/) to reduce homology to the native *vnfH* gene (*vnfH_{opt}*; sequence provided in **Appendix 3**). This fragment was synthesised by GeneArt (Thermo Scientific) and PCR amplified to be co-assembled downstream of the promoter in order to create a unified single operon. PCR products were purified by gel electrophoresis and extraction using the PureLink Quick Gel Extraction Kit (Invitrogen). Promoter and flanking fragments were then assembled into *Bam*HI/*Xba*I-digested pK18*mobSacB* (Schäfer et al., 1994) with the NEBuilder High-Fidelity DNA Assembly Cloning Kit (New England Biolabs) with a 90-minute incubation, followed by cloning into *E. coli* NEB5 α and blue-white screening for successful constructs. Component PCR fragments and final assembled plasmids were verified by Sanger sequencing before use (DNA Sequencing Facility, University of Cambridge). Plasmids used are detailed in **Table 5.1**.

5.4.3 Optimised *R. palustris* transformation and markerless strain generation

Electrocompetent cells were prepared from 50 mL log-phase cultures (OD₆₆₀: 0.3 – 0.6) grown in VNG medium. Cultures were chilled on ice for 10 min and centrifuged (4000 *g*, 4°C, 10 min), followed by 3 washes with 50 mL ice-cold 10% glycerol and final resuspension in 0.5 – 1 mL 10% glycerol. Cells were either used immediately or quick frozen on dry ice and stored at –80°C. No discernible difference in transformation efficiency was observed for frozen cells compared to those prepared from fresh cultures. Approximately 500 ng plasmid DNA was

Table 5.1. Plasmids used in this study

Plasmid	Description	Reference
pK18 <i>mobSacB</i>	Km ^r , <i>sacB</i> suicide vector	Schäfer et al. (1994)
pK18 <i>nif:puc</i>	pK18 <i>mobSacB</i> containing <i>puc</i> promoter targeted for in-frame insertion upstream of <i>nifH</i>	This study
pK18 <i>nif:cit</i>	pK18 <i>mobSacB</i> containing <i>cit</i> promoter targeted for in-frame insertion upstream of <i>nifH</i>	This study
pK18 <i>vnf:puc</i>	pK18 <i>mobSacB</i> containing <i>puc</i> promoter targeted for in-frame insertion upstream of <i>vnfH</i> ribosome binding site (-21 bp from start codon)	This study
pK18 <i>vnf:cit</i>	pK18 <i>mobSacB</i> containing <i>cit</i> promoter targeted for in-frame insertion upstream of <i>vnfH</i> ribosome binding site (-21 bp from start codon)	This study
pK18 <i>anf:puc</i>	pK18 <i>mobSacB</i> containing <i>puc</i> promoter targeted for in-frame insertion upstream of <i>anfH</i>	This study
pK18 <i>anf:cit</i>	pK18 <i>mobSacB</i> containing <i>cit</i> promoter targeted for in-frame insertion upstream of <i>anfH</i>	This study
pK18Δ <i>glnK2</i>	pK18 <i>mobSacB</i> containing <i>glnK2</i> 266 bp in-frame deletion construct (genome position 302318–302584)	Laing (2018)

mixed with 100 μ L electrocompetent cells in a pre-chilled 1 mm electroporation cuvette (VWR), electroporated (2.0 kV, 600 – 800 Ω , 25 μ F), followed by immediate addition of 1.8 mL ice-cold VNG medium and incubation on ice for 5 min. Cells were allowed to recover during overnight 18-hour incubation at 30°C under incandescent light (80 – 100 W.m⁻²) and subsequently plated on VNG agar with 200 μ g.mL⁻¹ kanamycin. Comprehensive protocols for electrocompetent cell preparation (**Protocol C**) and electro-transformation (**Protocol D**) are provided in **Appendix 6**.

Kanamycin-resistant transformants were promptly genotyped by colony PCR using GoTaq G2 DNA polymerase (Promega) and primers spanning and within the insertion site to confirm the presence of a single homologous recombination event. Screening of colony PCRs was rapidly performed by capillary electrophoresis using a QIAxcel Advanced system with DNA high-resolution kit (Qiagen). Confirmed single-recombination clones were cultured in 15 mL VNG medium for 2 days and plated on 10% sucrose VNG agar to select for double recombination events. Sucrose-resistant colonies were screened for kanamycin sensitivity and genotypes of resultant unmarked knock-in strains were verified by PCR using primers

flanking and within the insertion region (Table 5.2). Sequencing of the amplicon confirmed correct insertion of the promoter construct.

Table 5.2. Genotyping PCR Primers used in this study

Primer	Sequence (5' – 3')	Expected PCR product size (bp)		
		WT	<i>puc</i>	<i>cit</i>
Spanning	> primers span insertion regions	WT	<i>puc</i>	<i>cit</i>
GT Nif Fwd	AGCAAGGCGAGGGATGGTTGG	348	706	498
GT Nif Span Rev	TCTTCCACCGAACCCGCTTCC			
GT Anf Fwd	AAGGATGGCGAGGCGATGGATC	212	570	362
GT Anf Span Rev	GAGGATCAGGCGGGTCGAGTC			
GT Vnf Fwd	GGTCGTCTCAGCCGCCTCAG	167	1416	1208
GT Vnf Span Rev	TGGTCGGCGCGTTTGAAGCTG			
Internal: promoter specific	> all use spanning fwd primer		<i>nif</i>	
GT Int Puc Rev	TTGGGAGCTGCTGGGCCAAG	–	233	–
GT Int Cit Rev	CTTGCGAGCGAGACTGGTTGT	–	–	240
			<i>anf</i>	
		–	156	163
Internal: <i>vnfH_{opt}</i> specific			<i>vnf</i>	
GT Vnf Int Rev	CAGCCGACGATGAGGATCTTCTGG	–	499	349
<i>vnf</i> insertion orientation check	> fwd in <i>vnfH</i> , rev in 3' beyond insertion flanking region (<i>vnfD</i>)			
GT-Orient Vnf Fwd	CTCAACAGCAAGCTCATCCATTTTCG	–	1498	1498
GT-Orient Vnf Rev	TGAAGATCACGTCCGGCTTGAC			
<i>nif</i> + <i>anf</i> orientation check	> PCR product only if correctly inserted			
GT-Orient Puc Fwd	GTCCACAATAAAGCGGCCCAAC			
GTR-Orient Cit Fwd	CGCCAGCGCTTCAAGACAAC			
GTR-Orient Nif Rev	CCGGTGGTGCCCTTGTAGTAG		1479	1382
GTR-Orient Anf Rev	GTGGCGCAGGTCTGGTAGATC		1478	1381
Knockout		WT	Knockout	
GT glnK2 span Fwd	CGCTGATTCCGAAATGATTC	555	288	
GT glnK2 span Rev	GCCGTAGGGACGTTTGAA			
GT glnK2 int Fwd	TGGCGATCATTAAGCCATTC	205	–	
GT glnK2 int Rev	GTCTTCTCGACCTGCTCGTT			

5.4.4 Electroporation procedure refinement

Initial tests of electroporation parameters affecting transformation efficiency in *R. palustris* were performed using a pK18*mobSacB* plasmid targeting a deletion in RPA1309. This gene is a transposase pseudogene, which is thought to be frameshifted and incomplete, and thus inactivation is unlikely to have a deleterious effect on cell viability. 60 μL mid-log electrocompetent cells (prepared as above from culture OD_{660} : 0.3) were transformed with 250 ng of plasmid DNA in 1 mm electroporation cuvettes. Following electroporation (1.5 – 2.5 kV, 200 – 1000 Ω , 25 μF), 1 mL of either ice-cold or prewarmed SOC medium was added and samples were allowed to recover for 90 min at 37°C, before plating on YP agar plates with 100 $\mu\text{g}\cdot\text{mL}^{-1}$ kanamycin and incubation at 30°C. Protocol refinements leading to the highest transformation efficiencies are reflected in the optimised procedure above.

5.4.5 Optimised RNA isolation

Each strain was inoculated in triplicate from a 3-day preculture into 50 mL of Minimal medium supplemented with 0.3% yeast extract and 50 mM glycerol in completely-filled 25 cm^2 transparent polystyrene cell culture flasks (solid cap; Nunc, Thermo Scientific) at a starting OD_{660} of 0.05. Cultures were grown anaerobically at 35°C with shaking under 80 – 100 $\text{W}\cdot\text{m}^{-2}$ illumination (500 – 1100 nm) from incandescent lightbulbs for 48 hours ($\text{OD}_{660} < 3$). RNA was isolated in duplicate from 1 mL aliquots of each culture, with the remainder kept for protein extraction. Samples were chilled on ice and cells harvested by centrifugation (14000 g , 4°C, 5 min). The pellets were snap frozen in liquid nitrogen and stored at –80°C until further processing. Cell pellets were lysed by resuspension in 55 μL 2% SDS in RNase-free Tris-EDTA (TE) buffer (pH 8; Invitrogen) with incubation at 65°C for 20 minutes followed by thorough mixing with 640 μL TRI Reagent (Sigma-Aldrich). After 15 minutes of agitation, samples were centrifuged to pellet cell debris (20000 g , 10 min.). RNA was purified from the supernatant using the Direct-Zol RNA miniprep kit (Zymo Research) with on-column DNase digestion for 30 minutes, and 2-minute incubation prior to final elution. This method allows isolation of RNA directly from TRI reagent, obviating the chloroform phase separation normally required

and thereby minimising both complexity and the number of sample handling steps. The optimised protocol for RNA isolation is given in **Appendix 6 (Protocol E)**.

RNA quantity and purity were determined by UV spectrophotometry (NanoDrop 1000, Thermo Scientific). RNA integrity was rapidly assessed using 1% agarose TBE bleach gels (Aranda, LaJoie & Jorcyk, 2012) before further use and storage at -80°C . 5 μL containing 150 ng of each RNA sample were pre-incubated with 5 μL 2X formamide RNA loading buffer at 65°C for 5 minutes to denature RNA secondary structure followed by snap cooling on ice prior to electrophoresis. Densitometry of gel images was performed using the GelQuant program (Rehbein & Schwalbe, 2015).

Procedures tested during optimisation and not forming part of the final isolation procedure are described in the legends of **Figure 5.4** and **Figure 5.5**.

5.4.6 Gene expression analysis by RT-qPCR

A total of 300 ng of RNA from each sample was used for cDNA synthesis using SuperScript IV VILO Mastermix with EZDNase (Invitrogen) containing both oligo d(T) and random hexamer primers. This input quantity was optimal to ensure linearity of the RT step (Minshall & Git, 2020). Reverse transcription was performed at 65°C to minimise secondary structure interference due to the GC-rich template. Linearity of RT-qPCR was verified using a titration of a pool of input RNAs, which was also used to rule out gDNA contribution (RT-).

Quantitative PCR (qPCR) primers (**Table 5.3**) were designed using OligoArchitect (Sigma-Aldrich) with a target T_m of 66°C , strictly avoiding primer and cDNA secondary structure or dimer formation where possible. Product sizes were limited to 80 – 120 bp to enable fast reaction cycling, and primers were confirmed to be target-specific using PrimerBlast (NCBI). Efficiency of all primer sets was determined by titration over 4 orders of magnitude from 10 pg to 10 ng (MIQE guidelines; (Bustin et al., 2009)) using isolated gDNA from the *vnf:puc* strain (ChargeSwitch gDNA bacterial kit, Life Technologies), which contained all the target sequences. Multiple primer sets were tested for each gene and best-performing sets were selected. qPCR was performed using PowerUp SYBR green mastermix in 384-well plates on a

QuantStudio 5 real-time PCR system (both Applied Biosystems). Triplicate 10 μ L reactions contained 400 nM primers, 0.75 ng cDNA and 5% v/v 1,2-propanediol (0.68 M) to improve amplification of templates with problematic secondary structure due to the high GC content (Mousavian et al., 2014). The 2-step PCR fast-cycling program consisted of initial heat activation and DNA denaturation at 95°C, 2 min; and 40 cycles of 95°C, 1 s; 60°C, 30 s. C_q values were converted to gDNA ng equivalents using a reference titration of gDNA amplified alongside the cDNAs, and normalised to average quantification values of *rpoD* and *dnaA* reference genes (Fixen, Oda & Harwood, 2016).

Quality Control: The existence of a single end product was verified by melt-curve analysis. Genomic contribution to RT-qPCR was ruled out by processing a pool of input RNAs without reverse transcriptase (RT-), as well as ensuring negligible amplification from an untranscribed inter-operon genomic area (located between CAE27092–93) in the RT-qPCR samples. No substantial readings were obtained in reverse transcription or PCR samples performed with water alone (RT0 and NTC respectively).

Table 5.3. qPCR Primers used in this study

Primer	Sequence (5' – 3')	Notes
qPCR NifH-3 Fwd	AGAAGGTCCATGCCAACG	
qPCR NifH-3 Rev	CTGCTCGTCGGTCTTCAT	
qPCR NifK-2 Fwd	ATGACCGAGACCGCAGAGA	
qPCR NifK-2 Rev	TCCGCTTGTTCTCCATCAACTC	
qPCR NifE Fwd	ATGGGCGAGAACGATGTGAT	
qPCR NifE Rev	AGGTCTGATACACGAACACGG	
qPCR NifQ Fwd	CGACAACACCCGCAACAT	
qPCR NifQ Rev	TGCTACACATCACCATAACCGT	
qPCR VnfH-2 Fwd	CGTGATGAGCGGCGAAATG	Detection of inserted codon-optimised <i>vnfH</i> (<i>vnfH_{opt}</i>) transcript
qPCR VnfH-2 Rev	GCTCGACGCATACTTGAGGAT	
qPCR VnfD-2 Fwd	GCTGGGTCAACGAGAAGGT	
qPCR VnfD-2 Rev	ATGTTGTAGTCGCCGATGAAGT	
qPCR VnfK-2 Fwd	GGTTGCGAAGTCATTAGC	
qPCR VnfK-2 Rev	AATCCTTGACACCGATCC	
qPCR AnfH-3 Fwd	CAGGAAGTCTACATCGTCGC	
qPCR AnfH-3 Rev	TCTGCTTGCGTATTTGACA	
qPCR AnfK-2 Fwd	ACAAGAAGGTGGCGATCT	
qPCR AnfK-2 Rev	CCGGTTTCATTTCCAGGTC	
qPCR RpoD-3 Fwd	GCAACTATCAGGGCTCGG	<i>rpoD</i> reference gene
qPCR RpoD-3 Rev	CTTCTCGTGGTGGACAAAGT	
qPCR DnaA Fwd	GTGATGTTCAATCCGCTCTAC	<i>dnaA</i> reference gene
qPCR DnaA Rev	GATACAGCACCTTGCGTTC	
qPCR CisY Fwd	AGAAACTTGCTATCTCTTGCTGTA	Native <i>cit</i> promoter transcript
qPCR CisY Rev	CCATCTGCTCGTGAACCA	
qPCR PucBa Fwd	CTGACAAGACGCTGACCG	Native <i>puc</i> promoter transcript
qPCR PucBa Rev	GAAAATGCGGGTGCCATC	
qPCR NTSCR Fwd	ATCTCGCTCGCACCGATC	Non-transcribed control for detection of gDNA contamination (intergenic region between CAE27092–93)
qPCR NTSCR Rev	TAACTATCCGCCGCTCGC	

5.4.7 Western blot

Cells were harvested from the remaining 50 mL cultures by centrifugation (4°C, 5000 g, 10 min) and resuspended in 3 mL hypotonic STE buffer (20 mM NaCl, 50 mM Tris-HCl, 5 mM EDTA) and 1 mL lysis buffer (10% glycerol, 1% Triton X-100, 1 mM PMSF, 10 µg.ml⁻¹ RNase/DNase I, 10 mM MgCl₂). Samples were lysed by sonication on ice for 2 min (5 s on, 15 s off). After centrifugation at 14000 g for 2 min to pellet debris, protein concentration was measured using Pierce 660 nm protein assay reagent (Thermo Scientific). Samples were diluted to 1 µg. µl⁻¹ protein in 1X Laemmli sample buffer (with 50 mM DTT) and incubated at 40°C for 30 min. For each sample 40 µg protein was loaded into wells of 4 – 15% Mini-PROTEAN TGX gels (Bio-Rad) and run at 200 V. Transfer onto PVDF membranes was performed using the iBlot dry blotting system (Invitrogen) at 20V for 7 min. NifH was detected with chicken polyclonal anti-NifH (Agrisera AS01021A; 1:7500 dilution) and secondary goat anti-chicken horseradish peroxidase-conjugated IgG (ImmunoReagents Inc., 1:7500 dilution) with Pierce ECL Western Blotting Substrate (Thermo Scientific). Images were captured using a ChemiDoc system (Bio-Rad) and densitometry was performed using Image Studio lite (Li-Cor Biosciences).

5.4.8 Photobioreactor configuration and conditions

Strains were grown in 500 mL test-scale photobioreactors at 35°C and 200 W.m⁻² (± 20), as per the setup detailed in **Section 3.4.2**. 500 mL minimal medium, with 50 mM glycerol and 10 mM glutamate, was inoculated from a 4-day preculture to a starting OD₆₆₀ of 0.05 – 0.075 (~1% inoculum). Cell growth was determined by monitoring optical density (OD₆₆₀) and converting to dry cell weight concentration as described in **Section 3.4.3**.

5.5 Results and discussion

5.5.1 Generation of plasmids and identification of promoters for over-expression of genes encoding nitrogenase subunits

In order to facilitate rapid engineering of strains suitable for biotechnology applications, we set out to develop a versatile genetic modification toolset capable of both deletion of chromosomal regions and insertion of foreign DNA into the *R. palustris* genome. The suicide vector pK18*mobSacB* was chosen (Schäfer et al., 1994), as it has been widely used for genetic modification in a variety of organisms, including *R. palustris* (Xu et al., 2016; Jackson et al., 2018; Oshlag et al., 2020). This system exploits a two-step homologous recombination system. The plasmid vector is inserted into the genome under selection pressure incurred by encoded kanamycin resistance. Subsequent excision of the plasmid backbone is then selected by exposing recombinant strains to sucrose, which is lethal via the formation of levansucrase by *sacB*, resulting in stable markerless strains. The absence of selection markers in the final strain facilitates repeated modifications in this strain utilising the same method.

In order to over-express alternative *vnf* and *anf* nitrogenases, a suitably strong promoter was required, which is highly active under photoheterotrophic conditions. Transcriptomic studies of *R. palustris* strain CGA009 cultured under anaerobic phototrophic conditions showed *pucBa* to be strongly expressed under both high and low light (Fixen, Oda & Harwood, 2016). This gene encodes the light harvesting antenna protein LH2 peptide A, and is expressed only under low oxygen tension via action of the PpsR repressor mechanism (Braatsch et al., 2006). The *pucBa* promoter is therefore potentially ideal for inducible expression under photosynthetic conditions conducive to high cellular energy availability, with repression under aerobic conditions. This promoter has also successfully been used in the PNSB *Rhodobacter sphaeroides* for tuneable expression of membrane proteins by control of culture oxygenation (Erbakan et al., 2015) and in vectors designed for heterologous expression (Tikh, Held & Schmidt-Dannert, 2014). For comparison, the *cisY* promoter was chosen as a constitutively-expressed control, since citrate synthase forms part of the TCA cycle, which should be active under most environmental conditions (McKinlay, 2014).

The Nif nitrogenase enzyme complex consists of two subunits: iron-cofactor dinitrogenase reductase (NifH; Fe protein), which facilitates the maturation and ATP-mediated transfer of electrons to the molybdenum-containing catalytic component dinitrogenase (an $\alpha_2\beta_2$ tetramer of NifDK; MoFe protein) (Jasniewski et al., 2018). These genes are clustered on the CGA009 chromosome (**Figure 5.1A**) along with additional genes responsible for the complex process of cofactor synthesis and assembly of the catalytically-active holoenzyme (Hu & Ribbe, 2013). The alternative nitrogenases are similarly composed, with the exception of additional AnfG and VnfG subunits in the respective $\alpha_2\beta_2\gamma_2$ dinitrogenase complexes.

We thus designed plasmids to insert *pucBa* (*puc*) and *cisY* (*cit*) promoters directly upstream of these three putative nitrogenase operons in order to drive over-expression of all requisite nitrogenase H, D, G and K components (**Figure 5.1B**). These insertions preserved the native intergenic sequences to avoid disrupting terminators and potential downstream control regions for the preceding genes; elements that have not been well characterised in *R. palustris*. The native vanadium nitrogenase genes do not form a single cluster, since *vnfH* is transcribed from the reverse strand (**Figure 5.1A**). To consolidate the operon, we generated a second synthetic version (*vnfH_{opt}*), which was codon-optimised to limit potential off-target recombination with the native gene during co-insertion with the promoter. These constructs were designed for insertion upstream of the native *vnfD* ribosome binding site to facilitate translation from the polycistronic transcript.

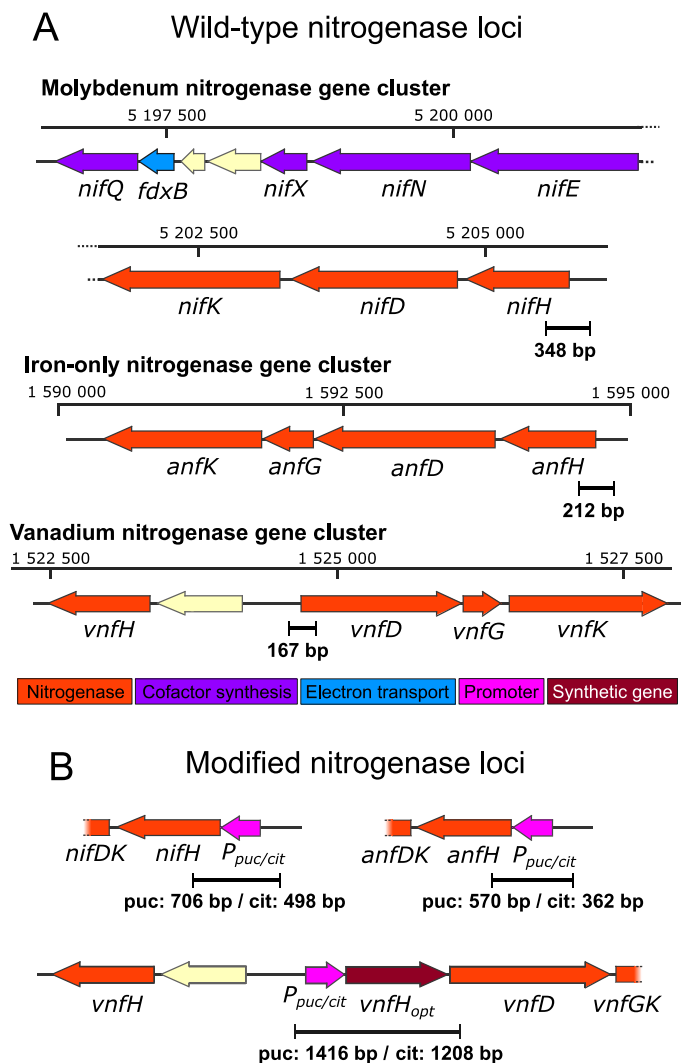


Figure 5.1 Organisation of nitrogenase genes in *R. palustris* (A) and summary of promoter insertion modifications (B).

Expected PCR product sizes are indicated for genotyping primer pairs spanning the insertion region. Promoters (P_{puc} or P_{cit}) were inserted upstream of gene clusters. A synthetic codon-optimised *vnfH* gene (*vnfH_{opt}*) was co-inserted with the promoter to create a unified vanadium nitrogenase operon. Gene functions annotated as per Oda et al., (2005); cream-coloured genes denote undefined functions.

5.5.2 Optimisation of a rapid electroporation-based genetic modification protocol

The pK18*mobSacB* plasmid was originally designed to be mobilised into target cells by conjugation. However, this process is slow and labour-intensive, since specific *E. coli* donor strains must be generated for each construct and subsequently eliminated after transfer (Laussermair & Oesterhelt, 1992; Ouchane et al., 1996). Published protocols require

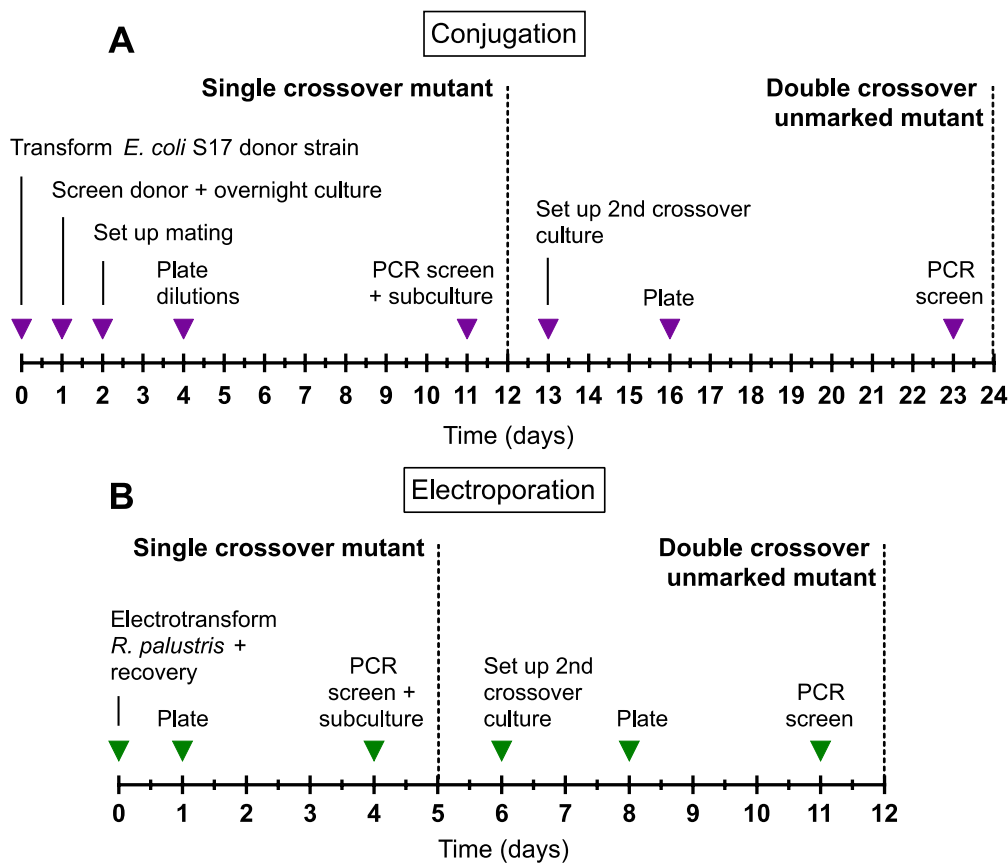


Figure 5.2 Timelines for transformation and generation of unmarked strains in *R. palustris*.

Time required for conjugation (**A**) and electroporation (protocol used in this study; **B**) are compared, and represent the minimum possible for each protocol under ideal conditions. Conjugation timeline constructed from protocol by Giraud et al. (2018).

approximately 24 days for *R. palustris* unmarked strain construction (Giraud et al., 2018) (**Figure 5.2A**). Therefore, we trialled transformation by electroporation, which is more rapid and flexible.

Initial attempts with published electroporation parameters for *R. palustris* (Inui et al., 2000; Pelletier et al., 2008) yielded very low transformation efficiency of around 200 colonies per μg of plasmid DNA. Replicative plasmids display much higher transformation efficiencies than vectors such as pK18*mobSacB*, which require chromosomal insertion for persistence; therefore, parameters need to be specifically optimised for insertional mutagenesis, in particular by allowing sufficient recovery time for integration to occur before selection pressure is applied (Ichimura et al., 2010).

In the PNSB *Rhodobacter sphaeroides*, increasing recovery time after transformation and before exposure to antibiotics has also been linked to markedly higher efficiency (Fornari & Kaplan, 1982). We thus attempted to identify the optimal electroporation parameters in terms of field strength (voltage), pulse duration (resistance), and optimal post-incubation conditions including growth medium and recovery time. Electroporation of cells at 2.0 kV and 800 Ω , immediate recovery in cold VNG medium and subsequent incubation in antibiotic-free medium at 30°C for 18 hours before plating on selective media, resulted in the highest transformation efficiency of $1.79 - 3.57 \times 10^3$ colonies per μg of plasmid DNA. Despite larger insert sizes of around 1.5 kb for the *vnf* constructs, these plasmids were integrated with similar efficiency to promoter-only insertions. Furthermore, use of frozen electrocompetent cells did not result in an observable decrease in transformation efficiency, which greatly enhances the convenience of the electro-transformation method.

Since *R. palustris* is a relatively slow-growing species with a doubling time of 8 – 11 hours in mineral medium (Rey & Harwood, 2010), obtaining transformants during selection steps has been one of the most time-consuming and thus major rate-limiting steps in published methods (**Figure 5.2A**) (Giraud et al., 2018). In order to reduce the time required for generation of visible colonies on agar plates, we tested a range of complex culture media, including Van Niel's yeast agar (van Niel, 1944), yeast peptone (YP), tryptone soy (TS) and nutrient agar (NA). In addition, defined mineral medium (PM), used in the majority of *R. palustris* genetic modification studies, was tested for comparison (Rey & Harwood, 2010; Fixen, Oda & Harwood, 2019). Culturing transformants on Van Niel's yeast agar (VN) at 30°C resulted in the fastest growth amongst the media tested, with colonies appearing approximately 3 days after electroporation, consistent with this medium being specifically developed for PNSB (van Niel, 1944, 1971). Equivalent growth on YP, TS, and NA required approximately 4 – 5 days, while colonies did not appear on minimal medium or PM plates for at least one week, consistent with previously reported times (Giraud et al., 2018). Further refinement of conditions by the addition of glycerol to VN medium as a carbon source (referred to as VNG

medium) and incubation at 35°C, resulted in even more rapid colony formation after only 2 – 3 days.

R. palustris displays high innate resistance to antibiotics due to the presence of drug efflux pumps (Larimer et al., 2004), which may contribute to the substantial frequency of false positives observed during screening. Use of kanamycin concentrations up to 400 µg.mL⁻¹ has been reported (Welander et al., 2009; Pechter et al., 2016), but the effect of high concentrations on the growth rate of transformants has not been definitively determined. In addition, long-term cultivation in the presence of kanamycin leads to spontaneous mutations in the 16S rRNA of many bacterial species, resulting in antibiotic resistance and further increasing the frequency of false positives over time (Higuchi-Takeuchi, Morisaki & Numata, 2020). In order to decrease the frequency of false positives seen in initial experiments using 100 µg.mL⁻¹ kanamycin, transformants were subsequently routinely cultured on agar plates containing kanamycin at a concentration of 200 µg.mL⁻¹ and screened as promptly as possible. These measures resulted in an average of 70% of colonies successfully showing a single cross-over event, with a range of 50 – 83%, perhaps reflecting variation in recombination efficiency for different constructs and loci (Table 5.4).

Table 5.4. Rate of false-positive transformants with wild-type genotype after selection on 200 µg.mL⁻¹ kanamycin.

Plasmid	% correct PCR genotype at 1 st crossover screening
<i>Insertion</i>	
pK18 <i>nif:puc</i>	83
pK18 <i>nif:cit</i>	50
pK18 <i>vnf:puc</i>	67
pK18 <i>vnf:cit</i>	83
pK18 <i>anf:puc</i>	67
pK18 <i>anf:cit</i>	75
<i>Deletion</i>	
pK18Δ <i>glnK2</i>	58

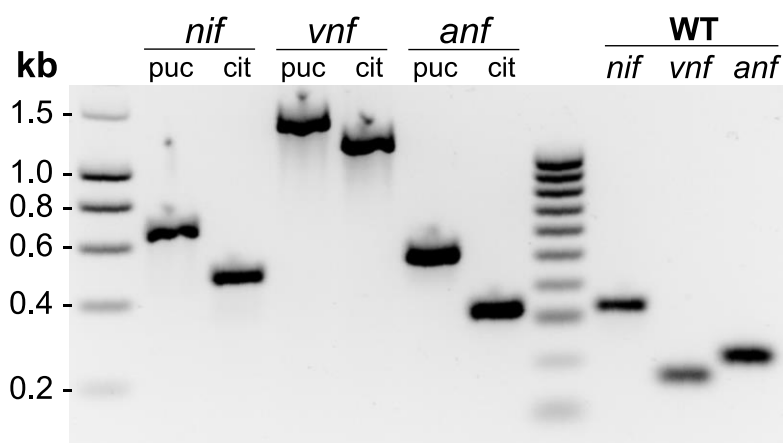


Figure 5.3 Genotyping of promoter-modified strains by PCR.

Gel electrophoresis indicates that PCR products conform to expected sizes, confirming genotypes of six modified strains which were additionally verified by sequencing.

Single cross-over strains were then cultured on sucrose-containing plates to generate unmarked strains. Screening by PCR showed ~50% of colonies were wild-type revertants as expected for the pK*mobSacB* vector system (Schäfer et al., 1994), and all six *R. palustris* insertion strains with either *puc* or *cit* promoters placed to drive expression of each putative nitrogenase operon were successfully generated (**Figure 5.3**), and confirmed by sequencing of the loci. In order to test the efficacy of the procedure for generating deletions rather than insertions, a pK*mobSacB* vector targeting *glnK2* was used. Deletion of *glnK2*, a component of the nitrogenase post-translational control mechanism, has previously been performed using an insertional mutagenesis technique (Heiniger et al., 2012b). Similar success rates using our optimised technique demonstrated that deletions can be achieved with comparable efficiency to insertions (**Table 5.4**). Together, these results confirm the versatility of the electro-transformation method for precise multi-unit modifications in *R. palustris*. Combining the advantages of electro-transformation and faster selection steps using VNG agar, markerless strains were generated in 12 days, approximately half the time required in previous conjugation-based protocols (**Figure 5.2B**).

5.5.3 Development of an optimised RNA extraction method for analysis of overexpressed genes

Confirmation of increased transcription of target genes is typically achieved by reverse-transcription followed by quantitative PCR (RT-qPCR). RNA-based expression analysis requires the purification of high-quality RNA. However, utilising widely-used kit-based methods for *R. palustris* (Oda et al., 2005b; Welander et al., 2009) resulted in poor yields, and degraded RNA (**Figure 5.4**). We thus tested RNA extraction methods *de novo* with the aim of addressing these problems, while simplifying the methodology as far as possible.

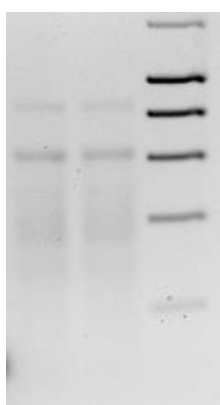


Figure 5.4 Test of kit-based RNA isolation from *R. palustris*.

RNA was isolated from cells harvested from 1 mL of culture grown in VNG medium ($OD_{660} \sim 1$), using the Qiagen RNeasy kit with bead beating pre-treatment. Cell pellet was resuspended in 1 mL buffer RLT (supplied in the kit) and added to a 2 mL screw-top tube containing 1 mL 0.1 - 0.2 mm silica beads (Sigma). Samples were mechanically disrupted in 1 min intervals on a Biospec mini beadbeater, followed by cooling on ice, for a total of 5 min. RNA was then isolated according to supplied protocol, including on-column DNase digestion. 5 μ L of each sample ($n = 2$) was examined on a 1% agarose bleach gel, indicating poor RNA yield. Right lane: 1 kb DNA ladder.

TRI reagent (acidic guanidinium thiocyanate-phenol) has an extensive track record for reliable isolation of intact RNA (Chomczynski & Sacchi, 2006), further improved by the more recent development of direct column-based purification. We therefore determined the efficacy of this method in combination with detergent and enzymatic pre-treatment methods to improve cell lysis and RNA extraction efficiency (**Figure 5.5**). Lysozyme digestion offered reasonably improved yield over samples with no additional treatment (**Figure 5.5A**, lane 1). Lysis in 1% sodium dodecyl sulfate (SDS) resulted in both the best yield and RNA integrity for the single treatments investigated, as determined by electrophoresis (**Figure 5.5A**, lane 4). The favourable denaturing environment in the presence of SDS offers additional protection of RNA integrity from the activity of RNases. Although the combination of lysozyme and SDS offered the most efficient RNA extraction (**Figure 5.5A**, lane 2), we focused further

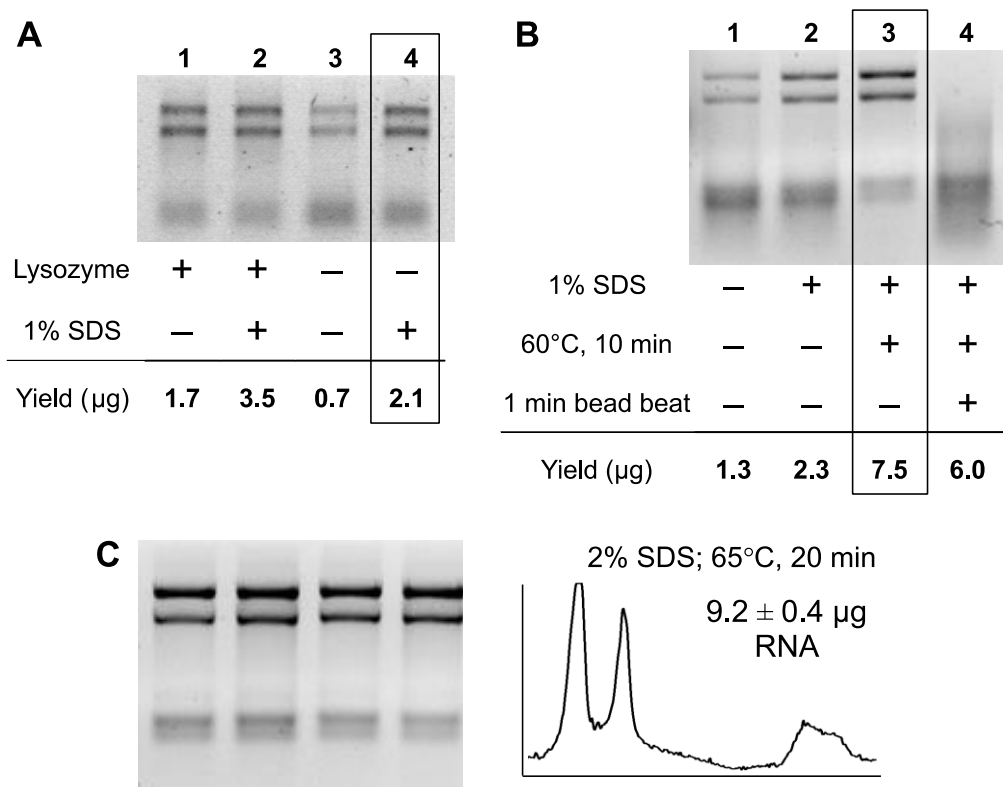


Figure 5.5 Evaluation of cell lysis pre-treatments for RNA extraction from *R. palustris* cultures.

Frozen pellets of 1 mL culture ($\text{OD}_{660} = 1$) were used for each test. Lysozyme digestion (**A**) was performed by addition of 250 U of Ready-Lyse lysozyme (Epicentre) with incubation at room temperature for 15 min. SDS and lysozyme treatments were aided by the presence of EDTA in the TE resuspension buffer (pH 8). For bead disruption (**B**), RNase-free 0.1 - 0.2 mm acid-washed glass beads (Sigma) were added after thorough mixing with TRI reagent (as per methods section). Pre-chilled samples were treated for 1 min in a Biospec mini-beadbeater and immediately cooled on ice. 150 ng RNA was loaded in each lane of 1% agarose TBE bleach gels for evaluation of RNA integrity. Optimal RNA quality and yield was seen using 2% SDS and 20 minutes of heat treatment (**C**; lanes represent 4 biological replicates). Densitometry analysis of the agarose gel allows comparison to Agilent Bioanalyzer electropherograms used to compute RNA integrity numbers (RIN).

optimisation on the SDS pre-treatment to simplify and expedite the extraction protocol with high sample throughput in mind.

In subsequent experiments RNA yield was further increased by the addition of a heat treatment step. Incubation at $\sim 65^\circ\text{C}$ has been reported to enhance lysis efficiency (Jahn, Charkowski & Willis, 2008), which corresponds with results seen here (**Figure 5.5B**, lane 3). Marked improvement in RNA quality was also observed, probably due to the synergistic disruptive action of heat and detergent, which also accelerates the inactivation of RNases.

Conventionally, mechanical disruption with silica beads is used to lyse resilient bacteria to improve yields and this method has been widely applied to isolate RNA from *R. palustris* (Harrison, 2005; Oda et al., 2005b; Fixen et al., 2018). However, when used in combination with SDS and heat treatment, even 1 minute of bead disruption resulted in severe RNA degradation (**Figure 5.5B**, lane 4). A higher 2% SDS concentration with a longer 20 minute incubation at 65°C ultimately offered the highest reproducible yields of up to 10 µg per 1 mL culture sample (OD₆₆₀ ~1) with excellent RNA integrity as evidenced by sharp rRNA bands and densitometry peaks (**Figure 5.5C**). Comparison of gel densitometry to reference electropherograms (Schroeder et al., 2006; Jahn, Charkowski & Willis, 2008) indicated all samples had RNA integrity number (RIN) values of at least 8. This reflects excellent RNA integrity suitable for expression studies.

Despite the high resistance to cell disruption, relatively gentle lysis of *R. palustris* with heat and detergent seems to give much higher quality RNA than bead beating. In addition, RT-qPCR controls showed little evidence of gDNA carryover with only two integrated DNase treatment steps, in contrast to extensive digestion required for bead beating protocols (Harrison, 2005). SDS and heat thus offer an effective method for extraction of high-quality RNA, with the added benefit of a simple, rapid protocol (**Protocol E; Appendix 6**).

5.5.4 Quantifying gene expression of recombinant strains

Using the optimised RNA extraction method we analysed transcript levels of multiple genes in each putative operon under nitrogen-fixing conditions in the six promoter-substitution strains by RT-qPCR (**Figure 5.6**). Transcript levels for all genes investigated in each putative operon showed significant overexpression in both *puc*- and *cit*-promoter strains, with the single exception of *nifH*, the first gene in the operon, which did not differ from wild-type levels (**Figure 5.6**; $p = 0.054 - 0.1$). Since the canonical molybdenum nitrogenase is well-known to be highly expressed under nitrogen fixing conditions, it would seem that the activities of these promoters offer only equivalent expression potential to the native *nif* promoter, albeit with

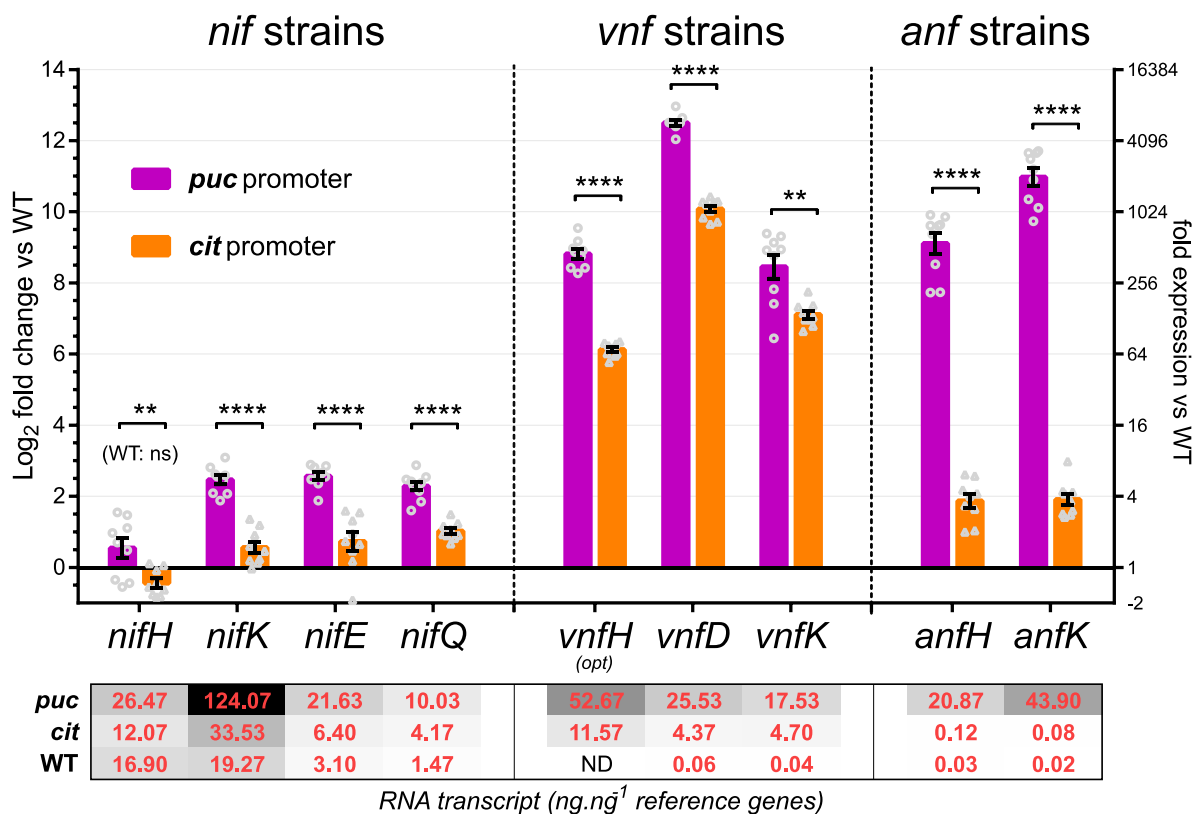


Figure 5.6. Quantification of gene expression by RT-qPCR from modified nitrogenase operons under control of *pucBa* (P_{puc}) or *cisY* (P_{cit}) promoters.

Cultures were grown under nitrogen-fixing conditions for 48 h. Transcript levels were normalised to reference genes and wild-type samples to give relative log₂ expression (left axis) and -fold difference (right axis). Heatmap below graph shows differences in normalised transcript abundance between strains (ND: not detected). Data reflects average \pm SEM from 3 biological and 3 technical triplicates, with datapoints shown as grey symbols. Statistical significance from two-tailed t-tests with Holm-Sidak correction ($\alpha = 0.05$) represented by: ****: $p < 0.0001$; **: $p < 0.01$; ns: not significant.

the distinction of being active under non nitrogen-fixing conditions as well. Interestingly, however, downstream genes in the operon were over-expressed despite the lack of change in transcript level of *nifH*. These downstream genes include the non-nitrogenase subunit genes *nifE* and *nifQ*, which encode assembly and helper proteins, confirming that these accessory genes are co-transcribed.

In the case of the alternative *vnf* and *anf* nitrogenase promoter-substitution strains, significantly higher relative expression was observed for all genes. As expected, promoter

insertion was much more effective here, since these nitrogenases are normally repressed due to their nature as fall-back isozymes, with the repression confirmed by very low transcript abundance in WT samples (**Figure 5.6**). Up-regulation of between 1000 to 4000-fold compared to wild-type were achieved for *vnf* and *anf* subunit genes under control of the *puc* promoter, indicating excellent activity under photoheterotrophic conditions. Expression of native *pucBa* transcripts in wild-type samples was 10-fold higher than those for *nifH*, while *cisY* transcripts were 23-fold lower, consistent with the nature of citrate synthase as a constitutively expressed but low-abundance protein. This highlights the usefulness of the *puc* promoter as a robust driver of gene expression with wider potential applications.

5.5.5 Nitrogenase protein expression

Detection of total nitrogenase protein in the modified strains was performed by western blot analysis (**Figure 5.7**) using antibodies against a peptide epitope conserved in all dinitrogenase

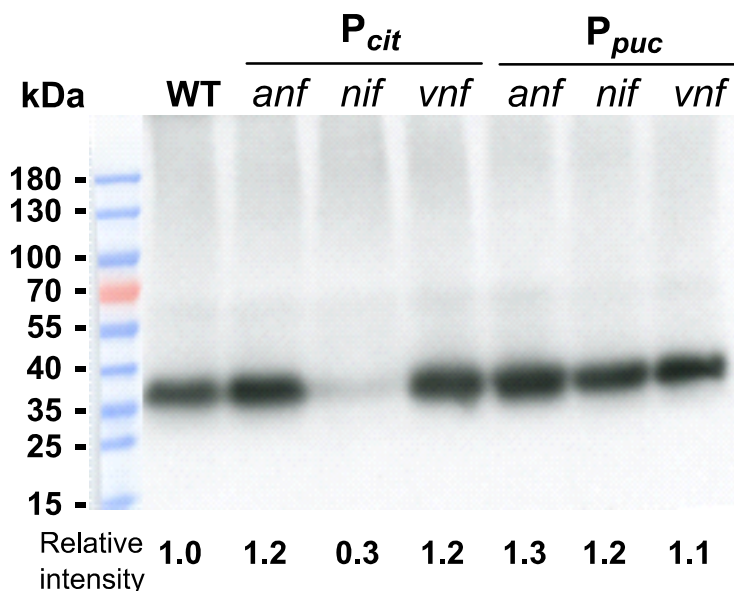


Figure 5.7. Quantification of nitrogenase protein in promoter-modified strains.

Western blot was used for the detection of total nitrogenase via a conserved peptide epitope in all dinitrogenase reductase subunits (NifH, VnfH, AnfH). 40 μ g protein loaded in each sample lane, extracted from each promoter-substitution strain in which *nif* (Mo), *vnf* (V) and *anf* (Fe) nitrogenase genes are expressed under control of either *pucBa* or *cisY* promoters (P_{puc} and P_{cit}). All strains grown under nitrogen-fixing conditions. Band intensity relative to wild-type determined by densitometry. Bands correspond to expected size of dinitrogenase reductase subunits.

reductase subunits (NifH, VnfH, AnfH), which further verified successful over-expression of the alternative nitrogenases. Nitrogenase protein abundance was increased in all strains relative to wild-type except for the *nif:cit* strain, following the same trend observed for transcript quantification. A modest increase in nitrogenase in the *nif:puc* strain suggests that *puc* promoter performs at least equivalently to the native *nif* promoter. In *Rhodospseudomonas capsulatus*, nitrogenase comprises up to 40% of intracellular protein under nitrogen-fixing conditions (Jouanneau, Wong & Vignais, 1985). If this level of abundance is similar in *R. palustris*, the success in further increasing protein concentration with the *puc* promoter demonstrates its potential for high-level expression of target genes. In the *nif:cit* strains, decreased nitrogenase protein is consistent with the lack of increase in transcript levels, indicating inferior performance of the *cit* promoter compared to the native promoter.

The *anf* and *vnf* strains possess intact *nif* genes, and under nitrogen-fixing conditions high-level expression of the main molybdenum nitrogenase would occur in addition to that of the modified loci. Assuming similar translation efficiency between *nif* and alternative nitrogenases, over-expressing *vnf* and *anf* transcripts to levels similar to that of *nif* should lead to a doubling in total nitrogenase protein. However, protein expression was raised only modestly with a maximum of 30% in the *anf:puc* strain. Thus, there is a possibility that the complex processes of translation, cofactor synthesis and enzyme assembly are saturated under these conditions, leading to competitive bottlenecks in expression of the alternative isozymes and a practical limit on the total nitrogenase present within the cell. In addition, post-transcriptional control mechanisms may reduce translational efficiency despite high transcript levels. However, these promoters may be useful for heterologous expression of other proteins under phototrophic conditions where nitrogenases are not expressed, allowing higher translation capacity.

In addition, a two amino acid difference in the VnfH antibody epitope target may affect the detection efficiency for the vanadium nitrogenase, which may lead to an underestimation of the total nitrogenase content in the *vnf* samples. Nevertheless, protein expression levels

further validate the over-expression of genes using the *puc* (and in some cases *cit*) promoters; and the optimised genetic modification method as a viable metabolic engineering strategy.

5.5.6 Hydrogen production by modified strains

Along with modest improvement of nitrogenase protein expression, subtle differences in the relative populations of expressed isozymes may yield distinct changes in hydrogen output due to the higher hydrogen production stoichiometries of the iron and vanadium nitrogenases (Schneider et al., 1997; Oda et al., 2005b; Heiniger & Harwood, 2015). To test this, growth and hydrogen production studies were conducted with the promoter-modified strains in 0.5 L test-scale bioreactors under nitrogen-fixing conditions. Initial growth of all modified strains was slightly slower than wild-type, perhaps reflecting a small metabolic burden on cells due to the modification, although the difference in growth rates was not significant (**Figure 5.8A**). The specific hydrogen production rate was in turn also lower, most notably in the case of the *nif* strains (**Figure 5.8B**) during the early phase of growth, when cultures are at low density and light availability per cell is highest. These strains only attained a maximal production rate of $\sim 10 \text{ mL}\cdot\text{g}^{-1}\cdot\text{h}^{-1}$ at 90 hours, around half of the wild-type maximum rate, which suggests that substitution of the native *nif* promoter does not enhance hydrogen production performance by Mo nitrogenase. Notwithstanding equivalent transcription in the *nif:puc* strain and wild-type, the replacement of native regulatory elements in the 5' untranslated region (UTR) may disrupt correct post-transcriptional processing, translation or the intricate enzyme assembly and maturation process (Rubio & Ludden, 2005), leading to decreased concentration of functional enzyme.

Despite the presence of unmodified *nif* loci in *vnf* and *anf* strains, a slight decrease in hydrogen productivity was observed relative to wild-type levels, especially in terms of the peak in production rate in the early culture phase (**Figure 5.8B**). In these strains, expressing an additional nitrogenase isozyme from a second locus, only increased or at the very least equivalent hydrogen productivity would be likely compared to wild-type unless the over-expression places a burden on the cell. Again, high transcript and protein levels from

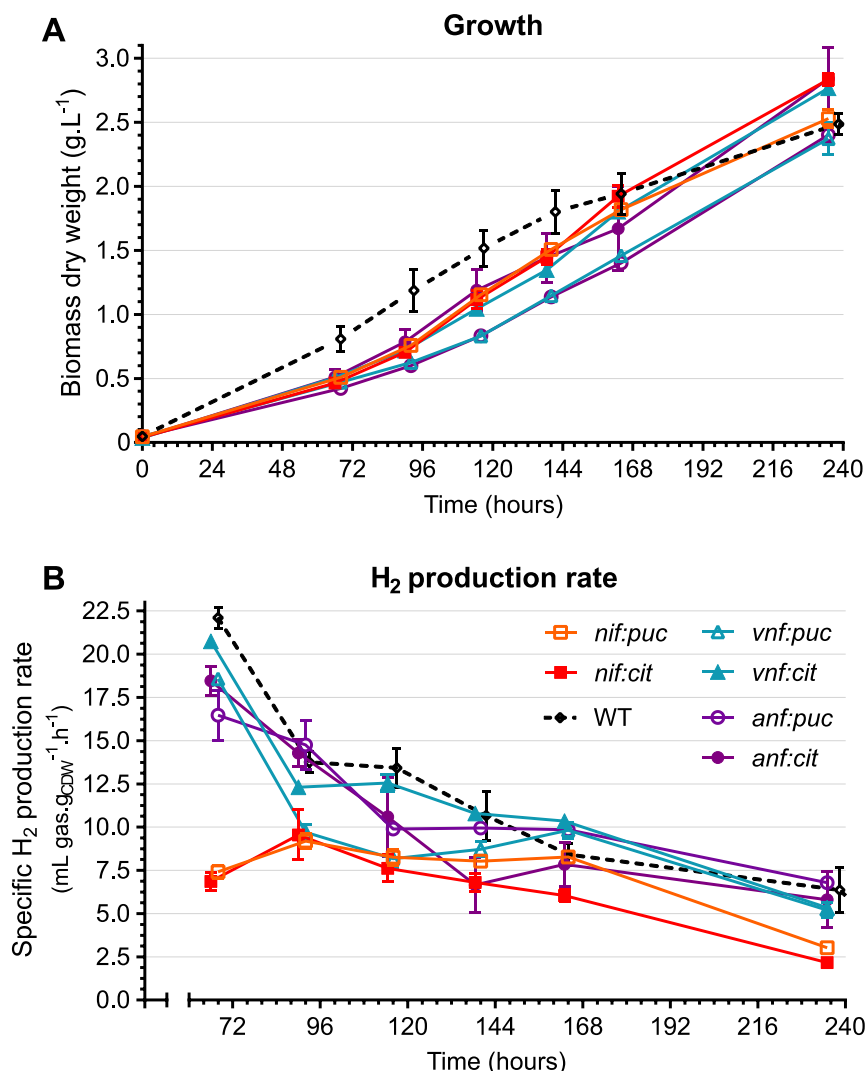


Figure 5.8 Growth and hydrogen production by nitrogenase promoter-modified strains under nitrogen-fixing conditions.

Cell growth in 0.5 L test bioreactors was tracked by converting OD_{660} to cell dry weight (**A**). Hydrogen production was normalised to biomass in the reactor to give specific production rate (**B**). Data reflects averages and error bars represent SEM for 3 to 6 biological replicates.

expression of two nitrogenase genes may reduce expression of other proteins required for optimal hydrogen production, including those involved in correct nitrogenase assembly. Alternatively, lower production rates may reflect innate limitation in terms of either ATP or electron availability for reduction of protons to H_2 . This may result from either non-optimal light availability within the relatively large 80 mm diameter bioreactor with a low surface-to-volume ratio, or saturation of the pathway supplying electrons to nitrogenase. This pathway is another potential target for production rate enhancement (Fixen et al., 2018). Deletion of

nifHDK from the *vnf:puc* and *anf:puc* strains in order to restrict expression to alternative nitrogenases would likely improve the hydrogen productivity of these strains.

While enhancing production rates is a key goal for the feasibility of biohydrogen, improving overall bioprocess compatibility is equally important for implementation. Production of hydrogen via nitrogenases expressed from native promoters will be strongly repressed by nitrogenous compounds such as ammonia and urea (Zumft & Castillo, 1978), which are commonly found in potential waste feedstocks. The NifA* strain, which expresses higher levels of constitutively-active nitrogenase due to a 16 amino acid deletion in the master transcriptional activator NifA (McKinlay & Harwood, 2010b), shows highly reduced sensitivity to the presence of ammonia (Adessi et al., 2012). The maintenance of nitrogenase activity was hypothesised to be due to the lack of expression of post-translational inactivation system GlnK2-DraT2, since the NtrBC control regulon is not activated under nitrogen-replete conditions (Heiniger et al., 2012b). This hypothesis should similarly apply to the promoter-modified strains under nitrogen replete conditions. However, no hydrogen was produced by these strains grown with 5 mM urea (which is converted to ammonia intracellularly), suggesting that over-expression is not sufficient to overwhelm basal activity of the switch-off system (data not shown). Additional factors thus seem to be involved with maintenance of nitrogenase activity in the NifA* strain, warranting further exploration of nitrogenase control mechanisms. Further engineering of the *vnf:puc* and *anf:puc* strains by knocking out the GlnK2-DraT2 control system may result in efficient hydrogen-producing strains insensitive to nitrogenous feedstocks.

Notably, improved hydrogen productivity was not achieved by the genetic modification applied in this study probably due to nitrogenase expression being an exceedingly complex, multifactorial process (Rubio & Ludden, 2005; Hu & Ribbe, 2013). Optimal nitrogenase activity is reliant on associated ATP and electron supply mechanisms operating at similar efficiency. Alongside biomass synthesis, the Calvin Cycle CO₂ fixation pathway is the main metabolic competitor for reducing equivalents (McKinlay & Harwood, 2010b), and

inactivation of this pathway resulted in 1.5 to 2.5 times higher specific H₂ production rates (McCully & McKinlay, 2016). It is thus also possible that promoter-substitution strains would show superior hydrogen production compared to wild-type under non-growing conditions with reduced competition from biomass accumulation (McKinlay et al., 2014). In addition, nitrogenase activity is highly sensitive to competitive binding of ADP to dinitrogenase reductase (Weston, Kotake & Davis, 1983). ADP to ATP ratios as low as 0.2 completely inhibit nitrogenase activity, despite abundant cellular ATP, requiring high light intensity to efficiently regenerate ATP from ADP via photosynthetic cyclic electron transport (Zheng & Harwood, 2019). Reduction in expression of photosynthetic antennae may thus increase light penetration to dense cultures (Kondo et al., 2002; Ma, Guo & Yang, 2012) as part of a multivalent strategy to address nitrogenase pathway limitations.

Nevertheless, the *pucBa* promoter shows great promise for high-level heterologous expression in *R. palustris*, applied to synthesis of products with fewer demands and in the absence of sophisticated native control mechanisms. Further investigation into the function of the promoter sequence, identification of core elements and clarification of post-transcriptional control mechanisms would allow full development of an effective heterologous expression system.

Exacting maximal hydrogen productivity from *R. palustris* will clearly require comprehensive metabolic engineering to address bottlenecks in highly-complex pathways. The optimised tools presented here expedite the repeated genetic modifications required for further genetic dissection, while also advancing the potential of *R. palustris* as a biotechnology platform for additional high-value products suited to its metabolic capabilities.

5.6 Conclusion

We present an efficient electro-transformation method for chromosomal insertions and deletions in *R. palustris*, with protocol refinements in terms of growth medium, electroporation parameters and post-electroporation recovery which maximise expediency. These allow generation of modified strains in around 12 days, greatly reducing the time required by previous methods. Further, characterisation of expression is assisted by high-quality RNA extracted using a simple method combining heat and SDS.

These genetic modification techniques were applied to replace the native promoters of alternative nitrogenases with the aim of enhancement of hydrogen productivity. The activity of the *pucBa* promoter resulted in robust transcriptional upregulation of *anf* and *vnf* operons of up to 4000-fold of wild-type, which in turn translated to increased protein expression. While hydrogen productivity was not ultimately enhanced, this system is ideally suited to metabolic engineering of pathways in *R. palustris* exploiting the robust redox driving force innate to phototrophic purple bacteria.

5.7 Acknowledgements

We thank Jeffrey Douglass for assistance with Western blotting, and Ruth Laing for initial data leading to the optimisation of the electroporation protocol. This work was supported by funding from the Cambridge-Africa ALBORADA Research Fund (UK), the Waste and Environmental Education Research Trust (WEERT; UK) and the Water Research Commission (WRC) of South Africa.

5.8 Author contributions

Declaration by the candidate:

With regard to Chapter 5, the nature and scope of my contribution were as follows:

Nature of contribution	Extent of contribution (%)
Conceptualisation Methodology Investigation Data analysis & Visualisation Writing & Editing	80%

The following co-authors have contributed to Chapter 5:

Name	e-mail address	Nature of contribution	Extent of contribution
David J. Lea-Smith	D.Lea-Smith@uea.ac.uk	Conceptualisation Methodology Review & Editing	5%
Anna Git	anna.git@cruk.cam.ac.uk	Methodology & Investigation: RT-qPCR Review & Editing	3%
John R. D. Hervey	jrdh2@cam.ac.uk	Methodology	2%
Christopher J. Howe	ch26@cam.ac.uk	Conceptualisation Review & Editing	5%
Robert W. M. Pott	rpott@sun.ac.za	Conceptualisation Review & Editing	5%

Signature of candidate: Jan-Pierre du Toit Date: 29 January 2021

Declaration by co-authors: The undersigned hereby confirm that

1. the declaration above accurately reflects the nature and extent of the contributions of the candidate and the co-authors to Chapter 5,
2. no other authors contributed to Chapters 5 besides those specified above, and
3. potential conflicts of interest have been revealed to all interested parties and that the necessary arrangements have been made to use the material in Chapters 5 of this dissertation.

Signature	Institutional affiliation	Date
David J. Lea-Smith	University of East Anglia	29 January 2021
Anna Git	University of Cambridge	29 January 2021
John R. D. Hervey	University of Cambridge	29 January 2021
Christopher J. Howe	University of Cambridge	29 January 2021
Robert W. M. Pott	Stellenbosch University	29 January 2021

Declaration with signatures in possession of candidate and supervisor

CHAPTER 6

CONCLUSIONS AND FUTURE PERSPECTIVES

6.1 Conclusions

Hydrogen shows great promise as a sustainable, clean source of energy in the ongoing quest to mitigate the existential threat of unrestrained carbon emissions. As part of a future circular bioeconomy, biohydrogen production via photofermentation by PNSB such as *R. palustris* is coupled to efficient conversion of organic wastes. This allows extraction of the latent value in biomass resources that would otherwise be lost, alleviating the concomitant disposal burden. Hydrogen production is enabled by the unique metabolism of *R. palustris* in which ATP production from photosynthesis is uncoupled from oxidation of organic substrates, leading to a redox imbalance, which is relieved by endergonic pathways including nitrogenase-catalysed proton reduction to H₂. High-rate hydrogen production thus necessitates maintenance of both this favourable redox state and high nitrogenase activity, supported by optimised process conditions and enhanced by metabolic engineering strategies.

The first objective of this dissertation was therefore to definitively determine the optimum temperature for hydrogen production by *R. palustris* to realise the maximum innate metabolic potential of the organism (Chapter 3). While previous studies suggested that 30°C is the ideal temperature, acclimation of strains CGA009 and ATH 2.1.37 to higher temperatures revealed optima of 35 and 40°C respectively with substantial 2 to 4-fold gains in hydrogen productivity. This work is the first investigation accounting for adaptation of *R. palustris* to cultivation temperature and demonstrates the importance of proper acclimation when optimising this fundamental process parameter which plays a key role in metabolic and catalytic efficiency. Further, the variability of temperature optima in strains with highly-similar genomes reaffirms the necessity of characterising strains individually. This also prompts caution when using laboratory strains which may exhibit much-reduced resistance to higher temperature due to loss of function induced by maintenance under mild conditions.

The feasibility of biohydrogen production will likely require continuous process operation, with separation of biomass from the liquid medium in order to optimise hydraulic retention time and reactor performance. To this end the development of a transparent bacterial

immobilisation matrix based on PVA cryogel was pursued (Chapter 4). Optimisation of PVA molecular weight and glycerol-water solvent composition resulted in a material with key properties well-suited to entrapment of photosynthetic bacteria and overall process efficiency. The material exhibited a high level of transparency, especially to the near-infrared wavelengths of light required by PNSB, as well a level of mechanical and chemical stability conferring robustness approaching indestructibility under typical bioprocess conditions. This level of durability is a solution to the most common problem encountered with current immobilisation materials such as alginate which are fragile and vulnerable to dissolution by salts or chelators commonly present in the feedstock. As an additional benefit, transparent cryogels offer the advantage of achieving these properties after a single low temperature cycle, in contrast to the multiple cycles required for conventional cryogels. The immobilisation process is thus greatly accelerated and the potential for deleterious impact on cells minimised. Methods employing differential fluorescent staining and confocal microscopy were developed for assessing both the porosity of the cryogels and the viability of entrapped cells, allowing examination of the material in the native hydrated state. This demonstrated excellent biocompatibility of both the immobilisation process and transparent cryogel over extended periods. Tests using common *R. palustris* substrates showed only a slight barrier to diffusion through the material, on the same order as alginate which is prized for high permeability. Comparison of non-growing immobilised cultures to identical free planktonic controls further confirmed these properties, where a slight increase in hydrogen production was seen with immobilised cultures versus planktonic controls confirming lack of detriment to cells. Further, long-term continuous cultivation showed sustained hydrogen production for at least 2 months. This work is the first comprehensive characterisation and optimisation of transparent PVA cryogel specifically applied to immobilisation of phototrophic bacteria. The techniques devised and improvements in material properties demonstrated represent a significant technological advancement in support of continuous process operation by bacterial immobilisation, and extends the applicability of transparent PVA cryogels to even non-photosynthetic bioprocesses.

The final section of work addressed challenges to metabolic engineering of *R. palustris* due to the lack of well-developed tools for genetic manipulation. This gap presents a barrier both to metabolic enhancement of biohydrogen production, and more importantly the widespread biotechnological utilisation of this organism. Here a chromosomal genetic modification technique was refined to expedite generation of markerless insertion and deletion strains. Markerless modifications allow persistent strains to be created with potentially numerous modifications, since selection markers such as antibiotic resistance are not required to maintain plasmids separate from the organism's chromosome. This technique, employing electroporation for transformation of a plasmid vector, was adjusted in terms of electroporation parameters, recovery conditions and growth medium composition in order to both maximise transformation efficiency and to reduce the time required to generate strains. These efforts resulted in a 10 to 17-fold increase in transformation efficiency, while allowing markerless strains to be created in 12 days; half the time required by previous methods. The optimised technique was applied to over-express the alternative *vnf* and *anf* nitrogenase gene clusters by insertion of strong promoters, since these isozymes have the potential to improve hydrogen productivity. This is, to our knowledge, the first instance of promoter substitution being successfully used to over-express a native gene in a PNSB, representing a new approach to metabolic engineering of photosynthetic bacteria. Transcript quantification, facilitated by a newly-devised and optimised RNA extraction procedure, showed successful overexpression up to 4000-fold of wild-type levels. However, hydrogen production rates were not enhanced in bioreactor studies, perhaps indicative of enzyme assembly saturation or electron supply deficiencies. Nevertheless, the genetic toolset developed tackles the current lack of detailed methods to create chromosomal modifications in *R. palustris*, while increasing expedience of several key steps dramatically. This would allow much more efficient genetic dissection of the hydrogen producing metabolism, in order to inform further metabolic engineering strategies to create a super-producing strain. In addition, these tools pave the way for further exploration of the biotechnological potential of the organism's innate redox imbalance for synthesis of energy-intensive bioproducts.

The work in this dissertation has thus advanced three key approaches to addressing hydrogen productivity by *R. palustris*. This multivalent process engineering strategy comprises strain selection and high-temperature acclimation, an immobilisation technology for process optimisation, and genetic engineering to co-opt cellular metabolism for high-rate production of hydrogen and a plethora of yet-to-be explored energy-intensive bioproducts.

6.2 Further work

The work described in this dissertation advances some key process engineering strategies for efficient biohydrogen production via photofermentation. However, this process is still far from sufficient maturity to be considered viable for implementation. Substantial further work is required to better understand the complex hydrogen-producing metabolism of *R. palustris* and other candidate PNSB, and to develop the requisite bioprocess technology for this and other photofermentative products taking advantage of the favourable redox imbalance. The work performed has informed potential avenues for further efficiency gains, as presented here.

Chapter 3 demonstrated the inherent link between temperature and hydrogen productivity, with drastically enhanced efficiency at higher temperatures. Despite highly-similar genomes, CGA009 had reduced temperature resistance than ATH 2.1.37, suggesting that laboratory strains are not ideal candidates when robustness is required. Isolation of new strains of *R. palustris*, which are widespread in the natural environment, or additional study of isolates from temperature extremes such as hot springs may thus further expand the feasible temperature range into the thermophilic range above 40°C. Long-term studies of candidate strains will likely be necessary to confirm that elevated temperatures are not deleterious to organism survival and efficacy during continuous hydrogen production. Along with the potential for much higher hydrogen productivity driven by wholesale increases in metabolic efficiency, higher operating temperatures offer further reductions in engineering considerations for sunlight-driven photofermentation.

The observation that increasing temperature results in higher hydrogen production despite poor light penetration in dense cultures poses some additional questions on the presumed link between mutual cell shading and light limitation. In this case, increased photosynthetic ATP production seems to be possible despite the level of mutual shading, indicating that light penetration may not have a significant impact on overall hydrogen production capacity since light conversion does not seem to be rate-limiting. Further study of the interaction of culture density, photosynthetic antenna expression and light conversion efficiency will thus be required to inform design considerations for optimal photobioreactor configurations which balance light penetration and density of catalytic biomass. This will be especially important for processes which are able to efficiently use this pool of light-derived ATP and may thus encounter rate limitation due to non-optimal ATP regeneration.

The optimised transparent PVA material described in Chapter 4 facilitates the maintenance of a stable pool of biomass irrespective of hydraulic retention time, which is relevant to design of effective continuous photobioreactors. In these experiments, nitrogen limitation was used to maintain cells in a non-growing state to prevent difficult-to-quantify biomass accumulation within the material. It thus remains unclear how cells respond to entrapment on a community level, and to what extent growth or biofilm formation occurs within the material. Here further application of the *in situ* imaging technique could contribute to study of matrix-cell interactions. As with the case of light conversion efficiency, creation of metabolically efficient strains of *R. palustris* may necessitate improved mass transfer characteristics of PVA cryogel beads to avoid substrate limitation. This can most immediately be achieved by reducing the size of the beads to increase surface area to volume ratio and thus limit diffusion distance. Since the diameter is currently constrained to around 2 – 3 mm due to the temperature and thus viscosity of the PVA solution and the dripping process used for immobilisation, new high-throughput bead formation techniques will need to be explored for production of smaller beads at low cost. Technologies such as the JetCutter allow rapid aseptic production of ~0.8 mm beads even with highly viscous 4% alginate solutions (Prüsse et al., 2008), and may

be adapted to cryogel formation by incorporation of efficient freezing methods. Such a system would greatly increase the accessibility, performance and cost-effectiveness of cryogel cell immobilisation for innovative bioprocesses.

The non-growing state also reduces competition from biomass synthesis and thus redirects more energy to hydrogen production (McKinlay et al., 2014). Recent studies have shown that long term survival in a non-growing state is influenced by the stringent response mediated by guanosine polyphosphate (Yin et al., 2019). Deeper understanding of these molecular signals controlling induction and maintenance of the persistent non-growing metabolic state would therefore also allow finer control over biomass accumulation and energy flux in the system without the need to limit nutrient availability.

The optimised genetic toolset detailed in Chapter 5 presents an excellent resource for future efforts to probe the photoheterotrophic metabolism of *R. palustris*, and resultant metabolic engineering strategies for high-rate production of hydrogen and other bioproducts. The alternative nitrogenase promoter-substitution strains did not ultimately yield increased hydrogen production despite efficient over-expression, which requires further investigation. Deletion of *nif* genes to limit expression to the alternative nitrogenases may reduce competition for both nitrogenase assembly processes and the electron pool, thus better realising the catalytic potential of the *vnf* and *anf* isozymes. Another solution may be inactivation of the Calvin cycle by deleting phosphoribulokinase (PRK), which unlike the more common target RuBisCo does not result in accumulation of deleterious intermediates (McCully & McKinlay, 2016). Eliminating competition from this significant electron sink would likely be a key step towards engineering of an obligate hydrogen super-producer, complemented by non-growing cultivation of immobilised biomass in a continuous bioreactor. Beyond biohydrogen, a $\Delta Nif/\Delta PRK$ strain would thus also serve as useful chassis for a multitude of endergonic biosynthetic pathways suited to the unique metabolism of *R. palustris* such as for high-value terpenoids or those with oxygen-sensitive or membrane-bound products or intermediates (Heck & Drepper, 2017). Here the redox imbalance under

photoheterotrophic conditions would be entirely funnelled towards the engineered pathway, with maintenance of the functional pathway ensured by the existential requirement of the electron sink for cell survival.

Indeed, the use of *R. palustris* for production of high-value products would also encourage the investment in further research & development required to reach process maturity. By increasing efficiency and reducing costs through economies of scale, this has the potential in turn to advance photofermentative biohydrogen production from waste towards commercial feasibility and eventual implementation as part of a future circular bioeconomy.

REFERENCES

- Acar, C. & Dincer, I. 2020. The potential role of hydrogen as a sustainable transportation fuel to combat global warming. *International Journal of Hydrogen Energy*. 45(5):3396–3406. DOI: 10.1016/j.ijhydene.2018.10.149.
- Adessi, A., McKinlay, J.B., Harwood, C.S. & De Philippis, R. 2012. A *Rhodospseudomonas palustris* nifA* mutant produces H₂ from NH₄⁺-containing vegetable wastes. *International Journal of Hydrogen Energy*. 37(21):15893–15900. DOI: 10.1016/j.ijhydene.2012.08.009.
- Adessi, A., Corneli, E. & De Philippis, R. 2017. Photosynthetic Purple Non Sulfur Bacteria in Hydrogen Producing Systems: New Approaches in the Use of Well Known and Innovative Substrates. In *Modern Topics in the Phototrophic Prokaryotes: Environmental and Applied Aspects*. P.C. Hallenbeck, Ed. Springer International Publishing. 321–350. DOI: 10.1007/978-3-319-46261-5_10.
- Albert, D.R. 2020. Monte Carlo Uncertainty Propagation with the NIST Uncertainty Machine. *Journal of Chemical Education*. 97(5):1491–1494. DOI: 10.1021/acs.jchemed.0c00096.
- Allen, M., Babiker, M., Chen, Y., de Coninck, H., Connors, S., van Diemen, R., Dube, O.P., Ebi, K.L., et al. 2018. Summary for policymakers Global Warming of 1.5 C: an IPCC Special Report on the Impacts of Global Warming of 1.5 C Above Pre-Industrial Levels and Related Global Greenhouse Gas Emissions Pathways, in the Context of Strengthening the Global Response to the Threat of Climate Change. *World Meteorological Organization*. 1–24.
- Alves, M.-H., Jensen, B.E.B., Smith, A.A.A. & Zelikin, A.N. 2011. Poly(Vinyl Alcohol) Physical Hydrogels: New Vista on a Long Serving Biomaterial. *Macromolecular Bioscience*. 11(10):1293–1313. DOI: 10.1002/mabi.201100145.
- Aranda, P.S., LaJoie, D.M. & Jorczyk, C.L. 2012. Bleach Gel: A Simple Agarose Gel for Analyzing RNA Quality. *Electrophoresis*. 33(2):366–369. DOI: 10.1002/elps.201100335.
- Ariga, O., Takagi, H., Nishizawa, H. & Sano, Y. 1987. Immobilization of microorganisms with PVA hardened by iterative freezing and thawing. *Journal of Fermentation Technology*. 65(6):651–658. DOI: 10.1016/0385-6380(87)90007-0.
- Ariga, O., Kubo, T. & Sano, Y. 1994. Effective diffusivity of glucose in PVA hydrogel. *Journal of Fermentation and Bioengineering*. 78(2):200–201. DOI: 10.1016/0922-338X(94)90267-4.
- Arnell, N.W., Lowe, J.A., Challinor, A.J. & Osborn, T.J. 2019. Global and regional impacts of climate change at different levels of global temperature increase. *Climatic Change*. 155(3):377–391. DOI: 10.1007/s10584-019-02464-z.
- Arnold, F.H., Wintrode, P.L., Miyazaki, K. & Gershenson, A. 2001. How enzymes adapt: lessons from directed evolution. *Trends in Biochemical Sciences*. 26(2):100–106. DOI: 10.1016/S0968-0004(00)01755-2.
- Austin, S., Kontur, W.S., Ulbrich, A., Oshlag, J.Z., Zhang, W., Higbee, A., Zhang, Y., Coon, J.J., et al. 2015. Metabolism of Multiple Aromatic Compounds in Corn Stover Hydrolysate by *Rhodospseudomonas palustris*. *Environmental Science & Technology*. 49(14):8914–8922. DOI: 10.1021/acs.est.5b02062.
- Ayers, K., Danilovic, N., Ouimet, R., Carmo, M., Pivovar, B. & Bornstein, M. 2019. Perspectives on Low-Temperature Electrolysis and Potential for Renewable Hydrogen at Scale. *Annual Review of Chemical and Biomolecular Engineering*. 10(1):219–239. DOI: 10.1146/annurev-chembioeng-060718-030241.
- Azbar, N. & Cetinkaya Dokgoz, F.T. 2010. The effect of dilution and l-malic acid addition on bio-hydrogen production with *Rhodospseudomonas palustris* from effluent of an acidogenic anaerobic reactor. *International Journal of Hydrogen Energy*. 35(10):5028–5033. DOI: 10.1016/j.ijhydene.2009.10.044.
- Baker, M.I., Walsh, S.P., Schwartz, Z. & Boyan, B.D. 2012. A review of polyvinyl alcohol and its uses in cartilage and orthopedic applications. *Journal of Biomedical Materials Research Part B: Applied Biomaterials*. 100B(5):1451–1457. DOI: 10.1002/jbm.b.32694.
- Barber, J. & Andersson, B. 1992. Too much of a good thing: light can be bad for photosynthesis. *Trends in Biochemical Sciences*. 17(2):61–66. DOI: 10.1016/0968-0004(92)90503-2.
- Barbosa, M.J., Rocha, J.M.S., Tramper, J. & Wijffels, R.H. 2001. Acetate as a carbon source for hydrogen production by photosynthetic bacteria. *Journal of Biotechnology*. 85(1):25–33. DOI: 10.1016/S0168-1656(00)00368-0.

- Barrande, M., Bouchet, R. & Denoyel, R. 2007. Tortuosity of Porous Particles. *Analytical Chemistry*. 79(23):9115–9121. DOI: 10.1021/ac071377r.
- Bercea, M., Morariu, S. & Rusu, D. 2012. In situ gelation of aqueous solutions of entangled poly(vinyl alcohol). *Soft Matter*. 9(4):1244–1253. DOI: 10.1039/C2SM26094H.
- Bergmeyer, H.-U. 2012. *Methods of Enzymatic Analysis*. Elsevier.
- Bettmann, H. & Rehm, H.J. 1984. Degradation of phenol by polymer entrapped microorganisms. *Applied Microbiology and Biotechnology*. 20(5):285–290. DOI: 10.1007/BF00270587.
- Boateng, E. & Chen, A. 2020. Recent advances in nanomaterial-based solid-state hydrogen storage. *Materials Today Advances*. 6:100022. DOI: 10.1016/j.mtadv.2019.100022.
- Bogachev, M.I., Volkov, V.Y., Markelov, O.A., Trizna, E.Y., Baydamshina, D.R., Melnikov, V., Murtazina, R.R., Zelenikhin, P.V., et al. 2018. Fast and simple tool for the quantification of biofilm-embedded cells sub-populations from fluorescent microscopic images. *PLoS ONE*. 13(5):e0193267. DOI: 10.1371/journal.pone.0193267.
- Braatsch, S., Bernstein, J.R., Lessner, F., Morgan, J., Liao, J.C., Harwood, C.S. & Beatty, J.T. 2006. Rhodospseudomonas palustris CGA009 Has Two Functional ppsR Genes, Each of Which Encodes a Repressor of Photosynthesis Gene Expression. *Biochemistry*. 45(48):14441–14451. DOI: 10.1021/bi061074b.
- Bucke C., Brown D. E., Hartley Brian Selby, Atkinson T., & Lilly Malcolm Douglas. 1983. Immobilized cells. *Philosophical Transactions of the Royal Society of London. B, Biological Sciences*. 300(1100):369–389. DOI: 10.1098/rstb.1983.0011.
- Buitelaar, R.M., Bucke, C., Tramper, J. & Wijffels, R.H. 1996. *Immobilized Cells: Basics and Applications*. Elsevier.
- Burris, R.H. 1991. Nitrogenases. *Journal of Biological Chemistry*. 266(15):9339–9342.
- Bustin, S.A., Benes, V., Garson, J.A., Hellems, J., Huggett, J., Kubista, M., Mueller, R., Nolan, T., et al. 2009. The MIQE Guidelines: Minimum Information for Publication of Quantitative Real-Time PCR Experiments. *Clinical Chemistry*. 55(4):611–622. DOI: 10.1373/clinchem.2008.112797.
- Call, T., Carey, T., Bombelli, P., J. Lea-Smith, D., Hooper, P., J. Howe, C. & Torrisi, F. 2017. Platinum-free, graphene based anodes and air cathodes for single chamber microbial fuel cells. *Journal of Materials Chemistry A*. 5(45):23872–23886. DOI: 10.1039/C7TA06895F.
- Carlozzi, P. & Lambardi, M. 2009. Fed-batch operation for bio-H₂ production by Rhodospseudomonas palustris (strain 42OL). *Renewable Energy*. 34(12):2577–2584. DOI: 10.1016/j.renene.2009.04.016.
- Cha, W.-I., Hyon, S.-H. & Ikada, Y. 1992. Transparent poly(vinyl alcohol) hydrogel with high water content and high strength. *Die Makromolekulare Chemie*. 193(8):1913–1925. DOI: 10.1002/macp.1992.021930812.
- Chen, C.-Y., Lu, W.-B., Wu, J.-F. & Chang, J.-S. 2007. Enhancing phototrophic hydrogen production of Rhodospseudomonas palustris via statistical experimental design. *International Journal of Hydrogen Energy*. 32(8):940–949. DOI: 10.1016/j.ijhydene.2006.09.021.
- Chomczynski, P. & Sacchi, N. 2006. The single-step method of RNA isolation by acid guanidinium thiocyanate–phenol–chloroform extraction: twenty-something years on. *Nature Protocols*. 1(2):581–585. DOI: 10.1038/nprot.2006.83.
- Chong, M.-L., Sabaratnam, V., Shirai, Y. & Hassan, M.A. 2009. Biohydrogen production from biomass and industrial wastes by dark fermentation. *International Journal of Hydrogen Energy*. 34(8):3277–3287. DOI: 10.1016/j.ijhydene.2009.02.010.
- Ciriminna, R., Pina, C.D., Rossi, M. & Pagliaro, M. 2014. Understanding the glycerol market. *European Journal of Lipid Science and Technology*. 116(10):1432–1439. DOI: 10.1002/ejlt.201400229.
- Clark, R.L., McGinley, L.L., Purdy, H.M., Korosh, T.C., Reed, J.L., Root, T.W. & Pflieger, B.F. 2018. Light-optimized growth of cyanobacterial cultures: Growth phases and productivity of biomass and secreted molecules in light-limited batch growth. *Metabolic Engineering*. 47:230–242. DOI: 10.1016/j.ymben.2018.03.017.
- Cogdell, R.J. & Frank, H.A. 1987. How carotenoids function in photosynthetic bacteria. *Biochimica et Biophysica Acta (BBA) - Reviews on Bioenergetics*. 895(2):63–79. DOI: 10.1016/S0304-4173(87)80008-3.

- Crabtree, G.W., Dresselhaus, M.S. & Buchanan, M.V. 2004. The Hydrogen Economy. *Physics Today*. 57(12):39–44.
- Dahiya, S., Chatterjee, S., Sarkar, O. & Mohan, S.V. 2021. Renewable hydrogen production by dark-fermentation: Current status, challenges and perspectives. *Bioresource Technology*. 321:124354. DOI: 10.1016/j.biortech.2020.124354.
- Dervakos, G.A. & Webb, C. 1991. On the merits of viable-cell immobilisation. *Biotechnology Advances*. 9(4):559–612. DOI: 10.1016/0734-9750(91)90733-C.
- Doud, D.F.R., Holmes, E.C., Richter, H., Molitor, B., Jander, G. & Angenent, L.T. 2017. Metabolic engineering of *Rhodospseudomonas palustris* for the obligate reduction of n-butyrate to n-butanol. *Biotechnology for Biofuels*. 10(1):178. DOI: 10.1186/s13068-017-0864-3.
- Doughty, D.M., Coleman, M.L., Hunter, R.C., Sessions, A.L., Summons, R.E. & Newman, D.K. 2011. The RND-family transporter, HpnN, is required for hopanoid localization to the outer membrane of *Rhodospseudomonas palustris* TIE-1. *Proceedings of the National Academy of Sciences*. 108(45):E1045–E1051. DOI: 10.1073/pnas.1104209108.
- Eady, R.R. 1996. Structure–Function Relationships of Alternative Nitrogenases. *Chemical Reviews*. 96(7):3013–3030. DOI: 10.1021/cr950057h.
- EI-Emam, R.S. & Özcan, H. 2019. Comprehensive review on the techno-economics of sustainable large-scale clean hydrogen production. *Journal of Cleaner Production*. 220:593–609. DOI: 10.1016/j.jclepro.2019.01.309.
- Erbakan, M., Curtis, B.S., Nixon, B.T., Kumar, M. & Curtis, W.R. 2015. Advancing *Rhodobacter sphaeroides* as a platform for expression of functional membrane proteins. *Protein Expression and Purification*. 115:109–117. DOI: 10.1016/j.pep.2015.05.012.
- Fergg, F., Keil, F.J. & Quader, H. 2001. Investigations of the microscopic structure of poly(vinyl alcohol) hydrogels by confocal laser scanning microscopy. *Colloid and Polymer Science*. 279(1):61–67. DOI: 10.1007/s003960000398.
- Firsow, N.N. & Drews, G. 1977. Differentiation of the intracytoplasmic membrane of *Rhodospseudomonas palustris* induced by variations of oxygen partial pressure or light intensity. *Archives of Microbiology*. 115(3):299–306. DOI: 10.1007/BF00446456.
- Fixen, K.R., Oda, Y. & Harwood, C.S. 2016. Clades of Photosynthetic Bacteria Belonging to the Genus *Rhodospseudomonas* Show Marked Diversity in Light-Harvesting Antenna Complex Gene Composition and Expression. *mSystems*. 1(1):e00006-15. DOI: 10.1128/mSystems.00006-15.
- Fixen, K.R., Zheng, Y., Harris, D.F., Shaw, S., Yang, Z.-Y., Dean, D.R., Seefeldt, L.C. & Harwood, C.S. 2016. Light-driven carbon dioxide reduction to methane by nitrogenase in a photosynthetic bacterium. *Proceedings of the National Academy of Sciences*. 113(36):10163–10167. DOI: 10.1073/pnas.1611043113.
- Fixen, K.R., Chowdhury, N.P., Martinez-Perez, M., Poudel, S., Boyd, E.S. & Harwood, C.S. 2018. The path of electron transfer to nitrogenase in a phototrophic alpha-proteobacterium. *Environmental Microbiology*. 20(7):2500–2508. DOI: 10.1111/1462-2920.14262.
- Fixen, K.R., Oda, Y. & Harwood, C.S. 2019. Redox Regulation of a Light-Harvesting Antenna Complex in an Anoxygenic Phototroph. *mBio*. 10(6). DOI: 10.1128/mBio.02838-19.
- Fißler, J., Kohring, G.W. & Giffhorn, F. 1995. Enhanced hydrogen production from aromatic acids by immobilized cells of *Rhodospseudomonas palustris*. *Applied Microbiology and Biotechnology*. 44(1–2):43–46. DOI: 10.1007/BF00164478.
- Fornari, C.S. & Kaplan, S. 1982. Genetic transformation of *Rhodospseudomonas sphaeroides* by plasmid DNA. *Journal of Bacteriology*. 152(1):89–97.
- Fowler, A. & Toner, M. 2006. Cryo-Injury and Biopreservation. *Annals of the New York Academy of Sciences*. 1066(1):119–135. DOI: 10.1196/annals.1363.010.
- Francou, N. & Vignais, P.M. 1984. Hydrogen production by *Rhodospseudomonas capsulata* cells entrapped in carrageenan beads. *Biotechnology Letters*. 6(10):639–644. DOI: 10.1007/BF00133829.
- Fu, S., Thacker, A., Sperger, D.M., Boni, R.L., Buckner, I.S., Velankar, S., Munson, E.J. & Block, L.H. 2011. Relevance of Rheological Properties of Sodium Alginate in Solution to Calcium Alginate Gel Properties. *AAPS PharmSciTech*. 12(2):453–460. DOI: 10.1208/s12249-011-9587-0.

- Fujimori, S., Hasegawa, T., Krey, V., Riahi, K., Bertram, C., Bodirsky, B.L., Bosetti, V., Callen, J., et al. 2019. A multi-model assessment of food security implications of climate change mitigation. *Nature Sustainability*. 2(5):386–396. DOI: 10.1038/s41893-019-0286-2.
- Garbayo, I., León, R. & Vílchez, C. 2002. Diffusion characteristics of nitrate and glycerol in alginate. *Colloids and Surfaces B: Biointerfaces*. 25(1):1–9. DOI: [https://doi.org/10.1016/S0927-7765\(01\)00287-9](https://doi.org/10.1016/S0927-7765(01)00287-9).
- Ghosh, D., Tourigny, A. & Hallenbeck, P.C. 2012. Near stoichiometric reforming of biodiesel derived crude glycerol to hydrogen by photofermentation. *International Journal of Hydrogen Energy*. 37(3):2273–2277. DOI: 10.1016/j.ijhydene.2011.11.011.
- Ghosh, D., Sobro, I.F. & Hallenbeck, P.C. 2012. Stoichiometric conversion of biodiesel derived crude glycerol to hydrogen: Response surface methodology study of the effects of light intensity and crude glycerol and glutamate concentration. *Bioresource Technology*. 106:154–160. DOI: 10.1016/j.biortech.2011.12.021.
- Gibson, D.G., Young, L., Chuang, R.-Y., Venter, J.C., Hutchison, C.A. & Smith, H.O. 2009. Enzymatic assembly of DNA molecules up to several hundred kilobases. *Nature Methods*. 6(5):343–345. DOI: 10.1038/nmeth.1318.
- Giraud, E., Zappa, S., Vuillet, L., Adriano, J.-M., Hannibal, L., Fardoux, J., Berthomieu, C., Bouyer, P., et al. 2005. A New Type of Bacteriophytochrome Acts in Tandem with a Classical Bacteriophytochrome to Control the Antennae Synthesis in *Rhodospseudomonas palustris*. *Journal of Biological Chemistry*. 280(37):32389–32397. DOI: 10.1074/jbc.M506890200.
- Giraud, E., Hannibal, L., Chaintreuil, C., Fardoux, J. & Verméglio, A. 2018. Synthesis of Carotenoids of Industrial Interest in the Photosynthetic Bacterium *Rhodospseudomonas palustris*: Bioengineering and Growth Conditions. In *Microbial Carotenoids: Methods and Protocols*. C. Barreiro & J.-L. Barredo, Eds. (Methods in Molecular Biology). New York, NY: Springer. 211–220. DOI: 10.1007/978-1-4939-8742-9_12.
- Golomysova, A., Gomelsky, M. & Ivanov, P.S. 2010. Flux balance analysis of photoheterotrophic growth of purple nonsulfur bacteria relevant to biohydrogen production. *International Journal of Hydrogen Energy*. 35(23):12751–12760. DOI: 10.1016/j.ijhydene.2010.08.133.
- Gough, J.E., Scotchford, C.A. & Downes, S. 2002. Cytotoxicity of glutaraldehyde crosslinked collagen/poly(vinyl alcohol) films is by the mechanism of apoptosis. *Journal of Biomedical Materials Research*. 61(1):121–130. DOI: 10.1002/jbm.10145.
- Guo, C.-L., Zhu, X., Liao, Q., Wang, Y.-Z., Chen, R. & Lee, D.-J. 2011. Enhancement of photo-hydrogen production in a biofilm photobioreactor using optical fiber with additional rough surface. *Bioresource Technology*. 102(18):8507–8513. DOI: 10.1016/j.biortech.2011.04.075.
- Gupta, S.K., Kumari, S., Reddy, K. & Bux, F. 2013. Trends in biohydrogen production: major challenges and state-of-the-art developments. *Environmental Technology*. 34(13–14):1653–1670. DOI: 10.1080/09593330.2013.822022.
- Gürkan, M., Koku, H., Eroglu, I. & Yücel, M. 2020. Microarray analysis of high light intensity stress on hydrogen production metabolism of *Rhodobacter capsulatus*. *International Journal of Hydrogen Energy*. 45(5):3516–3523. DOI: 10.1016/j.ijhydene.2018.12.205.
- Guzman, M.S., Rengasamy, K., Binkley, M.M., Jones, C., Ranaivoarisoa, T.O., Singh, R., Fike, D.A., Meacham, J.M., et al. 2019. Phototrophic extracellular electron uptake is linked to carbon dioxide fixation in the bacterium *Rhodospseudomonas palustris*. *Nature Communications*. 10(1):1–13. DOI: 10.1038/s41467-019-09377-6.
- Hallenbeck, P.C. 1983. Nitrogenase reduction by electron carriers: Influence of redox potential on activity and the ATP_{2e}- ratio. *Archives of Biochemistry and Biophysics*. 220(2):657–660. DOI: 10.1016/0003-9861(83)90460-5.
- Hallenbeck, P.C. & Benemann, J.R. 2002. Biological hydrogen production; fundamentals and limiting processes. *International Journal of Hydrogen Energy*. 27(11–12):1185–1193. DOI: 10.1016/S0360-3199(02)00131-3.
- Hallenbeck, P.C. & Ghosh, D. 2009. Advances in fermentative biohydrogen production: the way forward? *Trends in Biotechnology*. 27(5):287–297. DOI: 10.1016/j.tibtech.2009.02.004.
- Hallenbeck, P.C. & Liu, Y. 2016. Recent advances in hydrogen production by photosynthetic bacteria. *International Journal of Hydrogen Energy*. 41(7):4446–4454. DOI: 10.1016/j.ijhydene.2015.11.090.
- Hallenbeck, P.C., Ghosh, D., Skonieczny, M.T. & Yargeau, V. 2009. Microbiological and engineering aspects of biohydrogen production. *Indian Journal of Microbiology*. 49(1):48–59. DOI: 10.1007/s12088-009-0010-4.

- Hamngren Blomqvist, C., Abrahamsson, C., Gebäck, T., Altskär, A., Hermansson, A.-M., Nydén, M., Gustafsson, S., Lorén, N., et al. 2015. Pore size effects on convective flow and diffusion through nanoporous silica gels. *Colloids and Surfaces A: Physicochemical and Engineering Aspects*. 484:288–296. DOI: 10.1016/j.colsurfa.2015.07.032.
- Hanipa, M.A.F., Abdul, P.M., Jahim, J.M., Takriff, M.S., Reungsang, A. & Wu, S.-Y. 2020. Biotechnological approach to generate green biohydrogen through the utilization of succinate-rich fermentation wastewater. *International Journal of Hydrogen Energy*. 45(42):22246–22259. DOI: 10.1016/j.ijhydene.2019.09.192.
- Harrison, F.H. 2005. The pimFABCDE operon from *Rhodospseudomonas palustris* mediates dicarboxylic acid degradation and participates in anaerobic benzoate degradation. *Microbiology*. 151(3):727–736. DOI: 10.1099/mic.0.27731-0.
- Harwood, C.S. 2008. Nitrogenase-Catalyzed Hydrogen Production by Purple Nonsulfur Photosynthetic Bacteria. (January, 1):259–271. DOI: 10.1128/9781555815547.ch21.
- Harwood, C.S. & Gibson, J. 1988. Anaerobic and aerobic metabolism of diverse aromatic compounds by the photosynthetic bacterium *Rhodospseudomonas palustris*. *Applied and Environmental Microbiology*. 54(3):712–717.
- Hashimoto, H., Uragami, C. & Cogdell, R.J. 2016. Carotenoids and Photosynthesis. In *Carotenoids in Nature*. (Subcellular Biochemistry). Springer, Cham. 111–139. DOI: 10.1007/978-3-319-39126-7_4.
- Hassan, C. & Peppas, N. 2000. Structure and applications of poly (vinyl alcohol) hydrogels produced by conventional crosslinking or by freezing/thawing methods. In *Biopolymers: PVA Hydrogels, Anionic Polymerisation Nanocomposites*. (Advances in Polymer Science). Springer, Berlin, Heidelberg. 37–65. Available: <http://link.springer.com/content/pdf/10.1007/3-540-46414-X.pdf#page=46>.
- Haynes, W.M., Lide, D.R. & Bruno, T.J. 2016. *CRC handbook of chemistry and physics : a ready-reference book of chemical and physical data*. 97th ed. Boca Raton, Florida: CRC Press.
- Heck, A. & Drepper, T. 2017. Engineering Photosynthetic α -Proteobacteria for the Production of Recombinant Proteins and Terpenoids. In *Modern Topics in the Phototrophic Prokaryotes: Environmental and Applied Aspects*. P.C. Hallenbeck, Ed. Cham: Springer International Publishing. 395–425. DOI: 10.1007/978-3-319-46261-5_12.
- Heiniger, E.K. & Harwood, C.S. 2015. Posttranslational modification of a vanadium nitrogenase. *MicrobiologyOpen*. 4(4):597–603. DOI: 10.1002/mbo3.265.
- Heiniger, E.K., Oda, Y., Samanta, S.K. & Harwood, C.S. 2012a. How Posttranslational Modification of Nitrogenase Is Circumvented in *Rhodospseudomonas palustris* Strains That Produce Hydrogen Gas Constitutively. *Applied and Environmental Microbiology*. 78(4):1023–1032. DOI: 10.1128/AEM.07254-11.
- Heiniger, E.K., Oda, Y., Samanta, S.K. & Harwood, C.S. 2012b. How Posttranslational Modification of Nitrogenase Is Circumvented in *Rhodospseudomonas palustris* Strains That Produce Hydrogen Gas Constitutively. *Applied and Environmental Microbiology*. 78(4):1023–1032. DOI: 10.1128/AEM.07254-11.
- Hellingwerf, K.J., Crielaard, W., Hoff, W.D., Matthijs, H.C.P., Mur, L.R. & Rotterdam, B.J. van. 1994. Photobiology of Bacteria. *Antonie van Leeuwenhoek*. 65(4):331–347. DOI: 10.1007/BF00872217.
- Hénin, J., Tajkhorshid, E., Schulten, K. & Chipot, C. 2008. Diffusion of Glycerol through *Escherichia coli* Aquaglyceroporin GlpF. *Biophysical Journal*. 94(3):832–839. DOI: 10.1529/biophysj.107.115105.
- Higuchi-Takeuchi, M., Morisaki, K. & Numata, K. 2020. Method for the facile transformation of marine purple photosynthetic bacteria using chemically competent cells. *MicrobiologyOpen*. 9(1):e00953. DOI: 10.1002/mbo3.953.
- Hirakawa, H., Harwood, C.S., Pechter, K.B., Schaefer, A.L. & Greenberg, E.P. 2012. Antisense RNA that affects *Rhodospseudomonas palustris* quorum-sensing signal receptor expression. *Proceedings of the National Academy of Sciences*. 109(30):12141–12146. DOI: 10.1073/pnas.1200243109.
- Hirayama, O., Uya, K., Hiramatsu, Y., Yamada, H. & Moriwaki, K. 1986. Photoproduction of Hydrogen by Immobilized Cells of a Photosynthetic Bacterium, *Rhodospirillum rubrum* G-9 BM. *Agricultural and Biological Chemistry*. 50(4):891–897. DOI: 10.1271/bbb1961.50.891.
- Hisada, T., Okamura, K. & Hiraishi, A. 2007. Isolation and Characterization of Phototrophic Purple Nonsulfur Bacteria from *Chloroflexus* and Cyanobacterial Mats in Hot Springs. *Microbes and Environments*. 22(4):405–411. DOI: 10.1264/jsme2.22.405.

- Holloway, J.L., Lowman, A.M. & Palmese, G.R. 2013a. The role of crystallization and phase separation in the formation of physically cross-linked PVA hydrogels. *Soft Matter*. 9(3):826–833. DOI: 10.1039/C2SM26763B.
- Holloway, J.L., Lowman, A.M. & Palmese, G.R. 2013b. The role of crystallization and phase separation in the formation of physically cross-linked PVA hydrogels. *Soft Matter*. 9(3):826–833. DOI: 10.1039/C2SM26763B.
- Hu, Y. & Ribbe, M.W. 2013. Nitrogenase assembly. *Biochimica et Biophysica Acta (BBA) - Bioenergetics*. 1827(8):1112–1122. DOI: 10.1016/j.bbabi.2012.12.001.
- Hu, J., Jing, Y., Zhang, Q., Guo, J. & Lee, D.-J. 2017. Mesophilic and thermophilic photo-hydrogen production from micro-grinded, enzyme-hydrolyzed maize straws. *International Journal of Hydrogen Energy*. 42(45):27618–27622. DOI: 10.1016/j.ijhydene.2017.05.077.
- Hyon, S.-H., Cha, W.-I. & Ikada, Y. 1989. Preparation of transparent poly(vinyl alcohol) hydrogel. *Polymer Bulletin*. 22(2):119–122. DOI: 10.1007/BF00255200.
- Ichimura, M., Nakayama-Imaohji, H., Wakimoto, S., Morita, H., Hayashi, T. & Kuwahara, T. 2010. Efficient Electrotransformation of *Bacteroides fragilis*. *Applied and Environmental Microbiology*. 76(10):3325–3332. DOI: 10.1128/AEM.02420-09.
- Idi, A., Md Nor, M.H., Abdul Wahab, M.F. & Ibrahim, Z. 2015. Photosynthetic bacteria: an eco-friendly and cheap tool for bioremediation. *Reviews in Environmental Science and Bio/Technology*. 14(2):271–285. DOI: 10.1007/s11157-014-9355-1.
- Imhoff, J.F., Meyer, T.E. & Kyndt, J. 2020. Genomic and genetic sequence information of strains assigned to the genus *Rhodopseudomonas* reveal the great heterogeneity of the group and identify strain *Rhodopseudomonas palustris* DSM 123T as the authentic type strain of this species. *International Journal of Systematic and Evolutionary Microbiology*. DOI: 10.1099/ijsem.0.004077.
- Inada, T. & Lu, S.-S. 2003. Inhibition of Recrystallization of Ice Grains by Adsorption of Poly(Vinyl Alcohol) onto Ice Surfaces. *Crystal Growth & Design*. 3(5):747–752. DOI: 10.1021/cg0340300.
- Inui, M., Roh, J.H., Zahn, K. & Yukawa, H. 2000. Sequence Analysis of the Cryptic Plasmid pMG101 from *Rhodopseudomonas palustris* and Construction of Stable Cloning Vectors. *Applied and Environmental Microbiology*. 66(1):54–63. DOI: 10.1128/AEM.66.1.54-63.2000.
- Jackson, P.J., Hitchcock, A., Swainsbury, D.J.K., Qian, P., Martin, E.C., Farmer, D.A., Dickman, M.J., Canniffe, D.P., et al. 2018. Identification of protein W, the elusive sixth subunit of the *Rhodopseudomonas palustris* reaction center-light harvesting 1 core complex. *Biochimica et Biophysica Acta (BBA) - Bioenergetics*. 1859(2):119–128. DOI: 10.1016/j.bbabi.2017.11.001.
- Jahn, C.E., Charkowski, A.O. & Willis, D.K. 2008. Evaluation of isolation methods and RNA integrity for bacterial RNA quantitation. *Journal of Microbiological Methods*. 75(2):318–324. DOI: 10.1016/j.mimet.2008.07.004.
- Jasniewski, A.J., Sickerman, N.S., Hu, Y. & Ribbe, M.W. 2018. The Fe Protein: An Unsung Hero of Nitrogenase. *Inorganics*. 6(1):25. DOI: 10.3390/inorganics6010025.
- Jouanneau, Y., Wong, B. & Vignais, P.M. 1985. Stimulation by light of nitrogenase synthesis in cells of *Rhodopseudomonas capsulata* growing in N-limited continuous cultures. *Biochimica et Biophysica Acta (BBA) - Bioenergetics*. 808(1):149–155. DOI: 10.1016/0005-2728(85)90037-4.
- Kaftan, D., Bina, D. & Koblížek, M. 2019. Temperature dependence of photosynthetic reaction centre activity in *Rhodospirillum rubrum*. *Photosynthesis Research*. 142(2):181–193. DOI: 10.1007/s11120-019-00652-7.
- Kaiser, I. & Oelze, J. 1980. Growth and adaptation to phototrophic conditions of *Rhodospirillum rubrum* and *Rhodopseudomonas sphaeroides* at different temperatures. *Archives of Microbiology*. 126(2):187–194. DOI: 10.1007/BF00511226.
- Kanaya, T., Takahashi, N., Takeshita, H., Ohkura, M., Nishida, K. & Kaji, K. 2012. Structure and dynamics of poly(vinyl alcohol) gels in mixtures of dimethyl sulfoxide and water. *Polymer Journal*. 44(1):83–94. DOI: 10.1038/pj.2011.88.
- Kapdan, I.K. & Kargi, F. 2006. Bio-hydrogen production from waste materials. *Enzyme and Microbial Technology*. 38(5):569–582. DOI: 10.1016/j.enzmictec.2005.09.015.
- Karl, T.R. & Trenberth, K.E. 2003. Modern Global Climate Change. *Science*. 302(5651):1719–1723. DOI: 10.1126/science.1090228.

- Karpinets, T.V., Pelletier, D.A., Pan, C., Uberbacher, E.C., Melnichenko, G.V., Hettich, R.L. & Samatova, N.F. 2009. Phenotype Fingerprinting Suggests the Involvement of Single-Genotype Consortia in Degradation of Aromatic Compounds by *Rhodopseudomonas palustris*. *PLOS ONE*. 4(2):e4615. DOI: 10.1371/journal.pone.0004615.
- Keskin, T. & Hallenbeck, P.C. 2012. Hydrogen production from sugar industry wastes using single-stage photofermentation. *Bioresource Technology*. 112:131–136. DOI: 10.1016/j.biortech.2012.02.077.
- Kim, M.-K. & Harwood, C.S. 1991. Regulation of benzoate-CoA ligase in *Rhodopseudomonas palustris*. *FEMS Microbiology Letters*. 83(2):199–203. DOI: 10.1111/j.1574-6968.1991.tb04440.x-i1.
- Kim, B.W., Kim, I.K. & Chang, H.N. 1990. Bioconversion of hydrogen sulfide by free and immobilized cells of *Chlorobium thiosulfatophilum*. *Biotechnology Letters*. 12(5):381–386. DOI: 10.1007/BF01024436.
- Kim, M.K., Choi, K.-M., Yin, C.-R., Lee, K.-Y., Im, W.-T., Lim, J.H. & Lee, S.-T. 2004. Odorous swine wastewater treatment by purple non-sulfur bacteria, *Rhodopseudomonas palustris*, isolated from eutrophicated ponds. *Biotechnology Letters*. 26(10):819–822. DOI: 10.1023/B:BILE.0000025884.50198.67.
- Kolosova, O.Y., Kurochkin, I.N., Kurochkin, I.I. & Lozinsky, V.I. 2018. Cryostructuring of polymeric systems. 48. Influence of organic chaotropes and kosmotropes on the cryotropic gel-formation of aqueous poly(vinyl alcohol) solutions. *European Polymer Journal*. 102:169–177. DOI: 10.1016/j.eurpolymj.2018.03.010.
- Kondo, T., Arakawa, M., Hirai, T., Wakayama, T., Hara, M. & Miyake, J. 2002. Enhancement of hydrogen production by a photosynthetic bacterium mutant with reduced pigment. *Journal of Bioscience and Bioengineering*. 93(2):145–150. DOI: 10.1016/S1389-1723(02)80006-8.
- Kutsche, M., Leimkühler, S., Angermüller, S. & Klipp, W. 1996. Promoters controlling expression of the alternative nitrogenase and the molybdenum uptake system in *Rhodobacter capsulatus* are activated by NtrC, independent of sigma54, and repressed by molybdenum. *Journal of Bacteriology*. 178(7):2010–2017. DOI: 10.1128/jb.178.7.2010-2017.1996.
- Laing, R.M.L. 2018. Development of *Rhodopseudomonas palustris* as a chassis for biotechnological applications. Thesis. University of Cambridge. DOI: 10.17863/CAM.30560.
- Lane, L.B. 1925. Freezing Points of Glycerol and Its Aqueous Solutions. *Industrial & Engineering Chemistry*. 17(9):924–924. DOI: 10.1021/ie50189a017.
- Larimer, F.W., Chain, P., Hauser, L., Lamerdin, J., Malfatti, S., Do, L., Land, M.L., Pelletier, D.A., et al. 2004. Complete genome sequence of the metabolically versatile photosynthetic bacterium *Rhodopseudomonas palustris*. *Nature Biotechnology*. 22(1):55–61. DOI: 10.1038/nbt923.
- Laurinavichene, T. & Tsygankov, A. 2018. Inoculum density and buffer capacity are crucial for H₂ photoproduction from acetate by purple bacteria. *International Journal of Hydrogen Energy*. 43(41):18873–18882. DOI: 10.1016/j.ijhydene.2018.08.095.
- Laussermair, E. & Oesterhelt, D. 1992. A system for site-specific mutagenesis of the photosynthetic reaction center in *Rhodopseudomonas viridis*. *The EMBO Journal*. 11(2):777–783. DOI: 10.1002/j.1460-2075.1992.tb05111.x.
- Lazaro, C.Z., Varesche, M.B.A. & Silva, E.L. 2015. Sequential fermentative and phototrophic system for hydrogen production: An approach for Brazilian alcohol distillery wastewater. *International Journal of Hydrogen Energy*. 40(31):9642–9655. DOI: 10.1016/j.ijhydene.2015.06.003.
- Lee, H.-S., Salerno, M.B. & Rittmann, B.E. 2008. Thermodynamic Evaluation on H₂ Production in Glucose Fermentation. *Environmental Science & Technology*. 42(7):2401–2407. DOI: 10.1021/es702610v.
- Lee, H.-S., Krajmalnik-Brown, R., Zhang, H. & Rittmann, B.E. 2009. An electron-flow model can predict complex redox reactions in mixed-culture fermentative BioH₂: Microbial ecology evidence. *Biotechnology and Bioengineering*. 104(4):687–697. DOI: 10.1002/bit.22442.
- Letunic, I. & Bork, P. 2019. Interactive Tree Of Life (iTOL) v4: recent updates and new developments. *Nucleic Acids Research*. 47(W1):W256–W259. DOI: 10.1093/nar/gkz239.
- Li, S., Zheng, H., Zheng, Y., Tian, J., Jing, T., Chang, J.-S. & Ho, S.-H. 2019. Recent advances in hydrogen production by thermo-catalytic conversion of biomass. *International Journal of Hydrogen Energy*. 44(28):14266–14278. DOI: 10.1016/j.ijhydene.2019.03.018.

- Llorens, I., Untereiner, G., Jaillard, D., Gouget, B., Chapon, V. & Carriere, M. 2012. Uranium Interaction with Two Multi-Resistant Environmental Bacteria: *Cupriavidus metallidurans* CH34 and *Rhodopseudomonas palustris*. *PLOS ONE*. 7(12):e51783. DOI: 10.1371/journal.pone.0051783.
- Lozinsky, V.I. 2009. Polymeric cryogels as a new family of macroporous and supermacroporous materials for biotechnological purposes. *Russian Chemical Bulletin*. 57(5):1015–1032. DOI: 10.1007/s11172-008-0131-7.
- Lozinsky, V.I. & Plieva, F.M. 1998. Poly(vinyl alcohol) cryogels employed as matrices for cell immobilization. 3. Overview of recent research and developments. *Enzyme and Microbial Technology*. 23(3–4):227–242. DOI: 10.1016/S0141-0229(98)00036-2.
- Lozinsky, V.I., Vainerman, E.S., Domotenko, L.V., Mamtsis, A.M., Titova, E.F., Belavtseva, E.M. & Rogozhin, S.V. 1986. Study of cryostructurization of polymer systems VII. Structure formation under freezing of poly(vinyl alcohol) aqueous solutions. *Colloid and Polymer Science*. 264(1):19–24. DOI: 10.1007/BF01410304.
- Lozinsky, V.I., Solodova, E.V., Zubov, A.L. & Simenel, I.A. 1995. Study of cryostructuration of polymer systems. XI. The formation of PVA cryogels by freezing–thawing the polymer aqueous solutions containing additives of some polyols. *Journal of Applied Polymer Science*. 58(1):171–177. DOI: 10.1002/app.1995.070580119.
- Lozinsky, V.I., Zubov, A.L. & Titova, E.F. 1996. Swelling behavior of poly(vinyl alcohol) cryogels employed as matrices for cell immobilization. *Enzyme and Microbial Technology*. 18(8):561–569. DOI: 10.1016/0141-0229(95)00148-4.
- Lozinsky, V.I., Zubov, A.L. & Makhlis, T.A. 1996. Entrapment of *Zymomonas mobilis* cells into PVA-cryogel carrier in the presence of polyol cryoprotectants. In *Progress in Biotechnology*. V. 11. Elsevier. 112–117.
- Lozinsky, V.I., Galaev, I.Yu., Plieva, F.M., Savina, I.N., Jungvid, H. & Mattiasson, B. 2003. Polymeric cryogels as promising materials of biotechnological interest. *Trends in Biotechnology*. 21(10):445–451. DOI: 10.1016/j.tibtech.2003.08.002.
- Lozinsky, V.I., Damshkaln, L.G., Shaskol'skii, B.L., Babushkina, T.A., Kurochkin, I.N. & Kurochkin, I.I. 2007. Study of cryostructuring of polymer systems: 27. Physicochemical properties of poly(vinyl alcohol) cryogels and specific features of their macroporous morphology. *Colloid Journal*. 69(6):747–764. DOI: 10.1134/S1061933X07060117.
- Lu, C., Zhang, Z., Ge, X., Wang, Y., Zhou, X., You, X., Liu, H. & Zhang, Q. 2016. Bio-hydrogen production from apple waste by photosynthetic bacteria HAU-M1. *International Journal of Hydrogen Energy*. 41(31):13399–13407. DOI: 10.1016/j.ijhydene.2016.06.101.
- Ma, C., Guo, L. & Yang, H. 2012. Improved photo – Hydrogen production by transposon mutant of *Rhodobacter capsulatus* with reduced pigment. *International Journal of Hydrogen Energy*. 37(17):12229–12233. DOI: 10.1016/j.ijhydene.2012.05.148.
- Madigan, M.T. & Jung, D.O. 2009. An Overview of Purple Bacteria: Systematics, Physiology, and Habitats. In *The Purple Phototrophic Bacteria*. C.N. Hunter, F. Daldal, M.C. Thurnauer, & J.T. Beatty, Eds. (Advances in Photosynthesis and Respiration). Dordrecht: Springer Netherlands. 1–15. DOI: 10.1007/978-1-4020-8815-5_1.
- Mancini, M., Moresi, M. & Rancini, R. 1999. Mechanical properties of alginate gels: empirical characterisation. *Journal of Food Engineering*. 39(4):369–378. DOI: 10.1016/S0260-8774(99)00022-9.
- Mattiasson, B. 2014. Cryogels for Biotechnological Applications. In *Polymeric Cryogels: Macroporous Gels with Remarkable Properties*. O. Okay, Ed. Springer International Publishing. 245–281. DOI: 10.1007/978-3-319-05846-7_7.
- McCully, A.L. & McKinlay, J.B. 2016. Disrupting Calvin cycle phosphoribulokinase activity in *Rhodopseudomonas palustris* increases the H₂ yield and specific production rate proportionately. *International Journal of Hydrogen Energy*. 41(7):4143–4149. DOI: 10.1016/j.ijhydene.2016.01.003.
- McKinlay, J.B. 2014. Systems Biology of Photobiological Hydrogen Production by Purple Non-sulfur Bacteria. In *Microbial BioEnergy: Hydrogen Production*. D. Zannoni & R. De Philippis, Eds. (Advances in Photosynthesis and Respiration). Dordrecht: Springer Netherlands. 155–176. DOI: 10.1007/978-94-017-8554-9_7.
- McKinlay, J.B. & Harwood, C.S. 2010a. Photobiological production of hydrogen gas as a biofuel. *Current Opinion in Biotechnology*. 21(3):244–251. DOI: 10.1016/j.copbio.2010.02.012.

- McKinlay, J.B. & Harwood, C.S. 2010b. Carbon dioxide fixation as a central redox cofactor recycling mechanism in bacteria. *Proceedings of the National Academy of Sciences*. 107(26):11669–11675. DOI: 10.1073/pnas.1006175107.
- McKinlay, J.B. & Harwood, C.S. 2011. Calvin Cycle Flux, Pathway Constraints, and Substrate Oxidation State Together Determine the H₂ Biofuel Yield in Photoheterotrophic Bacteria. *mBio*. 2(2):e00323-10. DOI: 10.1128/mBio.00323-10.
- McKinlay, J.B., Oda, Y., Rühl, M., Posto, A.L., Sauer, U. & Harwood, C.S. 2014. Non-growing *Rhodospseudomonas palustris* Increases the Hydrogen Gas Yield from Acetate by Shifting from the Glyoxylate Shunt to the Tricarboxylic Acid Cycle. *Journal of Biological Chemistry*. 289(4):1960–1970. DOI: 10.1074/jbc.M113.527515.
- McRose, D.L., Zhang, X., Kraepiel, A.M.L. & Morel, F.M.M. 2017. Diversity and Activity of Alternative Nitrogenases in Sequenced Genomes and Coastal Environments. *Frontiers in Microbiology*. 8. DOI: 10.3389/fmicb.2017.00267.
- Melnicki, M.R., Bianchi, L., De Philippis, R. & Melis, A. 2008. Hydrogen production during stationary phase in purple photosynthetic bacteria. *International Journal of Hydrogen Energy*. 33(22):6525–6534. DOI: 10.1016/j.ijhydene.2008.08.041.
- Minshall, N. & Git, A. 2020. Enzyme- and gene-specific biases in reverse transcription of RNA raise concerns for evaluating gene expression. *Scientific Reports*. 10(1):8151. DOI: 10.1038/s41598-020-65005-0.
- Mishra, P., Krishnan, S., Rana, S., Singh, L., Sakinah, M. & Ab Wahid, Z. 2019. Outlook of fermentative hydrogen production techniques: An overview of dark, photo and integrated dark-photo fermentative approach to biomass. *Energy Strategy Reviews*. 24:27–37. DOI: 10.1016/j.esr.2019.01.001.
- Mitsukawa, H., Shimizu, O. & Nishi, H. 1971. Colorimetric Determination of α -Amino Nitrogen in Urine and Plasma with Ninhydrin Reaction. *Agricultural and Biological Chemistry*. 35(2):272–274. DOI: 10.1271/bbb1961.35.272.
- Mohanraj, S., Pandey, A., Venkata Mohan, S., Anbalagan, K., Kodhaiyoli, S. & Pugalenti, V. 2019. Chapter 17 - Metabolic Engineering and Molecular Biotechnology of Biohydrogen Production. In *Biohydrogen (Second Edition)*. A. Pandey, S.V. Mohan, J.-S. Chang, P.C. Hallenbeck, & C. Larroche, Eds. (Biomass, Biofuels, Biochemicals). Elsevier. 413–434. DOI: 10.1016/B978-0-444-64203-5.00017-4.
- Moradi, R. & Groth, K.M. 2019. Hydrogen storage and delivery: Review of the state of the art technologies and risk and reliability analysis. *International Journal of Hydrogen Energy*. 44(23):12254–12269. DOI: 10.1016/j.ijhydene.2019.03.041.
- Mota, M., Teixeira, J.A. & Yelshin, A. 2001. Immobilized Particles in Gel Matrix-Type Porous Media. Homogeneous Porous Media Model. *Biotechnology Progress*. 17(5):860–865. DOI: 10.1021/bp010064t.
- Mousavian, Z., Sadeghi, H.M.M., Sabzghabae, A.M. & Moazen, F. 2014. Polymerase chain reaction amplification of a GC rich region by adding 1,2 propanediol. *Advanced Biomedical Research*. 3(1):65. DOI: 10.4103/2277-9175.125846.
- Mullineaux, C.W. & Liu, L.-N. 2020. Membrane Dynamics in Phototrophic Bacteria. *Annual Review of Microbiology*. 74(1):633–654. DOI: 10.1146/annurev-micro-020518-120134.
- Muzziotti, D., Adessi, A., Faraloni, C., Torzillo, G. & De Philippis, R. 2016. H₂ production in *Rhodospseudomonas palustris* as a way to cope with high light intensities. *Research in Microbiology*. (April, 3). DOI: 10.1016/j.resmic.2016.02.003.
- Muzziotti, D., Adessi, A., Faraloni, C., Torzillo, G. & De Philippis, R. 2017. Acclimation strategy of *Rhodospseudomonas palustris* to high light irradiance. *Microbiological Research*. 197:49–55. DOI: 10.1016/j.micres.2017.01.007.
- Nagadomi, H., Hiromitsu, T., Takeno, K., Watanabe, M. & Sasaki, K. 1999. Treatment of aquarium water by denitrifying photosynthetic bacteria using immobilized polyvinyl alcohol beads. *Journal of Bioscience and Bioengineering*. 87(2):189–193. DOI: 10.1016/S1389-1723(99)89011-2.
- Namsaraev, Z.B., Gorlenko, V.M., Namsaraev, B.B., Buryukhaev, S.P. & Yurkov, V.V. 2003. The Structure and Biogeochemical Activity of the Phototrophic Communities from the Bol'shorechenskii Alkaline Hot Spring. *Microbiology*. 72(2):193–203. DOI: 10.1023/A:1023272131859.

- National Energy Act (34/2008): Draft Position on the South African Biofuels Regulatory Framework*. 2008. V. 34. Available: http://www.energy.gov.za/files/policies/Draft_position_paper_on_the_SA_Biofuels_Reg_Frmwrk.pdf.
- Nedovic, V. & Willaert, R. 2013. *Fundamentals of Cell Immobilisation Biotechnology*. Springer Netherlands. Available: <https://books.google.co.za/books?id=ts7tCAAQBAJ>.
- Neubauer, C., Dalleska, N.F., Cowley, E.S., Shikuma, N.J., Wu, C.-H., Sessions, A.L. & Newman, D.K. 2015. Lipid remodeling in *Rhodopseudomonas palustris* TIE-1 upon loss of hopanoids and hopanoid methylation. *Geobiology*. 13(5):443–453. DOI: 10.1111/gbi.12143.
- van Niel, C.B. 1944. The culture, general physiology, morphology, and classification of the non-sulfur purple and brown bacteria. *Bacteriological Reviews*. 8(1):1–118.
- van Niel, C.B. 1971. [1] Techniques for the enrichment, isolation, and maintenance of the photosynthetic bacteria. In *Methods in Enzymology*. V. 23. (Photosynthesis and Nitrogen Part A). Academic Press. 3–28. DOI: 10.1016/S0076-6879(71)23077-9.
- Obradovic, B., Nedović, V.A., Bugarski, B., Willaert, R.G. & Vunjak-Novakovic, G. 2004. Immobilised Cell Bioreactors. In *Fundamentals of Cell Immobilisation Biotechnology*. V. Nedović & R. Willaert, Eds. Dordrecht: Springer Netherlands. 411–436. DOI: 10.1007/978-94-017-1638-3_22.
- Oda, Y., Samanta, S.K., Rey, F.E., Wu, L., Liu, X., Yan, T., Zhou, J. & Harwood, C.S. 2005a. Functional Genomic Analysis of Three Nitrogenase Isozymes in the Photosynthetic Bacterium *Rhodopseudomonas palustris*. *Journal of Bacteriology*. 187(22):7784–7794. DOI: 10.1128/JB.187.22.7784-7794.2005.
- Oda, Y., Samanta, S.K., Rey, F.E., Wu, L., Liu, X., Yan, T., Zhou, J. & Harwood, C.S. 2005b. Functional Genomic Analysis of Three Nitrogenase Isozymes in the Photosynthetic Bacterium *Rhodopseudomonas palustris*. *Journal of Bacteriology*. 187(22):7784–7794. DOI: 10.1128/JB.187.22.7784-7794.2005.
- Oda, Y., Larimer, F.W., Chain, P.S.G., Malfatti, S., Shin, M.V., Vergez, L.M., Hauser, L., Land, M.L., et al. 2008. Multiple genome sequences reveal adaptations of a phototrophic bacterium to sediment microenvironments. *Proceedings of the National Academy of Sciences*. 105(47):18543–18548. DOI: 10.1073/pnas.0809160105.
- Oh, Y.-K., Seol, E.-H., Kim, M.-S. & Park, S. 2004. Photoproduction of hydrogen from acetate by a chemoheterotrophic bacterium *Rhodopseudomonas palustris* P4. *International Journal of Hydrogen Energy*. 29(11):1115–1121. DOI: 10.1016/j.ijhydene.2003.11.008.
- Oh, Y.-K., Raj, S.M., Jung, G.Y. & Park, S. 2013. Chapter 3 - Metabolic Engineering of Microorganisms for Biohydrogen Production. In *Biohydrogen*. A. Pandey, J.-S. Chang, P.C. Hallenbecka, & C. Larroche, Eds. Amsterdam: Elsevier. 45–65. DOI: 10.1016/B978-0-444-59555-3.00003-9.
- Okazaki, M., Hamada, T., Fujii, H., Mizobe, A. & Matsuzawa, S. 1995. Development of poly(vinyl alcohol) hydrogel for waste water cleaning. I. Study of poly(vinyl alcohol) gel as a carrier for immobilizing microorganisms. *Journal of Applied Polymer Science*. 58(12):2235–2241. DOI: 10.1002/app.1995.070581212.
- Oshlag, J.Z., Ma, Y., Morse, K., Burger, B.T., Lemke, R.A., Karlen, S.D., Myers, K.S., Donohue, T.J., et al. 2020. Anaerobic Degradation of Syringic Acid by an Adapted Strain of *Rhodopseudomonas palustris*. *Applied and Environmental Microbiology*. 86(3). DOI: 10.1128/AEM.01888-19.
- Ouchane, S., Picaud, M., Reiss-Husson, F., Vernotte, C. & Astier, C. 1996. Development of gene transfer methods for *Rubrivivax gelatinosus* S1: construction, characterization and complementation of apuf operon deletion strain. *Molecular and General Genetics MGG*. 252(4):379–385. DOI: 10.1007/BF02173002.
- Øyaas, J., Storrø, I., Svendsen, H. & Levine, D.W. 1995. The effective diffusion coefficient and the distribution constant for small molecules in calcium-alginate gel beads. *Biotechnology and Bioengineering*. 47(4):492–500. DOI: 10.1002/bit.260470411.
- Pechter, K.B., Gallagher, L., Pyles, H., Manoil, C.S. & Harwood, C.S. 2016. Essential Genome of the Metabolically Versatile Alphaproteobacterium *Rhodopseudomonas palustris*. *Journal of Bacteriology*. 198(5):867–876. DOI: 10.1128/JB.00771-15.
- Pechter, K.B., Yin, L., Oda, Y., Gallagher, L., Yang, J., Manoil, C. & Harwood, C.S. 2017. Molecular Basis of Bacterial Longevity. *mBio*. 8(6). DOI: 10.1128/mBio.01726-17.
- Pelletier, D.A., Hurst, G.B., Foote, L.J., Lankford, P.K., McKeown, C.K., Lu, T.-Y., Schmoyer, D.D., Shah, M.B., et al. 2008. A General System for Studying Protein–Protein Interactions in Gram-Negative Bacteria. *Journal of Proteome Research*. 7(8):3319–3328. DOI: 10.1021/pr8001832.

- Pereira, R., Carvalho, A., Vaz, D.C., Gil, M.H., Mendes, A. & Bártolo, P. 2013. Development of novel alginate based hydrogel films for wound healing applications. *International Journal of Biological Macromolecules*. 52:221–230. DOI: 10.1016/j.ijbiomac.2012.09.031.
- Ping, Z.H., Nguyen, Q.T., Chen, S.M., Zhou, J.Q. & Ding, Y.D. 2001. States of water in different hydrophilic polymers — DSC and FTIR studies. *Polymer*. 42(20):8461–8467. DOI: 10.1016/S0032-3861(01)00358-5.
- Plieva, F.M., Galaev, I.Yu., Noppe, W. & Mattiasson, B. 2008. Cryogel applications in microbiology. *Trends in Microbiology*. 16(11):543–551. DOI: 10.1016/j.tim.2008.08.005.
- Pott, R.W.M., Howe, C.J. & Dennis, J.S. 2013. Photofermentation of crude glycerol from biodiesel using *Rhodospseudomonas palustris*: Comparison with organic acids and the identification of inhibitory compounds. *Bioresource Technology*. 130:725–730. DOI: 10.1016/j.biortech.2012.11.126.
- Pott, R.W.M., Howe, C.J. & Dennis, J.S. 2014. The purification of crude glycerol derived from biodiesel manufacture and its use as a substrate by *Rhodospseudomonas palustris* to produce hydrogen. *Bioresource Technology*. 152:464–470. DOI: 10.1016/j.biortech.2013.10.094.
- Prüsse, U., Bilancetti, L., Bučko, M., Bugarski, B., Bukowski, J., Gemeiner, P., Lewińska, D., Manojlovic, V., et al. 2008. Comparison of different technologies for alginate beads production. *Chemical Papers*. 62(4):364. DOI: 10.2478/s11696-008-0035-x.
- Ranaivoarisoa, T.O., Singh, R., Rengasamy, K., Guzman, M.S. & Bose, A. 2019. Towards sustainable bioplastic production using the photoautotrophic bacterium *Rhodospseudomonas palustris* TIE-1. *Journal of Industrial Microbiology & Biotechnology*. 46(9):1401–1417. DOI: 10.1007/s10295-019-02165-7.
- Rehbein, P. & Schwalbe, H. 2015. Integrated protocol for reliable and fast quantification and documentation of electrophoresis gels. *Protein Expression and Purification*. 110:1–6. DOI: 10.1016/j.pep.2014.12.006.
- Rey, F.E. & Harwood, C.S. 2010. FixK, a global regulator of microaerobic growth, controls photosynthesis in *Rhodospseudomonas palustris*. *Molecular Microbiology*. 75(4):1007–1020. DOI: 10.1111/j.1365-2958.2009.07037.x.
- Rey, F.E., Heiniger, E.K. & Harwood, C.S. 2007. Redirection of Metabolism for Biological Hydrogen Production. *Applied and Environmental Microbiology*. 73(5):1665–1671. DOI: 10.1128/AEM.02565-06.
- Ribeiro, A.C.F., Rodrigo, M.M., Barros, M.C.F., Verissimo, L.M.P., Romero, C., Valente, A.J.M. & Esteso, M.A. 2014. Mutual diffusion coefficients of L-glutamic acid and monosodium L-glutamate in aqueous solutions at T=298.15K. *The Journal of Chemical Thermodynamics*. 74:133–137. DOI: 10.1016/j.jct.2014.01.017.
- Robert, B., Cogdell, R.J. & van Grondelle, R. 2003. The Light-Harvesting System of Purple Bacteria. In *Light-Harvesting Antennas in Photosynthesis*. B.R. Green & W.W. Parson, Eds. (Advances in Photosynthesis and Respiration). Dordrecht: Springer Netherlands. 169–194. DOI: 10.1007/978-94-017-2087-8_5.
- Roelfsema, M., van Soest, H.L., Harmsen, M., van Vuuren, D.P., Bertram, C., den Elzen, M., Höhne, N., Iacobuta, G., et al. 2020. Taking stock of national climate policies to evaluate implementation of the Paris Agreement. *Nature Communications*. 11(1):2096. DOI: 10.1038/s41467-020-15414-6.
- Rosenberg, M., Azevedo, N.F. & Ivask, A. 2019. Propidium iodide staining underestimates viability of adherent bacterial cells. *Scientific Reports*. 9(1):1–12. DOI: 10.1038/s41598-019-42906-3.
- Roszak, A.W., Howard, T.D., Southall, J., Gardiner, A.T., Law, C.J., Isaacs, N.W. & Cogdell, R.J. 2003. Crystal Structure of the RC-LH1 Core Complex from *Rhodospseudomonas palustris*. *Science*. 302(5652):1969–1972. DOI: 10.1126/science.1088892.
- Rubio, L.M. & Ludden, P.W. 2005. Maturation of Nitrogenase: a Biochemical Puzzle. *Journal of Bacteriology*. 187(2):405–414. DOI: 10.1128/JB.187.2.405-414.2005.
- Sabourin-Provost, G. & Hallenbeck, P.C. 2009. High yield conversion of a crude glycerol fraction from biodiesel production to hydrogen by photofermentation. *Bioresource Technology*. 100(14):3513–3517. DOI: 10.1016/j.biortech.2009.03.027.
- Sasikala, K., Ramana, Ch.V. & Raghuveer Rao, P. 1991. Environmental regulation for optimal biomass yield and photoproduction of hydrogen by *Rhodobacter sphaeroides* O.U. 001. *International Journal of Hydrogen Energy*. 16(9):597–601. DOI: 10.1016/0360-3199(91)90082-T.

- Schäfer, A., Tauch, A., Jäger, W., Kalinowski, J., Thierbach, G. & Pühler, A. 1994. Small mobilizable multi-purpose cloning vectors derived from the *Escherichia coli* plasmids pK18 and pK19: selection of defined deletions in the chromosome of *Corynebacterium glutamicum*. *Gene*. 145(1):69–73. DOI: 10.1016/0378-1119(94)90324-7.
- Scheuring, S., Gonçalves, R.P., Prima, V. & Sturgis, J.N. 2006. The Photosynthetic Apparatus of *Rhodospseudomonas palustris*: Structures and Organization. *Journal of Molecular Biology*. 358(1):83–96. DOI: 10.1016/j.jmb.2006.01.085.
- Schleussner, C.-F., Rogelj, J., Schaeffer, M., Lissner, T., Licker, R., Fischer, E.M., Knutti, R., Levermann, A., et al. 2016. Science and policy characteristics of the Paris Agreement temperature goal. *Nature Climate Change*. 6(9):827–835. DOI: 10.1038/nclimate3096.
- Schneider, K., Gollan, U., Dröttboom, M., Selsemeier-Voigt, S. & Müller, A. 1997. Comparative Biochemical Characterization of the Iron-Only Nitrogenase and the Molybdenum Nitrogenase from *Rhodobacter Capsulatus*. *European Journal of Biochemistry*. 244(3):789–800. DOI: 10.1111/j.1432-1033.1997.t01-1-00789.x.
- Schroeder, A., Mueller, O., Stocker, S., Salowsky, R., Leiber, M., Gassmann, M., Lightfoot, S., Menzel, W., et al. 2006. The RIN: an RNA integrity number for assigning integrity values to RNA measurements. *BMC Molecular Biology*. 7(1):3. DOI: 10.1186/1471-2199-7-3.
- Schüddekopf, K., Hennecke, S., Liese, U., Kutsche, M. & Klipp, W. 1993. Characterization of *anf* genes specific for the alternative nitrogenase and identification of *nif* genes required for both nitrogenases in *Rhodobacter capsulatus*. *Molecular Microbiology*. 8(4):673–684. DOI: 10.1111/j.1365-2958.1993.tb01611.x.
- See, S., Lim, P.-E., Lim, J.-W., Seng, C.-E. & Adnan, R. 2015. Evaluation of o-cresol removal using PVA-cryogel-immobilised biomass enhanced by PAC. *Water SA*. 41(1):55–60. DOI: 10.4314/wsa.v41i1.8.
- Seifert, K., Waligorska, M. & Laniecki, M. 2010a. Hydrogen generation in photobiological process from dairy wastewater. *International Journal of Hydrogen Energy*. 35(18):9624–9629. DOI: 10.1016/j.ijhydene.2010.07.015.
- Seifert, K., Waligorska, M. & Laniecki, M. 2010b. Brewery wastewaters in photobiological hydrogen generation in presence of *Rhodobacter sphaeroides* O.U. 001. *International Journal of Hydrogen Energy*. 35(9):4085–4091. DOI: 10.1016/j.ijhydene.2010.01.126.
- Siefert, E., Irgens, R.L. & Pfennig, N. 1978. Phototrophic purple and green bacteria in a sewage treatment plant. *Applied and Environmental Microbiology*. 35(1):38–44.
- Simmons, S.S., Isokpehi, R.D., Brown, S.D., McAllister, D.L., Hall, C.C., McDuffy, W.M., Medley, T.L., Udensi, U.K., et al. 2011. Functional Annotation Analytics of *Rhodospseudomonas palustris* Genomes. *Bioinformatics and Biology Insights*. 5:115–129. DOI: 10.4137/BBI.S7316.
- Singh, S.P., Srivastava, S.C. & Pandey, K.D. 1994. Hydrogen production by *Rhodospseudomonas* at the expense of vegetable starch, sugarcane juice and whey. *International Journal of Hydrogen Energy*. 19(5):437–440. DOI: 10.1016/0360-3199(94)90020-5.
- Sippel, S., Meinshausen, N., Fischer, E.M., Székely, E. & Knutti, R. 2020. Climate change now detectable from any single day of weather at global scale. *Nature Climate Change*. 10(1):35–41. DOI: 10.1038/s41558-019-0666-7.
- Smidsrød, O. & Skjåk-Braek, G. 1990. Alginate as immobilization matrix for cells. *Trends in Biotechnology*. 8:71–78. DOI: 10.1016/0167-7799(90)90139-O.
- Staffell, I., Scamman, D., Abad, A.V., Balcombe, P., E. Dodds, P., Ekins, P., Shah, N. & R. Ward, K. 2019. The role of hydrogen and fuel cells in the global energy system. *Energy & Environmental Science*. DOI: 10.1039/C8EE01157E.
- Stamatakis, A. 2014. RAxML version 8: a tool for phylogenetic analysis and post-analysis of large phylogenies. *Bioinformatics*. 30(9):1312–1313. DOI: 10.1093/bioinformatics/btu033.
- Stepanov, N. & Efremenko, E. 2017. Immobilised cells of *Pachysolen tannophilus* yeast for ethanol production from crude glycerol. *New Biotechnology*. 34:54–58. DOI: 10.1016/j.nbt.2016.05.002.
- Szczęsna-Antczak, M. & Galas, E. 2001. *Bacillus subtilis* cells immobilised in PVA-cryogels. *Biomolecular Engineering*. 17(2):55–63. DOI: 10.1016/S1389-0344(00)00065-4.

- Takei, T., Ikeda, K., Ijima, H., Yoshida, M. & Kawakami, K. 2012. A comparison of sodium sulfate, sodium phosphate, and boric acid for preparation of immobilized *Pseudomonas putida* F1 in poly(vinyl alcohol) beads. *Polymer Bulletin*. 69(3):363–373. DOI: 10.1007/s00289-012-0756-4.
- Takehita, H., Kanaya, T., Nishida, K. & Kaji, K. 2002. Small-angle neutron scattering studies on network structure of transparent and opaque PVA gels. *Physica B: Condensed Matter*. 311(1):78–83. DOI: 10.1016/S0921-4526(01)01059-6.
- Tanaka, H., Irie, S. & Ochi, H. 1989. A novel immobilization method for prevention of cell leakage from the Gel matrix. *Journal of Fermentation and Bioengineering*. 68(3):216–219. DOI: 10.1016/0922-338X(89)90141-4.
- Taylor, M., Song, Y. & Brockbank, K. 2004. Vitrification in Tissue Preservation: New Developments. In *Life in the Frozen State*. Boca Raton, Florida: CRC Press. 604–641.
- Thorneley, R.N.F., Eady, R.R. & Yates, M.G. 1975. Nitrogenases of *Klebsiella pneumoniae* and *Azotobacter chroococcum*: Complex formation between the component proteins. *Biochimica et Biophysica Acta (BBA) - Enzymology*. 403(2):269–284. DOI: 10.1016/0005-2744(75)90057-1.
- Tian, X., Liao, Q., Liu, W., Wang, Y.Z., Zhu, X., Li, J. & Wang, H. 2009. Photo-hydrogen production rate of a PVA-boric acid gel granule containing immobilized photosynthetic bacteria cells. *International Journal of Hydrogen Energy*. 34(11):4708–4717. DOI: 10.1016/j.ijhydene.2009.03.042.
- Tiang, M.F., Fitri Hanipa, M.A., Abdul, P.M., Jahim, J.M. d., Mahmod, S.S., Takriff, M.S., Lay, C.-H., Reungsang, A., et al. 2020. Recent advanced biotechnological strategies to enhance photo-fermentative biohydrogen production by purple non-sulphur bacteria: An overview. *International Journal of Hydrogen Energy*. 45(24):13211–13230. DOI: 10.1016/j.ijhydene.2020.03.033.
- Tikh, I.B., Held, M. & Schmidt-Dannert, C. 2014. BioBrick™ compatible vector system for protein expression in *Rhodobacter sphaeroides*. *Applied Microbiology and Biotechnology*. 98(7):3111–3119. DOI: 10.1007/s00253-014-5527-8.
- du Toit, J.-P. & Pott, R.W.M. 2020. Transparent polyvinyl-alcohol cryogel as immobilisation matrix for continuous biohydrogen production by phototrophic bacteria. *Biotechnology for Biofuels*. 13(1):105. DOI: 10.1186/s13068-020-01743-7.
- Tsygankov, A. & Kosourov, S. 2014. Immobilization of Photosynthetic Microorganisms for Efficient Hydrogen Production. In *Microbial BioEnergy: Hydrogen Production*. D. Zannoni & R. De Philippis, Eds. Dordrecht: Springer Netherlands. 321–347. DOI: 10.1007/978-94-017-8554-9_14.
- Tsygankov, A.A. & Khusnutdinova, A.N. 2015. Hydrogen in metabolism of purple bacteria and prospects of practical application. *Microbiology*. 84(1):1–22. DOI: 10.1134/S0026261715010154.
- Turner, J., Sverdrup, G., Mann, M.K., Maness, P.-C., Kroposki, B., Ghirardi, M., Evans, R.J. & Blake, D. 2008. Renewable hydrogen production. *International Journal of Energy Research*. 32(5):379–407. DOI: 10.1002/er.1372.
- Ubando, A.T., Felix, C.B. & Chen, W.-H. 2020. Biorefineries in circular bioeconomy: A comprehensive review. *Bioresour Technol*. 299:122585. DOI: 10.1016/j.biortech.2019.122585.
- Uyar, B. 2016. Bioreactor design for photofermentative hydrogen production. *Bioprocess and Biosystems Engineering*. 39(9):1331–1340. DOI: 10.1007/s00449-016-1614-9.
- Uyar, B. & Kapucu, N. 2015. Passive temperature control of an outdoor photobioreactor by phase change materials. *Journal of Chemical Technology & Biotechnology*. 90(5):915–920. DOI: 10.1002/jctb.4398.
- Vasilyeva, L., Miyake, M., Khatipov, E., Wakayama, T., Sekine, M., Hara, M., Nakada, E., Asada, Y., et al. 1999. Enhanced hydrogen production by a mutant of *Rhodobacter sphaeroides* having an altered light-harvesting system. *Journal of Bioscience and Bioengineering*. 87(5):619–624. DOI: 10.1016/S1389-1723(99)80124-8.
- Vincenzini, M., Materassi, R., Tredici, M.R. & Florenzano, G. 1982. Hydrogen production by immobilized cells—I. light dependent dissimilation of organic substances by *Rhodospseudomonas palustris*. *International Journal of Hydrogen Energy*. 7(3):231–236. DOI: 10.1016/0360-3199(82)90086-6.
- Vredenberg, W.J. & Ames, J. 1966. Absorption bands of bacteriochlorophyll types in purple bacteria and their response to illumination. *Biochimica et Biophysica Acta (BBA) - Biophysics including Photosynthesis*. 126(2):244–253. DOI: 10.1016/0926-6585(66)90060-4.

- Wang, Y.-Z., Liao, Q., Zhu, X., Tian, X. & Zhang, C. 2010. Characteristics of hydrogen production and substrate consumption of *Rhodospseudomonas palustris* CQK 01 in an immobilized-cell photobioreactor. *Bioresource Technology*. 101(11):4034–4041. DOI: 10.1016/j.biortech.2010.01.045.
- Wang, Y.-Z., Liao, Q., Zhu, X., Li, J. & Lee, D.-J. 2011. Effect of culture conditions on the kinetics of hydrogen production by photosynthetic bacteria in batch culture. *International Journal of Hydrogen Energy*. 36(21):14004–14013. DOI: 10.1016/j.ijhydene.2011.04.005.
- Wattam, A.R., Davis, J.J., Assaf, R., Boisvert, S., Brettin, T., Bun, C., Conrad, N., Dietrich, E.M., et al. 2017. Improvements to PATRIC, the all-bacterial Bioinformatics Database and Analysis Resource Center. *Nucleic Acids Research*. 45(D1):D535–D542. DOI: 10.1093/nar/gkw1017.
- Weaver, P.F., Wall, J.D. & Gest, H. 1975. Characterization of *Rhodospseudomonas capsulata*. *Archives of Microbiology*. 105(1):207–216. DOI: 10.1007/BF00447139.
- Welander, P.V., Hunter, R.C., Zhang, L., Sessions, A.L., Summons, R.E. & Newman, D.K. 2009. Hopanoids Play a Role in Membrane Integrity and pH Homeostasis in *Rhodospseudomonas palustris* TIE-1. *Journal of Bacteriology*. 191(19):6145–6156. DOI: 10.1128/JB.00460-09.
- Westmacott, D. & Primrose, S.B. 1976. Synchronous Growth of *Rhodospseudomonas palustris* from the Swarmer Phase. *Journal of General Microbiology*. 94(1):117–125. DOI: 10.1099/00221287-94-1-117.
- Weston, M.F., Kotake, S. & Davis, L.C. 1983. Interaction of nitrogenase with nucleotide analogs of ATP and ADP and the effect of metal ions on ADP inhibition. *Archives of Biochemistry and Biophysics*. 225(2):809–817. DOI: 10.1016/0003-9861(83)90093-0.
- Willaert, R.G. & Baron, G.V. 1996. Gel entrapment and micro-encapsulation: methods, applications and engineering principles. *Reviews in Chemical Engineering*. 12(1–2):1–205. DOI: 10.1515/REVCE.1996.12.1-2.1.
- Wovk, B., Leitl, E., Rasch, C.M., Mesbah-Karimi, N., Harris, S.B. & Fahy, G.M. 2000. Vitrification Enhancement by Synthetic Ice Blocking Agents. *Cryobiology*. 40(3):228–236. DOI: 10.1006/cryo.2000.2243.
- Wu, K.-Y.A. & Wisecarver, K.D. 1992. Cell immobilization using PVA crosslinked with boric acid. *Biotechnology and Bioengineering*. 39(4):447–449. DOI: 10.1002/bit.260390411.
- Wu, X.-M., Zhu, L.-Y., Zhu, L.-Y. & Wu, L. 2016. Improved ammonium tolerance and hydrogen production in *nifA* mutant strains of *Rhodospseudomonas palustris*. *International Journal of Hydrogen Energy*. 41(48):22824–22830. DOI: 10.1016/j.ijhydene.2016.10.093.
- Xu, W., Chai, C., Shao, L., Yao, J. & Wang, Y. 2016. Metabolic engineering of *Rhodospseudomonas palustris* for squalene production. *Journal of Industrial Microbiology & Biotechnology*. 43(5):719–725. DOI: 10.1007/s10295-016-1745-7.
- Yang, H., Zhang, J., Wang, X., Feng, J., Yan, W. & Guo, L. 2015. Coexpression of Mo- and Fe-nitrogenase in *Rhodobacter capsulatus* enhanced its photosynthetic hydrogen production. *International Journal of Hydrogen Energy*. 40(2):927–934. DOI: 10.1016/j.ijhydene.2014.11.087.
- Yang, J., Yin, L., Lessner, F.H., Nakayasu, E.S., Payne, S.H., Fixen, K.R., Gallagher, L. & Harwood, C.S. 2017. Genes essential for phototrophic growth by a purple alphaproteobacterium. *Environmental Microbiology*. 19(9):3567–3578. DOI: 10.1111/1462-2920.13852.
- Yang, Z.-Y., Ledbetter, R., Shaw, S., Pence, N., Tokmina-Lukaszewska, M., Eilers, B., Guo, Q., Pokhrel, N., et al. 2016. Evidence That the Pi Release Event Is the Rate-Limiting Step in the Nitrogenase Catalytic Cycle. *Biochemistry*. 55(26):3625–3635. DOI: 10.1021/acs.biochem.6b00421.
- Yin, L., Ma, H., Nakayasu, E.S., Payne, S.H., Morris, D.R. & Harwood, C.S. 2019. Bacterial Longevity Requires Protein Synthesis and a Stringent Response. *mBio*. 10(5). DOI: 10.1128/mBio.02189-19.
- Yoch, D.C. & Gotto, J.W. 1982. Effect of light intensity and inhibitors of nitrogen assimilation on NH₄⁺ inhibition of nitrogenase activity in *Rhodospirillum rubrum* and *Anabaena* sp. *Journal of Bacteriology*. 151(2):800–806.
- Young, C.S. & Beatty, J.T. 2003. Multi-level Regulation of Purple Bacterial Light-harvesting Complexes. In *Light-Harvesting Antennas in Photosynthesis*. (Advances in Photosynthesis and Respiration). Springer, Dordrecht. 449–470. DOI: 10.1007/978-94-017-2087-8_16.
- Zagrodnik, R., Seifert, K., Stodolny, M. & Laniecki, M. 2015. Continuous photofermentative production of hydrogen by immobilized *Rhodobacter sphaeroides* O.U.001. *International Journal of Hydrogen Energy*. 40(15):5062–5073. DOI: 10.1016/j.ijhydene.2015.02.079.

- Zamost, B.L., Nielsen, H.K. & Starnes, R.L. 1991. Thermostable enzymes for industrial applications. *Journal of Industrial Microbiology*. 8(2):71–81. DOI: 10.1007/BF01578757.
- Zhai, Z., Du, J., Chen, L., Hamid, M.R., Du, X., Kong, X., Cheng, J., Tang, W., et al. 2019. A genetic tool for production of GFP-expressing *Rhodospseudomonas palustris* for visualization of bacterial colonization. *AMB Express*. 9(1):141. DOI: 10.1186/s13568-019-0866-6.
- Zhang, H., Chen, G., Zhang, Q., Lee, D.-J., Zhang, Z., Li, Y., Li, P., Hu, J., et al. 2017. Photosynthetic hydrogen production by alginate immobilized bacterial consortium. *Bioresource Technology*. 236:44–48. DOI: 10.1016/j.biortech.2017.03.171.
- Zheng, Y. & Harwood, C.S. 2019. Influence of Energy and Electron Availability on In Vivo Methane and Hydrogen Production by a Variant Molybdenum Nitrogenase. *Applied and Environmental Microbiology*. 85(9). DOI: 10.1128/AEM.02671-18.
- Zhu, H., Wakayama, T., Suzuki, T., Asada, Y. & Miyake, J. 1999. Entrapment of *Rhodobacter sphaeroides* RV in cationic polymer/agar gels for hydrogen production in the presence of NH₄⁺. *Journal of Bioscience and Bioengineering*. 88(5):507–512. DOI: 10.1016/S1389-1723(00)87667-7.
- Zumft, W.G. & Castillo, F. 1978. Regulatory properties of the nitrogenase from *Rhodospseudomonas palustris*. *Archives of Microbiology*. 117(1):53–60. DOI: 10.1007/BF00689351.
- Żur, J., Wojcieszńska, D. & Guzik, U. 2016. Metabolic Responses of Bacterial Cells to Immobilization. *Molecules*. 21(7):958. DOI: 10.3390/molecules21070958.

APPENDICES

APPENDIX 1. Supplementary information for Chapter 3.

Heat-acclimatised strains of Rhodopseudomonas palustris reveal higher temperature optima with concomitantly enhanced hydrogen production rates.

Multiple sequence alignments of essential hopanoid biosynthesis and transport genes.

Amino acid coding sequences of RefSeq-annotated genes from strain CGA009 and ATH2.1.37 were compared to those in strains TIE1 and R1 to investigate potential differences in temperature resistance due to hopanoid production and localisation functionality (Doughty et al., 2011). No sequence differences between ATH2.1.37 and CGA009 were evident.

Hopanoid biosynthesis:

HpnP: hopanoid 2-methyltransferase. Refseq locus tags: ATH2.1.37: D4Q71_08190; CGA009: RPA3748; TIE1: Rpal_4269; R1: D1920_07285.

ATH2.1.37_D4Q71	1	MKAESGQTSRRILCVFPRYTKSFGTFQHSYPLMDDVAAFMPQGLLVIAAYLPDEWSVRF
CGA009_RPA3748	1	MKAESGQTSRRILCVFPRYTKSFGTFQHSYPLMDDVAAFMPQGLLVIAAYLPDEWSVRF
TIE1_Rpal_4269	1	MKAESGQTSRRILCVFPRYTKSFGTFQHSYPLMDDVAAFMPQGLLVIAAYLPDEWSVRF
R1_D1920_07285	1	MKAESGQTSRRILCVFPRYTKSFGTFQHSYPLMDDVAAFMPQGLLVIAAYLPDEWSVRF
ATH2.1.37_D4Q71	61	VDENIRPATADDFAWADAVFVSGMHIQRQQMNDICRRAHDFDLPVALGGPSVSACPDYYP
CGA009_RPA3748	61	VDENIRPATADDFAWADAVFVSGMHIQRQQMNDICRRAHDFDLPVALGGPSVSACPDYYP
TIE1_Rpal_4269	61	VDENIRPATADDFAWADAVFVSGMHIQRQQMNDICRRAHDFDLPVALGGPSVSACPDYYP
R1_D1920_07285	61	VDENIRPATADDFAWADAVFVSGMHIQRQQMNDICRRAHDFDLPVALGGPSVSACPDYYP
ATH2.1.37_D4Q71	121	NFDYLHVGE LGDATDQLIAKLTHDVTRPKRQVVFTTEDRLDMTLFPIPAYELAEC SKYLL
CGA009_RPA3748	121	NFDYLHVGE LGDATDQLIAKLTHDVTRPKRQVVFTTEDRLDMTLFPIPAYELAEC SKYLL
TIE1_Rpal_4269	121	NFDYLHVGE LGDATDQLIAKLTHDVTRPKRQVVFTTEDRLDMTLFPIPAYELAEC SKYLL
R1_D1920_07285	121	NFDYLHVGE LGDATDQLIAKLTHDVTRPKRQVVFTTEDRLDMTLFPIPAYELAEC SKYLL
ATH2.1.37_D4Q71	181	GSIQYSSGCPYQCEFCDI PGLYGRNPR LKTPEQIITELDRMIECGIRGSVYFVDDNFIGN
CGA009_RPA3748	181	GSIQYSSGCPYQCEFCDI PGLYGRNPR LKTPEQIITELDRMIECGIRGSVYFVDDNFIGN
TIE1_Rpal_4269	181	GSIQYSSGCPYQCEFCDI PGLYGRNPR LKTPEQIITELDRMIECGIRGSVYFVDDNFIGN
R1_D1920_07285	181	GSIQYSSGCPYQCEFCDI PGLYGRNPR LKTPEQIITELDRMIECGIRGSVYFVDDNFIGN
ATH2.1.37_D4Q71	241	RKAALDLLPHLVEWQKRTGFQLQ LACEATLNI AKRPEI IELMREAYFCTIFVGIETPDPT
CGA009_RPA3748	241	RKAALDLLPHLVEWQKRTGFQLQ LACEATLNI AKRPEI IELMREAYFCTIFVGIETPDPT
TIE1_Rpal_4269	241	RKAALDLLPHLVEWQKRTGFQLQ LACEATLNI AKRPEI IELMREAYFCTIFVGIETPDPT
R1_D1920_07285	241	RKAALDLLPHLVEWQKRTGFQLQ LACEATLNI AKRPEI IELMREAYFCTIFVGIETPDPT
ATH2.1.37_D4Q71	301	ALKAMHKDHNMMVPILEGVRTISSYGI EVVSGI I LGLD TDPETGEFLMQFIEQSQIPLL
CGA009_RPA3748	301	ALKAMHKDHNMMVPILEGVRTISSYGI EVVSGI I LGLD TDPETGEFLMQFIEQSQIPLL
TIE1_Rpal_4269	301	ALKAMHKDHNMMVPILEGVRTISSYGI EVVSGI I LGLD TDPETGEFLMQFIEQSQIPLL
R1_D1920_07285	301	ALKAMHKDHNMMVPILEGVRTISSYGI EVVSGI I LGLD TDPETGEFLMQFIEQSQIPLL
ATH2.1.37_D4Q71	361	TINLLQALPKTPLWDR LQREGRLVHDD SRESNVDFLLPHDQVVAMWKDCMARAYQPEALL
CGA009_RPA3748	361	TINLLQALPKTPLWDR LQREGRLVHDD SRESNVDFLLPHDQVVAMWKDCMARAYQPEALL
TIE1_Rpal_4269	361	TINLLQALPKTPLWDR LQREGRLVHDD SRESNVDFLLPHDQVVAMWKDCMARAYQPEALL
R1_D1920_07285	361	TINLLQALPKTPLWDR LQREGRLVHDD SRESNVDFLLPHDQVVAMWKDCMARAYQPEALL

ATH2.1.37_D4Q71	421	KRYEYQIAHAYATRLHPSTPQRASKANIKRAMIMLRNVIWQIGIRGDYKLAFWKFAFRRL
CGA009_RPA3748	421	KRYEYQIAHAYATRLHPSTPQRASKANIKRAMIMLRNVIWQIGIRGDYKLAFWKFAFRRL
TIE1_Rpal_4269	421	KRYEYQIAHAYATRLHPSTPQRASKANIKRAMIMLRNVIWQIGIRGDYKLAFWKFAFRRL
R1_D1920_07285	421	KRYEYQIAHAYATRLHPSTPQRASKANIKRAMIMLRNVIWQIGIRGDYKLAFWKFAFRRL
ATH2.1.37_D4Q71	481	FRGDIENLLVMVVAHHLIIYAREASRGHANASNYSIRLREAAVPAAE
CGA009_RPA3748	481	FRGDIENLLVMVVAHHLIIYAREASRGHANASNYSIRLREAAVPAAE
TIE1_Rpal_4269	481	IRGDIENLLVMVVAHHLIIYAREASRGHANASNYSIRLREAAVPAAE
R1_D1920_07285	481	IRGDIENLLVMVVAHHLIIYAREASRGHANASNYSIRLREAAVPAAE

Shc: squalene-hopene cyclase. Refseq locus tags: ATH2.1.37: D4Q71_08230; CGA009: RPA3740; TIE1: Rpal_4261; R1: D1920_07245.

ATH2.1.37	1	MDSGSYTTGVERNALIASIDAARSALLNYRRDDGHVFELEADCTIPAEYVLLRHLYLGEF
CGA009_RPA3740	1	MDSGSYTTGVERNALIASIDAARSALLNYRRDDGHVFELEADCTIPAEYVLLRHLYLGEF
TIE1_Rpal_4261	1	MDSGSYTTGVERNALIASIDAARSALLNYRRDDGHVFELEADCTIPAEYVLLRHLYLGEF
R1_D1920_07245	1	MDSGSYTTGVERNALIASIDAARSALLNYRRDDGHVFELEADCTIPAEYVLLRHLYLGEF
ATH2.1.37	61	VDAELEAKIAVYLRRIQGAHGGWPLVHDGDFDMSASVKGYFALKMIGDSIDAPHMVRARE
CGA009_RPA3740	61	VDAELEAKIAVYLRRIQGAHGGWPLVHDGDFDMSASVKGYFALKMIGDSIDAPHMVRARE
TIE1_Rpal_4261	61	VDAELEAKIAVYLRRIQGAHGGWPLVHDGDFDMSASVKGYFALKMIGDSIDAPHMVRARE
R1_D1920_07245	61	VDAELEAKIAVYLRRIQGAHGGWPLVHDGDFDMSASVKGYFALKMIGDSIDAPHMVRARE
ATH2.1.37	121	AIRSRGGAIHSNVFTRFLLTLYGVTTWRAVPVLPVEIMLLPSWSPFTLTKISYWARTTMV
CGA009_RPA3740	121	AIRSRGGAIHSNVFTRFLLTLYGVTTWRAVPVLPVEIMLLPSWSPFTLTKISYWARTTMV
TIE1_Rpal_4261	121	AIRSRGGAIHSNVFTRFLLTLYGVTTWRAVPVLPVEIMLLPSWSPFTLTKISYWARTTMV
R1_D1920_07245	121	AIRSRGGAIHSNVFTRFLLTLYGVTTWRAVPVLPVEIMLLPSWSPFTLTKISYWARTTMV
ATH2.1.37	181	PLLVLCAKPKRAKNPKGVDTIDELFLQDPKTI GMPVKAPHQNWALFKLFGSIDAVLRVIEP
CGA009_RPA3740	181	PLLVLCAKPKRAKNPKGVDTIDELFLQDPKTI GMPVKAPHQNWALFKLFGSIDAVLRVIEP
TIE1_Rpal_4261	181	PLLVLCAKPKRAKNPKGVDTIDELFLQDPKTI GMPVKAPHQNWALFKLFGSIDAVLRVIEP
R1_D1920_07245	181	PLLVLCAKPKRAKNPKGVDTIDELFLQDPKTI GMPVKAPHQNWALFKLFGSIDAVLRVIEP
ATH2.1.37	241	VMPKSIKRAIDKALAFIEERLNGEDGMGAIFPPMANAVMMYEALGYPEDYPPRASQRRG
CGA009_RPA3740	241	VMPKSIKRAIDKALAFIEERLNGEDGMGAIFPPMANAVMMYEALGYPEDYPPRASQRRG
TIE1_Rpal_4261	241	VMPKGIKRAIDKALAFIEERLNGEDGMGAIFPPMANAVMMYEALGYPEDYPPRASQRRG
R1_D1920_07245	241	VMPKGIKRAIDKALAFIEERLNGEDGMGAIFPPMANAVMMYEALGYPEDYPPRASQRRG
ATH2.1.37	301	IDLLLVDRGDEAYCQPCVSPVWDTALASHAVLEADGHEGAKSVRPALDWLLPRQVLDLKG
CGA009_RPA3740	301	IDLLLVDRGDEAYCQPCVSPVWDTALASHAVLEADGHEGAKSVRPALDWLLPRQVLDLKG
TIE1_Rpal_4261	301	IDLLLVDRGDEAYCQPCVSPVWDTALASHAVLEADGHEGAKSVRPALDWLLPRQVLDLKG
R1_D1920_07245	301	IDLLLVDRGDEAYCQPCVSPVWDTALASHAVLEADGHEGAKSVRPALDWLLPRQVLDLKG
ATH2.1.37	361	DWAVKAPNVRPGGWAFQYNNAHYPDLDDTAVVVMALDRARKDQPNPAYDAATARAREWIE
CGA009_RPA3740	361	DWAVKAPNVRPGGWAFQYNNAHYPDLDDTAVVVMALDRARKDQPNPAYDAATARAREWIE
TIE1_Rpal_4261	361	DWAVKAPNVRPGGWAFQYNNAHYPDLDDTAVVVMALDRARKDQPNPAYDAATARAREWIE
R1_D1920_07245	361	DWAVKAPNVRPGGWAFQYNNAHYPDLDDTAVVVMALDRARKDQPNPAYDAATARAREWIE
ATH2.1.37	421	GMQSDDDGGWGAFFDINNTEYLLNIPFSDHGAMLDPPTEDVTARCVSMLAQLGETMDSSPA
CGA009_RPA3740	421	GMQSDDDGGWGAFFDINNTEYLLNIPFSDHGAMLDPPTEDVTARCVSMLAQLGETMDSSPA
TIE1_Rpal_4261	421	GMQSDDDGGWGAFFDINNTEYLLNIPFSDHGAMLDPPTEDVTARCVSMLAQLGETMDSSPA
R1_D1920_07245	421	GMQSDDDGGWGAFFDINNTEYLLNIPFSDHGAMLDPPTEDVTARCVSMLAQLGETMDSSPA
ATH2.1.37	481	LARAVGYLRDTQLAEGSWYGRWGMNYIYGTWSVLCALNAAGVPHADPMIRKAVAWLESVQ
CGA009_RPA3740	481	LARAVGYLRDTQLAEGSWYGRWGMNYIYGTWSVLCALNAAGVPHADPMIRKAVAWLESVQ
TIE1_Rpal_4261	481	LARAVGYLRDTQLAEGSWYGRWGMNYIYGTWSVLCALNAAGVPHADPMIRKAVAWLESVQ
R1_D1920_07245	481	LARAVGYLRDTQLAEGSWYGRWGMNYIYGTWSVLCALNAAGVPHADPMIRKAVAWLESVQ
ATH2.1.37	541	NRDGGWGEDAVSYRLDYRGYESAPSTASQTAWALLALMAAGEVDHPPAVARGIEYLKSTQT
CGA009_RPA3740	541	NRDGGWGEDAVSYRLDYRGYESAPSTASQTAWALLALMAAGEVDHPPAVARGIEYLKSTQT
TIE1_Rpal_4261	541	NRDGGWGEDAVSYRLDYRGYESAPSTASQTAWALLALMAAGEVDHPPAVARGIEYLKSTQT
R1_D1920_07245	541	NRDGGWGEDAVSYRLDYRGYESAPSTASQTAWALLALMAAGEVDHPPAVARGIEYLKSTQT

ATH2.1.37	601	EKGLWDEQRYTATGFPRVFLRYHGYSKFFPLWALARYRNLOATNSKVVGVGM
CGA009_RPA3740	601	EKGLWDEQRYTATGFPRVFLRYHGYSKFFPLWALARYRNLOATNSKVVGVGM
TIE1_Rpal_4261	601	EKGLWDEQRYTATGFPRVFLRYHGYSKFFPLWALARYRNLOATNSKVVGVGM
R1_D1920_07245	601	EKGLWDEQRYTATGFPRVFLRYHGYSKFFPLWALARYRNLOATNSKVVGVGM

HpnG: adenosyl-hopane nucleosidase. Refseq locus tags: ATH2.1.37: D4Q71_08235; CGA009: RPA3739; TIE1: Rpal_4260; R1: D1920_07240.

ATH2.1.37_D4Q71	1	MILGAVDDQAAALRQDPRPVLIVTGLIQEARIAAGPGLTVICSSSDPKQLRAIMADFDPS
CGA009_RPA3739	1	MILGAVDDQAAALRQDPRPVLIVTGLIQEARIAAGPGLTVICSSSDPKQLRAIMADFDPS
TIE1_Rpal_4260	1	MILGAVDDQAAALRQDPRPVLIVTGLIQEARIAAGPGLTVICSSSDPKQLRAIMADFDAS
R1_D1920_07240	1	MILGAVDDQAAALRQDPRPVLIVTGLIQEARIAAGPGLTVICSSSDPKQLRAIMADFDAS
ATH2.1.37_D4Q71	61	SIRGVISFGVAGGLDPSLEAGDIVIATEVVAGERRWTSEVALTDELLRSAGLGRQRVVRG
CGA009_RPA3739	61	SIRGVISFGVAGGLDPSLEAGDIVIATEVVAGERRWTSEVALTDELLRSAGLGRQRVVRG
TIE1_Rpal_4260	61	SIRGVISFGVAGGLDPSLEAGDIVIATEVVAGERRWTSEVALTDELLRSAGLGRQRVVRG
R1_D1920_07240	61	SIRGVISFGVAGGLDPSLEAGDIVIATEVVAGERRWTSEVALTDELLRSAGLGRQRVVRG
ATH2.1.37_D4Q71	121	GLVGAEQVIAARSAKAAALRSETGAAAVDMESHIAADFAAAAKLPFAALRVISDPANRSLP
CGA009_RPA3739	121	GLVGAEQVIAARSAKAAALRSETGAAAVDMESHIAADFAAAAKLPFAALRVISDPANRSLP
TIE1_Rpal_4260	121	GLVGAEQVIAARSAKAAALRSETGAAAVDMESHIAADFAAAAKLPFAALRVISDPANRSLP
R1_D1920_07240	121	GLVGAEQVIAARSAKAAALRSETGAAAVDMESHIAADFAAAAKLPFAALRVISDPANRSLP
ATH2.1.37_D4Q71	181	QIVSSAIKPNGDIDLRKVLRGARHPTSIRSLVSTGIDFNRALRSLRGCRNFVQEA VLGR
CGA009_RPA3739	181	QIVSSAIKPNGDIDLRKVLRGARHPTSIRSLVSTGIDFNRALRSLRGCRNFVQEA VLGR
TIE1_Rpal_4260	181	QIVSSAIKPNGDIDLRKVLRGARHPTSIRSLVSTGIDFNRALRSLRGCRNFVQEA VLGR
R1_D1920_07240	181	QIVSSAIKPNGDIDLRKVLRGARHPTSIRSLVSTGIDFNRALRSLRGCRNFVQEA VLGR
ATH2.1.37_D4Q71	241	GGLVAEI
CGA009_RPA3739	241	GGLVAEI
TIE1_Rpal_4260	241	GGLVAEI
R1_D1920_07240	241	GGLVAEI

HpnH: adenosyl-hopene transferase. Refseq locus tags: ATH2.1.37: D4Q71_08255; CGA009: RPA3735; TIE1: Rpal_4256; R1: D1920_07220.

ATH2.1.37_D4Q71	1	MAIPFHKELVIGGYLLKQKLLGRKRYPLVLMLEPLFRCNLACAGCGKIDYPDAILNRRMT
CGA009_RPA3735	1	MAIPFHKELVIGGYLLKQKLLGRKRYPLVLMLEPLFRCNLACAGCGKIDYPDAILNRRMT
TIE1_Rpal_4256	1	MAIPFHKELVIGGYLLKQKLLGRKRYPLVLMLEPLFRCNLACAGCGKIDYPDAILNRRMT
R1_D1920_07220	1	MAIPFHKELVIGGYLLKQKLLGRKRYPLVLMLEPLFRCNLACAGCGKIDYPDAILNRRMT
ATH2.1.37_D4Q71	61	AQECWDAAECEGAPMVAIPGGEPLIHKEIGEIVRGLVARKKFVSLCTNALLLEKKLHLFE
CGA009_RPA3735	61	AQECWDAAECEGAPMVAIPGGEPLIHKEIGEIVRGLVARKKFVSLCTNALLLEKKLHLFE
TIE1_Rpal_4256	61	AQECWDAAECEGAPMVAIPGGEPLIHKEIGEIVRGLVARKKFVSLCTNALLLEKKLHLFE
R1_D1920_07220	61	AQECWDAAECEGAPMVAIPGGEPLIHKEIGEIVRGLVARKKFVSLCTNALLLEKKLHLFE
ATH2.1.37_D4Q71	121	PSPYLFFSVHLDGLKEHHDKAVSQQGVFDRAVAAIKAAKAKGFTVNVNCTVFDGYAAEDI
CGA009_RPA3735	121	PSPYLFFSVHLDGLKEHHDKAVSQQGVFDRAVAAIKAAKAKGFTVNVNCTVFDGYAAEDI
TIE1_Rpal_4256	121	PSPYLFFSVHLDGLKEHHDKAVSQQGVFDRAVAAIKAAKAKGFTVNVNCTVFDGYAAEDI
R1_D1920_07220	121	PSPYLFFSVHLDGLKEHHDKAVSQQGVFDRAVAAIKAAKAKGFTVNVNCTVFDGYAAEDI
ATH2.1.37_D4Q71	181	AKFMDFTEELGVGVSI SPGYAYERAPDQEHFLNRTKTKNLFREVFARGKGGKWSFMHSSM
CGA009_RPA3735	181	AKFMDFTEELGVGVSI SPGYAYERAPDQEHFLNRTKTKNLFREVFARGKGGKWSFMHSSM
TIE1_Rpal_4256	181	AKFMDFTEELGVGVSI SPGYAYERAPDQEHFLNRTKTKNLFREVFARGKGGKWSFMHSSM
R1_D1920_07220	181	AKFMDFTEELGVGVSI SPGYAYERAPDQEHFLNRTKTKNLFREVFARGKGGKWSFMHSSM
ATH2.1.37_D4Q71	241	FLDFLAGNQEFECTPWGMPARNIFGWQKPCYLLGEGYAKTFQELMETTDWDSYGTGKYEK
CGA009_RPA3735	241	FLDFLAGNQEFECTPWGMPARNIFGWQKPCYLLGEGYAKTFQELMETTDWDSYGTGKYEK
TIE1_Rpal_4256	241	FLDFLAGNQEFECTPWGMPARNIFGWQKPCYLLGEGYAKTFQELMETTDWDSYGTGKYEK
R1_D1920_07220	241	FLDFLAGNQEFECTPWGMPARNIFGWQKPCYLLGEGYAKTFQELMETTDWDSYGTGKYEK
ATH2.1.37_D4Q71	301	CADCMACGYEPTAAMASLNNPLKAAWVALRGIKTSGPMAPEIDMSKQRPAYVFSEQVQ
CGA009_RPA3735	301	CADCMACGYEPTAAMASLNNPLKAAWVALRGIKTSGPMAPEIDMSKQRPAYVFSEQVQ
TIE1_Rpal_4256	301	CADCMACGYEPTAAMASLNNPLKAAWVALRGIKTSGPMAPEIDMSKQRPAYVFSEQVQ
R1_D1920_07220	301	CADCMACGYEPTAAMASLNNPLKAAWVALRGIKTSGPMAPEIDMSKQRPAYVFSEQVQ

```

ATH2.1.37_D4Q71 361 KTLTQIRQDEAAEAKDKRQAERSTAA
CGA009_RPA3735 361 KTLTQIRQDEAAEAKDKRQAERSTAA
TIE1_Rpal_4254 361 KTLTQIRQDEAAEAKDKRQAERSTAA
R1_D1920_07220 361 KTLTQIRQDEAAEAKDKRQAERSTAA

```

Hopanoid transport and localisation:

HpnN: hopanoid biosynthesis-associated RND transporter. Refseq locus tags: ATH2.1.37: D4Q71_08265; CGA009: RPA3733; TIE1: Rpal_4254; R1: D1920_07210.

Differences in initial sequence from CGA009 is likely due to automatic genome annotation process and ambiguous start codon positions.

```

ATH2.1.37_D4Q71 1 --MLKSAIVSIVRASTRFAAFTVLIGVFLAVAAGFYTYQHFGINTDINHLISSDLDRKR
CGA009_RPA3733 1 MNLKSAIVSIVRASTRFAAFTVLIGVFLAVAAGFYTYQHFGINTDINHLISSDLDRKR
TIE1_Rpal_4254 1 --MLKSAIVSIVRASTRFAAFTVLIGVFLAVAAGFYTYQHFGINTDINHLISSDLDRKR
R1_D1920_07210 1 --MLKSAIVSIVRASTRFAAFTVLIGVFLAVAAGFYTYQHFGINTDINHLISSDLDRKR

ATH2.1.37_D4Q71 59 DIAFEKAFDQERLILAVVEAPTPEFANAAAAKLTAEISKNNINFDSVKRLGGGPPFFDRSG
CGA009_RPA3733 61 DIAFEKAFDQERLILAVVEAPTPEFANAAAAKLTAEISKNNINFDSVKRLGGGPPFFDRSG
TIE1_Rpal_4254 59 DIAFEKAFDQERLILAVVEAPTPEFANAAAAKLTAEISKNNINFDSVKRLGGGPPFFDRSG
R1_D1920_07210 59 DIVFEKAFDQERLILAVVEAPTPEFANAAAAKLTAEISKNNINFDSVKRLGGGPPFFDRSG

ATH2.1.37_D4Q71 119 LLFLPKDEVAKATGQFQQAVPLIEIMAGDPSIRGLTAALETGLVGLKRGELTLDATAKPF
CGA009_RPA3733 121 LLFLPKDEVAKATGQFQQAVPLIEIMAGDPSIRGLTAALETGLVGLKRGELTLDATAKPF
TIE1_Rpal_4254 119 LLFLPKDEVAKATGQFQQAVPLIEIMAGDPSIRGLTAALETGLVGLKRGELTLDATAKPF
R1_D1920_07210 119 LLFLPKDEVAKATGQFQQAVPLIEIMAGDPSIRGLTAALETGLVGLKRGELTLDATAKPF

ATH2.1.37_D4Q71 179 NTVAATVEDVLGKQQAFFSWRGLVNPEPLTDGDKRAFIEVKPILDFKALEPGKAATDAIR
CGA009_RPA3733 181 NTVAATVEDVLGKQQAFFSWRGLVNPEPLTDGDKRAFIEVKPILDFKALEPGKAATDAIR
TIE1_Rpal_4254 179 NTVAATVEDVLGKQQAFFSWRGLVNPEPLTDGDKRAFIEVKPILDFKALEPGKAATDAIR
R1_D1920_07210 179 NTVAATVEDVLGKQQAFFSWRGLVNPEPLTDGDKRAFIEVKPILDFKALEPGKAATDAIR

ATH2.1.37_D4Q71 239 QAAVDLKIEQDFGARVRLTGPVPIANEEFATVKDGAVVNGIGTVVVVLLILWMALHSSKI
CGA009_RPA3733 241 QAAVDLKIEQDFGARVRLTGPVPIANEEFATVKDGAVVNGIGTVVVVLLILWMALHSSKI
TIE1_Rpal_4254 239 QAAVDLKIEQDFGARVRLTGPVPIANEEFATVKDGAVVNGIGTVVVVLLILWMALHSSKI
R1_D1920_07210 239 QAAVDLKIEQDFGARVRLTGPVPIANEEFATVKDGAVVNGIGTVVVVLLILWMALHSSKI

ATH2.1.37_D4Q71 299 IFAVAANLVIGLSITTAVGLMLVDSLNLLSIAFAVLFVGLGVDFGIQFSVRYRSEHKTG
CGA009_RPA3733 301 IFAVAANLVIGLSITTAVGLMLVDSLNLLSIAFAVLFVGLGVDFGIQFSVRYRSEHKTG
TIE1_Rpal_4254 299 IFAVAANLVIGLSITTAVGLMLVDSLNLLSIAFAVLFVGLGVDFGIQFSVRYRSEHKTG
R1_D1920_07210 299 IFAVAANLVIGLSITTAVGLMLVDSLNLLSIAFAVLFVGLGVDFGIQFSVRYRSEHKTG

ATH2.1.37_D4Q71 359 DLEKALVQAAEYSAVPLSLAAMSTTAGFLSFLPTSYPKIGISELGEIAGAGMAIAFFTSITV
CGA009_RPA3733 361 DLEKALVQAAEYSAVPLSLAAMSTTAGFLSFLPTSYPKIGISELGEIAGAGMAIAFFTSITV
TIE1_Rpal_4254 359 DLEKALVQAAEYSAVPLSLAAMSTTAGFLSFLPTSYPKIGISELGEIAGAGMAIAFFTSITV
R1_D1920_07210 359 DLEKALVQAAEYSAVPLSLAAMSTTAGFLSFLPTSYPKIGISELGEIAGAGMAIAFFTSITV

ATH2.1.37_D4Q71 419 LPALLKLLNPAGEKEPLGYAFLAPVDHFLEKHRIAIIIVGTIGVALAGLPLLYFMHDFNPF
CGA009_RPA3733 421 LPALLKLLNPAGEKEPLGYAFLAPVDHFLEKHRIAIIIVGTIGVALAGLPLLYFMHDFNPF
TIE1_Rpal_4254 419 LPALLKLLNPAGEKEPLGYAFLAPVDHFLEKHRIAIIIVGTIGVALAGLPLLYFMHDFNPF
R1_D1920_07210 419 LPALLKLLNPAGEKEPLGYAFLAPVDHFLEKHRIAIIIVGTIGVALAGLPLLYFMHDFNPF

ATH2.1.37_D4Q71 479 INLRSPKVESIATFLDLRKPNTGANAVNVMAPNEQTAREIEAKLAKLPQVSRTISLDTF
CGA009_RPA3733 481 INLRSPKVESIATFLDLRKPNTGANAVNVMAPNEQTAREIEAKLAKLPQVSRTISLDTF
TIE1_Rpal_4254 479 INLRSPKVESIATFLDLRKPNTGANAVNVMAPNEQTAREIEAKLAKLPQVSRTISLDTF
R1_D1920_07210 479 INLRSPKVESIATFLDLRKPNTGANAVNVMAPNEQTAREIEAKLAKLPQVSRTISLDTF

ATH2.1.37_D4Q71 539 VPPDQPEKLLKLIQAGAKVLEPALNPEQVDPPPSDQDNIA SLKSSAEALSRRAAGEATGPGA
CGA009_RPA3733 541 VPPDQPEKLLKLIQAGAKVLEPALNPEQVDPPPSDQDNIA SLKSSAEALSRRAAGEATGPGA
TIE1_Rpal_4254 539 VPPDQPEKLLKLIQAGAKVLEPALNPEQVDPPPSDQDNIA SLKSSAEALSRRAAGEATGPGA
R1_D1920_07210 539 VPPDQPEKLLKLIQAGAKVLEPALNPEQVDPPPSDQDNIA SLKSSAEALSRRAAGEATGPGA

ATH2.1.37_D4Q71 599 DASRRRLATALT KLAGADQAMREKAQDVFRPRLLLDFELLRNMLKAQPVTLDNLPADIVSS
CGA009_RPA3733 601 DASRRRLATALT KLAGADQAMREKAQDVFRPRLLLDFELLRNMLKAQPVTLDNLPADIVSS
TIE1_Rpal_4254 599 DASRRRLATALT KLAGADQAMREKAQDVFRPRLLLDFELLRNMLKAQPVTLDNLPADIVSS
R1_D1920_07210 599 DASRRRLATALT KLAGADQAMREKAQDVFRPRLLLDFELLRNMLKAQPVTLDNLPADIVSS

```

ATH2.1.37_D4Q71	659	WKT	KD	GQ	I	R	V	E	V	L	P	S	G	D	P	N	D	N	D	T	L	R	K	F	A	A	V	L	Q	A	E	P	L	A	T	G	G	P	V	S	I	L	K	S	G	D	T	I	V	A	S	F	I	Q	A					
CGA009_RPA3733	661	WKT	KD	GQ	I	R	V	E	V	L	P	S	G	D	P	N	D	N	D	T	L	R	K	F	A	A	V	L	Q	A	E	P	L	A	T	G	G	P	V	S	I	L	K	S	G	D	T	I	V	A	S	F	I	Q	A					
TIE1_Rpal_4254	659	WKT	KD	GQ	I	R	V	E	V	L	P	S	G	D	P	N	D	N	D	T	L	R	K	F	A	A	V	L	Q	A	E	P	L	A	T	G	G	P	V	S	I	L	K	S	G	D	T	I	V	A	S	F	I	Q	A					
R1_D1920_07210	659	WKT	KD	GQ	I	R	V	E	V	L	P	S	G	D	P	N	D	N	D	T	L	R	K	F	A	A	V	L	Q	A	E	P	L	A	T	G	G	P	V	S	I	L	K	S	G	D	T	I	V	A	S	F	I	Q	A					
ATH2.1.37_D4Q71	719	L	W	A	L	L	S	I	S	I	L	L	W	I	T	L	R	R	I	S	D	V	A	L	T	L	V	P	L	L	V	A	G	A	V	T	L	E	I	C	V	L	I	D	L	P	L	N	F	A	N	I	V	A	L	P	L	L	L	G
CGA009_RPA3733	721	L	W	A	L	L	S	I	S	I	L	L	W	I	T	L	R	R	I	S	D	V	A	L	T	L	V	P	L	L	V	A	G	A	V	T	L	E	I	C	V	L	I	D	L	P	L	N	F	A	N	I	V	A	L	P	L	L	L	G
TIE1_Rpal_4254	719	L	W	A	L	L	S	I	S	I	L	L	W	I	T	L	R	R	I	S	D	V	A	L	T	L	V	P	L	L	V	A	G	A	V	T	L	E	I	C	V	L	I	D	L	P	L	N	F	A	N	I	V	A	L	P	L	L	L	G
R1_D1920_07210	719	L	W	A	L	L	S	I	S	I	L	L	W	I	T	L	R	R	I	S	D	V	A	L	T	L	V	P	L	L	V	A	G	A	V	T	L	E	I	C	V	L	I	D	L	P	L	N	F	A	N	I	V	A	L	P	L	L	L	G
ATH2.1.37_D4Q71	779	G	V	A	F	K	I	Y	Y	V	T	A	W	R	S	G	R	T	N	L	L	Q	S	A	L	T	R	A	I	F	F	S	A	L	T	T	A	T	A	F	G	S	L	W	L	S	S	H	P	G	T	A	S	M	G	K	L	L	A	L
CGA009_RPA3733	781	G	V	A	F	K	I	Y	Y	V	T	A	W	R	S	G	R	T	N	L	L	Q	S	A	L	T	R	A	I	F	F	S	A	L	T	T	A	T	A	F	G	S	L	W	L	S	S	H	P	G	T	A	S	M	G	K	L	L	A	L
TIE1_Rpal_4254	779	G	V	A	F	K	I	Y	Y	V	T	A	W	R	S	G	R	T	N	L	L	Q	S	A	L	T	R	A	I	F	F	S	A	L	T	T	A	T	A	F	G	S	L	W	L	S	S	H	P	G	T	A	S	M	G	K	L	L	A	L
R1_D1920_07210	779	G	V	A	F	K	I	Y	Y	V	T	A	W	R	S	G	R	T	N	L	L	Q	S	A	L	T	R	A	I	F	F	S	A	L	T	T	A	T	A	F	G	S	L	W	L	S	S	H	P	G	T	A	S	M	G	K	L	L	A	L
ATH2.1.37_D4Q71	839	L	L	T	T	L	G	A	V	L	L	F	Q	P	A	L	M	G	K	P	R	H	I	D	E	S	G	D	T	D	L																													
CGA009_RPA3733	841	L	L	T	T	L	G	A	V	L	L	F	Q	P	A	L	M	G	K	P	R	H	I	D	E	S	G	D	T	D																														
TIE1_Rpal_4254	839	L	L	T	T	L	G	A	V	L	L	F	Q	P	A	L	M	G	K	P	R	H	I	D	E	S	G	D	T	D																														
R1_D1920_07210	839	L	L	T	T	L	G	A	V	L	L	F	Q	P	A	L	M	G	K	P	R	H	I	D	E	S	G	D	T	D																														

RND-family hopanoid exporter. Refseq locus tags: ATH2.1.37: D4Q71_08200; CGA009: RPA3746; TIE1: Rpal_4267; R1: D1920_07275.

ATH2.1.37_D4Q71	1	M	L	D	K	N	V	S	D	T	E	V	A	E	L	K	R	R	R	V	S	I	A	F	G	L	E	R	L	G	L	I	P	L	R	A	P	V	V	S	C	I	I	L	L	A	L	I	V	G	A	V	F	G	I	E	R	I	K	I	D
CGA009_RPA3746	1	M	L	D	K	N	V	S	D	T	E	V	A	E	L	K	R	R	R	V	S	I	A	F	G	L	E	R	L	G	L	I	P	L	R	A	P	V	V	S	C	I	I	L	L	A	L	I	V	G	A	V	F	G	I	E	R	I	K	I	D
TIE1_Rpal_4267	1	M	L	D	K	N	V	S	D	T	E	V	A	E	L	K	R	R	R	V	S	I	A	F	G	L	E	R	L	G	L	I	P	L	R	A	P	V	V	S	C	I	I	L	L	A	L	I	V	G	A	V	F	G	I	E	R	I	K	I	D
R1_D1920_07275	1	M	L	D	K	N	V	S	D	T	E	V	A	E	L	K	R	R	R	V	S	I	A	F	G	L	E	R	L	G	L	I	P	L	R	A	P	V	V	S	C	I	I	L	L	A	L	I	V	G	A	V	F	G	I	E	R	I	K	I	D
ATH2.1.37_D4Q71	61	D	S	L	S	Q	L	F	R	S	D	T	K	E	F	K	Q	Y	E	E	V	T	K	R	F	P	S	T	E	F	D	V	L	L	V	E	G	K	E	L	L	A	R	N	L	E	K	L	R	D	T	V	T	D	L	Q	L	I	D		
CGA009_RPA3746	61	D	S	L	S	Q	L	F	R	S	D	T	K	E	F	K	Q	Y	E	E	V	T	K	R	F	P	S	T	E	F	D	V	L	L	V	E	G	K	E	L	L	A	R	N	L	E	K	L	R	D	T	V	T	D	L	Q	L	I	D		
TIE1_Rpal_4267	61	D	S	L	S	Q	L	F	R	S	D	T	K	E	F	K	Q	Y	E	E	V	T	K	R	F	P	S	T	E	F	D	V	L	L	V	E	G	K	E	L	L	A	R	N	L	E	K	L	R	D	T	V	T	D	L	Q	L	I	D		
R1_D1920_07275	61	D	S	L	S	Q	L	F	R	S	D	T	K	E	F	K	Q	Y	E	E	V	T	K	R	F	P	S	T	E	F	D	V	L	L	V	E	G	K	E	L	L	A	R	N	L	E	K	L	R	D	T	V	T	D	L	Q	L	I	D		
ATH2.1.37_D4Q71	121	G	V	R	G	L	I	S	L	F	S	A	R	Q	A	P	E	P	G	K	L	P	A	A	L	F	P	S	E	L	P	E	G	E	A	Y	D	Q	F	A	Q	T	V	K	T	N	E	I	I	R	G	K	L	L	S	E	D	G	T	L	
CGA009_RPA3746	121	G	V	R	G	L	I	S	L	F	S	A	R	Q	A	P	E	P	G	K	L	P	A	A	L	F	P	S	E	L	P	E	G	E	A	Y	D	Q	F	A	Q	T	V	K	T	N	E	I	I	R	G	K	L	L	S	E	D	G	T	L	
TIE1_Rpal_4267	121	G	V	R	G	L	I	S	L	F	S	A	R	Q	A	P	E	P	G	K	L	P	A	A	L	F	P	S	E	L	P	E	G	E	A	Y	D	Q	F	A	Q	T	V	K	T	N	E	I	I	R	G	K	L	L	S	E	D	G	T	L	
R1_D1920_07275	121	G	V	R	G	L	I	S	L	F	S	A	R	Q	A	P	E	P	G	K	L	P	A	A	L	F	P	S	E	L	P	E	G	E	A	Y	D	Q	F	A	Q	T	V	K	T	N	E	I	I	R	G	K	L	L	S	E	D	G	T	L	
ATH2.1.37_D4Q71	181	L	V	V	L	S	L	D	P	K	V	V	A	D	N	T	R	L	R	A	T	I	G	E	M	R	K	V	M	T	E	D	L	E	G	S	G	L	S	R	Q	L	S	G	V	P	V	M	Q	L	E	I	R	N	A	V	E	R	D	G	
CGA009_RPA3746	181	L	V	V	L	S	L	D	P	K	V	V	A	D	N	T	R	L	R	A	T	I	G	E	M	R	K	V	M	T	E	D	L	E	G	S	G	L	S	R	Q	L	S	G	V	P	V	M	Q	L	E	I	R	N	A	V	E	R	D	G	
TIE1_Rpal_4267	181	L	V	V	L	S	L	D	P	K	V	V	A	D	N	T	R	L	R	A	T	I	G	E	M	R	K	V	M	T	E	D	L	E	G	S	G	L	S	R	Q	L	S	G	V	P	V	M	Q	L	E	I	R	N	A	V	E	R	D	G	
R1_D1920_07275	181	L	V	V	L	S	L	D	P	K	V	V	A	D	N	T	R	L	R	A	T	I	G	E	M	R	K	V	M	T	E	D	L	E	G	S	G	L	S	R	Q	L	S	G	V	P	V	M	Q	L	E	I	R	N	A	V	E	R	D	G	
ATH2.1.37_D4Q71	241	I	Y	N	I	A	G	I	L	A	G	C	V	I	A	I	L	F	F	R	K	I	S	F	M	V	V	A	A	F	P	P	L	L	A	I	L	L	A	I	G	V	L	G	W	A	G	F	S	L	N	M	F	L	N	V	M	T	P	L	
CGA009_RPA3746	241	I	Y	N	I	A	G	I																																																					

ATH2.1.37_D4Q71	541	KEYVDLLPPNLVRRFISEDQSAVVVSGRVPDLSSEILPVVQKLDHALDSVRQKHPGYEV
CGA009_RPA3746	541	KEYVDLLPPNLVRRFISEDQSAVVVSGRVPDLSSEILPVVQKLDHALDSVRQKHPGYEV
TIE1_Rpal_4267	541	KEYVDLLPPNLVRRFISEDQSAVVVSGRVPDLSSEILPVVQKLDHALDSVRQKHPGYEV
R1_D1920_07275	541	KEYVDLLPPNLVRRFISEDQSAVVVSGRVPDLSSEILPVVQKLDHALDSVRQKHPGYEV
ATH2.1.37_D4Q71	601	AVTGLSATAARNSADMISKLNHGLTIEFVLVAIFIGLAFRSVVVMLACILPGIFPVVLSG
CGA009_RPA3746	601	AVTGLSATAARNSADMISKLNHGLTIEFVLVAIFIGLAFRSVVVMLACILPGIFPVVLSG
TIE1_Rpal_4267	601	AVTGLSATAARNSADMISKLNHGLTIEFVLVAIFIGLAFRSVVVMLACILPGIFPVVLSG
R1_D1920_07275	601	AVTGLSATAARNSADMISKLNHGLTIEFVLVAIFIGLAFRSVVVMLACILPGIFPVVLSG
ATH2.1.37_D4Q71	661	TLLWLMGEGLOFASVVALTVSFGLGLSATIHFLNRLRLESPPGVSAGLAVERATVLVGPA
CGA009_RPA3746	661	TLLWLMGEGLOFASVVALTVSFGLGLSATIHFLNRLRLESPPGVSAGLAVERATVLVGPA
TIE1_Rpal_4267	661	TLLWLMGEGLOFASVVALTVSFGLGLSATIHFLNRLRLESPPGVSAGLAVERATVLVGPA
R1_D1920_07275	661	TLLWLMGEGLOFASVVALTVSFGLGLSATIHFLNRLRLESPPGVSAGLAVERATVLVGPA
ATH2.1.37_D4Q71	721	LILTTVVLACGLGVTVFSDLPRLRFGWLSAFAMVAALIADLFILRPTAMWLISVAHRLR
CGA009_RPA3746	721	LILTTVVLACGLGVTVFSDLPRLRFGWLSAFAMVAALIADLFILRPTAMWLISVAHRLR
TIE1_Rpal_4267	721	LILTTVVLACGLGVTVFSDLPRLRFGWLSAFAMVAALIADLFILRPTAMWLISVAHRLR
R1_D1920_07275	721	LILTTVVLACGLGVTVFSDLPRLRFGWLSAFAMVAALIADLFILRPTAMWLISVAHRLR
ATH2.1.37_D4Q71	781	GGRGAGSVV
CGA009_RPA3746	781	GGRGAGSVV
TIE1_Rpal_4267	781	GGRGAGSVV
R1_D1920_07275	781	GGRGAGSVV

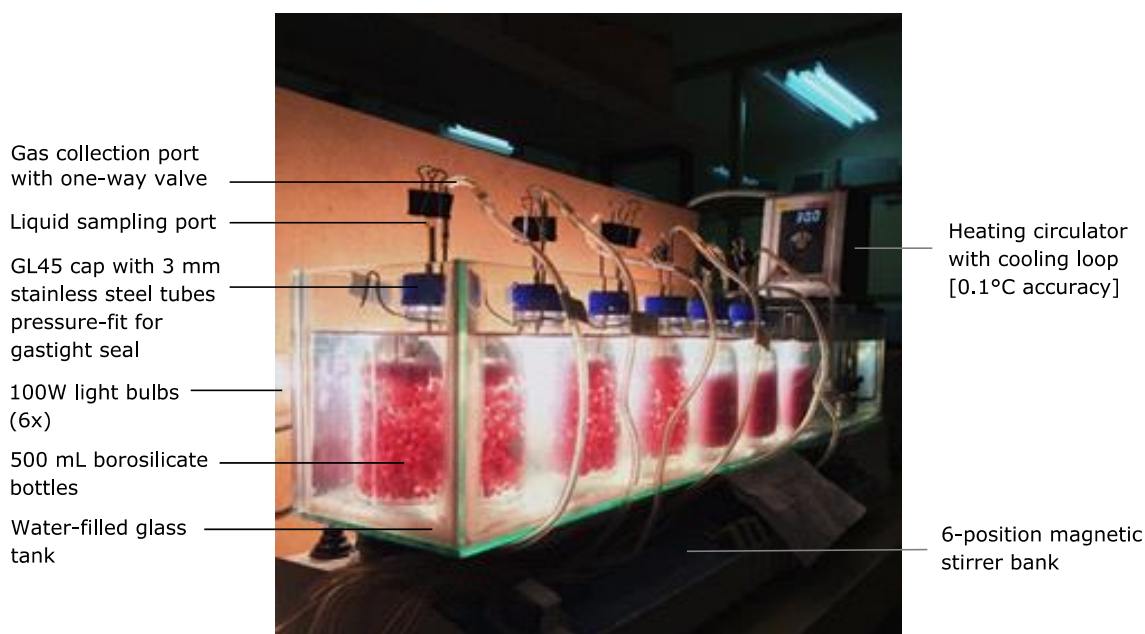


Figure A1.1. Setup of temperature-controlled 0.5 L test photobioreactors for growth and hydrogen production studies.

Additional details are described in **Section 3.4.2**.

APPENDIX 2. Supplementary information for Chapter 4.

Transparent poly vinyl-alcohol cryogel as immobilisation matrix for continuous biohydrogen production by phototrophic bacteria.

Supplementary methods for determination of diffusion coefficient

In order to determine the effective diffusivity D_{eff} , the partition coefficient defined according to the equilibrium relationship between substrate contained in the PVA cryogel cube (c_{cube}) and the solution (c_{sol}) such that $c_{sol} = K_H c_{cube}$, must first be determined. Cubes were equilibrated with a solution of known substrate concentration ($c_{sol,eq}$) and subsequently placed in a substrate free solution ($c_{sol} = 0$ at $t = 0$) until a new equilibrium was reached such that $\lim_{t \rightarrow \infty} c_{sol} = c_{sol,f}$, as described in the experimental methods, **section 4.4.4**. The equilibrium relationship with the initial solution (eq. 1), final solution (eq. 2) and a mass balance over the diffusion experiment (eq. 3) yields a system of linear equations which can be readily solved for the unknown values K_H , $c_{cube,0}$ and $c_{cube,f}$:

$$c_{sol,eq} = K_H c_{cube,0} \quad (1)$$

$$c_{sol,f} = K_H c_{cube,f} \quad (2)$$

$$V_{sol} c_{sol,f} = V_{cube} (c_{cube,0} - c_{cube,f}) \quad (3)$$

Where V_{sol} and V_{cube} are the liquid solution and cube volumes, respectively. Once the initial cube concentration $c_{cube,0}$ and the partition coefficient K_H are known, the intra-cube substrate diffusion can be modelled by approximating the cube as a sphere with radius equal to the surface-volume radius of the cube ($R = 3V_{cube}/A_{cube}$ where A_{cube} is the surface area of the cube). The partial differential equation describing the diffusion process is given by eq. 4, with accompanying boundary conditions (eqns. 5-6) and initial condition (eq. 7):

$$\frac{\partial c}{\partial t} = D_{eff} \left(\frac{\partial c}{\partial r^2} + \frac{2}{r} \frac{\partial c}{\partial r} \right) \quad \text{for } 0 < r < R, t > 0 \quad (4)$$

$$\frac{\partial c}{\partial r} = 0 \quad \text{for } r = 0, t > 0 \quad (5)$$

$$-D_{eff} \frac{\partial c}{\partial r} = k_L (K_H c - c_{sol}) \quad \text{for } r = R, t > 0 \quad (6)$$

$$c = c_{cube,0} \quad \text{for } 0 \leq r \leq R, t = 0 \quad (7)$$

Equation 6 represents the flux balance at the surface of the cube, where the flux out of the cube is equal to the rate of mass transfer from the surface of the cube to the bulk solution, with mass transfer coefficient k_L . The concentration of the bulk solution is modelled using the ordinary differential equation (ODE) given by eq. 8, with the initial condition $c_{sol}(0) = 0$:

$$V_{sol} \frac{dc_{sol}}{dt} = k_L A_{cube} (K_H c - c_{sol}) \quad (8)$$

The partial differential equation (eq. 4) was discretized using the finite difference method and combined with eq. 8, yielding a system of ODEs. This system of ODEs is readily solved using MATLAB (Natick, MA) and the built-in numerical integrator ode45.

The substrate concentration was measured at time points t_i during the diffusion experiment, yielding the experimental measurements $\hat{c}_{sol}(t_i)$. The unknown parameters \mathcal{D}_{eff} and k_L was determined by regressing the model predicted values $c_{sol}(t_i)$ against the experimental measurements $\hat{c}_{sol}(t_i)$. The regression was performed using the MATLAB built-in least-squares optimization function lsqnonlin.

Results

The regression results showed that the effective diffusivity \mathcal{D}_{eff} was insensitive to k_L when $k_L > 10^{-3}$. In fact, a basic identifiability analysis indicated that k_L was practically unidentifiable. This is illustrated in **Figure A2.1** for transparent cryogels with glycerol substrate. The optimal effective diffusivity was determined to be $\mathcal{D}_{eff} = 7.32 \times 10^{-6} \text{ cm}^2 \cdot \text{s}^{-1}$. Model results compared to experimental measurements are shown in **Figure A2.2**, indicating an excellent fit.

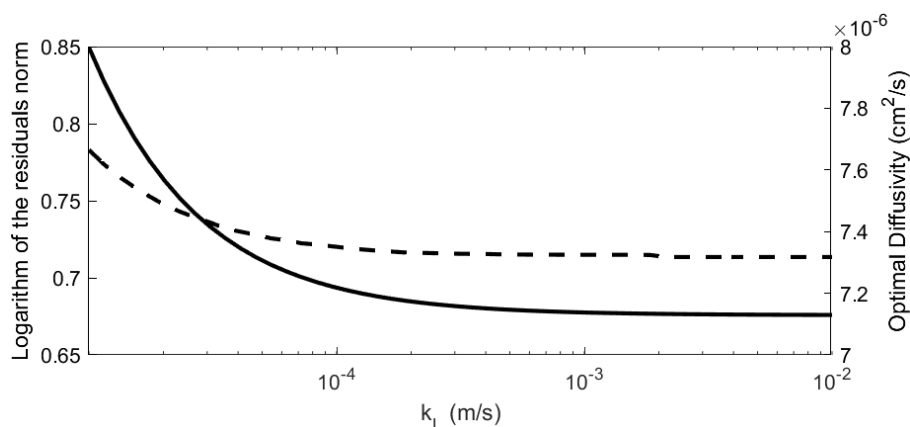


Figure A2.1. The minimum residual error (solid line) decreases asymptotically as the mass transfer coefficient k_L increases, indicating practical unidentifiability.

The optimal diffusivity \mathcal{D}_{eff} (dashed line) is insensitive to variations in k_L above a value of 10^{-3} and tends to a value of $\mathcal{D}_{eff} = 7.32 \times 10^{-6} \text{ cm}^2 \cdot \text{s}^{-1}$.

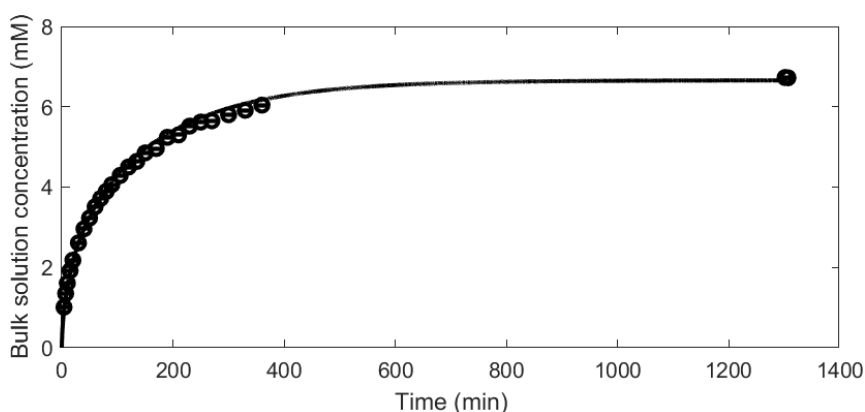


Figure A2.2. Model predictions (solid line) using $\mathcal{D}_{eff} = 7.32 \times 10^{-6} \text{ cm}^2 \cdot \text{s}^{-1}$, compared to experimental measurements (circles) for diffusion of glycerol from transparent cryogel.

APPENDIX 3. Supplementary information for Chapter 5.

Expression of alternative nitrogenases in Rhodospseudomonas palustris is enhanced using a novel genetic toolset for rapid, markerless modifications.

Sequence of maximum-diversity codon-optimised *vnfH* gene (*vnfH_{opt}*):

```
ATGCCGCGCCAGATCGCGTTCTACGGCAAGGGCGGCATCGGCAAGAGCACCACCTCGCAGAATACGCTGGCGGGCC
CTGGTGGAAATGGGCCAGAAGATCCTCATCGTTCGGCTGCGACCCGAAGGCCGACAGCACGCGCCTGATCCTGAAC
ACGAAGCTCCAGGATACGGTGTCTGGCCCTGGCGGGCGGAAGCCGGCTCGGTGGAAGATCTGGAACCTGGAAGATGTC
ATGAAGATCGGCTATAAGGGCATCAAGTGCACGGAAGCGGGCGGCCCGGAACCGGGCGTGGGCTGCGCCGGCCGG
GGCGTCATCACGGCCATCAATTTCTCGAGGAAAAATGGCGGTACGAGGATGTGGACTACGTGTCTGATGACGTC
CTGGGCGACGTCTGCTGCGGGCGGCTTCGCCATGCCGATCCGCGAAAAATAAGGCCAGGAAATCTATATCGTGATG
AGCGGCGAAATGATGGCCCTCTATGCGGGCAACAACATCAGCAAGGGCATCCTCAAGTATGCGTTCGAGCGGCGGC
GTGCGCCTCGGCGGCCTCATCTGCAATGAACGGCAGACGGATCGCGAACTGGACCTGGCGGAGGCGCTGGCCGCG
AAGCTCAACAGCAAGCTCATCCATTTCTGTCGCCGGGATAATATCGTCCAGCACGCGGAACTGCGCCGCGAAACC
GTCATCCAGTATGCGCCGGACAGCCAGCAGGCGAAGGAATATCGCGCCCTGGCGTCGAAGATCCACGCGAACAGC
GGCAATGGCACGATCCCGACCCGATCACGATGGAAGAAGCTCGAGGAAATGCTCCTGGATTTTCGGCATCATGAAG
ACGGAAGAACAGCAGCTGGCGGAACTCGCGGCGAAGGAAGCGGCGAAGGCCGCGGCCGTGGCGTAA
```

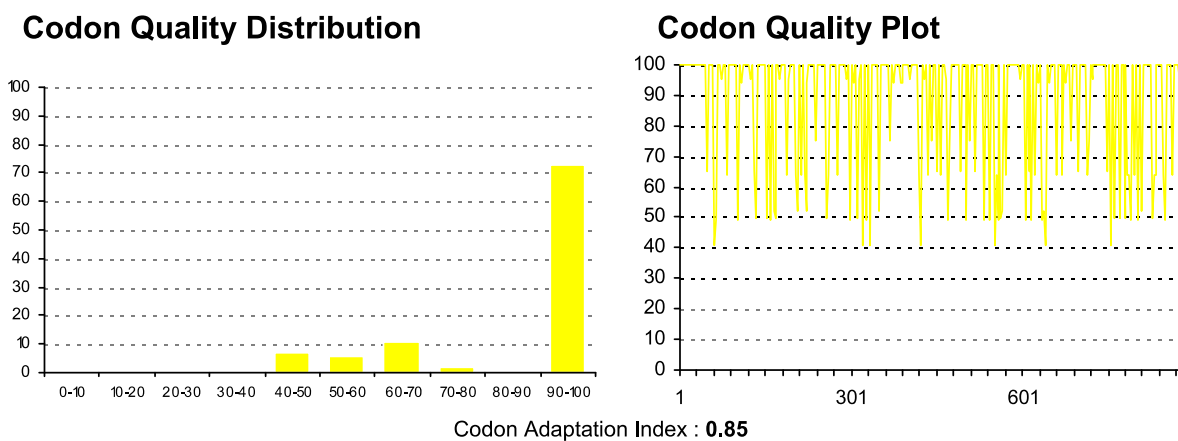


Figure A3.1. Codon quality distribution and codon quality plot of *vnfH_{opt}*.

Codon optimisation was performed to maximise diversity relative to native gene, using the Kazusa codon usage database and GeneOptimiser tool (GeneArt; Thermo Scientific). The quality value of the most frequently used codon for a given amino acid is set to 100, with the remaining codons scaled according to usage frequency. The Codon Adaptation Index is a measure how well the codons match the usage preference of *R. palustris*. (1.0 reflects a perfect score).

Table A3.1. PCR Primers used to generate fragments for plasmid construction by Gibson assembly. Uppercase denotes gene-specific primer portion; lowercase is overlapping portion for assembly (as output by NEBuilder tool). PCR fragments assembled in order as listed.

Primer	Sequence (5' – 3')	Note
<i>nif:puc</i> plasmid	>All 5' and 3' flanking regions designed to overlap with <i>Bam</i> HI/ <i>Xba</i> I-digested pK18 <i>mobSacB</i>	
<i>nif</i> 5' - Fwd	atgattacgaattcgagctcggtaccgggCATTGGGTGAATTACTATCGGCC	<i>nif</i> 5' homologous flank
<i>nif</i> 5': <i>puc</i> - Rev	tgacgagtaaggcgcGTTTTCTCTCCGTTGACCTAATGC	
<i>puc</i> prom (<i>nif</i>) - Fwd	caacggagagaaaacGCGCCTTACTCGTCAGATCG	<i>puc</i> promoter (for <i>nif</i> plasmids)
<i>puc</i> prom (<i>nif</i>) - Rev	ttgccgaagtgccatTTTGAGACCTCATAATGGGGTTTC	
<i>nif</i> 3': <i>puc</i> - Fwd	ttatgaggtctcaaaATGGCACTTCGGCAAATCG	<i>nif</i> 3' homologous flank
<i>nif</i> 3' - Rev	gtccaagctgcatgcctgcaggtcgactCTTGCCGACTTGTCGG	
<i>nif:cit</i> plasmid		
<i>nif</i> 5': <i>cit</i> - Rev	cgtttcccgggtttGTTTTCTCTCCGTTGACCTAATGC	Uses <i>nif</i> 5' - Fwd as above
<i>cit</i> prom (<i>nif</i>) - Fwd	caacggagagaaaacAAAACCCGGGAAACGGCTC	<i>cit</i> promoter (for <i>nif</i> plasmids)
<i>cit</i> prom (<i>nif</i>) - Rev	ttgccgaagtgccatCGTGTGGTCCCGATGTTC	
<i>nif</i> 3': <i>cit</i> - Fwd	atcggggaccacacgATGGCACTTCGGCAAATCG	Uses <i>nif</i> 3' - Rev as above
<i>anf:puc</i> plasmid		
<i>anf</i> 5' - Fwd	atgattacgaattcgagctcggtaccgggCGAGATGGTCGCTGAGGGC	
<i>anf</i> 5': <i>puc</i> - Rev	tgacgagtaaggcgcGGTCCGAAGCTCCTGCGATG	
<i>puc</i> prom (<i>anf</i>) - Fwd	caggagcttcggaccGCGCCTTACTCGTCAGATCG	
<i>puc</i> prom (<i>anf</i>) - Rev	caccttgcggtcatTTTGAGACCTCATAATGGGGTTTC	
<i>anf</i> 3': <i>puc</i> - Fwd	ttatgaggtctcaaaATGACCCGCAAGGTGGCG	
<i>anf</i> 3' - Rev	gtccaagctgcatgcctgcaggtcgactATCACATGCTTTGCGCCGC	
<i>anf:cit</i> plasmid		
<i>anf</i> 5': <i>cit</i> - Rev	cgtttcccgggtttGGTCCGAAGCTCCTGCGATG	Uses <i>anf</i> 5' - Fwd as above
<i>cit</i> prom (<i>anf</i>) - Fwd	caggagcttcggaccAAAACCCGGGAAACGGCTC	
<i>cit</i> prom (<i>anf</i>) - Rev	caccttgcggtcatCGTGTGGTCCCGATGTTC	
<i>anf</i> 3': <i>cit</i> - Fwd	atcggggaccacacgATGACCCGCAAGGTGGCG	Uses <i>anf</i> 3' - Rev as above
<i>vnf:puc</i> plasmid		
<i>vnf</i> 5' - Fwd	atgattacgaattcgagctcggtaccgggTCGCTCCAGTTGAACACCAGC	
<i>vnf</i> 5': <i>puc</i> - Rev	tgacgagtaaggcgcGGGATCGGCTGAGGCGG	
<i>puc</i> prom (<i>vnf</i>) - Fwd	gcctcagccgatcccGCGCCTTACTCGTCAGATCGAAG	
<i>puc</i> prom (<i>vnf</i>) - Rev	gatctggcggcatTTTGAGACCTCATAATGGGGTTTCTG	
<i>vnfH</i> sub: <i>puc</i> - Fwd	ttatgaggtctcaaaATGCCGCGCCAGATCGC	
<i>vnfH</i> sub - Rev	tctcctcgtcagacTTACGCCACGGCCGCG	
<i>vnf</i> 3' - Fwd	gcgccgtggcgtaaGTCTGAACGAGGAGATCCGCC	
<i>vnf</i> 3' - Rev	gtccaagctgcatgcctgcaggtcgactGTCGTCTCGACCGACTTGG	
<i>vnf:cit</i> plasmid		
<i>vnf</i> 5': <i>cit</i> - Rev	cgtttcccgggtttGGGATCGGCTGAGGCGG	Uses <i>vnf</i> 5' - Fwd as above
<i>cit</i> prom (<i>vnf</i>) - Fwd	gcctcagccgatcccAAAACCCGGGAAACGGCTC	
<i>cit</i> prom (<i>vnf</i>) - Rev	gatctggcggcatCGTGTGGTCCCGATGTTC	
<i>vnfH</i> sub: <i>cit</i> - Fwd	atcggggaccacacgATGCCGCGCCAGATCGC	Uses <i>vnfH</i> sub - Rev as above, and <i>vnf</i> 3' PCR fragment for assembly

APPENDIX 4. Light source selection, calibration and conversion factors

Illumination of photobioreactors employed incandescent tungsten-filament bulbs as a light source, which provide key wavelengths of light in the near-infrared region which the photosystem of *R. palustris* requires. Other common light sources such as fluorescent tubes neglect this range, as seen in **Figure A4.1**. In addition, incandescent light better-approximates sunlight, maintaining the relevance of bioreactors studies to development of outdoor sunlit photo-bioprocesses.

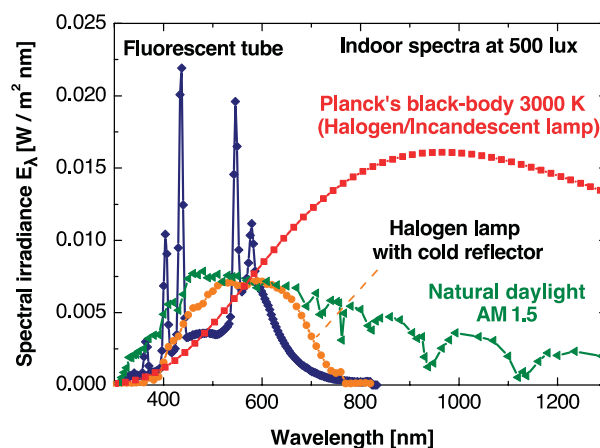


Figure A4.1. Spectra of commonly-used indoor light sources at 500 lux.

Figure reproduced from Virtuani, Lotter & Powalla (2006), with permission from *Elsevier*.

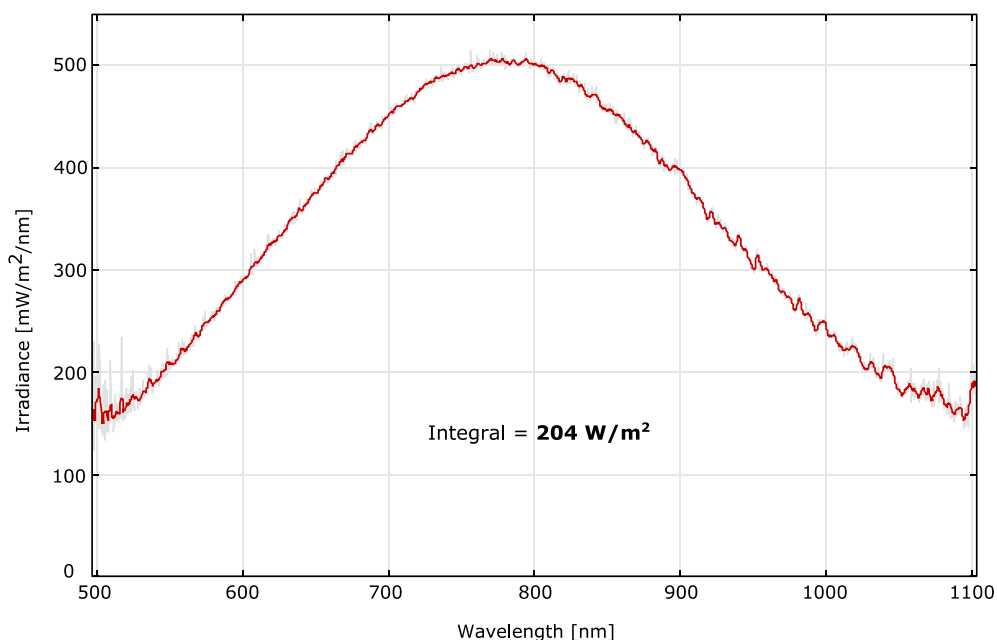


Figure A4.2. Irradiance intensity spectrum at inner surface of photobioreactors provided by 100 W incandescent lightbulbs.

Light bulbs supplied by Eurolux (South Africa), catalog #: G715 (rough service type, 2700 K colour temperature, 1152 lumen rated flux)

Irradiance was measured at the inner surface of the photobioreactors using a calibrated compact spectrometer and cosine correction probe (RBG photonics Qmini Vis-NIR) in the wavelength range 500 – 1100 nm critical for *R. palustris* photosynthesis. Distance between lights and bioreactors was adjusted to yield an average irradiance intensity of $200 (\pm 20) \text{ W/m}^2$, shown along with a representative spectrum in **Figure A4.2**.

Irradiance can also be expressed in terms of photon flux, commonly used in photosynthesis research where quantity of discrete photons is more relevant than the overall power. As such, the use of a spectrometer allows conversion between the units W/m^2 , and $\mu\text{mol photons/s/m}^2$ (otherwise referred to as microEinsteins, μE), as shown by the spectrum in **Figure A4.3**; equating 204 W/m^2 to $1350 \mu\text{mol/s/m}^2$.

Over a range of irradiance intensities between $30 - 680 \text{ W/m}^2$, the conversion factor was determined as $\mu\text{E} = 6.75 \pm 0.14 \times \text{W/m}^2$ for the specific system and light bulbs used in this work.

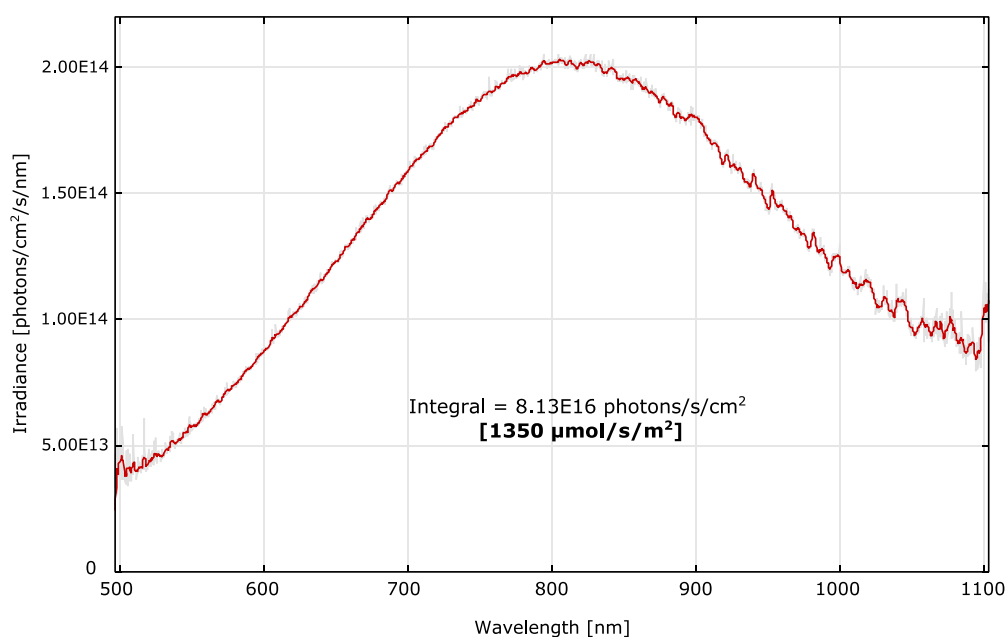


Figure A4.3. Photon flux intensity spectrum at inner surface of photobioreactors illuminated by 100 W incandescent lightbulbs.

Data from the same measurement as in **Figure A4.2**.

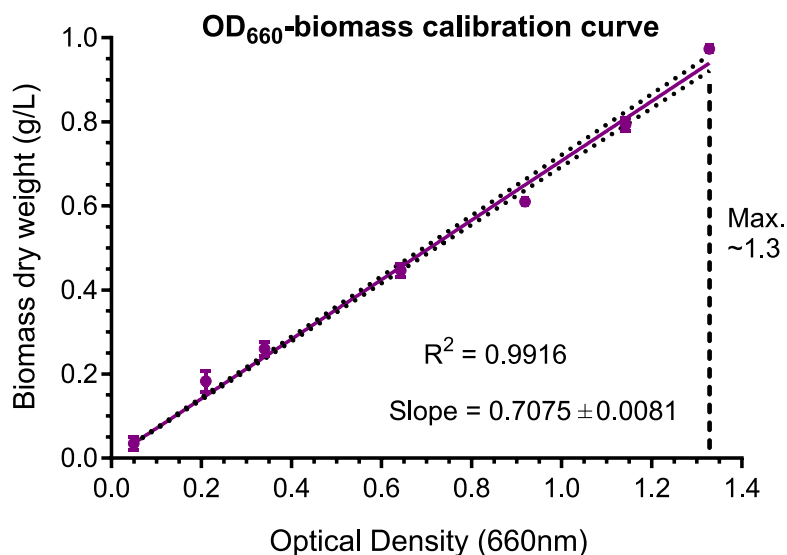
APPENDIX 5. Calibration curves for determination of biomass and glutamate concentration

Figure A5.1. Calibration curve for determination of biomass concentration using optical density at a wavelength of 660 nm.

Data points reflect mean \pm standard deviation for 3 – 5 replicates, performed as described in **Section 3.4.3**. Best fit line is shown bracketed by 95% confidence interval. Curve deviates from linear response above OD ~ 1.3; samples above this value are diluted for accurate measurement.

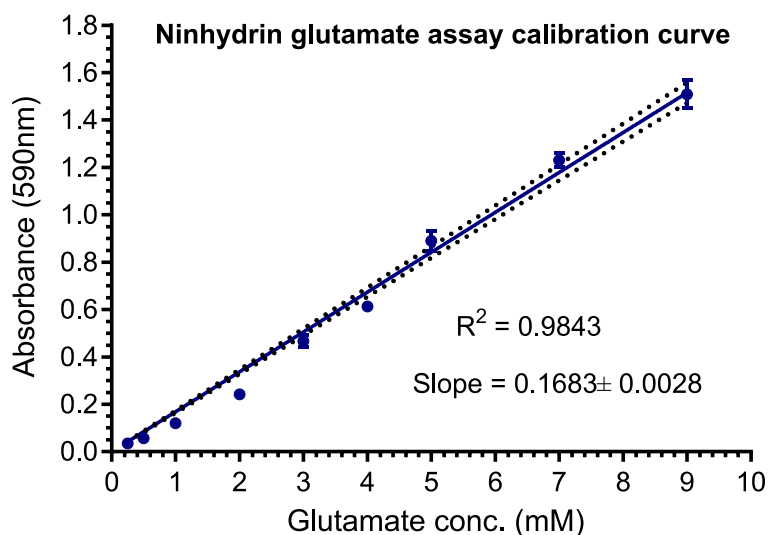


Figure A5.2. Calibration curve for determination of glutamate concentration using absorbance of ninhydrin colorimetric assay at a wavelength of 590 nm.

Data points reflect mean \pm standard deviation for 4 – 5 replicates. Best fit line is shown bracketed by 95% confidence interval. Curve generated using standard concentrations in minimal medium, as detailed in **Section 4.4.10**.

APPENDIX 6. Protocols**Protocol A. Modified *Rhodospirillacea* minimal medium**Stock solutions:**Buffers (250X):** 4 mL/L of each = final pH ~7.2 at 30 – 35°C

1. **KH₂PO₄** (acid): 1.05 M = 14.29 g / 100 mL
2. **K₂HPO₄** (base): 2.675 M = 46.6 g / 100 mL

Bulk nutrients (10X):

For 1 L (in deionised water):

Yeast extract:	2.0 g
Na thiosulfate (Na ₂ S ₂ O ₃):	1.6 g
PABA (4-aminobenzoic acid):	0.02 g
MgSO ₄ .7H ₂ O:	2.0 g
CaCl ₂ .2H ₂ O:	0.5 g
NaCl:	4.0 g
Ferric citrate:	0.05 g

- Heat with stirring to dissolve ferric citrate
- Autoclave in 250 mL aliquots for long-term storage (shake to re-dissolve precipitate)
- ***Nitrogen-free version for non-growing cultures: omit yeast extract***

1X Media preparation (1L):

- Make up 4 mL of each buffer component + 100 mL bulk nutrients to 1 L with deionised water
- For solid media: + 15 g agar (1.5% w/v)
- Autoclave 20 – 30 mins. Precipitate re-dissolves after cooling and shaking
- Final volume reduces by ~15 mL after autoclaving; sterile additions restore correct concentration

Sterile additions:

- 1 mL trace elements (per L; filtered sterile – small aliquots advisable):

ZnCl ₂	70 mg
MnCl ₂ .4H ₂ O	100 mg
H ₃ BO ₃	60 mg
CoCl ₂ .6H ₂ O	200 mg
CuCl ₂ .2H ₂ O	20 mg
NiCl ₂ .6H ₂ O	20 mg
NaMoO ₄ .2H ₂ O	40 mg

- Carbon source: 10 mL glycerol (5 M solution, autoclaved) = 50 mM final concentration.
- Nitrogen source: 4 mL glutamate (monosodium; 2.5 M solution, autoclaved) = 10 mM final concentration.

Protocol B. Transparent PVA cryogel bead immobilisation procedure

Materials:

- Poly-vinyl alcohol: highly hydrolysed (>98%) with MW ~80 – 100 kDa.
 - *PVA with standard specified viscosity ~30 cP (4% solution, 20°C) combines sufficiently low viscosity for dripping procedure with good gel strength.*
 - *Powder is preferable to granules for ease / speed of dissolution.*
 - *We use 88 kDa PVA, 98% hydrolysed: **Scientific Polymer Products Inc, USA; Cat # 362***
- 50% v/v glycerol in deionised water (plus **sterile aliquot**)
- Dripping setup with peristaltic pump and sterile tubing (e.g. silicone)
 - *Pre-tested and refined using non-sterile PVA solution*
- Dripping head with multiple nozzles (increases speed)
- Heating wrap for tubing: 20 W terrarium heating cable, available from reptile pet suppliers
 - *Keeps PVA solution warm & viscosity low for efficient dripping*
- Heated water bath
- Magnetic stirrer hotplate and X-shaped stirrer bars
- Liquid nitrogen & open-top dewar (e.g. Thermo Scientific Thermo-flask benchtop, 2 L)
- Sterile centrifuge tubes (50 mL) or bottles (250 mL; e.g. Nalgene)
- Log-phase bacterial culture

Procedure:

- Make 11% w/v PVA solution in 50% v/v glycerol: mix PVA with room temperature 50% glycerol and heat with magnetic stirring to ~95°C in loosely capped reagent bottle for a few hours until dissolved (up to overnight)
 - *Do not add PVA to hot solvent or it will clump and not dissolve properly.*
 - *PVA in powder form makes this process significantly quicker.*
- Autoclave known mass (200 g) in 250 mL reagent bottles whilst solution is still warm/melted.
- Prepare water bath heated to 45°C
- Melt autoclaved PVA solution thoroughly in microwave (if solidified), ensuring no lumps remain and solution is *completely* liquid to prevent clogging of dripping setup. Avoid boiling or overheating the solution. Allow to cool for 10 – 15 minutes before placing in water bath to equilibrate to 45°C.
- Centrifuge log-phase culture (3000 x g, 10 min) in pre-weighed 50 mL tubes or 250 mL bottles (15 min). Wash pellet with suitable sterile media or PBS if required and centrifuge again. Remove as much supernatant as possible and weigh cell pellets.

- Calculate volume of 50% glycerol to resuspend pellet in for desired biomass loading: this needs to be determined empirically eg. 1.5% (cell pellet : PVA mass) for *R. palustris* results in a bead with sufficient cell density balanced with good light transmittance.

Example calculation for 1.5% loading: require 1.5 g cells in 8.75 mL 50% glycerol for every 100 g PVA solution (final PVA concentration = 10 %).

- Resuspend cells in glycerol by shaking or pipetting and add to PVA (17.5 mL suspension for every 200 g). Mix with sterile spatula until homogeneous. Connect tubing to bottle and seal.
- Place PVA bottle back in water bath and drip into liquid nitrogen dewar
- Once finished, strain liquid nitrogen through sterile sieve to collect beads
- For later use, place in sterile container and store at -80°C immediately
- For immediate use, allow to thaw quickly in suitable sterile container at room temp. Before using thawed beads, the glycerol co-solvent can be removed if necessary, using successive sterile PBS washes or by incubating overnight in excess volume of growth media under suitable culturing conditions.

Protocol C. *R. palustris* electrocompetent cell preparation**Materials: all sterile**

- Van Niel's Yeast medium with 50 mM glycerol (VNG medium):
1 g K₂HPO₄, 0.5 g MgSO₄, 10 g yeast extract per litre (final pH ~7.1).
Add 10 mL sterile 5 M glycerol solution after autoclaving.
- 10% glycerol solution, sterile-filtered
- 50 mL centrifuge tubes

Electrocompetent cell preparation:

1. Inoculate 50 mL VNG medium in 50 mL tubes. Grow in light with shaking (35°C) ~2 days until OD₆₆₀ = 0.3 – 0.6 (max 1.0)
Fast growth in VNG results in high cell viability; freshly-grown nonstationary-phase cells are important for high transformation efficiency.
2. Chill tubes and 10% glycerol on ice ~15 min
3. Centrifuge ~4000 x g at 4°C; 10 mins.
Higher force makes pellet difficult to resuspend.
4. Resuspend / wash cell pellet 3X with 50 mL aliquots of ice-cold 10% glycerol; centrifuging as before for 10 min.
Pellets are easier to resuspend in small volume by vortexing, before topping up to 50ml.
5. Resuspend pellet in 0.5 – 1 mL 10% glycerol
(or just enough for homogeneous suspension with no clumps)
6. 100 µL aliquots can be quick-frozen on dry ice and stored at –80°C

Notes:

- It is advisable to routinely streak cultures on VNG plates before preparing electrocompetent cells; contamination shows up overnight at 35°C

Protocol D. *R. palustris* electro-transformation procedure**Materials: all sterile**

- Purified plasmid in water (high concentration preferable, with low or no salt present)
- Microfuge tubes
- 2 mL screw-cap tubes
- 1 mm gap electroporation cuvettes
- Electroporator e.g. BioRad GenePulser
- Electrocompetent cells (from above)
- VNG agar plates with 200 – 400 µg/mL kanamycin (or antibiotic suitable for plasmid)

Electroporation procedure:

1. Chill electroporation cuvettes and VNG medium on ice
2. Add ~500 ng plasmid to 1.5 mL tube on ice (*for VWR brand electroporation cuvettes with 100 µl capacity*)
3. Add 100 µL electrocompetent cells, mix gently by pipetting
4. Pipette into chilled cuvette, tap to remove any bubbles
5. Electroporate: 2.0 kV, 800 Ω, 25 µF pulse (time constant <17 mSec is good) – *chill on ice immediately and keep cold throughout*
Depending on construct, 600 Ω may result in higher transformation efficiency
6. Promptly add 900 µL ice-cold VNG medium. Transfer to 2 mL screw cap tube and use another 900 µL to rinse out cuvette and add to tube
7. Keep on ice 5 min
8. Incubate overnight at 30°C in light with shaking (~18 hours)
9. Plate 50 – 150 µL volumes on VNG plates with antibiotic
10. Incubate at 30 – 35°C until colonies form (3 – 5 days typically)
11. Patch colonies out onto fresh plates and screen by colony PCR

Notes:

- *R. palustris* is naturally resistant to antibiotics in general so higher concentration may reduce rate of false positives.
- Marked, 1st recombination strains with pK18*mobSacB* are unstable so second recombination step should be completed promptly after PCR screening.

Protocol E. Optimised RNA isolation procedure**Materials:**

- RNase-free microfuge tubes (from unopened package, *not autoclaved*)
- 2% SDS in RNase-free Tris-EDTA (TE) buffer, pH 8 (Invitrogen)
- Tri reagent (Sigma), TriZol (Thermofisher) or equivalent
- Zymo Research Direct-zol RNA miniprep kit
- RNase-free 96% ethanol

User should be familiarised with requirements for avoidance of RNase contamination

Procedure:

Reagents in **bold** are supplied with the Direct-zol kit

1. Grow cultures under desired conditions to medium density – *not opaque*; $OD_{660} < 2$
2. Centrifuge 1 mL of culture, 5 min at 14000 x g
Smaller volume should be used if dense culture – not more than 2 OD x mL to maintain high RNA integrity e.g. OD 3 = 2/3 mL
3. Pipette off supernatant
4. Resuspend cells in 55 μ L 2% SDS in RNase free TE buffer, pH 8 (Invitrogen) in 1.5 mL tube
5. Incubate at 65°C for 20 min
Preferably in thermomixer; 30s mix, 1:30 off
6. Add 640 μ L Tri reagent, mix by pipetting until homogeneous
7. Leave on carousel mixer for ~15 min at room temp. (RT)
8. *Stopping point: store at -20°C*
9. Centrifuge to pellet cell debris (5 min, 14000 x g)
10. Pipette off supernatant and add to equal volume 96% ethanol – 700 μ L
11. Apply to Zymo Direct-Zol column in 2 aliquots of 700 μ L (30s spins, as per supplied protocol)
12. Wash with 400 μ L **RNA wash buffer**
13. Transfer column to new collection tube
14. Mix 5 μ L **DNase I** + 75 μ L **DNA digestion buffer** in RNase free tube, apply to column matrix
15. Incubate at least 20 min at RT (*30 mins preferable*)
16. Centrifuge 30 s
17. Wash with 400 μ L **RNA pre-wash**
18. Discard flow-through & repeat washing with **pre-wash** solution
19. Wash with 700 μ L **RNA WASH buffer**, centrifuge 1 min.
20. Empty collection tube & centrifuge another 2 min.
21. Transfer to RNase free 1.5 mL tube
22. To elute add 50 μ L Nuclease free water directly to matrix, incubate >1 min. Centrifuge 1 min.
23. Store at -80°C, keeping 5 μ L sample aside for nanodrop (concentration/purity) and gel electrophoresis or Agilent BioAnalyzer to determine RNA integrity.